BODEA MARIUS

LABORATORY
MATERIALS SCIENCE ENGINEERING
Metallography and Microstructures

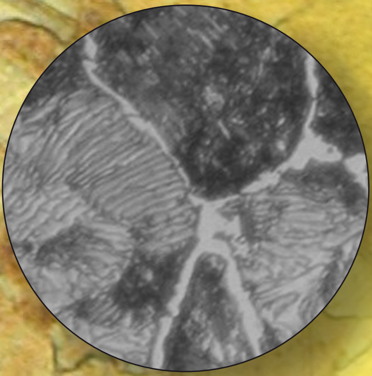

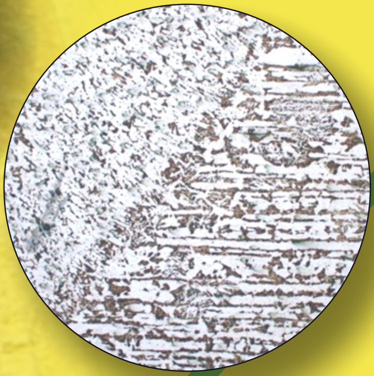

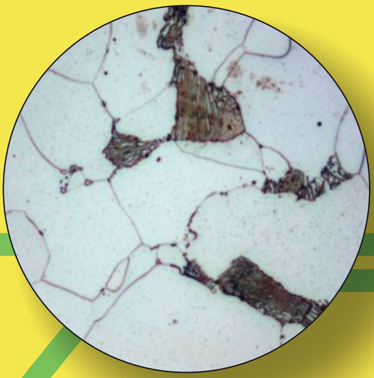

UTPRESS
Cluj-Napoca, 2025
ISBN 978-606-737-766-8

Marius BODEA

LABORATORY
MATERIALS SCIENCE ENGINEERING
Metallography and Microstructures

U.T. PRESS
Cluj-Napoca,2025
ISBN 978-606-737-766-8

Editura U.T.PRESS
Str. Observatorului nr. 34
400775 Cluj-Napoca
Tel.: 0264-401.999
e-mail: utpress@biblio.utcluj.ro
www.utcluj.ro/editura

Recenzia: Conf.dr. ing. Mariana Pop
Conf.dr. ing. Dan Frunză

Pregătire format electronic on-line: Gabriela Groza

ISBN 978-606-737-766-8

LABORATORY
MATERIALS SCIENCE ENGINEERING
Metallography and Microstructures

Materials Science and Engineering Department
Faculty of Materials Science and Environmental Engineering

"Materials science is to engineering as anatomy is to medicine; without a deep understanding of the structure, behavior, and properties, one cannot truly comprehend the performance and possibilities".

Chat GPT

Dr.eng. IWE Bodea Marius

PREFACE

This laboratory support is primarily intended for the first-year students pursuing specializations in the fields of Materials Engineering, Environmental Engineering, Industrial Engineering, Mechanical Engineering, and Economic Engineering in English language. The book can also be a useful resource for students enrolled in Romanian programs, but which aim to improve their communication skills in the English language.

The works presented throughout the book address essential aspects for the characterization of materials, highly useful in understanding the behavior of materials in various industrial applications or in understanding the causes that led to the failure's occurrence. The information and experimental techniques presented for conducting quantitative metallographic determinations will assist students in better understanding how the microstructural characteristics of materials are reflected in their properties.

Moreover, through the case studies presented, the students will be able to broaden their knowledge in the realm of materials, their characterization methods, as well as the risks and potential for causing failures with extremely serious consequences. Modern graphic and text editing tools, such as ChatGPT were employed in the preparation of the works (ChatGPT is a conversational artificial intelligence language model developed by OpenAI).

To facilitate the transfer of information to students, the book contains 272 hyperlinks that enable navigation to various sections of the course, video materials, technical expertise, EN, ISO, and ASTM standards, diverse case studies, and web pages with educational resources from professional organizations or companies such as Buehler, Nikon, Struers, Olympus, Zeiss, Leica, etc.

The bibliography includes 50 carefully selected references of the highest quality and updated to the year 2024. To reduce the volume of the work, some information can be explored during individual study, a [more info] link being introduced in the text and providing the web address for the respective content. These hyperlinks have not been included in the bibliography, because some of these addresses undergo changes and may not necessarily have a permanent character.

With the hope that the course support will be a reliable companion in your journey into the materials universe, the author wishes you much success in your future career.

> *"Materials are the foundation of our civilization, whether they be the bricks and steel of our buildings or the semiconductors in our electronics." - Mildred Dresselhaus*

Cluj-Napoca *Dr.eng.IWE Bodea Marius*

January 2024

1. Introduction in Metallography

1.1.Theoretical background

Materials characterization is a crucial aspect of materials science and engineering, playing a vital role in understanding, designing, and optimizing materials for various applications. Understanding and tailoring materials based on their properties are fundamental for successful exploitation in diverse industries (e.g. automotive, aeronautics, shipbuilding, oil-gas, energy, nuclear, etc.)

The specific requirements of each application guide the selection and design of materials to ensure optimal performance and reliability. The exploitation or application of materials often requires careful consideration of their mechanical, thermal, electrical, and chemical properties used in the materials selection process.

Selecting materials with consideration for safety and performance indicators is critical in various industries. The goal is to choose materials that not only meet the functional requirements of a given application, but also ensure the safety and performance of the product, process, or structure. A comprehensive approach that balances technical requirements, regulatory compliance, and sustainability goals is key to successful materials selection.

Materials characterization involves various techniques to analyze and understand the properties, structure, and composition of materials. The choice of characterization method depends on the specific properties of interest and the nature of the material being studied. The materials characterization processes are performed through the following techniques:

- Optical Microscopy
- Scanning Electron Microscopy (SEM)
- Transmission Electron Microscopy (TEM)
- X-ray Diffraction (XRD)
- Fourier Transform Infrared Spectroscopy (FTIR)
- Raman Spectroscopy
- Nuclear Magnetic Resonance (NMR)
- Atomic Force Microscopy (AFM)
- Differential Scanning Calorimetry (DSC)
- Thermogravimetric Analysis (TGA)
- Mechanical Testing
- Electron Paramagnetic Resonance (EPR) Spectroscopy.

These techniques are enabling materials scientists and engineers to gain insights into the materials properties and behavior across different scales. The choice of characterization method depends on the specific goals of the analysis and the nature of the material being studied. In this volume we will focus only on optical microscopy techniques, for a large range of materials used in different industries.

Metallography is a branch of materials science that involves the study of the physical structure and components of metals and alloys, typically at the microscopic and macroscopic levels. Metallography employs various techniques to prepare, examine, and analyze the microstructure of metallic materials.

The main benefits of the metallography analysis are:

- **Understanding Material Properties**. Metallography allows specialists to study the microstructure of metals, revealing information about grain size, phases present, and the distribution of different constituents. This, in turn, provides insights into the material's mechanical, thermal, and chemical properties.

- **Quality Control.** In manufacturing processes, metallography helps assess the quality of metal components by examining factors like grain structure, inclusions, and the presence of defects. This ensures that the material meets specified standards and that manufacturing processes are consistent.
- **Research and Development.** Researchers use metallography to investigate new alloy compositions or processing methods. By analyzing the microstructure, they can understand how changes at the atomic and microscopic levels impact the material's properties.
- **Performance Optimization.** Metallography aids in optimizing the performance of metals by studying factors such as heat treatment effects, phase transformations, and the relationship between microstructure and mechanical properties.
- **Failure Analysis.** When metal components fail, metallography is a valuable tool for identifying the root causes. It helps determine whether failures are due to factors like fatigue, corrosion, or manufacturing defects, enabling engineers to address these issues in subsequent designs.
- **Tailoring Properties for Specific Applications.** Different applications demand specific material properties. Metallography allows specialists to tailor the microstructure of metals through techniques like alloying or heat treatment, ensuring that materials meet the requirements of specific industries.
- **Advancements in Nanotechnology.** Metallography has evolved to explore the nanoscale structure of metals using advanced microscopy techniques. This is essential for understanding the behavior of materials at the nanoscale, especially in the development of nanomaterials and nanocomposites.
- **Environmental Impact.** Metallography can contribute to assessing the environmental impact of metal processing methods. By studying microstructure, specialists can identify ways to optimize processes for sustainability, reduce waste, and enhance the recyclability of metals.
- **Innovation in Emerging Technologies.** Metallography plays a crucial role in the development of new materials for emerging technologies. For example, it is vital in understanding the microstructure of advanced alloys used in aerospace, high-performance materials, and other cutting-edge applications.
- **Regulatory Compliance.** Metallography is used to ensure that metals and alloys comply with industry and regulatory standards. By examining the microstructure, specialists can verify that materials meet specific requirements for strength, corrosion resistance, and other critical properties.

Fig.1 Examples of catastrophic structural failures: Rena, Stellar Daisy and Alexander L. Kielland platform [1].

Metallography is a powerful technique in materials characterization, offering detailed insights into the microstructure of metals and alloys. This information is foundational for addressing a wide range of concerns, from quality control to performance optimization and the development of innovative materials for diverse applications. It facilitates innovation, quality control, and the advancement of technology, making it an indispensable tool for specialists in the field.

Also, metallography plays a crucial role in failure analysis and material expertise by providing detailed insights into the microstructure of materials. The technique involves the preparation of metal specimens for microscopic examination, allowing experts to observe and analyze the material's internal features.

Based on advanced metallographic analysis we can:

- **Identify the Failure Mechanisms.** Metallography allows experts to examine the microstructure of failed components. This includes features such as grain size, inclusions, phase distribution, and any abnormalities that might contribute to the failure. Microscopic observations correlate with macroscopic features of the failed component, identifying the primary failure mechanisms, such as fatigue, corrosion, overheating or manufacturing defects.
- **Detection of Defects and Anomalies.** Metallography can reveal grain boundary characteristics, including grain boundary cracks or other anomalies. This is crucial for understanding how defects propagate and contribute to failure.
- **Inclusion Analysis.** Examination of inclusions in the material provides information about the cleanliness of the material and the potential role of inclusions in initiating or propagating cracks or in corrosion attacks.
- **Stress Analysis.** Metallography can reveal the residual stresses in materials. Residual stresses can be a factor in failure, but also in corrosion mechanisms (e.g. strees corrosion cracking).
- **Heat Treatment Assessment.** Metallography helps in assessing the effectiveness of heat treatment processes. This is critical in determining whether the material was heat-treated correctly and if deviations from the specified process contributed to the failure or to insuficient mechanical strength.
- **Phase Transformation Analysis:** Metallography allows the identification of different phases in the material, providing information on the material's heat treatment history and its impact on properties.
- **Corrosion Analysis.** Metallography is used to examine corrosion products and determine the extent of corrosion attack. This information is valuable in understanding the corrosion mechanism and the material's susceptibility to corrosion (e.g. in identifying localized corrosion features, such as pitting or crevice corrosion, which may contribute to the failure).
- **Microstructural Changes.** Metallography can detect changes in the material's microstructure due to environmental exposure, temperature, wear, or other factors. This is crucial in understanding how the material's properties may have evolved over time (e.g. in creep – long term exposure to pressure and high service temperatures).
- **Material Expertise.** Metallography is used to verify the material composition and quality. This is important in cases where the material specifications are critical for performance and safety.
- **Forensic Analysis.** Metallography can be employed in forensic investigations to reconstruct events leading to failure and provide expert testimony in legal proceedings.
- **Documentation and Reporting.** Based on metallographic observations, experts can provide recommendations for corrective actions, design improvements, or changes in material selection to prevent future failures or to gain new performances.

1.2. Working procedure

The microstructure of a material can only be viewed in a light microscope only after a specimen has been properly prepared. The main steps of specimen preparation for light microscopy include the following steps:

- Sectioning
- Mounting
- Grinding
- Polishing
- Etching**.**

Almost always, the component of interest is too big for a direct observation/analysis. First, we need to cut a small amount of the material from the area of interest (e.g. near the fractured surface, or the heat-treated surfaces, near welds, corrosion attacks, deformed zones etc.).

Sectioning serves two purposes:

- Generating a cross section of the specimen to be examined.
- Reducing the size of a specimen to be placed on a stage of a light microscope or reducing the size of a specimen to be embedded in mounting media for further preparation processes.

Fig.2 Equipment for abrasive cutting with abrasive blades/discs [2].

Abrasive cutting is the most common method of sectioning to achieve a clean and efficient cut. Abrasive blades are designed to provide high quality sectioning results with no burning and minimal surface deformation. The main methods of sectioning are through:

- Abrasive cutting,
- Electric discharge machining.

During the cutting operation it should be avoided the plastic deformation of the material, the overheating phenomena (material burning during cutting) and to prevent cracking or excessive surface damaging. In the case of composite materials or for very heterogeneous phases it should be prevented the delamination phenomena or the damaging of secondary phases (e.g. graphite flakes, nodules, grain or particles/fibers pull-out). Proper clamping or sample fixturing is required to prevent blade breakage and to optimize the cut.

The selection of the abrasive blade is based on the sample material properties (hardness). Cutting hard materials require a softer bond of the abrasive grains.

Used corundum grains can be detached more easily to expose new sharp grains. For softer materials, cut-off wheels are used in which the abrasive grains are enclosed in a hard bond. Resin-bonded corundum cut-off wheels (Al_2O_3) are ideally suited for metallographic specimen removal. The separated surfaces should result smooth, low in deformation and free of tarnish. More information about the selection of the abrasive blades and coolants can be read on [3, 4], Table 1.

a) b)

Fig. 3 a) Abrasive Cut-off Wheels Ø300x2,0x32 for cutting materials up to 65 HRC; b) Diamond Cut-Off Wheel Ø75 x 0,2 x 12,7 mm, metal bond for cutting of sintered carbides and brittle materials [3,4].

Table 1. Abrasive blades selection for cutting materials.

Sample Material	Abrasive
Ferrous metals	Al_2O_3
Non-ferrous metals	SiC
Very hard ferrous metals	Cubic Boron Nitride (CBN)
Very hard materials with low metal content	Diamond
Sintered carbides	Diamond
Hard ceramics	Diamond
Composites	Diamond

Mounting refers to embedding specimens commonly in thermosetting polymers, to allow them for further processing. Mounting is not necessary for bulky specimens, but it is required for specimens that are too small or oddly shaped to be handled, or when the edge of a specimen needs to be examined in transverse section, Fig. 4.

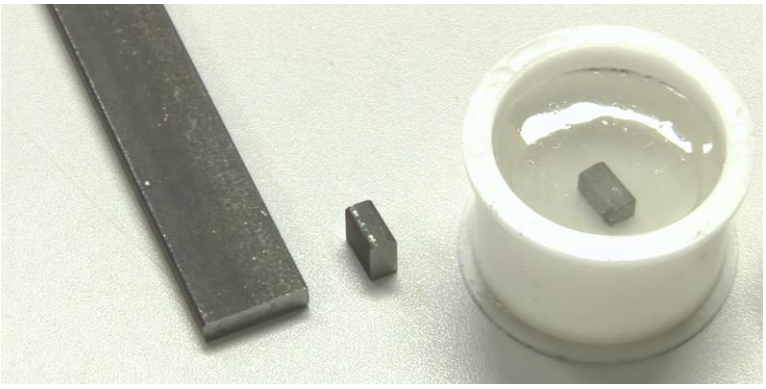

Fig. 4 Metallic specimen mounted in transparent resin [video].

In hot mounting process, the specimen is mounted in a mounting press under temperature and pressure with a plastic granulate, Fig.5. Advantages of the process are the high hardness of the mounting material (e.g. glass fiber reinforced) and the good gap-free properties of the mounting material.

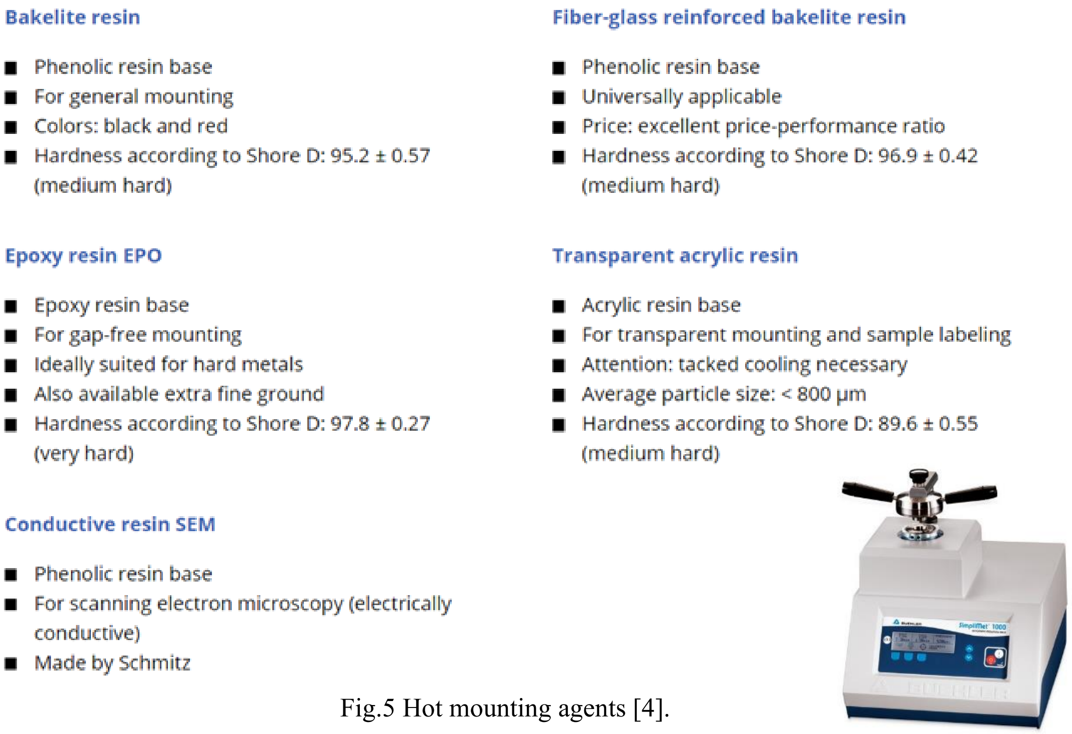

Bakelite resin

- Phenolic resin base
- For general mounting
- Colors: black and red
- Hardness according to Shore D: 95.2 ± 0.57 (medium hard)

Fiber-glass reinforced bakelite resin

- Phenolic resin base
- Universally applicable
- Price: excellent price-performance ratio
- Hardness according to Shore D: 96.9 ± 0.42 (medium hard)

Epoxy resin EPO

- Epoxy resin base
- For gap-free mounting
- Ideally suited for hard metals
- Also available extra fine ground
- Hardness according to Shore D: 97.8 ± 0.27 (very hard)

Transparent acrylic resin

- Acrylic resin base
- For transparent mounting and sample labeling
- Attention: tacked cooling necessary
- Average particle size: < 800 µm
- Hardness according to Shore D: 89.6 ± 0.55 (medium hard)

Conductive resin SEM

- Phenolic resin base
- For scanning electron microscopy (electrically conductive)
- Made by Schmitz

Fig.5 Hot mounting agents [4].

In case of cold mounting, two components are required. Both are mixed in a mixing cup according to the mixing ratio. After stirring, the mixture is poured into the mounting cup. Curing takes place via a chemical reaction (polymerization or polyaddition). Polymerization is an exothermic reaction and depending on the specimen mass, temperatures of up to 90 °C can be reached for a short time.

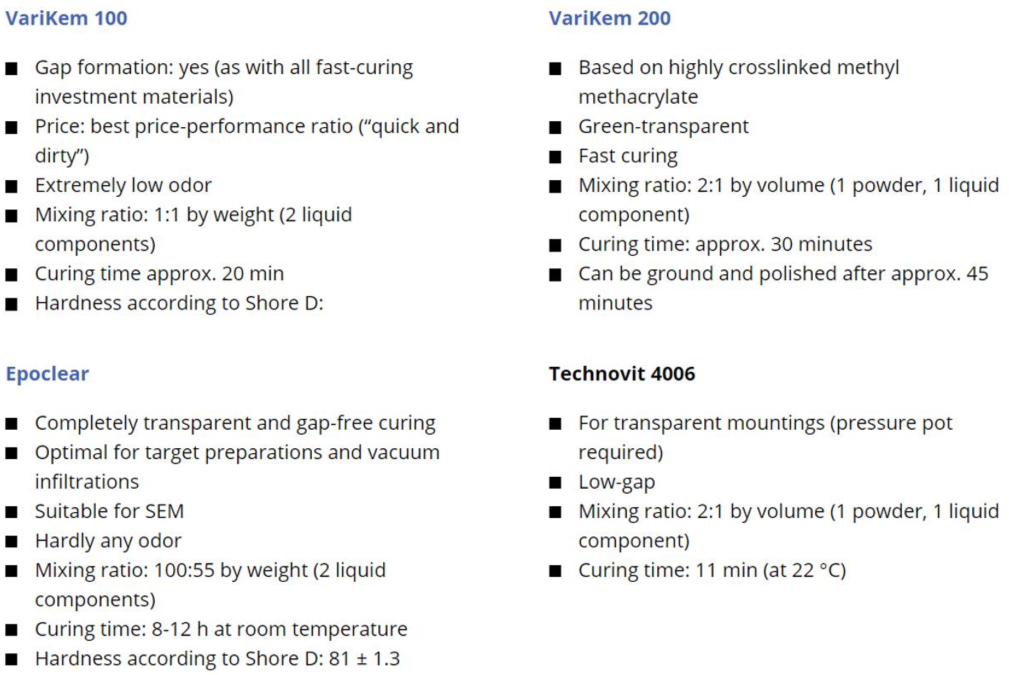

VariKem 100

- Gap formation: yes (as with all fast-curing investment materials)
- Price: best price-performance ratio ("quick and dirty")
- Extremely low odor
- Mixing ratio: 1:1 by weight (2 liquid components)
- Curing time approx. 20 min
- Hardness according to Shore D:

VariKem 200

- Based on highly crosslinked methyl methacrylate
- Green-transparent
- Fast curing
- Mixing ratio: 2:1 by volume (1 powder, 1 liquid component)
- Curing time: approx. 30 minutes
- Can be ground and polished after approx. 45 minutes

Epoclear

- Completely transparent and gap-free curing
- Optimal for target preparations and vacuum infiltrations
- Suitable for SEM
- Hardly any odor
- Mixing ratio: 100:55 by weight (2 liquid components)
- Curing time: 8-12 h at room temperature
- Hardness according to Shore D: 81 ± 1.3

Technovit 4006

- For transparent mountings (pressure pot required)
- Low-gap
- Mixing ratio: 2:1 by volume (1 powder, 1 liquid component)
- Curing time: 11 min (at 22 °C)

Fig.6 Cold mounting agents [4].

Basically, there are two types of cold-mounting resins available: epoxy and acrylic resins [6]. A short review of the cold mounting agents is given in Fig.6.

Grinding refers to flattening the surface to be examined and removing any damage caused by sectioning. The specimen surface to be examined is abraded using a graded sequence of abrasives, starting with a coarse grit. Commonly, abrasives (such as silicon carbide) are bonded to abrasive paper. Abrasive paper is graded according to particle size of abrasives such as 80, 120, 220, 320, 500, 800, 1000, 1200, 2000, 2400 and 4000 grit paper, Fig.7 [7].

Fig.7 Silicon carbide foils and papers, grinding machines [7].

Supplying running water during grinding is essential to cool specimen surfaces and to remove material and particles debris from the SiC papers/foils. Grinding produces surface traces that must be minimized by subsequent grinding with finer abrasives.

Specimens are rinsed with running water to remove surface debris and then are rotated 90° from the previous orientation. Rotation ensures that grinding traces generated by a coarse grit is completely removed by a subsequent finer grit.

Nowadays on the market are available diamond grinding discs that have a prolonged service life and assure maximum stock removal rate [4,7]. They have a wear-optimized coating geometry with wear indicator and a self-sharpening feature, Fig.8 and Fig.9.

Fig.8 Diamond grinding disc for advanced grinding operation of varied materials [4].

ADAMANT (Diamond grinding disc)

- Resin bond
- Very high coating thicknesses, stock removal rates and service life
- Self-sharpening
- With wear indicator
- Grit sizes: P80 to P1200
- Diameter: 250 and 300 mm

DSS (Diamond grinding disc)

- Nickel or synthetic resin bond
- Very high surface quality and edge sharpness
- Nickel: High stock removal rate with long tool life
- Synthetic resin: For fine grinding
- Grit sizes: P80 to P1000 (nickel bond)
- Grit sizes: P400 to P2500 (resin bonded)
- Diameter: 200, 250 and 300 mm

IDAMANT (Diamond grinding and polishing disc)

- Resin bond
- High stock removal rates, flatness and service life
- Grit sizes: 15 to 3 µm
- Diameter: 250 and 300 mm

DPS (Diamond plane grinding disc)

- Nickel bond
- For hard and brittle materials
- Self-adhesive or on carrier plate
- Grit sizes: P60 to P1000
- Diameter: 200, 250 and 300 mm

Fig.9 Diamond grinding discs features [4].

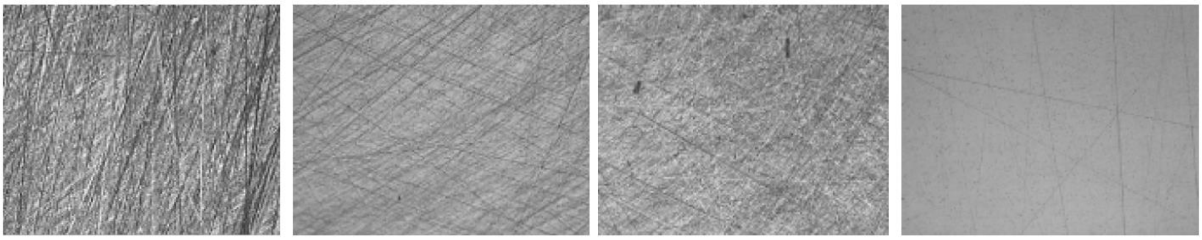

240 grit surface roughness 400 grit surface roughness 600 grit surface roughness 1200 grit surface roughness

Table 2. Surface roughness R_a [µm] vs. grit size of SiC paper [data source].

FEPA paper	P80	P120	P220	P320	P500	P800	P1000	P1200	P2000
R_a [µm]	185	129	69	44.5 ±2	29.2 ±1.5	22.8 ±1.5	17.3 ±1	12.8 ±1	9.3 ±1

Fig.10 Specimen surface roughness after grinding with SiC paper.

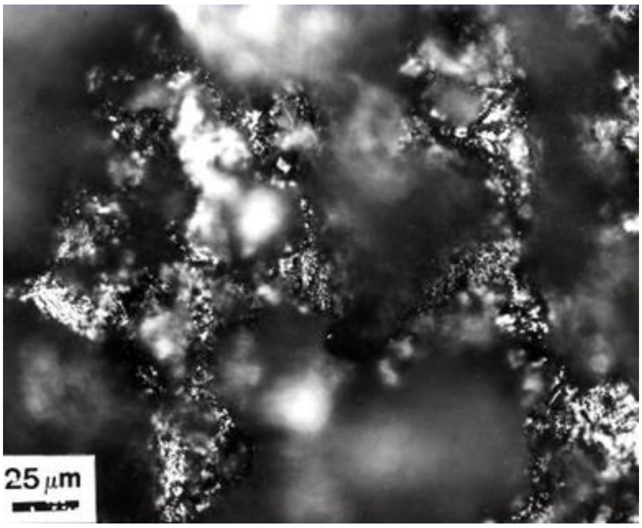

Polishing is the last step in producing a flat, scratch-free surface. After being ground to a 1000 grit finish, the specimen should be further polished to remove all visible scratches remaining from grinding. A correct polishing generates a mirror-like finish on the specimen surface to be examined. The flatness of the prepared surface is critical to image quality. Small deviations from planarity could lead to blurring effects at higher magnifications, Fig. 11.

Fig.11 Blurred image of a fracture surface due to limited depth of field in optical microscopy [8].

Abrasives for polishing are usually diamond paste, alumina, or other metal-oxide slurries. Polishing includes coarse and fine polishing. Coarse polishing uses abrasives with a grit size in the range from 3 to 30 μm; 6 μm diamond paste is the most popular. The abrasive size for fine polishing is usually less than 1 μm. Alumina slurries provide a wide range of abrasive size, ranging down to 0.05 μm.

It is important to remember that by pushing the specimen too hard against the polishing wheel, a plastic deformation of the grains can be produced in the top layer of the polished surface, especially in the case of ductile materials, Fig. 12.

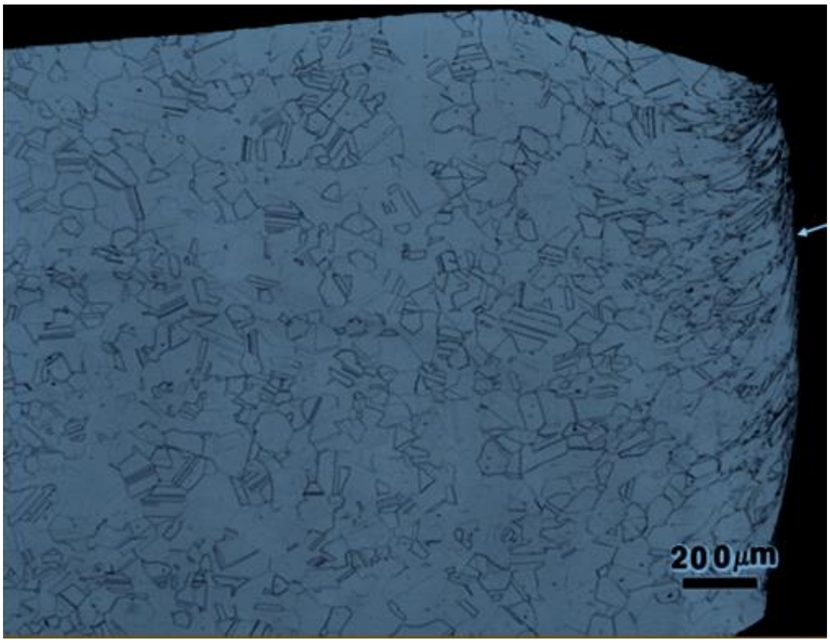

Fig.12 Grain plastic deformations in the top layers of polished specimens [8].

Etching is a controlled corrosion process by electrolytic action between specimen surface areas with differences in electrochemical potential. Thus, etching is used to highlight microstructural features or different phases present in alloys [read more].

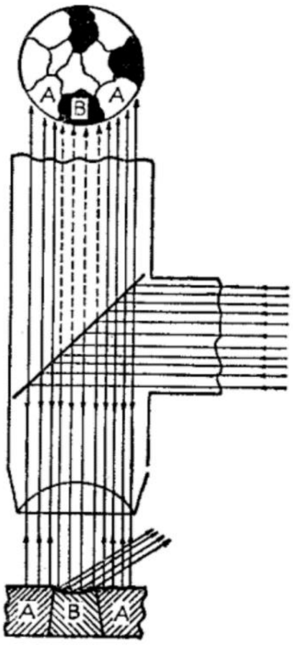

Grain boundaries in polycrystalline materials are more severely attacked by etchant, and thus are revealed by light microscopy because they reflect light differently. Grains are etched at different rates because of differences in grain orientation and some crystallographic planes are more subject to etching. Thus, the grains appear in the ocular field with different brightness and contrast.

Etching a specimen that has a multiphase microstructure will result in selective dissolution of the phases, Fig. 13. The changes in the rate of chemical attack produce deviations both in angle and depth of incident light. Thus the light is reflected in varying amounts depending on the angle and depressions of the portion of the surfaces resulting in light and dark regions. Thus, the crystalline microstructure of the specimens is revealed.

Fig.13 Schematic representation of the reflected light path on the specimen surface, according to the surface micro-morphology.

Many chemical etchants are mixtures of acids with a solvent such as water or alcohol. For etching more noble materials, etchants must contain oxidizers, such as nitric acid, chromic acid, iron chloride, and peroxides, Table 3. More etchant recipes for a variety of metals and alloys can be found at [9, 23].

Table 3. Examples of chemical etchants used for steels [more info].

Chemical composition	**Etchant name**
1-10 ml HNO_3, 90-99 ml methanol or ethanol	**Nital**. This is the most used solution for the etching of iron, low alloyed steels and cast iron. It reveals the ferrite grain boundaries and phases within the specimen microstructure.
4 gr picric acid, 100 ml ethanol	**Pikral**. It is recommended to be used for samples having ferrites and cementite phase. This reactive do not demonstrate ferrite’s grain boundaries.
1-4 gr $K_3Fe(CN)_6$, 10 gr KOH, 100 ml water	It has to be used freshly. The Cementite phases are seen as black and the perlite phases are noticed as brown.
100 ml ethanol, 5 ml HCl, 1 gr picric acid	**Vilella**. It is used for samples having ferrite and carbide structures. It gives information about the austenite grain size and notices the phases present in the stainless steel.
30 ml water, 25 ml ethanol, 40 ml HCl, 5 gr $CuCl_2$	**Fry**. It is used to demonstrate the defects in the steel resulted from the cold deformation process.
15 ml HCl, 20 ml water, 1 gr $CuCl_2$, 5 gr picric acid, 135 ml ethanol	**Noren**. It is used to show the cracks formed in the region affected by the welding process.
10 gr oxalic acid, 100 ml water	**Electrolytic etching reactive** used for steels. The distance between the cathode and the anode material is kept as 25 mm, the applied voltage is set to 6V. The carbides are revealed in 15-30 seconds, and the grain boundaries become visible in 45-60 seconds.

Many of the etching solutions represent **safety hazard**, all cyanides are extremely toxic. Fluorine compounds are extremely dangerous as they attack nerve tissue, yet do not show an immediate "burn" reaction like most acids. Chlorine gas and silanes are irritants on exposed skin, unbreathable, with attack of mucous membranes. Alkalies are most dangerous when being used hot and the strong acids give immediate skin burns [9].

1.3.Discussion and results interpretation

All the next chapters include case studies and some microstructures of the main alloys used in industry. The case studies are selected to illustrate the possible applications of metallographic analysis for the considered topic (see summary). For each set of microstructures type the students should use simple methods for quantitative analysis, e.g. grain size, phases distribution, particles size etc.

The discussion will be focused on the correlation between the identified phases and microstructural constituents and the mechanical characteristics of the material subjected to analysis. The quantitative analysis results will be analyzed from the material behavior in exploitation perspective. Coupled with the presented case studies, each set of microstructures will reveal the importance and applications of such analysis. Video recommended material is presented for each practical work and also supplementary references are given for further individual study.

2. Metallographic microscopes

2.1.Theoretical background

Henry Clifton Sorby is the inventor of the metallurgical microscope in 1863, and the founder of modern metallography [10]. As early as 1841, the Russian Ансов studied the patterns on the steel swords under the magnifying glass, and by 1863 the British (H.C. Sorby) transplanted the petrographic methods including sample preparation, polishing and etching, into the research of iron and steel, developing the metallographic technology.

A metallurgical microscope is used to analyze/view opaque objects, like metals, plastics, ceramics, composites or rocks. Basically, a metallurgical microscope is made up of an illumination and optical system. According to their design, the metallographic microscopes present two types:

- Upright Microscopes – most frequently used type, where the objective lens is above the specimen, Fig.14.
- Inverted Microscopes – used for larger specimens, where the objectives are located under the specimen, Fig.15.

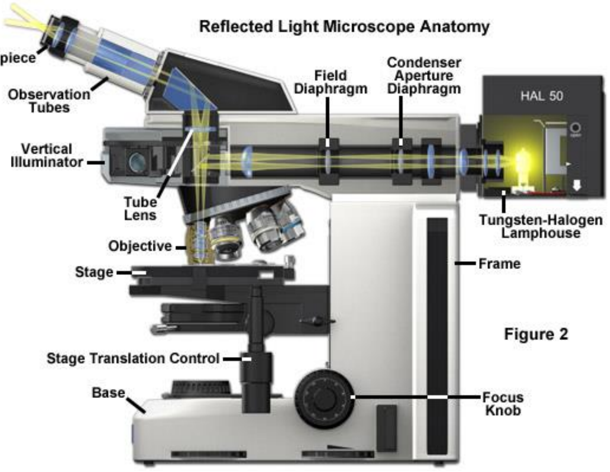

Fig.14 Upright microscope

Fig.15 Inverted microscope

According to their application, there are several types of microscopes and each of them solves unique problems:

- Stereo microscope (Fig. 16)
- Compound or biological microscope (Fig. 17)
- Metallurgical microscope
- Polarizing microscope

Fig.16 Stereo microscope

Fig.17 Biological microscope

Fig.18 Polarizing microscope

Stereo microscopes provide a 3D image or "stereo" image and typically will provide magnification between 10x - 40x. The stereo microscope is used in manufacturing, quality control, coin collecting, science high school projects, and botany. A stereo microscope typically provides both transmitted and reflected illumination and can be used to view a sample that will not allow light to pass through it.

The compound or biological microscope can be used to view biological samples (blood cells, cheek cells, parasites, bacteria, algae, tissue, and thin sections of organs). The magnification of a compound microscope is most commonly 40x, 100x, 400x, and sometimes 1000x. In the later half of the 20th century in the attempts to achieve improved image resolution in biological samples analysis, fluorescence microscopy or widefield fluorescence microscopy has been developed. In the 1990s, has been produced the first commercial confocal microscopes. The confocal microscopes use high intensity lasers and sensitive electronic detectors, that allows to obtain a z-series images, providing a three-dimensional view of the tissue samples or cells being examined.

Metallurgical microscopes have several unique features that are not always found on a biological or stereo microscope, like:

- Polarizer & Analyzer
- Aperture Diaphragm & Field Diaphragm
- Differential Interference Contrast (DIC)
- High Magnification & High-Resolution objectives
- Brightfield & Darkfield imaging
- Reflected & Transmitted illumination.

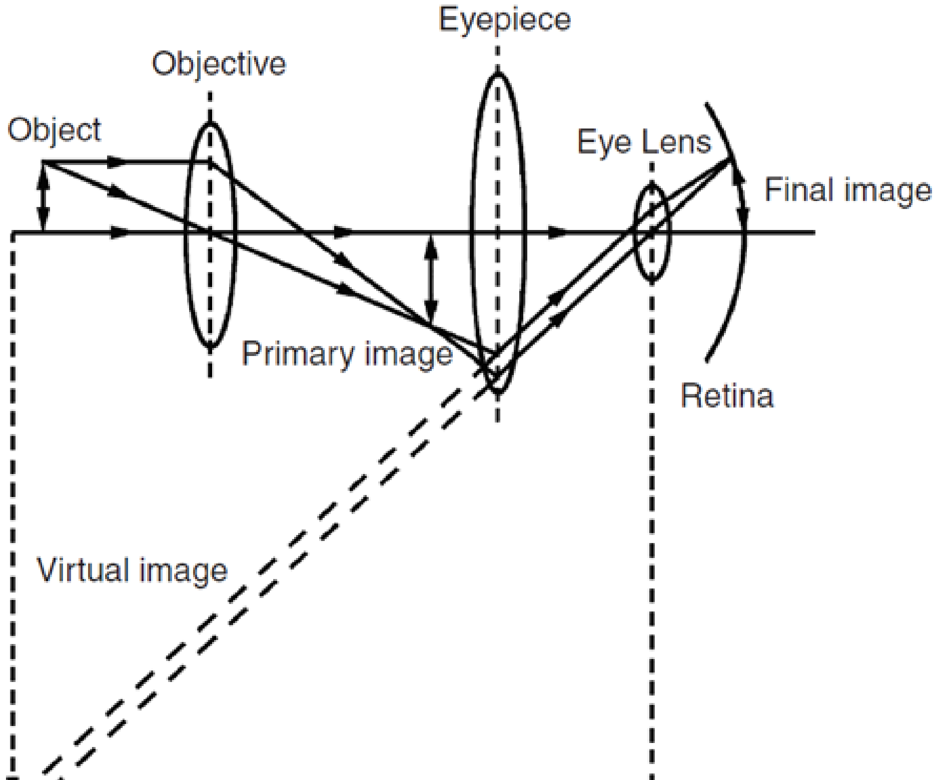

Fig.19 Schematic path of light in a microscope. Virtual image of a magnified object.

The grain size of metallic alloys and others microstructural constituents are in the micron range size, so it is obvious that in order to analyze them we need usually to magnify the area of interest up to several hundred times. Magnification in microscopy refers to the process of enlarging an object's apparent size when viewed through a microscope. Magnification is a crucial aspect of microscopy because it enables scientists to examine specimens at a much higher level of detail (in optical microscopy the magnification goes up to 2000x and in electronic microscopy up to 2.000.000x). The $27 million electron microscope from Lawrence Berkeley National Lab is able to make images to a resolution half the width of a hydrogen atom, that made it the most powerful microscope in the world [11].

The magnification achieved in optical microscopy is produced by a combination of lenses. There are typically two sets of lenses in a microscope, Fig. 20 and Fig. 21:

1. **Objective Lens**. The objective lens is the primary lens closest to the specimen being observed. It collects light rays coming from the specimen and forms an enlarged, real, and inverted image of the specimen. The objective lenses could provide different magnification levels (e.g., 4x, 10x, 40x, 100x).
2. **Ocular Lens** (Eyepiece). The ocular lens is the lens closest to the viewer's eye. It further magnifies the image produced by the objective lens.

Fig. 20 Ocular lens (Eyepiece)
More info about eyepieces [12].

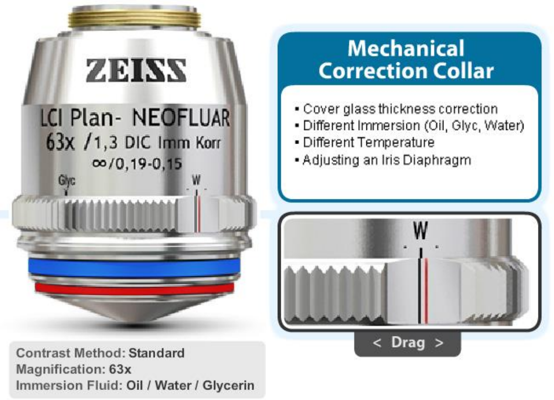

Fig. 21 Objective lens
More info about objectives lens [13, 14].

The total magnification of a microscope is calculated by multiplying the magnification of the objective lens by the magnification of the ocular lens. Mathematically, it is expressed as:

Total Magnification = **Magnification of Objective Lens** × **Magnification of Ocular Lens**

It's important to note that while higher magnification allows for more detailed observation, it comes with certain limitations. As magnification increases, the depth of field or the thickness of the specimen that remains in focus at one time decreases, and more light may be needed for a clear image. Additionally, the lateral resolution of the microscope, which is the ability to distinguish between two closely spaced objects, also plays a crucial role in obtaining detailed images at high resolution.

The resolution of a microscope is controlled by the diffraction of light phenomena. When the point object is magnified, its image is a central spot (the Airy disk) surrounded by a series of diffraction rings, not a single spot. To distinguish between two such point objects separated by a short distance, the Airy disks should not severely overlap with each other, Fig.22.

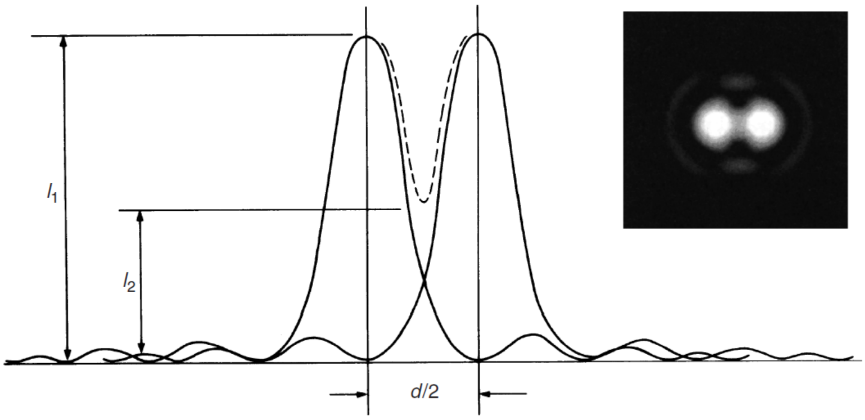

Intensity distribution of two airy disks with a distance $d/2$. I_1 indicates the maximum intensity of each point and I_2 represents the overlap intensity.

Fig. 22 Airy disc and diffraction rings in optical image.

The resolving power of an objective determines the size of the Airy diffraction pattern formed, and the radius of the central disk is determined by the combined numerical apertures of the objective and condenser. Thus, controlling the size of the Airy disk is the key to controlling resolution.

The size of the Airy disk (d) is related to the wavelength of light (λ) and the angle of light coming into the lens. The resolution of a microscope (R) is defined as the minimum distance between two Airy disks that can be distinguished.

$$R = \frac{d}{2} = \frac{0.61\lambda}{\mu \sin\alpha}$$

where μ is the refractive index of the medium between the object and objective lens and α is the half-angle of the cone of light entering the objective lens, Fig. 23.

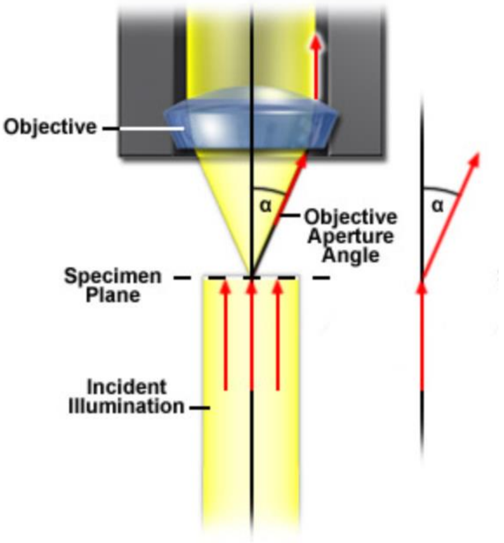

Fig. 23 Numerical aperture NA.
The product **μ·sin α**, is called the numerical aperture.

Reflected light illuminator.

Light emitted from the tungsten-halogen lamp filament first passes through the collector lens located close to the lamp housing, and then through the second lens in the light path, which are called the field lens, being responsible for bringing the image of the filament into focus at the plane of the substage condenser aperture diaphragm.

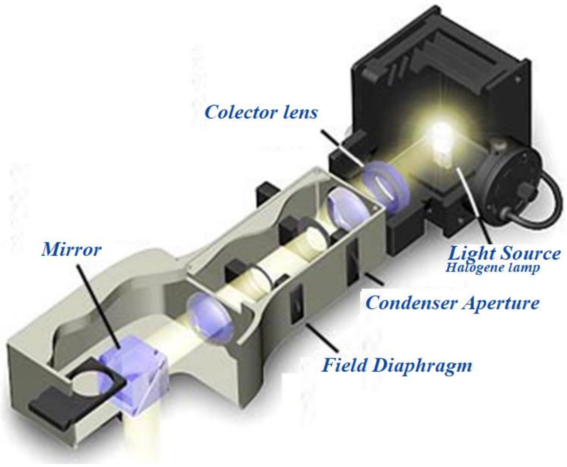

Fig. 24 Köhler illumination of a microscope [16].

As can be observed in Fig. 25, the metallurgical microscopes used the reflected light by opaque specimens, the illumination system being referred as episcopic illumination, epi-illumination, or vertical illumination, meaning that the light is originating from above. This contrasts with diascopic or transmitted illumination that passes through a specimen (case of compound or biological microscopes).

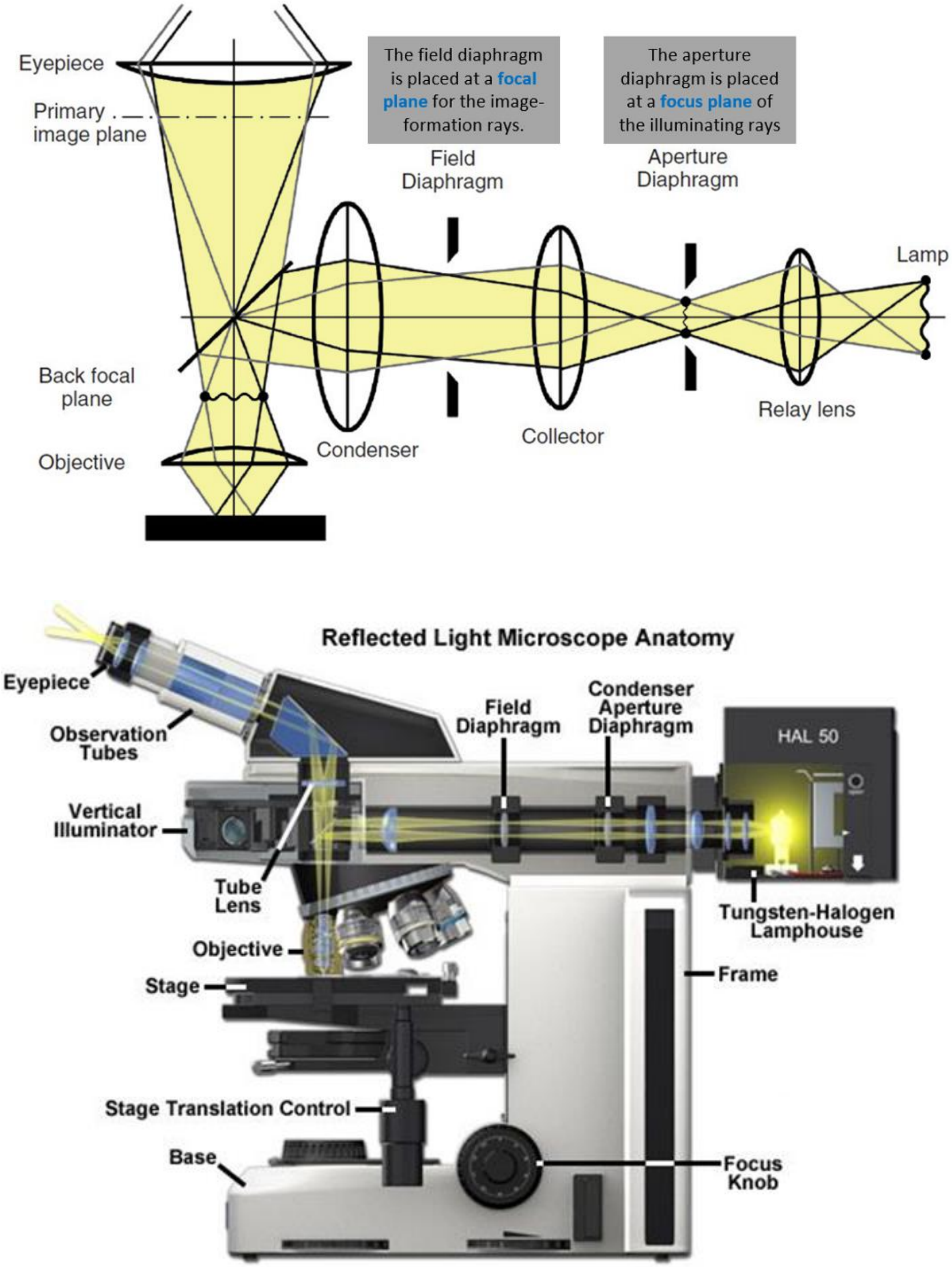

Fig. 25 The reflected light upright microscope components and the light path [15].

The Köhler system provides uniform intensity of illumination on the area of specimen. There are two important controllable diaphragms in the Kohler system: **the field diaphragm** and **the aperture diaphragm,** Fig. 24 and Fig. 25. The field diaphragm function controls the diameter of the illuminated area of the specimen, while the aperture diaphragm function controls α, and thus is affecting the image resolution and the depth of field. Köhler illumination is crucial for the correct illumination of the specimen, providing an optimum combination between contrast and resolution.

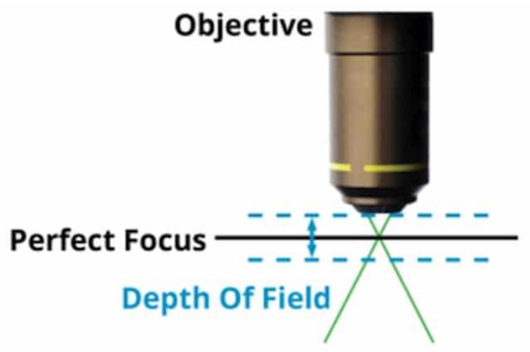

$$\text{Depth Of Field} = \pm \frac{\lambda \cdot \sqrt{n^2 - NA^2}}{2 \cdot NA^2}$$

where λ is the wavelength of the illuminating light, n is the refractive index of the medium between the specimen and the objective lens, and NA is the numerical aperture of the objective lens.

Fig. 26 Schematic representation of depth of field D [video].

The specimen metallographic analysis requires high quality image (image is clear and in focus) with an optimum contrast and high resolution. Because the depth of field is inversely proportional to the numerical aperture *NA* of the objective lens, then is directly proportional to image resolution and contrast, working distance, and is also affected by magnification.

The depth of field is defined as the distance between the nearest and farthest object planes that are both in focus at any given moment, Fig.26. Basically, the depth of field is the distance above and below the specimen surface plane, while the image remains in perfect focus.

The average depth of field at certain magnifications and apertures is:
- 3 to 5 µm at 10x objective,
- 0.5 µm at a 0.8 numerical aperture, 20x objective
- 0.1 to 0.2 µm at a 1.47 numerical aperture, 100x oil immersion objective.

The refractive index of the medium is important in optical microscopy. Air and vacuum both have an index of 1.00, water has 1.33, and immersion oil is at 1.52. Thus, the numerical aperture of the objective lens is the main factor that determines the depth of field in optical microscopy. According to magnification used for analysis, in order to achieve a clear image on microscope, the surface planarity of the specimen should vary less than depth of field for that magnification. The out-of-focus light will add blur to the image, reducing the resolution.

2.2. Working procedure

Metallographic microscopes use episcopic illumination which is often configured with specialized optics and lighting arrangements to optimize the imaging of reflective specimens. This may include the use of darkfield stops, polarizers, filters, and other accessories to control the illumination and to enhance image contrast. The choice of illumination method depends on the specific characteristics of the specimen and the information sought by the specialists. By selecting the appropriate illumination technique, researchers can optimize the visibility of microstructural features and gain deeper insights into the properties and performance of metallic materials in various applications.

The light interacts with the surface of the specimen, and the reflected or scattered light carries information about the surface morphology and features. So, bellow we present the methods of illumination that should be used according to the analysis specific:

Brightfield Illumination

Brightfield illumination is the most basic and common form of illumination in optical metallography. The light comes from the illuminator source, passes through the objective lens is reflected by the specimen surface, and the features within the sample scatter and absorb light to varying degrees, creating contrast. Brightfield illumination is suitable for general microstructural analysis.

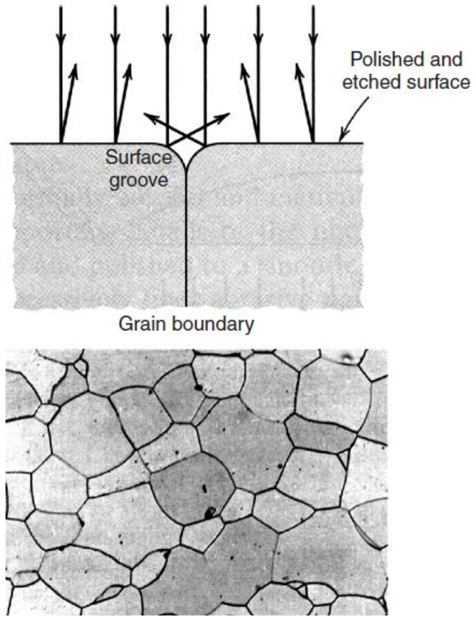

Flat surfaces produce a bright background due to reflection of a large amount of the incident light into the objective lens, while non-flat features, such as cracks, pores, etched grain boundaries or features with distinct reflectivity, such as precipitate and second phase inclusions on the surface appear darker as incident light is scattered and reflected at a variety of angles or even partially absorbed, Fig. 27.

Fig.27 Brightfield Illumination Method. The light interacts with the surface of the specimen, and the reflected or scattered light carries information about the surface morphology and features.

Darkfield Illumination

Darkfield illumination is used to enhance the contrast of light-colored or transparent features against a dark background. It is achieved by using a special condenser that prevents direct light from entering the objective lens. Only the scattered light from the sample reaches the objective, resulting in a bright image of the specimen against a dark background. Darkfield illumination is particularly useful for highlighting small particles, voids, pores, precipitates, or etched grain boundary.

Polarized Light Illumination

Polarized light microscopy involves the use of polarizers to control the orientation of light waves. This technique is useful for studying materials (metals with non-cubic crystalline structures, like magnesium and alpha-titanium) that exhibit birefringence[1], such as certain crystalline structures, revealing details related to crystal orientation and stress within the anisotropic materials.

---

[1] Birefringence is the optical property of a material having a refractive index that depends on the polarization and propagation direction of light. These optically anisotropic materials are said to be birefringent or birefractive. The birefringence is often quantified as the maximum difference between refractive indices. exhibited by the material. Crystals with non-cubic crystal structures are often birefringent, as are plastics under mechanical stress.

Differential Interference Contrast Illumination (DIC)

DIC microscopy is an advanced technique that provides three-dimensional information about the sample's surface morphology. It uses polarized light and a specialized optical system to create an interference pattern, which enhances the contrast of fine surface details. DIC is particularly useful for examining transparent or low-contrast samples, or to study features not seen otherwise in brightfield magnification, due to a difference in height as low as 0.002 µm, Fig. 28.

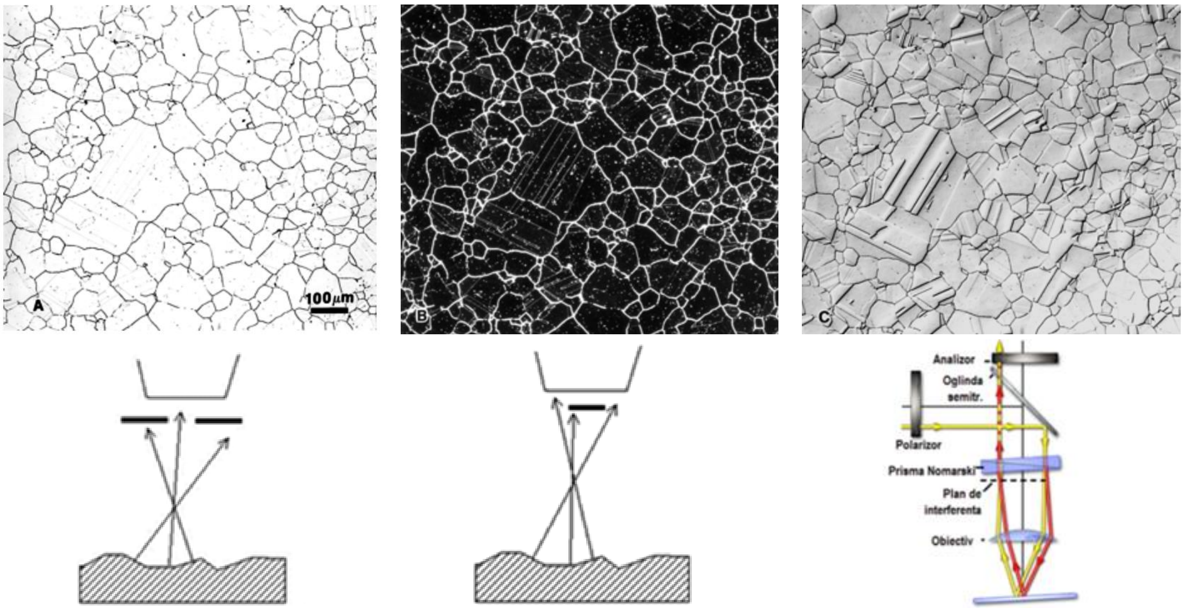

A) Brightfield illumination, 0.5 µm resolution

B) Darkfield illumination, 0.5 µm resolution

C) DIC illumination, 0.002 µm resolution

Fig.28 Comparison of illumination methods.

Oblique Illumination

Oblique illumination involves illuminating the sample at an angle, creating shadows that enhance the visibility of surface irregularities and topographical features. This technique is useful for examining surface relief and evaluating the quality of polished surfaces, Fig. 29.

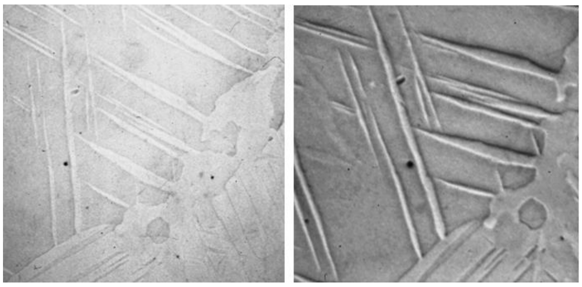

Fig.28 Examination in brightfield illumination (left) and oblique illumination (right).

Fluorescence Illumination

Fluorescence microscopy involves the use of fluorescent dyes or compounds that emit light when exposed to specific wavelengths. This technique is valuable for studying specific features or phases within a metal sample. Fluorescence can be used to highlight certain elements or structures, providing additional information about the composition and distribution of different components in the material.

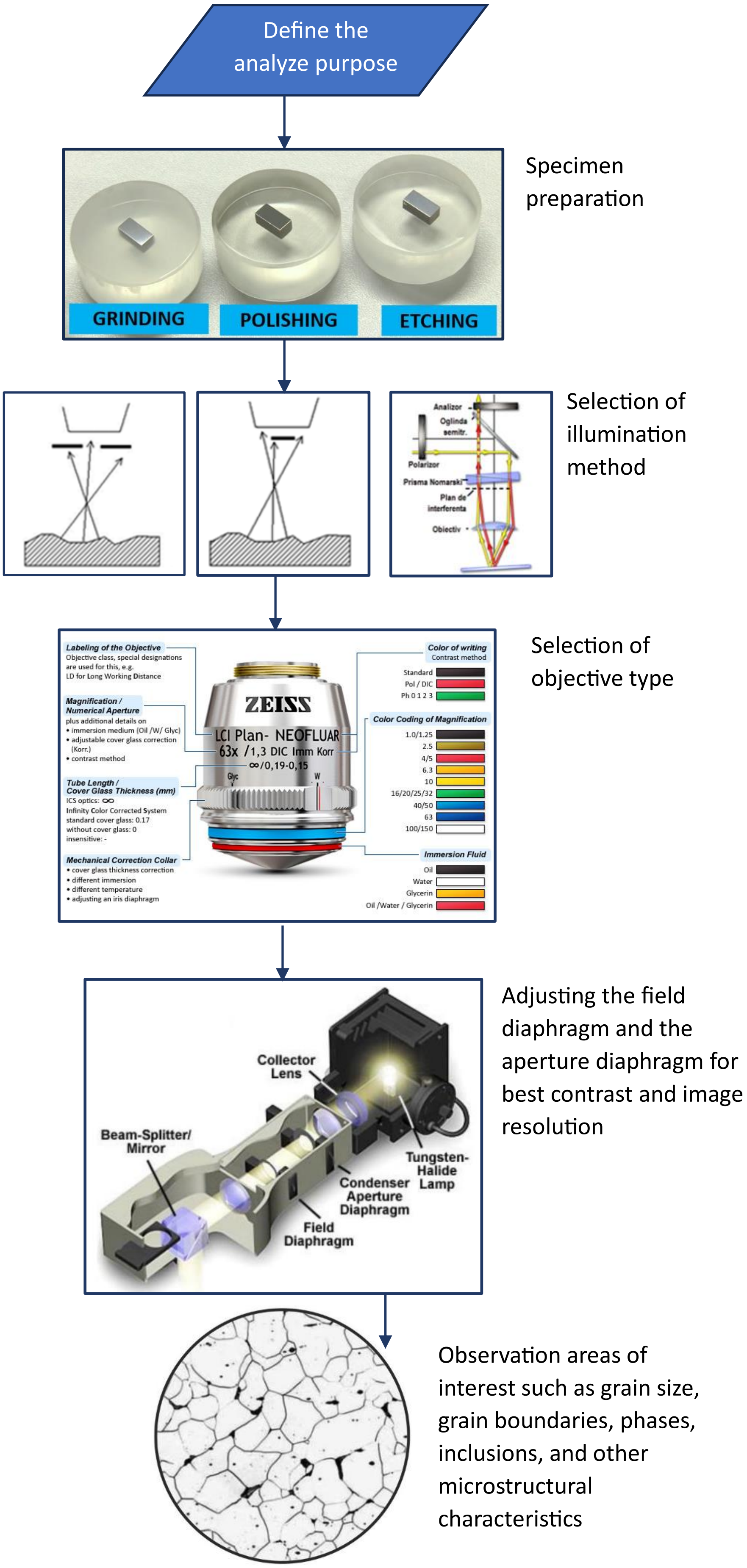

Fig. 29 The working procedure in metallographic analysis.

2.3.Discussion and results interpretation

The students should be able to identify the microscope components on to the microscopes available in the laboratory. The discussions will be focused on the possible applications of the metallographic analyses conducted in the laboratory class (quality control, failure analysis, study of the surface topography, grain structure, and defects of metallic materials, welded samples analysis etc.).

In the field of metallography, the integration of cameras and digital tools has revolutionized the way researchers and engineers analyze the microstructures of metallic materials. Cameras, coupled with advanced imaging software, offer enhanced capabilities for documentation, analysis, and sharing of microscopic details. This technological synergy not only improves the efficiency of metallographic studies but also enables precise quantitative analysis.

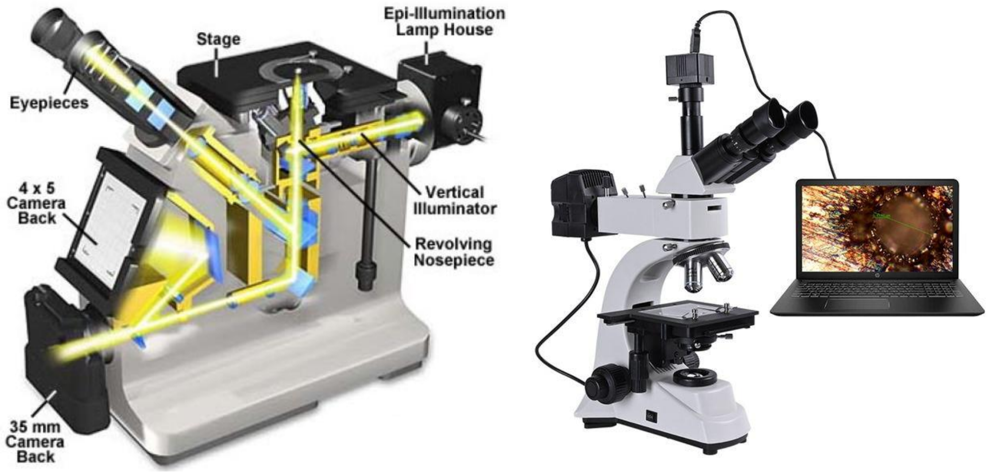

Fig. 30 Inverted reflected light microscope (left) and Trinocular HD Metallographic Microscope (right).

From capturing high-resolution images of microstructural features to employing digital tools for image processing, the integration of cameras and digital technologies has become indispensable in the pursuit of deeper insights into the composition and behavior of metallic materials. This introduction explores the pivotal role that cameras and digital tools play in modern metallography, facilitating a more comprehensive understanding of materials' microstructures and contributing to advancements in metallurgical science and engineering.

In Fig. 30 is presented an inverted metallographic microscope and a trinocular microscope equipped with a digital camera that allows the view in real time the image captured on microscope. Other essential features in a metallurgical microscope are mechanical stages, digital display, fine focus, image analysis processing software, and computer interfaces.

3. Stereology principles and basic notions. Basics of quantitative analysis in metallography

3.1. Theoretical background

Stereology is a branch of science that involves the systematic and quantitative study of the three-dimensional structure of objects based on their two-dimensional images. It is commonly used in materials science, metallography and in other fields such as biology, medicine and geology.

Key concepts and techniques within stereology include geometric principles, Cavalieri Principle and Deconvolution method:

- Geometric principles are used to estimate various structural features, such as volume, surface area, length, and number of objects within a three-dimensional space.
- The Cavalieri principle involves estimating volume by summing the areas of cross-sections obtained at regular intervals along the structure. This method is often applied to irregularly shaped objects.
- Deconvolution techniques are employed to make corrections of the effects of sectioning and imaging processes, allowing for more accurate estimations of three-dimensional parameters (e.g. separating crystal grains in microstructure, in particles analyses etc.).

In stereology are used several techniques, such as:

- Mean Linear Intercept. This method is used in materials science to estimate the mean distance between intercepts of a line with the interfaces of different phases in a material. It provides information about the size and distribution of particles or phases within the microstructure.

- Point Counting. One common stereological technique involves counting points or intersections of a grid or probe on two-dimensional sections of a structure. This information is then used to estimate the volume or other parameters of the three-dimensional object.

- Optical Fractionator. In the field of neuroscience, the optical fractionator is a stereological method used to estimate the number of objects (such as neurons) within a three-dimensional volume. It involves systematic sampling of sections and counting objects within a known fraction of the volume.

ASTM[2], ISO[3] and other international professional organizations develop voluntary standards that are not legally binding but are widely adopted by industries and organizations globally. **Compliance with those standards is often seen as a mark of quality and conformity to best practices**.

---

[2] **ASTM International**, formerly known as the American Society for Testing and Materials, is a globally recognized organization that develops and publishes voluntary consensus standards for a wide range of materials, products, systems, and services. ASTM standards are used by manufacturers, testing laboratories, regulatory agencies, and consumers worldwide to ensure the quality and safety of products and services. ASTM is one of the largest voluntary standards developing organizations in the world. Is a not-for-profit organization that provides standards for materials, products, systems and services. Members from more than 140 countries.

[3] **ISO (International Organization for Standardization)** is an independent, non-governmental international organization with a membership of 169 national standards bodies. The organization develops and publishes voluntary international standards that facilitate international trade, ensure the quality, safety, and efficiency of products, services, and systems, and promote innovation and interoperability.

At the European level we have more than 200.000 technical experts from industry, associations, public administrations, academia and societal organizations that are involved in the CEN[4] and CENELEC network being affiliated 34 national member countries (2022).

Based on the standards issued by these organizations we have valuable guidelines for evaluating and improving the laboratory's performance, and also there are specific standards related to quantitative analysis in metallography. These standards provide guidelines and methods for the quantitative assessment of the microstructure of metallic materials (e.g. bellow):

ASTM Standards:

- ASTM E562-19e1. Standard Test Method for Determining Volume Fraction by Systematic Manual Point Count. This standard provides procedures for determining the volume fraction of constituents in metals using a systematic manual point count method.

- ASTM E1245-03R23. Standard Practice for Determining the Inclusion or Second-Phase Constituent Content of Metals by Automatic Image Analysis. This practice covers the use of automatic image analysis equipment to statistically measure the volume fraction of an inclusion or second-phase constituent based on point counting.

- ASTM E1382-97-R23. Standard Test Methods for Determining Average Grain Size Using Semiautomatic and Automatic Image Analysis. These test methods cover the measurement of average grain size using semiautomatic and automatic image analysis.

- ASTM E112-13-R21. Standard Test Methods for Determining Average Grain Size. These test methods cover procedures for estimating and rules for expressing the average grain size of all metals consisting entirely, or principally, of a single phase. The grain size of specimens with two phases, or a phase and a constituent, can be measured using a combination of two methods, a measurement of the volume fraction of the phase and an intercept or planimetric count.

- ASTM E2567-16AR(23). Standard Test Method for Determining Nodularity and Nodule Count In Ductile Iron Using Image Analysis.

- ASTM A247-19. Standard Test Method for Evaluating the Microstructure of Graphite in Iron Castings. This test method covers the classification of graphite in cast irons in terms of type, distribution, and size by visual comparison to reference photomicrographs. This test method is intended to be applicable for all iron-carbon alloys containing graphite particles, and may be applied to gray irons, malleable irons, compacted graphite irons, and the ductile (nodular) irons.

ISO Standards:

- ISO 4967:2013 - Steel - Determination of content of nonmetallic inclusions - Micrographic method using standard diagrams. This standard specifies a micrographic method for determining the content of nonmetallic inclusions in steel using standard diagrams.

---

[4] CEN - European Committee for Standardization. CEN supports standardization activities in relation to a wide range of fields and sectors including air and space, chemicals, construction, consumer products, defense and security, energy, the environment, food and feed, health and safety, healthcare, ICT, machinery, materials, pressure equipment, services, smart living, transport and packaging.

ASTM Committee E-4 on Metallography was founded in 1916. Their first standard, ASTM E2 was proposed in 1917, and it included a detailed description of how to measure grain size using the planimetric method written by Zay Jeffries [17]. Later[5], in 1951 it was introduced the ASTM grain size number *G*, and the equation relating the number of grains per in^2 at 100X magnification (E 91-51T).

Measurement of the grain size of metals and alloys is the most important quantitative measurement performed due to the influence of grain size upon properties and materials service performance [17]. Furthermore, they may be observing several types of grain structures:

- non-twinned "*ferrite*" grains from BCC (body centered cubic) metals and FCC (face centered cubic) , e.g. aluminum.
- FCC grain structures containing twin boundaries.
- prior-austenite grain boundaries in heat treated steels.

Definition of Feret Diameters

This is not a diameter in its actual sense but the common basis of a group of diameters derived from the distance of two tangents to the contour of the particle in a well-defined orientation.

In simpler words, the method corresponds to the measurement by a slide gauge (slide gauge principle). In general it is defined as the distance between two parallel tangents of the particle at an arbitrary angle.

In practice the Minimum xF_{min} and Maximum Feret Diameter xF_{max}, the Mean Feret Diameter and the Feret Diameters obtained at 90° to direction of the Minimum and Maximum Feret Diameters xF_{90} are used. The minimum Feret diameter is often used as the diameter equivalent to a sieve analysis.

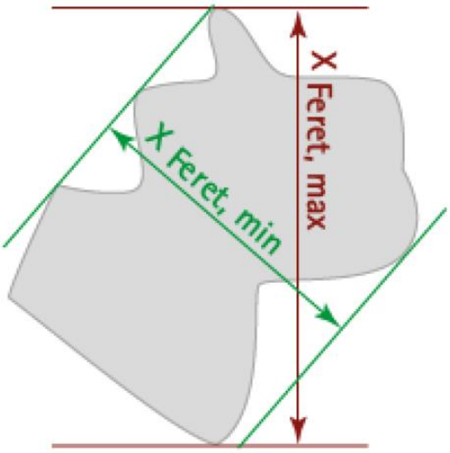

Fig. 31 Feret diameter or caliper diameter. The diameter of an object measured with a caliper is sometimes called the caliper diameter; it is the same as Feret diameter.

---

[5] Every ASTM standard must be reviewed every 5 years. A task group is assigned to review the standard. It decides if the standard is acceptable as written, if technology has changed and it must be modified, or that the standard is of no value and can be made obsolete (e.g. R23 – means revised in 2023. Standard is active).

One of the most common measurements, determination of the **amount of phases present**, can be done using three different methods:

- Areal analysis: Delesse in 1848, says that the area percent of a phase on a 2-D plane is equal to its volumetric percent, that is, AA = VV.
- Lineal analysis: Rosiwal in 1898, says that the lineal fraction of test lines in a phase on the 2-D plane is equal to its volumetric percentage, that is, LL = VV.
- Points analysis: Starting around 1930, several workers in different fields and countries showed that the percentage of points on a test grid lying in the phase of interest was equal to the volumetric percentage, that is, PP = VV. The point counting technique is described fully in ASTM E 562 (also ISO 9042).

Image analyzers use essentially the same procedure; that is, the amount of a phase (usually called the area fraction or volume fraction even if it actually is a point fraction) is determined by the number of picture elements or “pixels” in the phase of interest divided by the total number of pixels, expressed usually as a percentage. However, the latest software packages for image analysis use Artificial Intelligence and Machine Learning algorithms for a very accurate grain boundary detection or secondary phases, that makes those analyses extremely precise and fast.

3.2. Working procedure

According to ASTM E112 – 13, there are three basic procedures for grain size estimation:

Comparison Procedure	*Planimetric Procedure*	*Intercept Procedure*
The comparison procedure does not require counting of either grains, intercepts, or intersections but, as the name suggests, involves comparison of the grain structure to a series of graded images, either in the form of a wall chart, clear plastic overlays, or an eyepiece reticle. Repeatability and reproducibility of comparison chart ratings are generally ± 1 grain size number.	The planimetric method involves an actual count of the number of grains within a known area. The number of grains per unit area, is used to determine the ASTM grain size number *G*. The precision of the method is a function of the number of grains counted. A precision of ±0.25 grain size units can be attained with a reasonable amount of effort.	The intercept method involves an actual count of the number of grains intercepted by a test line or the number of grain boundary intersections with a test line, per unit length of test line, used to calculate the mean lineal intercept length. A precision of better than ± 0.25 grain size units can be attained. The intercept method is faster than the planimetric method for the same level of precision.

Note: The intercept procedure is particularly useful for structures consisting of elongated grains.

The average grain size of an alloy is generally expressed in terms of the **grain size number *G***, as indicated in the standard ASTM E112 – 13.

$N = 2^{G-1}$	N = number of grains/in^2 at 100X magnification G= ASTM grain size number (00 to 14)

The value of ***G*** ranges from **00 to 14**, where 00 corresponds to an average grain diameter of 0.508 mm with a area of 0.2581 mm^2 , and G=14 corresponds to a diameter of 2.8 µm and a area of 7.9 µm^2, see Table 4 from ASTM E112 [20].

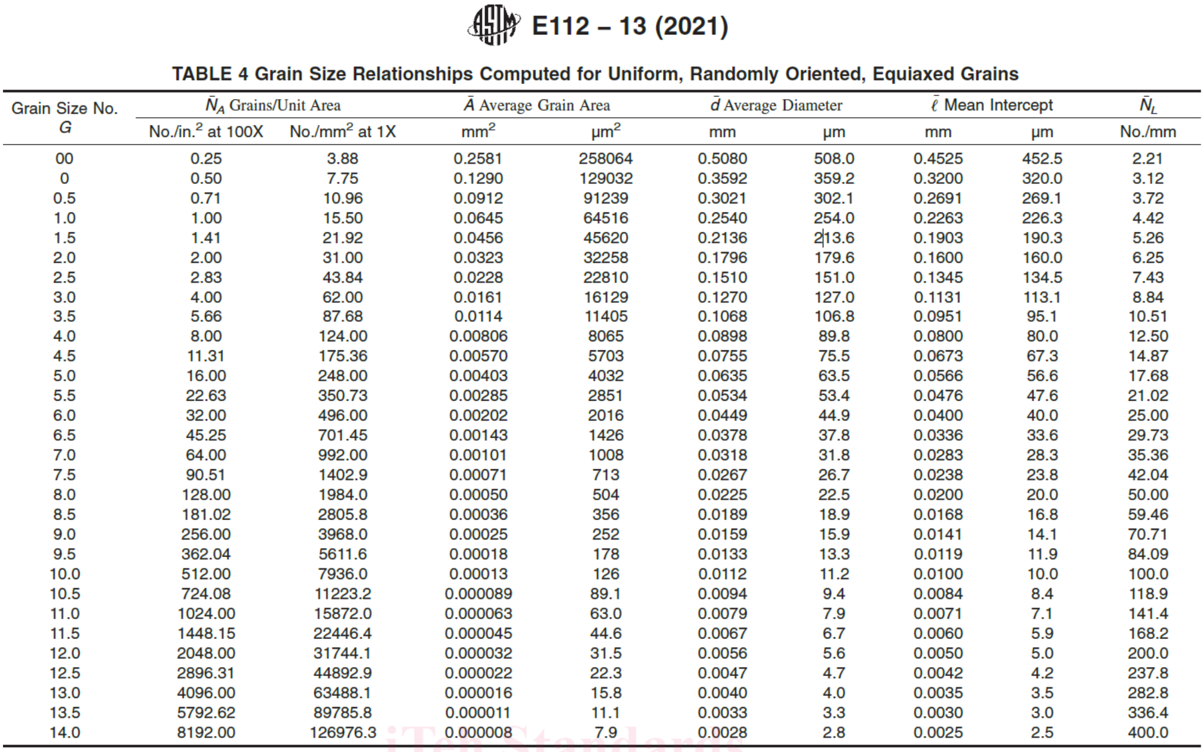

E112 – 13 (2021)

TABLE 4 Grain Size Relationships Computed for Uniform, Randomly Oriented, Equiaxed Grains

Grain Size No. G	$\bar{N}_A$ Grains/Unit Area		$\bar{A}$ Average Grain Area		$\bar{d}$ Average Diameter		$\bar{\ell}$ Mean Intercept		$\bar{N}_L$
	No./in.^{2} at 100X	No./mm^2 at 1X	mm^2	µm^2	mm	µm	mm	µm	No./mm
00	0.25	3.88	0.2581	258064	0.5080	508.0	0.4525	452.5	2.21
0	0.50	7.75	0.1290	129032	0.3592	359.2	0.3200	320.0	3.12
0.5	0.71	10.96	0.0912	91239	0.3021	302.1	0.2691	269.1	3.72
1.0	1.00	15.50	0.0645	64516	0.2540	254.0	0.2263	226.3	4.42
1.5	1.41	21.92	0.0456	45620	0.2136	213.6	0.1903	190.3	5.26
2.0	2.00	31.00	0.0323	32258	0.1796	179.6	0.1600	160.0	6.25
2.5	2.83	43.84	0.0228	22810	0.1510	151.0	0.1345	134.5	7.43
3.0	4.00	62.00	0.0161	16129	0.1270	127.0	0.1131	113.1	8.84
3.5	5.66	87.68	0.0114	11405	0.1068	106.8	0.0951	95.1	10.51
4.0	8.00	124.00	0.00806	8065	0.0898	89.8	0.0800	80.0	12.50
4.5	11.31	175.36	0.00570	5703	0.0755	75.5	0.0673	67.3	14.87
5.0	16.00	248.00	0.00403	4032	0.0635	63.5	0.0566	56.6	17.68
5.5	22.63	350.73	0.00285	2851	0.0534	53.4	0.0476	47.6	21.02
6.0	32.00	496.00	0.00202	2016	0.0449	44.9	0.0400	40.0	25.00
6.5	45.25	701.45	0.00143	1426	0.0378	37.8	0.0336	33.6	29.73
7.0	64.00	992.00	0.00101	1008	0.0318	31.8	0.0283	28.3	35.36
7.5	90.51	1402.9	0.00071	713	0.0267	26.7	0.0238	23.8	42.04
8.0	128.00	1984.0	0.00050	504	0.0225	22.5	0.0200	20.0	50.00
8.5	181.02	2805.8	0.00036	356	0.0189	18.9	0.0168	16.8	59.46
9.0	256.00	3968.0	0.00025	252	0.0159	15.9	0.0141	14.1	70.71
9.5	362.04	5611.6	0.00018	178	0.0133	13.3	0.0119	11.9	84.09
10.0	512.00	7936.0	0.00013	126	0.0112	11.2	0.0100	10.0	100.0
10.5	724.08	11223.2	0.000089	89.1	0.0094	9.4	0.0084	8.4	118.9
11.0	1024.00	15872.0	0.000063	63.0	0.0079	7.9	0.0071	7.1	141.4
11.5	1448.15	22446.4	0.000045	44.6	0.0067	6.7	0.0060	5.9	168.2
12.0	2048.00	31744.1	0.000032	31.5	0.0056	5.6	0.0050	5.0	200.0
12.5	2896.31	44892.9	0.000022	22.3	0.0047	4.7	0.0042	4.2	237.8
13.0	4096.00	63488.1	0.000016	15.8	0.0040	4.0	0.0035	3.5	282.8
13.5	5792.62	89785.8	0.000011	11.1	0.0033	3.3	0.0030	3.0	336.4
14.0	8192.00	126976.3	0.000008	7.9	0.0028	2.8	0.0025	2.5	400.0

The Comparison Chart procedure is a very fast method, but less accurate, Fig. 32. The etched microstructure taken usually at 100X magnification is compared to a series of pictures from the chart and is picked out the chart picture closest in size to the test specimen. Repeatability and reproducibility of comparison chart ratings are generally ± 1 grain size number *G* [20].

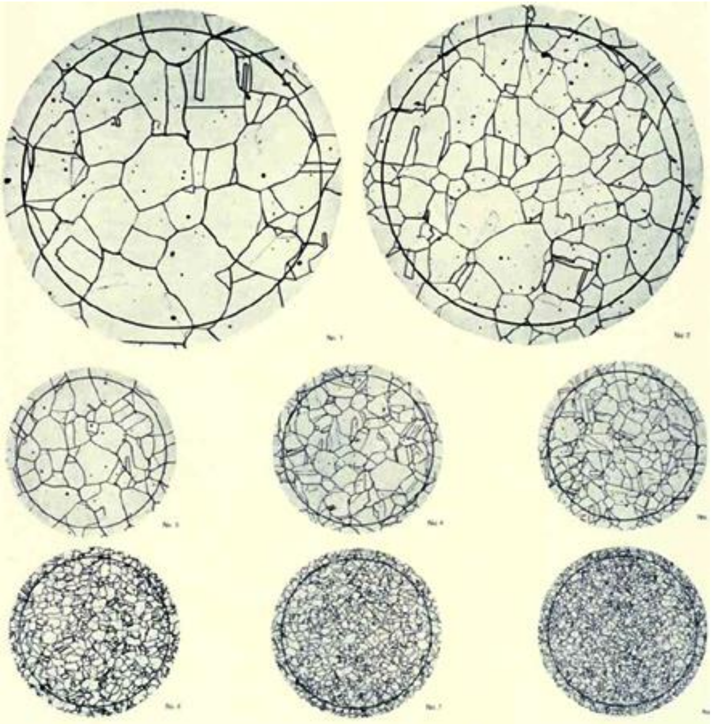

Fig. 32 ASTM chart for rating grain size of austenitic twined alloys.

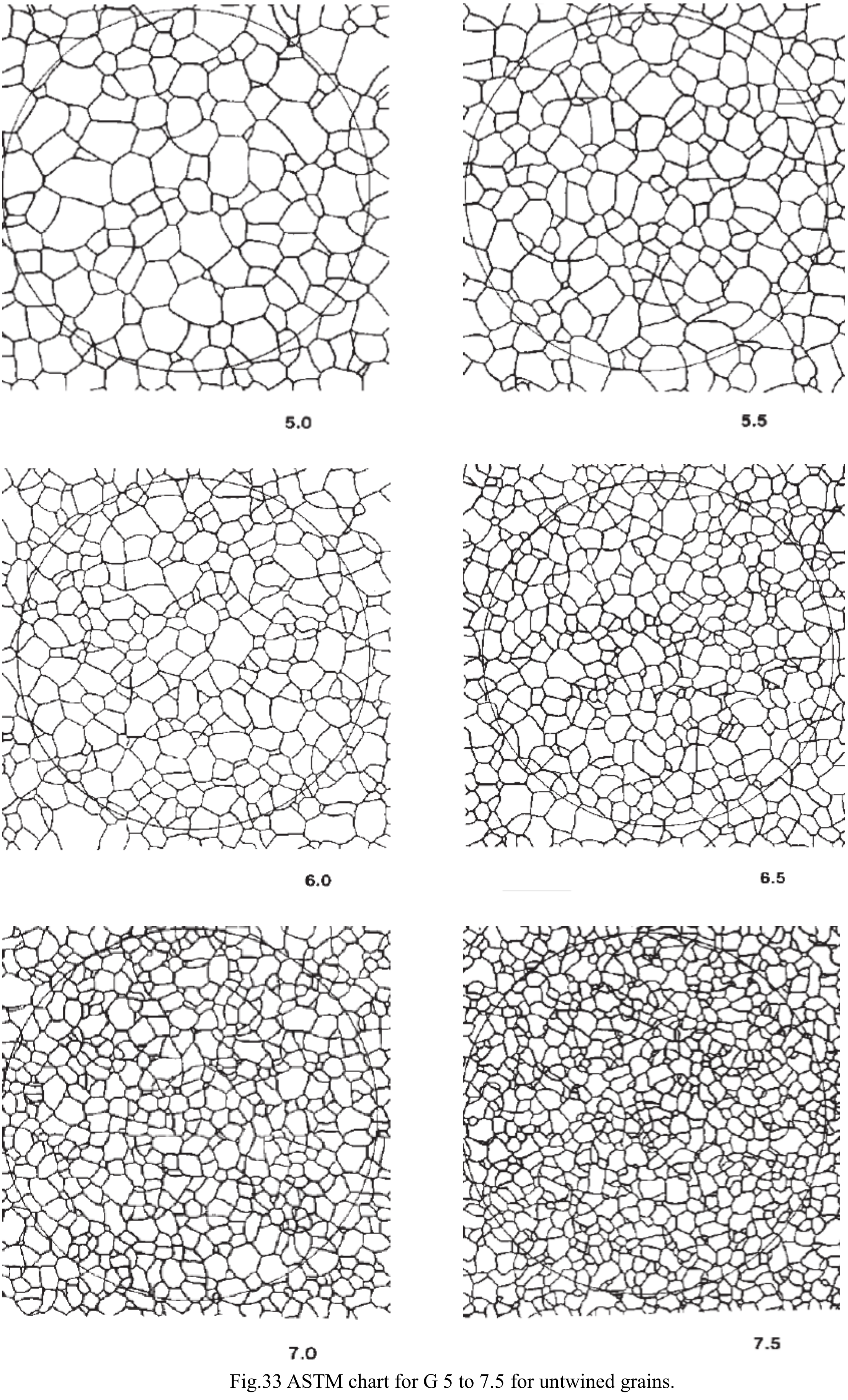

5.0

5.5

6.0

6.5

7.0

7.5

Fig.33 ASTM chart for G 5 to 7.5 for untwined grains.

If the grain structure is very fine, raise the magnification on the microscope, pick out the closest chart picture and correct for the difference in magnification according to the following relations:

$$G = \text{Chart } G + 6.64 \cdot \text{Log10}(M/M_b)$$

where:

Chart G is the ASTM grain size number indicated in the chart picture.
M is the magnification used.
M_b is the chart magnification.

An eyepiece reticle (or graticules) is a glass disc with a pattern on it that fits at the optical plane inside a microscope eyepiece. It is used to provide alignment, measurement, size or shape comparison, or area counting of specimens by having the reticle pattern superimposed over the specimen image, Fig. 34.

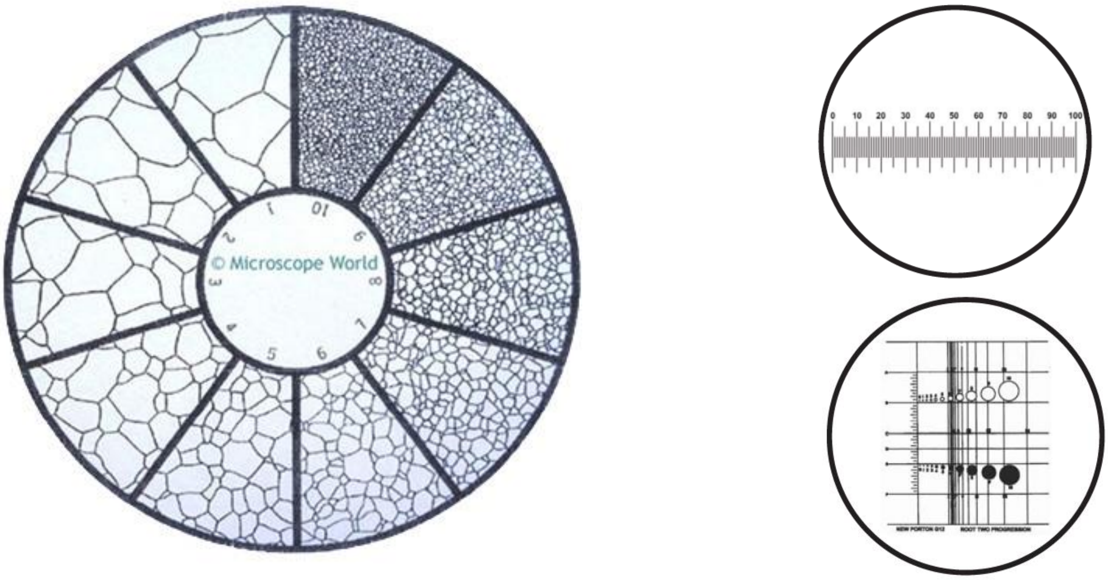

Fig. 34 Reticle with grain sizing disc. Other types of reticles [19].

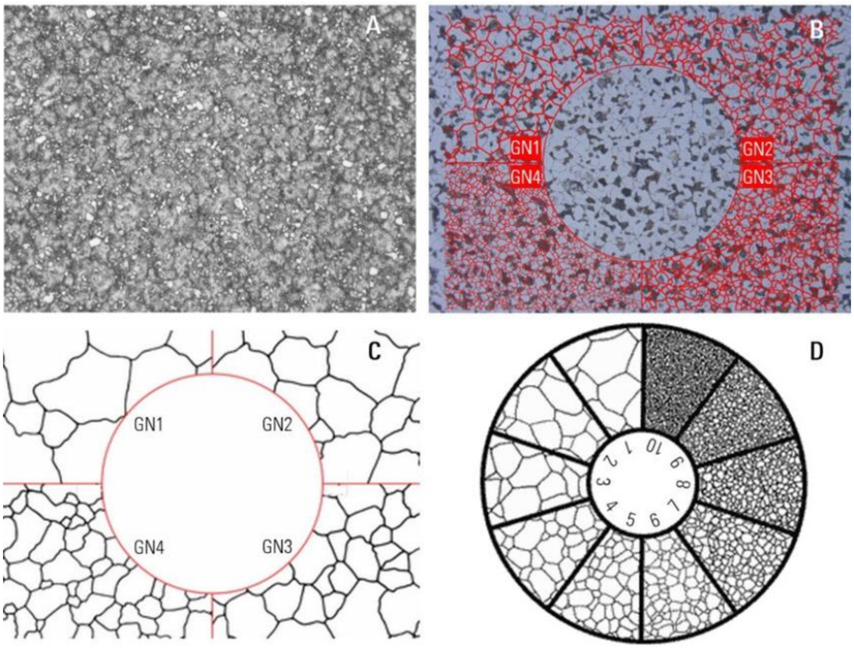

Fig. 35 Example of comparison method used to measure the grain size of a steel alloy [18].

The comparison method does not require to count the grains whitin a specified area, but rather to compare the grain structure (M = 100X) to a series of graded images printed on engraved on reticles. In Fig. 35 is illustrated the comparison method used to measure the grain size of a steel alloy, directly on the microscope using a graticule or an eyepiece reticle with a grain gradation, where:

A) Raw image of the steel microstructure.
B) Digital reticules with image overlays for comparison to determine grain size numbers.
C) Digital reticules for grain size comparison (G = 1, 2, 3, and 4) as seen without an underlying image.
D) Example of a microscope eyepiece reticule with overlays for G from 1 to 10 which can be compared directly with a live microscope image of the alloy.

The planimetric method involves an actual count of the number of grains within a known area. The Jeffries planimetric grain size method utilizes a test circle with a diameter of 79.8 mm which is superimposed over the microstructure. The magnification is chosen to give at least 50 grains to be counted [17]. The students should count all the grains that are completely inside the test circle and all the grains that are intercepted by the circle. To get an accurate measurement, the students must mark the grains as they are counted using a pen. Thus, makes the method slow and less popular [17]. A precision of ±0.25 grain size units *G* can be attained with a reasonable amount of effort [20], Fig. 36.

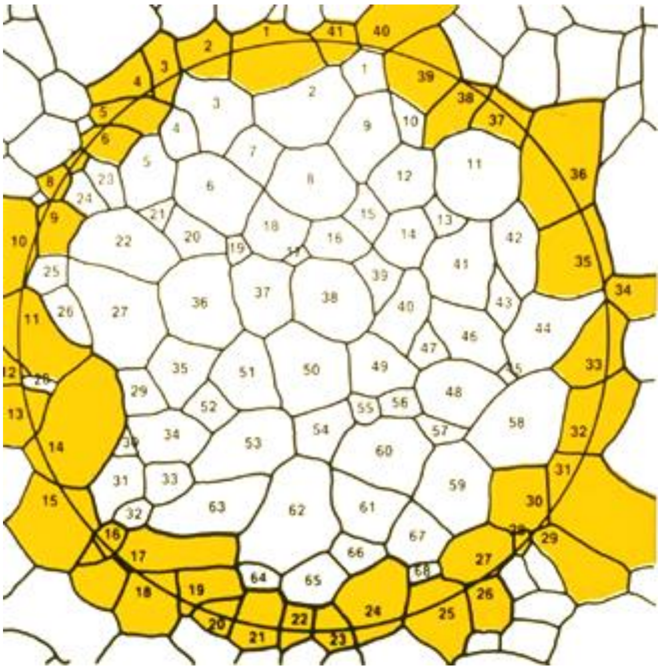

Fig. 36 Jeffries planimetric grain size method (n_{inside} =68, $n_{intercepted}$=41), M=100X.

$$N_A = (M^2/A)*(n_{inside}+[n_{intercepted}/2])$$

$$G = 3.322*\log[N_A] - 2.954$$

where:

- The number of grains per unit area N_A is used to determine grain size number *G*. The value of N_A is calculated with the relation from Fig. 36.
- M is the magnification,
- A is the circular area,
- n_{inside} is the number of grains falling completely within the circle,
- $n_{outside}$ is the number of grains intercepted by the circle's perimeter.

For data presented in Fig. 36, we have :

M=100X
D = 79.8 mm
$n_{inside} = 68$
$n_{intercepted} = 41$
$N_A = \frac{100^2}{20106.2}\left(68 + \frac{41}{2}\right) = 44.02mm^{-2}$
$G = 3.322 \cdot Log(N_A) - 2.954 = 2.5$

The Intercept Procedure. The intercept method involves an actual count of the number of grains intercepted by a test line or the number of grain boundary intersections with a test line, per unit length of test line, used to calculate the mean lineal intercept length, which is used to determine the ASTM grain size number, *G* [20].

The precision of the method is a function of the number of intercepts or intersections counted. A precision of better than ±0.25 grain size units can be attained with a reasonable amount of effort [20]. Results are free of bias; repeatability and reproducibility are less than ±0.5 grain size units. Because an accurate count can be made without need of marking off intercepts or intersections, the intercept method is faster than the planimetric method for the same level of precision.

Intercept procedures are recommended particularly for all structures that depart from the uniform equiaxed form. For anisotropic structures, procedures are available to make separate size estimates in each of the three principal directions.

Heyn Lineal Intercept Procedure

The average grain size by counting the number of grains intercepted by one or more straight lines sufficiently long to yield at least 50 intercepts. The precision of grain size *G* estimates by the intercept method is a function of the number of grain interceptions counted.

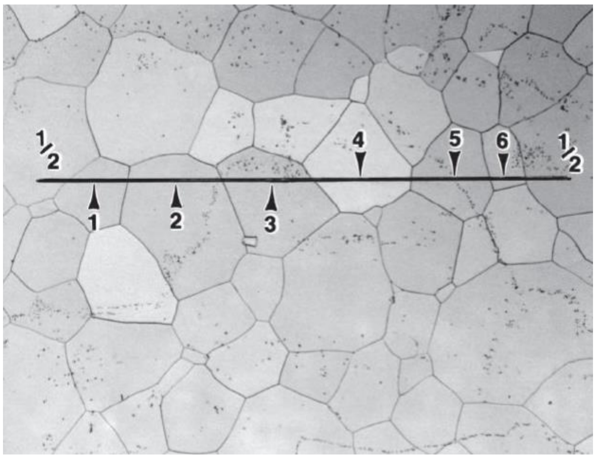

Number of grains intercepted:

$$N_i = ½ + 6 + ½ = 7$$

Fig. 37 Lineal Intercept Method. Number of grains intercepted by a line. For a two-phase structure, one must do N (grains intercepted) counts.

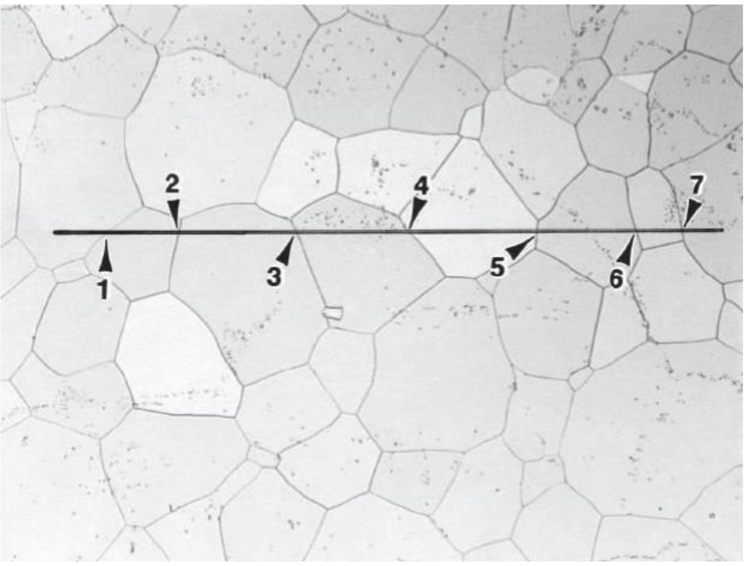

Number of grain boundaries intersections:

$$P_i = 7$$

Fig. 38 Lineal Intercept Method. The number of grains boundaries intersected by a line. For a single-phase structure, it is easier to do P (grain boundary intersections) counts.

1. N_i and P_i are the number of intercepts or intersections counted on the line, L is the total test line length and M is the magnification.
2. Calculate the **mean lineal intercept** value for each field:

$$\bar{N}_L = \frac{N_i}{L/M}$$

$$\bar{L} = \frac{1}{\bar{N}_L} = \frac{1}{\bar{P}_L}$$

$$\bar{P}_L = \frac{P_i}{L/M}$$

The P or N count is divided by the true line length, L, which is the line length divided by the magnification, L/M. These yields $\bar{N}$ or $\bar{P}$, the number of intersections per unit length or the number of interceptions per unit length. The reciprocal of $\bar{P}$ or $\bar{N}$ is the mean lineal intercept length $\bar{L}$. The mean lineal intercept $\bar{L}$ is related to G by the following empirical equation:

$$G = (-6.6457 \log \bar{L}) - 3.298$$

The effects of moderate departure from an equiaxed structure may be eliminated by making intercept counts on a line array containing lines having four or more orientations, Fig. 39 [20].

Hilliard Single-Circle Procedure

When the grain shape is not equiaxed but is distorted by deformation or other processes, obtaining an average lineal intercept value using straight test lines requires averaging of values made at a variety of orientations. Use of a circle as the test line eliminates this problem, as the circle will test all orientations equally and without bias. Hilliard recommended test conditions that produce about 35 counts per circle with the test circle applied blindly over as large a specimen area as feasible until the desired total number of counts is obtained.

Abrams Three-Circle Procedure

Based on an experimental finding that a total of 500 counts per specimen normally yields acceptable precision, Abrams developed a specific procedure for routine average grain size rating of commercial steels. Use of the chi-square test on real data demonstrated that the variation of intercept counts is close to normal, allowing the observations to be treated by the statistics of normal distributions [20].

The test pattern consists of three concentric and equally spaced circles having a total circumference of 500 mm, as shown in Fig. 39. Successively this pattern is applied to at least five blindly selected and widely spaced fields. Then, is recorded separately the count of intersections per pattern for each of the test. Then, the mean lineal intercept is determined with the standard deviation in 95 % confidence limit, and the relative accuracy of the test.

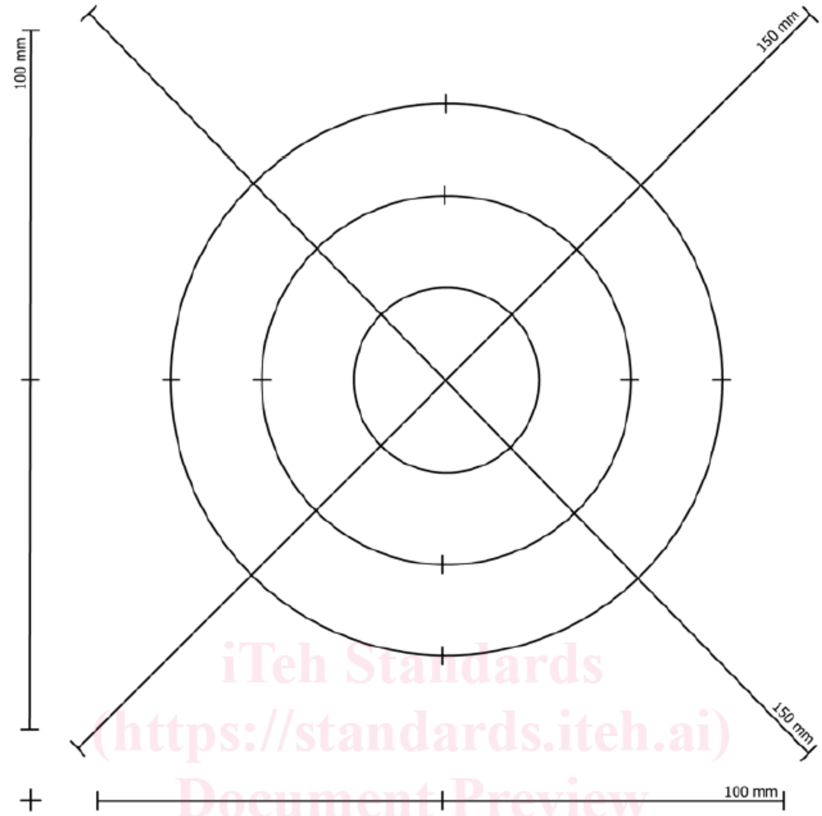

NOTE 1—If reproduced to make straight lines marked length:
Straight lines total: 500 mm

Circles are:	Circumference, mm,	Diameter, mm
	250.0	79.58
	166.7	53.05
	83.3	26.53
	Total 500.0	

NOTE 2—See Footnote 9.

Test Pattern for Intercept Counting

Fig. 39 Abrams Three-Circle Procedure Method for grain size estimation [20].

3.3. Discussion and results interpretation

The precision and bias of grain size measurements depend on the representativeness of the specimens selected and the areas on the plane-of-polish chosen for measurement.

The comparison chart rating procedure may provide acceptable precision for most commercial applications if the second phase (or constituent) consists of islands or patches of essentially the same size as the matrix grains; or, the amount and size of the second phase particles are both small and the particles are located primarily along grain boundaries.

The planimetric method may be applied if the matrix grain boundaries are clearly visible and the second phase (constituent) particles are mainly present between the matrix grains rather than within the grains.

Always should be determined the amount of the phase of least concentration, usually the second phase or constituent. Then, it can be determined the matrix phase by difference.

Circular intercept procedures are most suitable for use as fixed routine manual procedures for grain size estimation in quality control. When the grain shape is not equiaxed but is distorted by deformation or other processes, obtaining an average lineal intercept value using straight test lines requires averaging of values made at a variety of orientations. If this is not done carefully, bias may be introduced.

3.4. Case study

The captured images can be used to perform advanced image quantitative analysis with specialized software such as (search conducted with the Chat GPT help):

1. **ImageJ:**
   - **Link:** ImageJ
   - **Description:** ImageJ is a powerful open-source image processing and analysis software developed by the National Institutes of Health (NIH). It offers a wide range of plugins and tools for tasks such as particle analysis, measurements, and image enhancement. ImageJ is versatile and widely used in various scientific fields, including materials science and metallography.
   - Fiji is an extended distribution of ImageJ that comes with additional plugins, libraries, and features. It is designed to streamline the use of ImageJ for scientific image analysis and includes a user-friendly interface. Fiji is particularly popular in bioimaging, but its extensibility makes it suitable for a range of applications, including metallography.
2. **Olympus Stream Image Analysis Software:**
   - **Link:** Olympus Stream
   - **Description:** Olympus Stream is dedicated imaging and analysis software designed for metallurgical microscopes. It provides tools for image acquisition, documentation, and analysis, with features tailored to the needs of metallurgists. The software supports tasks such as phase analysis, grain size measurement, and reporting.
3. **NIS Elements:**
   - **Link:** NIS Elements
   - **Description:** NIS Elements is imaging software from Nikon Instruments that is widely used in microscopy, including metallography. It offers a range of features for image acquisition, analysis, and 3D reconstruction. NIS Elements is compatible with Nikon's microscopy systems and provides tools for quantitative analysis of microstructures.
4. **HKL Technology - HKL-3000:**
   - **Link:** HKL-3000

- **Description:** While originally developed for X-ray crystallography, HKL-3000 from HKL Research is a comprehensive software suite that includes image analysis tools for various applications, including metallography. It is capable of handling data from different imaging techniques and supports tasks such as grain boundary analysis and texture determination.

6. **ZEN Imaging Software by Zeiss:**

   - **Link:** ZEN Imaging Software

   - **Description:** ZEN (Zeiss Efficient Navigation) is imaging software provided by Zeiss for their microscopy systems. It offers a user-friendly interface for image acquisition, processing, and analysis. ZEN is applicable to various microscopy techniques, including metallography, and provides tools for quantitative analysis of microstructural features.

7. **Leica LAS X Software:**

   - **Link:** Leica LAS X

   - **Description:** Leica LAS X is imaging and analysis software designed for Leica Microsystems' microscopy solutions. It offers features for image acquisition, processing, and analysis, making it suitable for metallography applications. LAS X supports tasks such as particle analysis, measurement, and documentation.

8. **Gatan DigitalMicrograph:**

   - **Link:** DigitalMicrograph

   - **Description:** Gatan DigitalMicrograph is a software suite commonly used in transmission electron microscopy (TEM), but it is also applicable to other microscopy techniques, including metallography. It provides tools for image processing, analysis, and visualization, offering advanced capabilities for studying microstructures at high resolution.

9. **MetalImage™ by Nucor Digital Solutions:**

   - **Link:** MetalImage™

   - **Description:** MetalImage™ is a specialized image analysis software developed for metallography and materials science applications. It offers features for quantitative analysis of microstructures, including grain sizing, phase identification, and inclusion analysis. The software is designed to work seamlessly with metallographic images.

10. **MIPAR™ by MIPAR Image Analysis:**

- **Link:** Mipar™

   - **Description:** From manufacturing to research and development, MIPAR has a wide variety of applications. If you're ready to experience the power of MIPAR for yourself, visit our website at https://www.mipar.us and download a free 14-day trial. MIPAR Image Analysis is a world-leading algorithm development and image analysis software company. We specialize in efficiently, accurately, and reliably extracting measurements from complex images. From material and life sciences to aerospace and manufacturing solutions, our extensive portfolio can assist a variety of real-world applications.

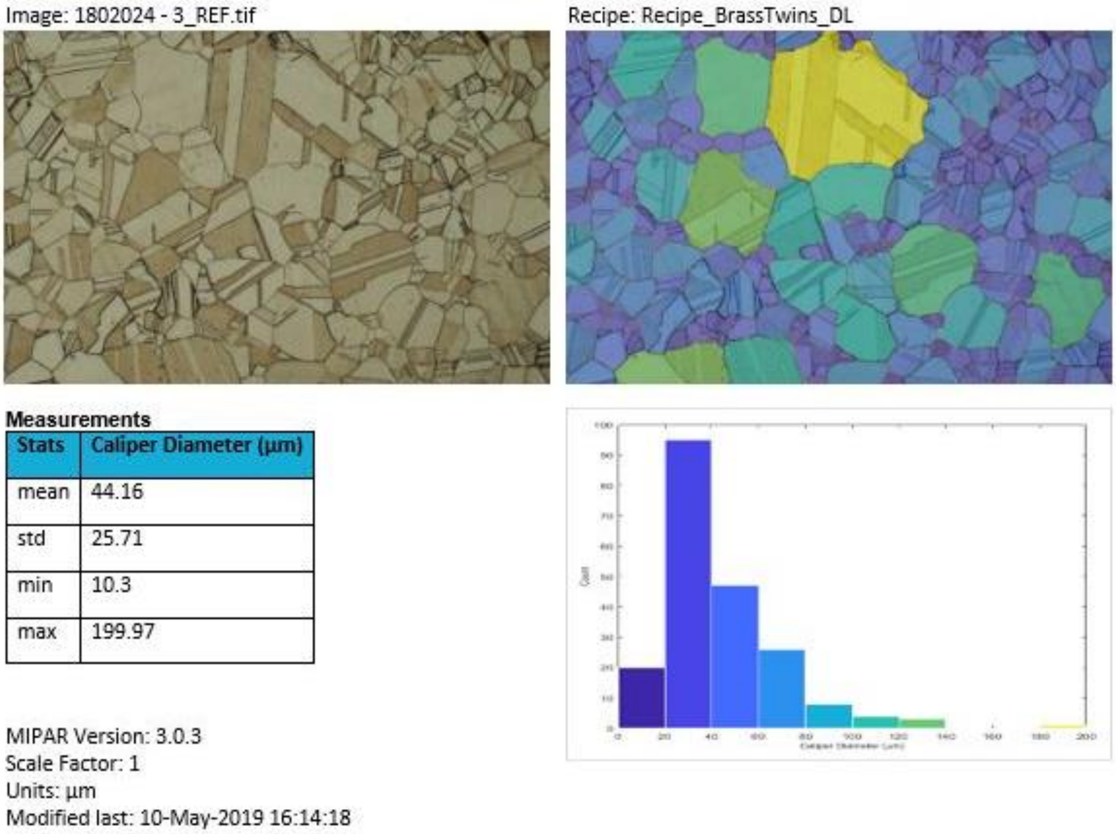

Image: 1802024 - 3_REF.tif

Recipe: Recipe_BrassTwins_DL

Measurements

Stats	Caliper Diameter (µm)
mean	44.16
std	25.71
min	10.3
max	199.97

MIPAR Version: 3.0.3
Scale Factor: 1
Units: µm
Modified last: 10-May-2019 16:14:18

Fig. 40 Example of image quantitative analysis performed with MIPAR software using deep learning algorithms in image processing.

4. Macrostructural characterization of metals and alloys

4.1. Theoretical background

Macrostructural characterization is a specialized field within materials science that focuses on the examination and analysis of large-scale features in materials, especially in metals and alloys. The macrostructural characterization involves the examination and analysis of large-scale features that are visible to the naked eye or with minimal magnification, providing specialists with valuable insights into the overall structure and properties of these materials at a macroscopic level.

The macrostructural characterization focuses on macroscopic features, such as grain fiber lines in forged parts, segregation, dendritic patterns, non-metallic inclusions, material discontinuities and geometric non-conformities produced in different manufacturing processes. Macrostructural characterization is also used to identify and analyze defects such as porosity, cracks, and inclusions that may have significant implications for the material's integrity and performance. Usually, this activity is part of the quality control process, but also plays a key role in expertise reports. Macrostructural characterization is often employed in quality control processes, ensuring that materials meet specified standards and exhibit the desired macroscopic properties. This is particularly important in industries such as aerospace, automotive, and construction.

Understanding these features is essential for predicting mechanical properties, heat treatment responses, and overall performance of the equipment's and machines in general and their safety requirements in exploitation. The observed macrostructural features are correlated with the mechanical, thermal, and chemical properties of the material. This correlation is crucial for designing and optimizing materials for specific applications.

Macrostructural characterization is complementary used with optical microscopy and etching technique to reveal and understand the macroscopic structure, leading to insights that are vital for materials design, quality control, and performance optimization.

The macrostructural characterization of materials is based on visual inspection of the manufactured parts. The standards used in industry for visual inspection are:

- EN 13018:2016 Non-destructive testing - Visual testing - General principles.
- ISO 17637 - Non-destructive testing of welds - Visual testing of fusion-welded joints.
- ASME[6] Section V, Article 9 - Visual Examination.

Visual inspection in the industry follows certain standards and guidelines to ensure consistency, accuracy, and reliability in evaluating the quality and integrity of materials and products. The specific standards used can vary depending on the industry and the type of materials being inspected. Visual inspection refers to the manual examination of an object or product by a human inspector using their eyes[7] and judgment to identify defects, anomalies, or deviations from specifications through direct visual observation and thus, to assess its quality, appearance, and adherence to standards. This process is subjective and may vary between different inspectors.

---

[6] The American Society of Mechanical Engineers (ASME) provides a set of standards for nondestructive examination, including visual inspection. These standards cover various methods, and Section V specifically addresses visual examination requirements.

[7] The inspectors can use tools such as magnifiers, borescopes, and cameras.

Nowadays, visual inspection can use automated systems with machine vision capabilities and powerful software analysis based on AI and machine learning algorithms. Advanced algorithms enable real-time processing of visual data, allowing for rapid decision-making in industrial settings. This is essential for high-speed production lines.

The macrostructural characterization of materials and visual inspection are complementary processes within the broader field of quality assessment. While macrostructural characterization provides in-depth insights into the internal structure of materials, visual inspection assesses the external features, surface quality, and overall appearance. Together, these approaches contribute to a comprehensive evaluation of materials in various industries.

Surface Inspection: A visual examination of the material's surface is conducted to identify any visible defects, such as cracks, scratches, or corrosion. The inspection includes also a dimensional inspection, ensuring that the dimensions and shapes of the final product conform to specified tolerances is essential for meeting design requirements.

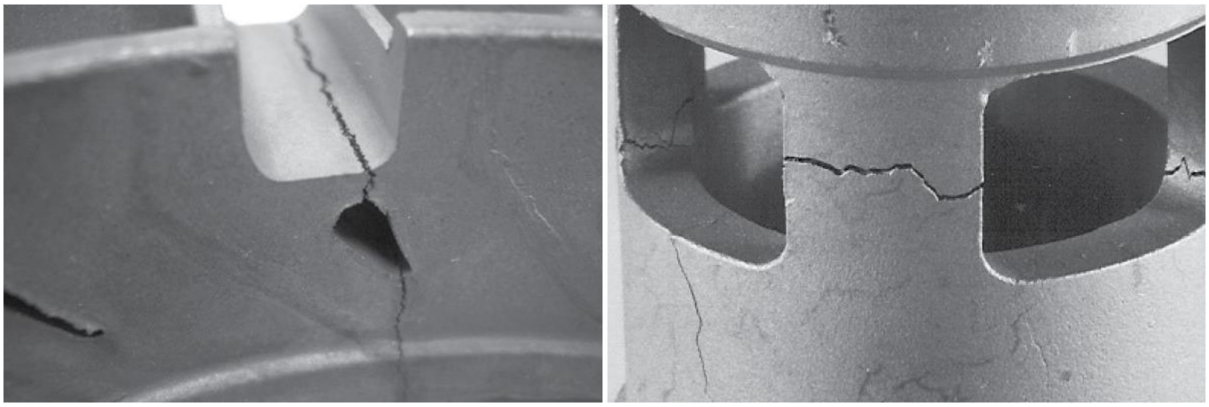

During casting cooling, the strength of the shell or gating system exceeds that of the solidifying metal. The crack presents an irregular path, typically with an oxidized fracture face. Typical location is in areas where the part geometry involves seriously restrained contraction. May occur at the intersection of thick and thin section.

Fig. 41 Hot tear in casting product [21].

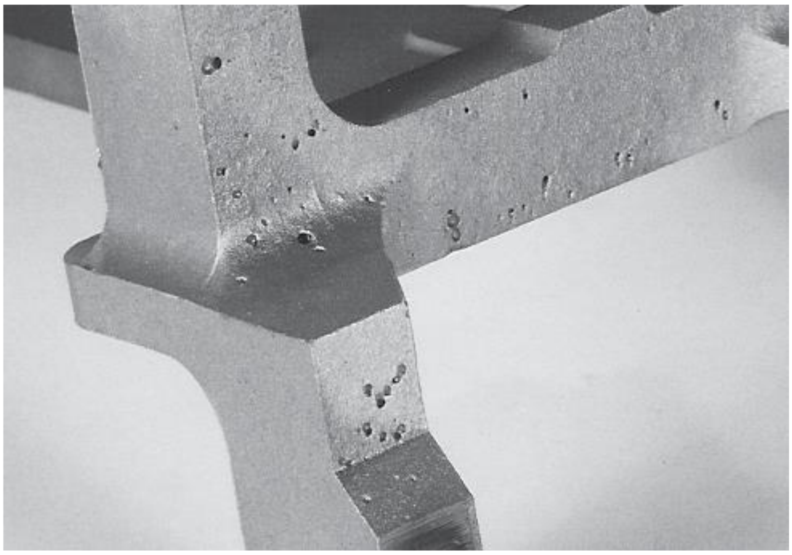

Gases are absorbed in metal during melting. If the gas level in the melt exceeds the solid state solubility limit, bubbles are formed during solidification. The gases most responsible for this defect are hydrogen and nitrogen.

Fig. 42 Pinholes in casting product [21].

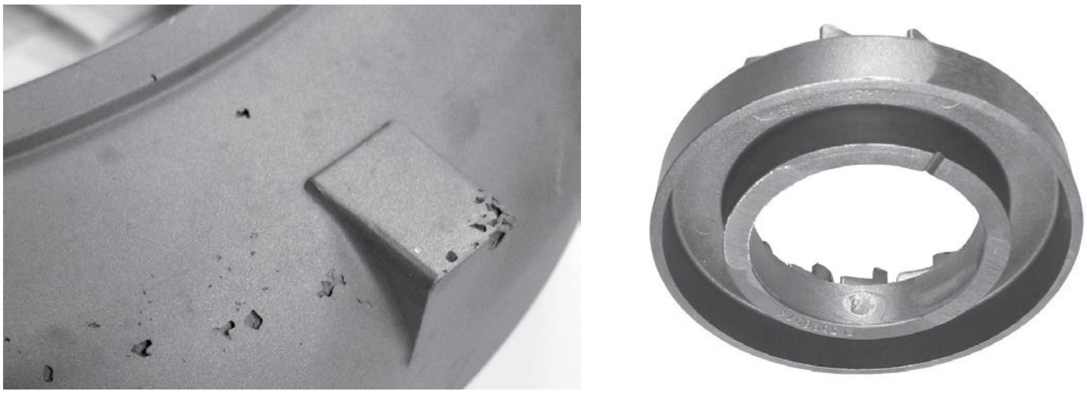

During melting or casting, slag is produced as a function of time, temperature and availability of oxygen. This slag is mixed with the metal during pouring and being less dense than the metal, floats to the top surface of the casting.

Fig. 43 Slag inclusions in casting product [21].

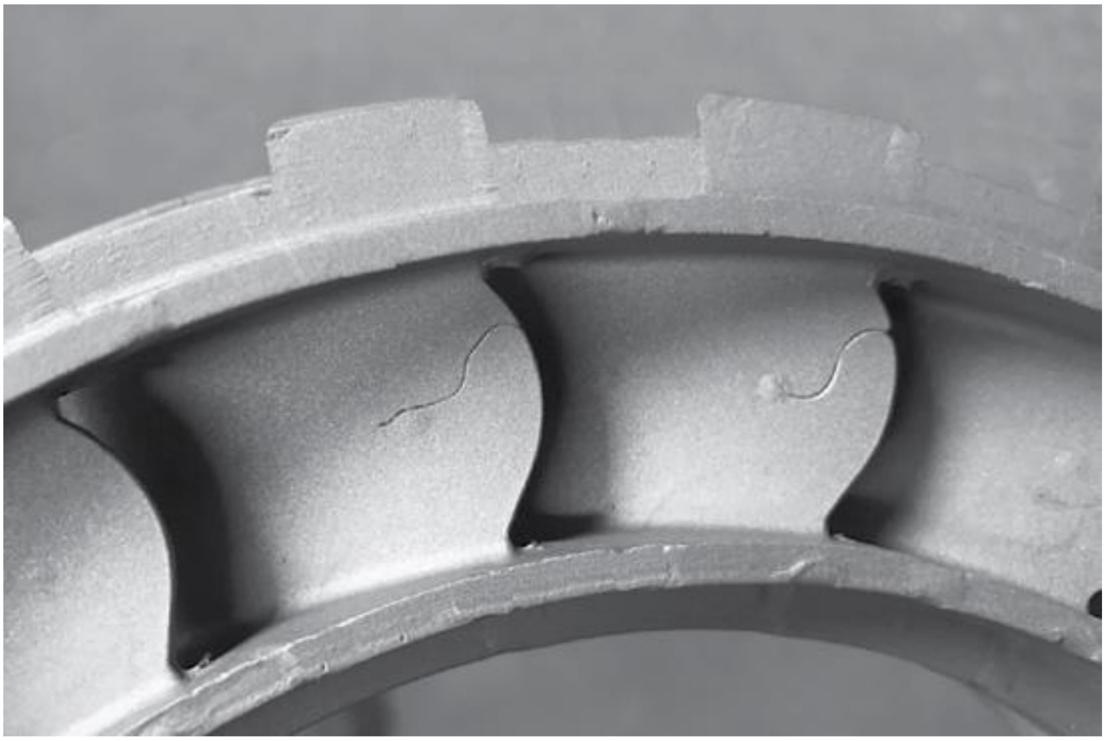

This defect takes the form of a crack or discontinuity in the surface with rounded edges indicating the freezing or solidification of two or more streams of metal before they had time to completely fuse together.

Fig. 44 Cold shut defect in casting product [21].

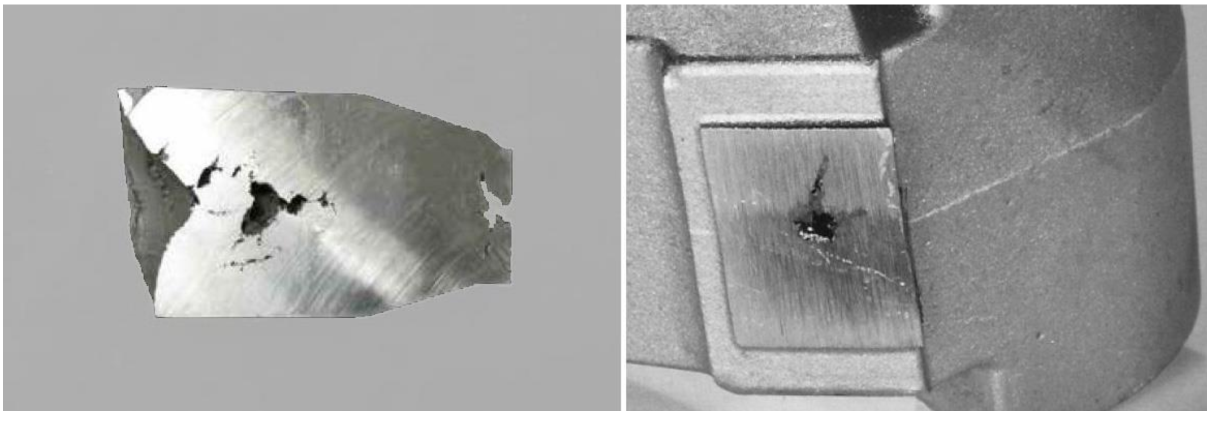

Fig. 45 Shrink-gate defect in casting product [21].

The molten alloy shrinks as it solidifies. Inadequate feed metal from the gating system is available to prevent a cavity from forming. Internal irregular cavity exhibiting an open or porous coarsely crystalline or dendritic structure usually exposed upon removal of the gate, Fig. 45.

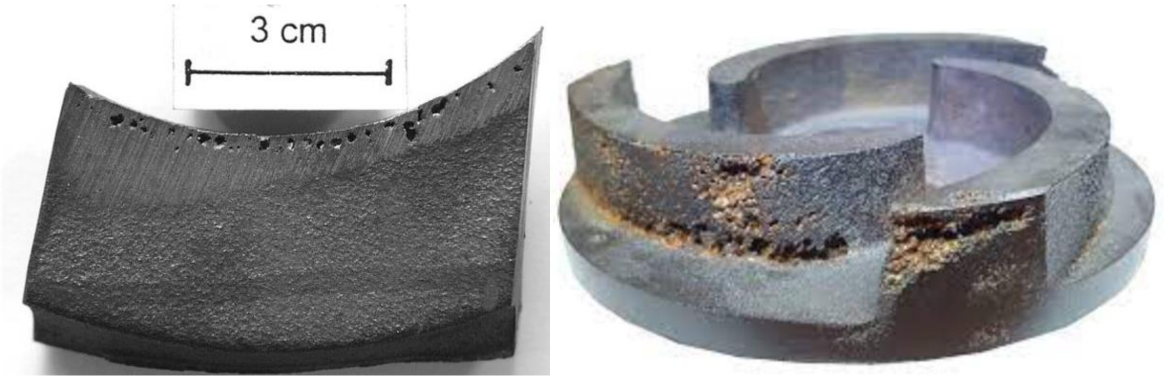

Fig. 46 Cavities (in a cast part left) and in a pump part due to cavitation (right picture).

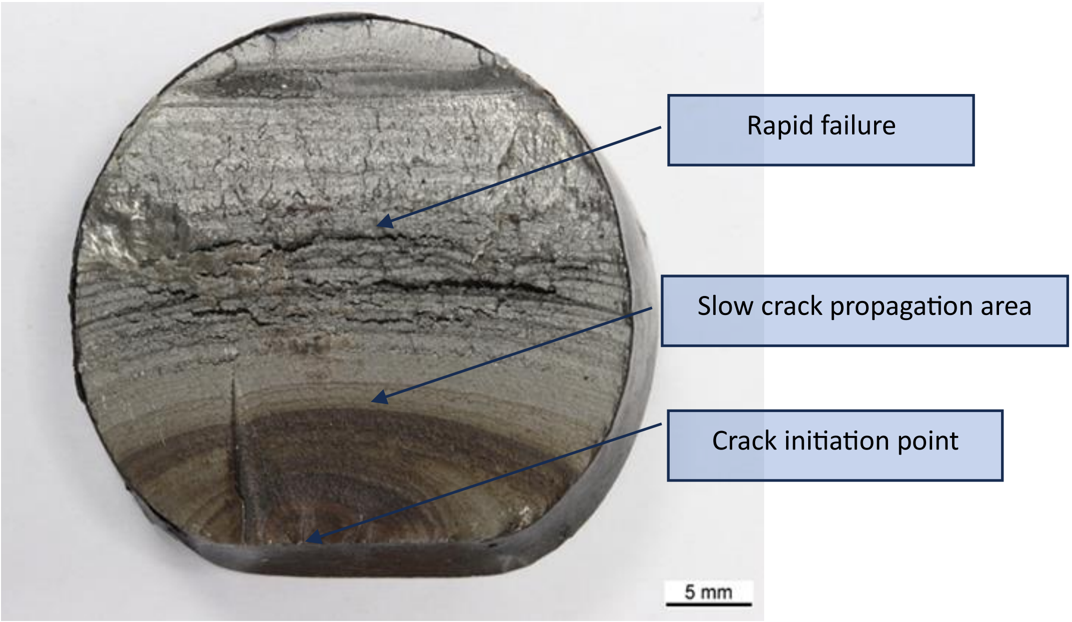

A small crack is initiated at the part surface (on non-metallic inclusions, scratches, or in geometric stress raisers area, corrosions pits, etc.). The smooth region of fractured surface corresponds to a slow crack propagation and rapid failure has occurred in the fibrous texture area.

Fig. 47 Fatigue failure surface in a hitch, S355J2 [22].

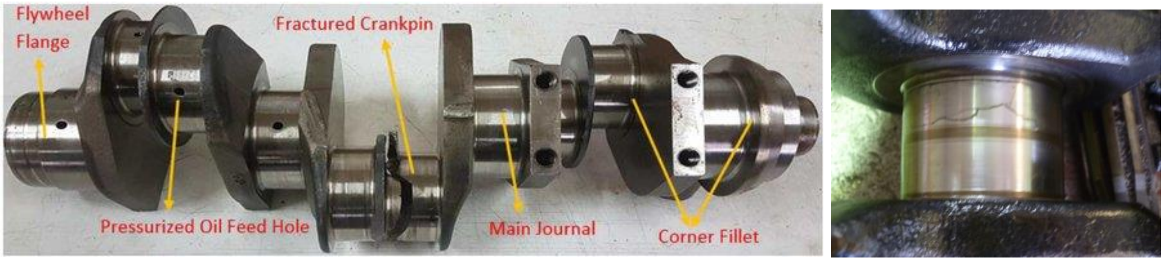

Fatigue failure of crankshaft takes place in the regions of maximum bending and maximum twisting. The maximum bending may be found at the center or at either end of the crankshaft. The crankshaft fails due to cyclic twisting, which results in shear stress. The crack initiation can occur due to high-stress concentration or as a defect during manufacture which eventually propagates under cyclic loads.

Fig. 48 Fatigue failure in a crankshaft.

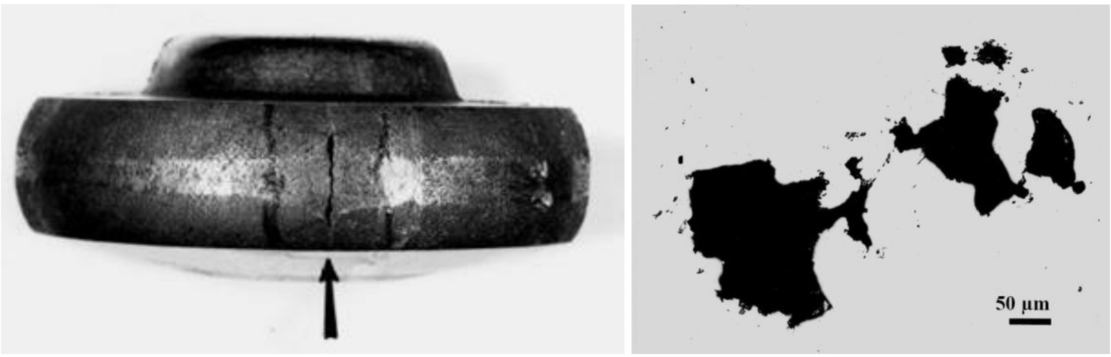

Fig. 49 Crack in upset forged EX33 steel initiated by oxide inclusions [more info].

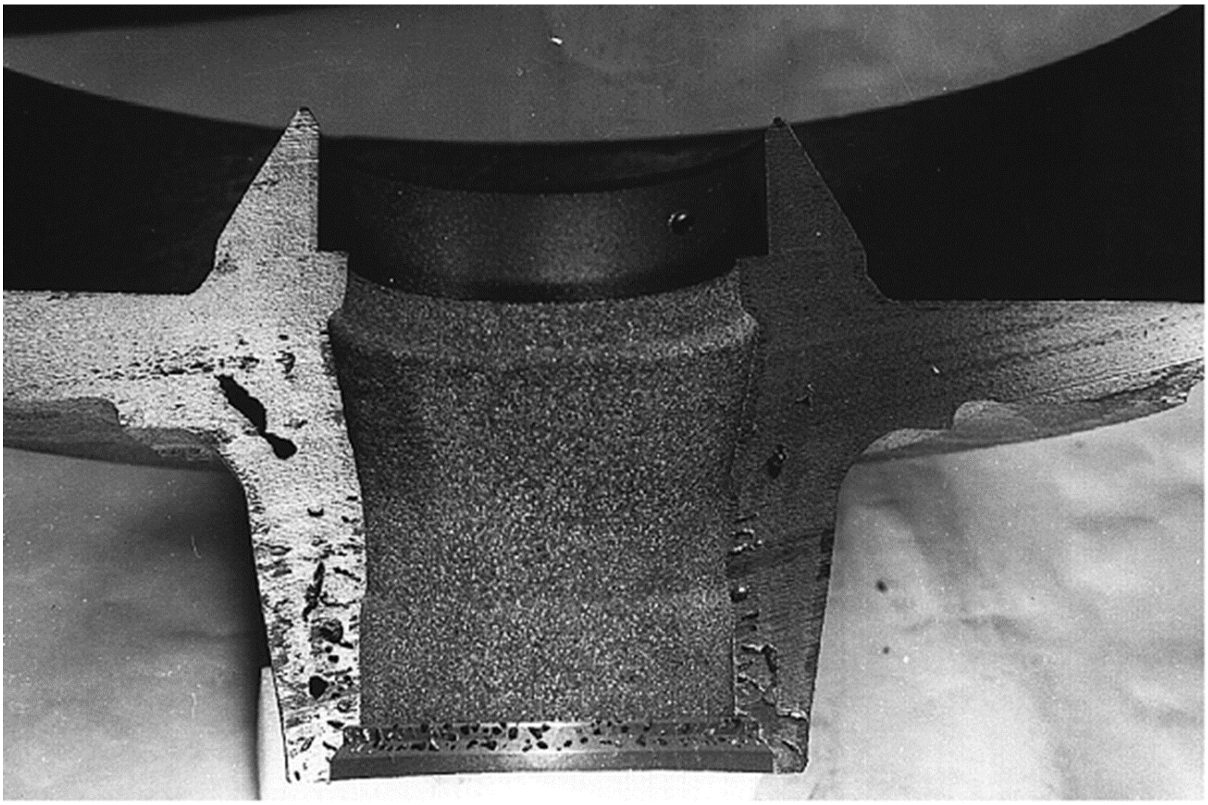

Fig. 50 Dispersed shrinkage. This defect is mainly observed in castings made of flake graphite cast iron, but this phenomenon may also occur in nodular graphite cast iron and cast steels [more info].

The macro examination may be performed on the transverse or longitudinal cross section of the test sample. The sample is viewed with the unaided eye or at low magnification, usually no greater than 10 times. Hole steel casting defects include pores, shrinkage holes, shrinkage porosity, slag holes, trachoma, and iron beans. Also known as gas eyes, bubbles, holes casting defects caused by gas. Casting pores are generally round, and the inner surface of the holes is smooth.

The macro etch inspection is a testing technique used to examine the macrostructure of metallic materials. It involves etching the surface of a metal part to reveal its macroscopic features, such as grain size, grain flows, inclusions, segregations, and different material discontinuities (surface cracks, laps, seams, porosity). By identifying these defects early on, manufacturers can take corrective measures to prevent further propagation or failure.

Macro etch examination is also performed on welds to assess quality and strength of the welded joints.

For welds, etching the cross section may reveal internal discontinuities, weld profile, extent of penetration and the quality of weld, Fig.51. The macro structural properties of a weld can be used for procedure qualification or personnel qualification.

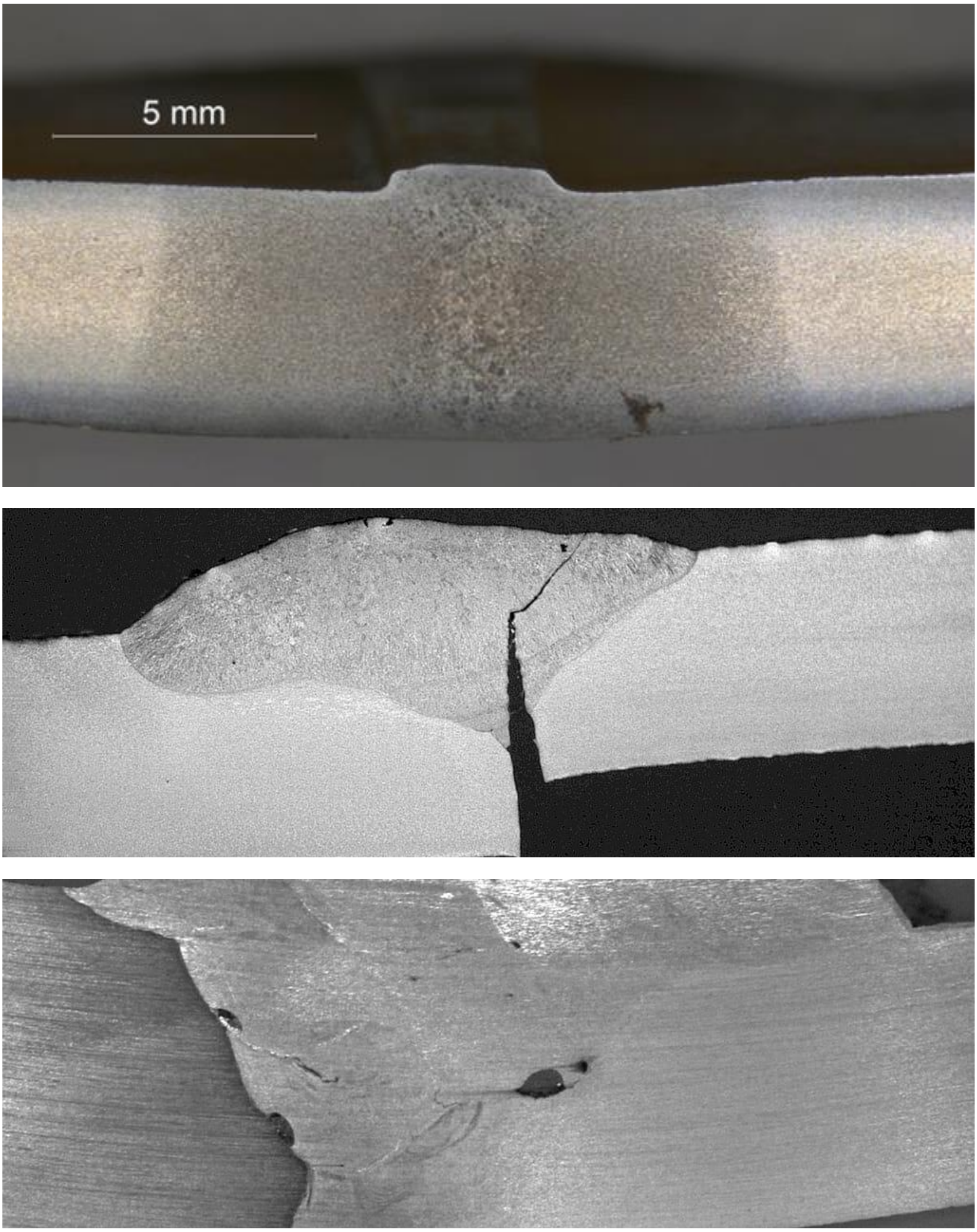

Fig. 51 Macro etch inspection of welded joints.

Fatigue life and impact strength in aerospace, automotive and other industrial applications is achieved by optimizing grain flow in forged components. Orienting the grain structure can enhance mechanical properties, boosting service life several times (this is one of the intrinsic benefits of forgings).

Fig. 52 Macro etch of forged parts, revealing the grain flow pattern.

Macro etch test, according to ASTM E340 is the controlled surface etching of a metal or alloy sample to reveal a structure such as grain flow lines and ingot patterns that are visible at the low magnification. Grain flow lines are the resulting fiber pattern observed in a hot or cold worked material, showing the manner in which the metal flowed during the forming process.

The machined part retains the unaltered grain structure of the original raw material, which creates the potential for weakness along the grain lines in the final part. In contrast, the cold forging compression process creates a reformed and strengthened grain structure to eliminate these weaknesses, Fig. 53.

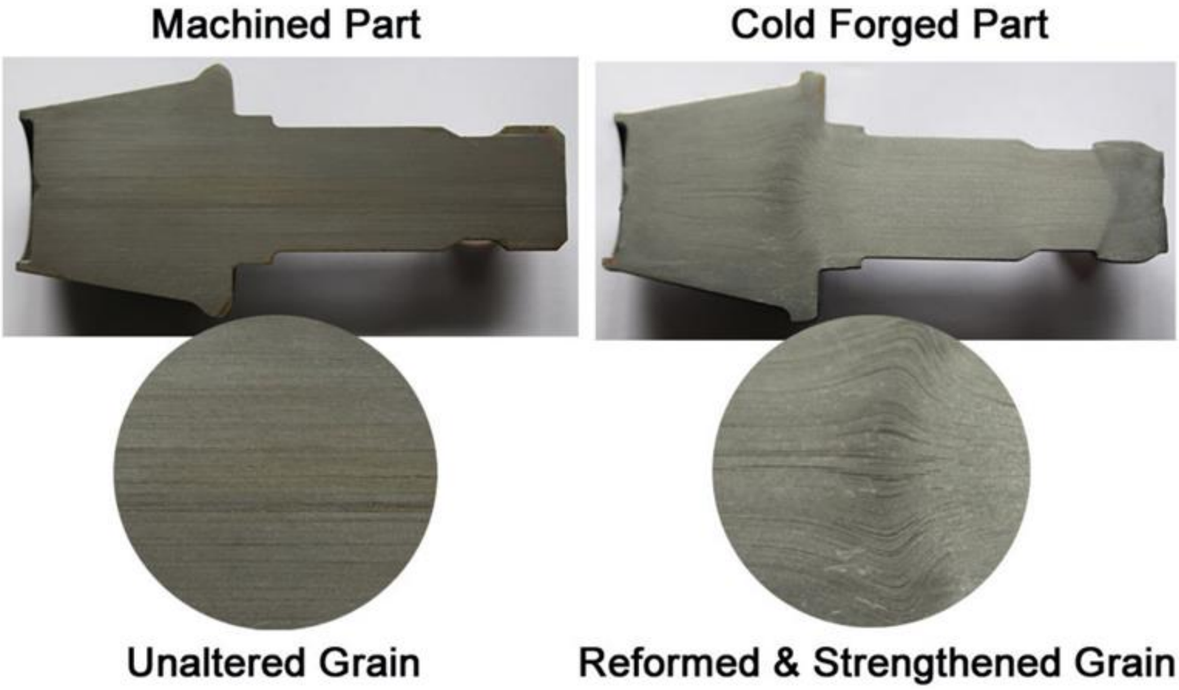

Fig. 53 Macroetch of a machined part vs. a cold forged part [more info].

Table 4. Macro Etching Agents [more info].

Etching name	Chemical composition		Designation
Oberhoffer	$FeCl_3$	7.2 gr.	Detection of phosphorus segregation (fiber flow) and visualization of the dendritic microstructure in steel. A thin, firmly adhering copper skin forms on the phosphorus-rich areas, which prevents acid attack. The P-segregations are not etched (thus remain white). Immersion or swabbing etch at 20ºC.
	$SnCl_2$	0.12 gr.	
	Hydrochloric acid	10 ml	
	Distiled water	120 ml	
	Ethanol	120 ml	
Adler	Copper ammonium chloride	9 gr.	Suitable for etching cast iron, high-alloy and corrosion-resistant steels as well as nickel alloys for visualization of welded joints and coarse grit. For etching 300 series stainless steel and Hastelloy superalloys. Immersion is recommended for several seconds.
	Hydrochloric acid	150 ml	
	$FeCl_3$	45 gr.	
	Distiled water	75 ml	
Frys	Hydrochloric acid	100 ml	Martensitic 400 series stainless steels. Grain flows for cold worked steels.
	Copper Chloride	12.5 gr.	
	Distilled Water	75 ml	
	Alcohol	65 ml	
Heyn	Copper ammonium chloride solution $Cl_4CuH_8N_2 \cdot 2\ H_2O$	10 ml	This a macro etchant rarely used nowadays to detect phosphorus segregations in steel. The phosphorus segregations are etched brown by the copper ammonium chloride solution. The copper precipitate that forms is removed under running water by rubbing with absorbent cotton. Repeated etching and wiping enhance the contrast.
	Distilled Water	100 ml	
Baumann print	Distilled water	100 ml	Sulfide inclusions. Soak photographic paper with the solution and press firmly onto the sample surface. After 3 min, rinse, photo fix, wash, and dry. Sulfur-rich regions will turn brown.
	Sulfuric acid (95–97%)	5 ml	

Examples of macroetched specimens:

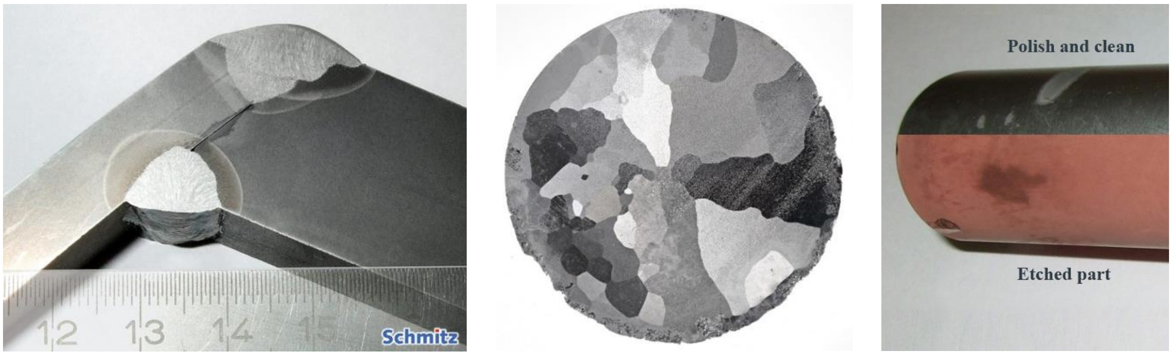

Macro etchant: Nital 5%

Nital is a macro etchant for welding joints and heat affected zone for mild and low alloy steels. Are available the following variants:

- Nital 5% (aq)
- Nital 5% (alc)
- Nital 10% (aq)

Macro etchant: NaOH

NaOH is used as a macro-etching agent for aluminum alloys for welded joints and grain formation on extrusions. It is available as NaOH 10% and NaOH 15%.

Macro etchant: Heyn

The presence of a dense compound layer on (gas) nitrided workpieces can be determined by means of the spot test (Heyn etchant).

Fig. 54 Macro etched specimens: low alloy steel, aluminum alloy, nitrided steel.

Chemically, the copper ammonium chloride ($Cl_4CuH_8N_2 \cdot 2 H_2O$) interacts with the nitriding zones of metallic specimens, resulting in visible discoloration. This discoloration is a direct response to the nitrogen content in the material, thus allowing qualitative analysis of the nitriding zones. The red coloration, see Fig. 54 (right picture) is due to a chemical reaction (copper is forced out of its compound by iron). This causes the free copper on the steel surface to precipitate. The spot test is a non-destructive testing method. Polished surfaces, however, become dull.

4.2. Working procedure

In the materials science laboratory are available a series of parts manufactured by using different technologies: hot and cold rolling, welding, casting, forging, extrusion, bar drawing, powder metallurgy. The students should be able to identify the technology used for fabrication of these parts (Fig.55), and to perform a macrostructural characterization can be applied for a specific purpose.

Fig. 55 Metallic parts manufactured by different technologies for macrostructural analysis.

Many of these parts contain a series of defects and imperfections. The students should identify on each part the visible defects based on a macrostructural analysis. They can take photos of these parts and prepare a short *e*-report with the identified material problems. The *e*-report should contain a brief description of the identified defects and their possible implications on the material performance and safety-related concerns. The *e*-report should refer also to the new technologies that can enhance the defects detection and reduce costs by automatization: machine vision, AI, machine learning algorithms, NDE methods, etc. The individual/team reports should be uploaded on the TEAM class.

4.3. Case study

Scope of discussion: highlighting the importance of the macrostructural characterization over large-scale features of materials, such as grain structure, segregation, and overall morphology; checking for surface defects, dimensional changes, and general appearance of the metallic parts.

Sayano-Shushenskaya dam[8] is considered as the most powerful hydroelectric power station in Russian Federation and one of the most powerful hydroelectric power stations in the world [more info].

---

[8] Sayano-Shushenskaya dam is the 6th most powerful hydroelectric power station in the world.

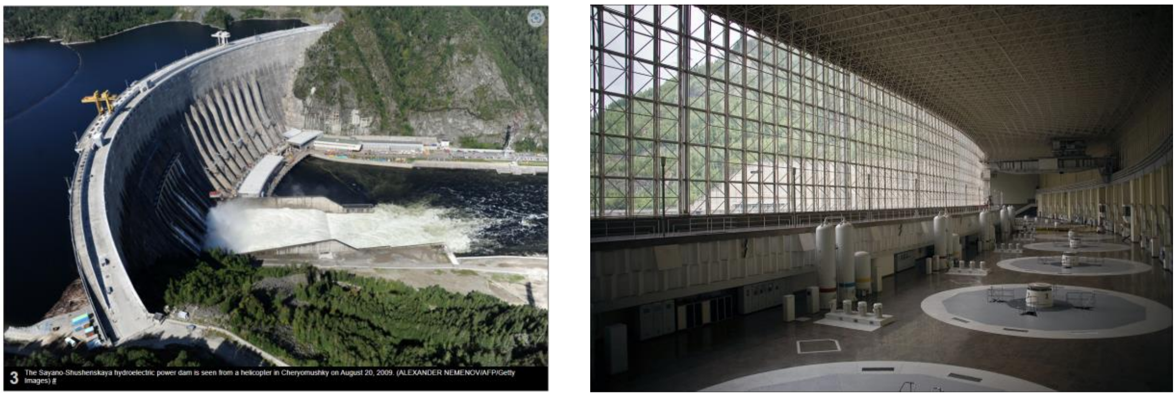

Fig. 56 The Sayano-Shushenskaya hydroelectric power dam and the Generator Hall seen before the accident occurred on 17 August 2009 [more info].

The Sayano–Shushenskaya hydroelectric power station accident occurred on 17 August 2009, when turbine from the Unit 2 of the Sayano–Shushenskaya hydroelectric power station near Sayanogorsk in Khakassia, Russia, broke apart violently. Under the 20 atmospheres of water pressure, the spinning turbine, with its cover, rotor, and upper parts, jumped out of the casing, destroying the machinery hall, the equipment in it, and the building. The turbine unit (for Unit 2) weighing 1,860 metric tons had flown 14 meters into the air (Fig. 57) after the screws (anchor bolts) holding it down had come loose, causing flooding and debris that killed dozens of workers in seconds.

As result, the turbine hall and engine room were flooded, the ceiling of the turbine hall collapsed, 9 of 10 turbines were damaged or destroyed, and 75 people were killed [press report].

Fig. 57 The turbine Unit 2 of the Sayano-Shushenskaya dam weighing 1,860 metric tons, spinning at 14 m in the air in the Generator Hall, destroying everything in its path [24].

Because of the gyroscopic effect, the spinning mass of 1,860 tons descended back into the turbine generator pit. The rotor then disintegrated, and the remains of the rotor spider became wrapped around the generator shaft, Fig.58.

The probable cause of the failure was excessive vibration causing long term fatigue of the bolts holding the turbine cover to the stayring. According to the 3rd October report, many of the bolts had major fatigue cracks. In the final moments they broke off in sequence until they could no longer contain the pressure under the turbine cover. At this point, the remaining bolts broke simultaneously. Inspection of the bolts after the accident revealed that several of them had cracked right through from long-term metal fatigue, some time before the accident. After the accident 49 recovered bolts (out of 80) were investigated, of which 41 had fatigue cracks. On 8 bolts, the fatigue damaged area exceeded 90% of the total cross-sectional area.

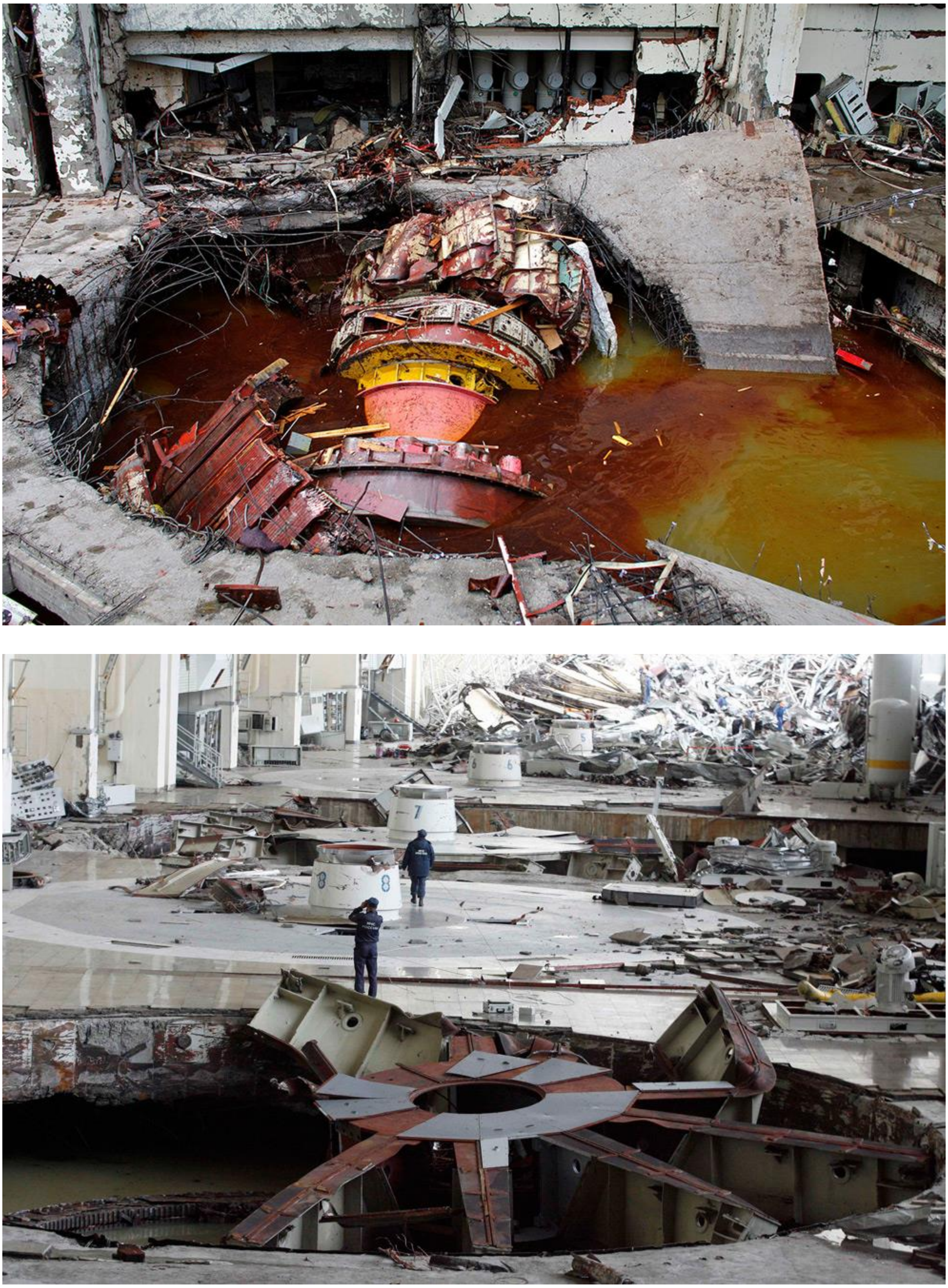

Fig.58 A general view of the damaged turbine Unit 2 and the generator hall of Sayano-Shushenskaya hydroelectric power station [24].

Others expertise’s in hydropower energy field: Hydropower (bryanleyland.co.nz)

Materials Science Laboratory

Materials Science and Engineering Department

eReport

Type of the work	Macrostructural characterization of metals and alloys
Scop of inspection	Short description: Macrostructural characterization
Specimen G17Mn2 EN 10213-2007	Photo/Microstructure 
Preparation Machined, non-etched	
Manufacturing Technology Cast Steel	
Magnification	
Equipment Magnifying glass 5X	
Observations Steel castings for pressure purposes	Specimen characterization. Results Analysis Identified defects, results of visual inspection: • Type of fracture • Origin of fracture • Presence of secondary cracks • Presence of external debris or corrosion products • Discoloration • Presence of wear marks in the vicinity of fracture • Plastic deformation preceding fracture • Dimensional changes in the component • Evidence of any overheating • Post-fracture damage such as rub marks.

Date:	Specialization:	Authorization Student Name

5. Determination of non-metallic inclusions in alloys

5.1. Theoretical background

Standards used for determination of non-metallic inclusion in steels:

- ASTM E45 - 18a. Standard Test Methods for Determining the Inclusion Content of Steel.
- ASTM E1245-03(2016). Practice for Determining the Inclusion or Second-Phase Constituent Content of Metals by Automatic Image Analysis.
- ISO 3763:1976 (reviewed 2023). Wrought Steels - Macroscopic Methods for Assessing the Content of Nonmetallic Inclusions.
- ISO 4967:2013. Steel - Determination of Content of Nonmetallic Inclusions - Micrographic Methods Using Standard Diagrams.
- SR EN 10247:2017. Micrographic examination of the non-metallic inclusion content of steels using standard pictures (english version)

The rating of non-metallic inclusions in steel is critical for many industrial applications. In structural applications (e.g. in construction, aerospace, automotive, oil-gas etc.), materials need to withstand loads without failing. Mechanical properties such as tensile strength, compressive strength, toughness, and elasticity are critical for assessing a material's structural integrity. Non-metallic inclusions disrupt the homogeneity of the steel's metallic matrix. They can have considerable impact on the steel's mechanical properties, affecting performance and lifetime cycle of the machines and equipment's. Therefore, rating non-metallic inclusions is important for evaluating steel quality in all industries.

Finding and assessing the non-metallic inclusions in steels can be challenging. Often a large sample area is inspected and detected inclusions of interest are analyzed in greater detail (by optical microscopy, EDX and XRD analysis).

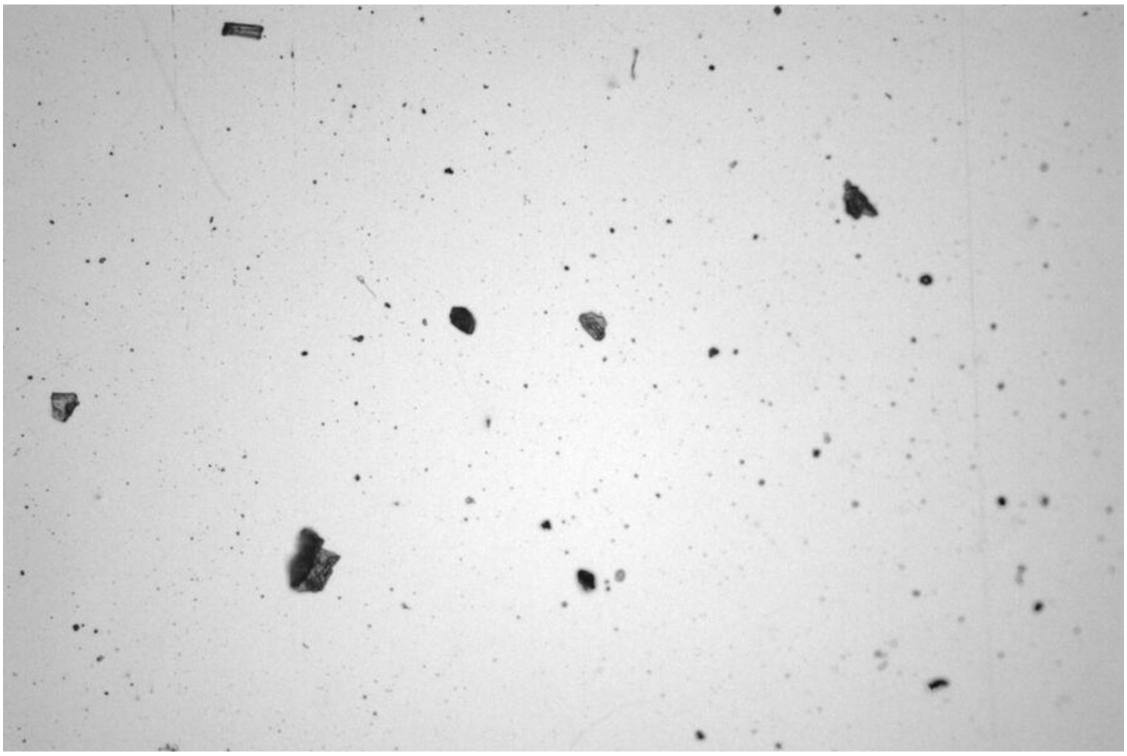

Fig. 59 General aspects of non-metallic inclusions in steel [photo credit].

Rating inclusions can take a long time and considerable effort, different standards requiring different inclusion classifications, mainly based on inclusion length or area. The length is typically defined as the largest inclusion dimension. However, there are various definitions for inclusion width which are often difficult to apply in optical microscope analysis. Thus, inclusions rating by visual comparison to references charts and manual measurement have some limits in results reproducibility [more info].

During the hot working process, individual inclusions and inclusion clusters are either deformed or fractured and dispersed depending on the inclusion plasticity. In Fig 60 is depicted cast and rolled morphology of various types of inclusions. Inclusions that have little to no plasticity at hot working temperatures include Al_2O_3, calcium aluminates, silica, and spinels. Clusters of inclusion particles are broken up and separated during hot working, resulting in oxide stringers elongated in the rolling direction. Individual hard oxide particles often exhibit voids in the rolling direction of the inclusion as illustrated in Fig. 60. Large globular oxide particles are more susceptible to the formation of these voids.

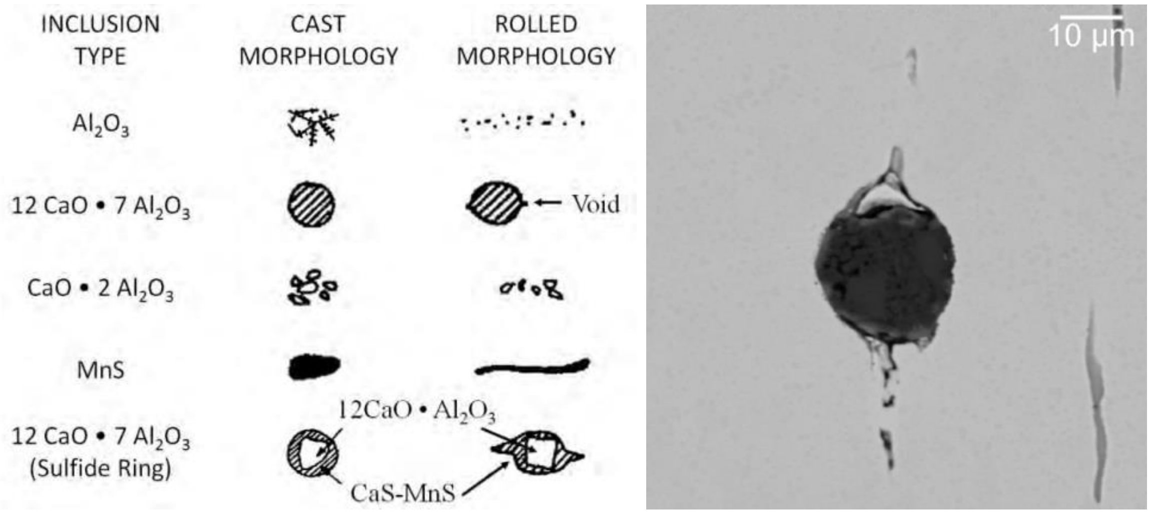

Fig. 60 Voids formation in hot rolled steel due to large globular oxide particles [27].

The macroscopic methods of determination of non-metallic inclusion include macro etch, fracture, step-down, and magnetic particle tests. The macroscopic test methods evaluate larger surface areas than microscopic test methods and because examination is visual or at low magnifications, these methods are best suited for detecting larger inclusions, Fig. 61.

Fig. 61 Exogenous non-metallic inclusion in cast steel [30].

Exogenous inclusions are originating from outside of the melt, e.g. furnace lining, mould sand or slag/oxides in the feed material, while endogenous inclusions are caused by a reaction of the molten metal or alloy with dissolved gases within the melt oxygen, sulphur, or nitrogen.

Macroscopic methods are not suitable for detecting inclusions smaller than about 400 μm in length and the methods do not discriminate inclusions by type.

- Macro-etch Test. The macro-etch test is used to indicate inclusion content and distribution, usually in the cross section or transverse to the direction of rolling or forging. Only large oxides are revealed by this test method.
- Fracture Test. The fracture test is used to determine the presence and location of inclusions as shown on the fracture. ISO 3763 provides a chart method for fracture surface inclusion ratings. In some instances, indications as small as 400 μm in length are recorded. Blue fracture testing is an historically well-established technique used to reveal macro inclusions larger than 0.5 mm. It is performed on a bar cross-section area that has been hardened, fractured and then tempered blue to increase the visibility of defects [29].
- Step-Down Method. The step-down test method is used to determine the presence of inclusions on machined surfaces of rolled or forged steel. The test sample is machined to specified diameters below the surface and surveyed for inclusions under good illumination with the unaided eye or with low magnification. This test is essentially used to determine the presence of inclusions 3 mm in length and longer.
- Magnetic Particle Method. The magnetic particle method is a variation of the step-down method for ferromagnetic materials in which the test sample is machined, magnetized, and magnetic powder is applied. Discontinuities as small as 0.40 mm in length create magnetic leakage fields that attract the magnetic powder, thereby outlining the inclusion.

The microscopic methods include five generally accepted methods of examination (**Method A, B, C, D and E**). In these microscopic methods, inclusions are assigned to a category based on similarities in morphology, and not necessarily on their chemical identity. Inclusions are characterized by size, shape, concentration, and distribution rather than chemical composition [26].

Microscopic methods are used to characterize the size, distribution, number, and type of inclusions on a polished specimen surface. The microscopic methods place non-metallic inclusions into one of several composition related categories sulfides, oxides, and silicates.

In these microscopic methods, **inclusions are classified into four categories** (called **Type**) **based on their morphology** and two subcategories based on their width or diameter (**Heavy** and **Thin**), Fig. 62:

- A - Sulfide Type,
- B - Alumina Type,
- C - Silicate Type
- D - Globular Oxide Type

The non-metallic inclusions are partitioned into **Severity Levels** based on the number or length of the particles present in a 0.50 mm^2 microscope field of view, see Table 5 [26].

Methods of specimen preparation must be such that a polished, microscopically flat section is achieved in order that the sizes and shapes of inclusions are accurately shown. To obtain satisfactory and consistent inclusion ratings, the specimen must have a polished surface free of artifacts such as pitting, foreign material (for example, polishing media), and scratches. When polishing the specimen it is very important that the inclusions not be pitted, dragged, or obscured [26].

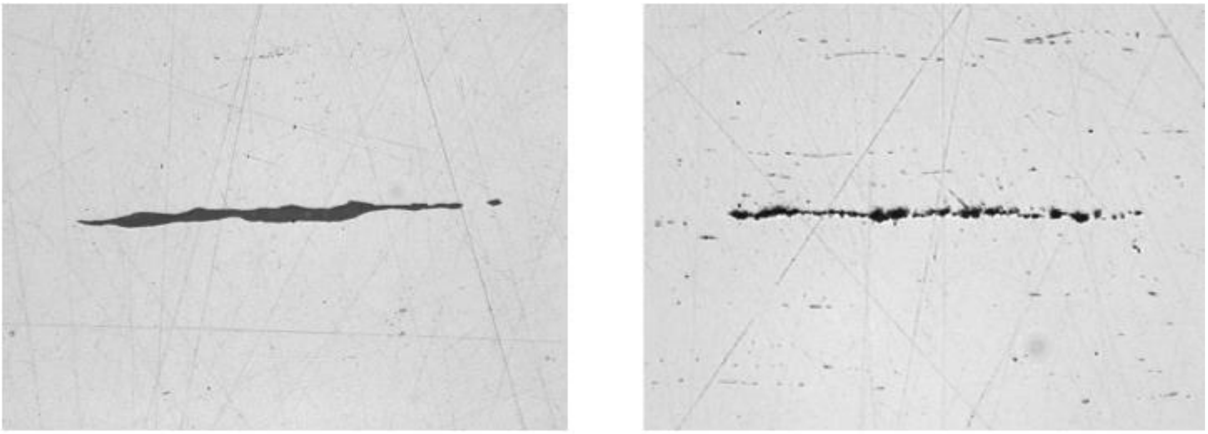

A) Sulfide

B) Alumina

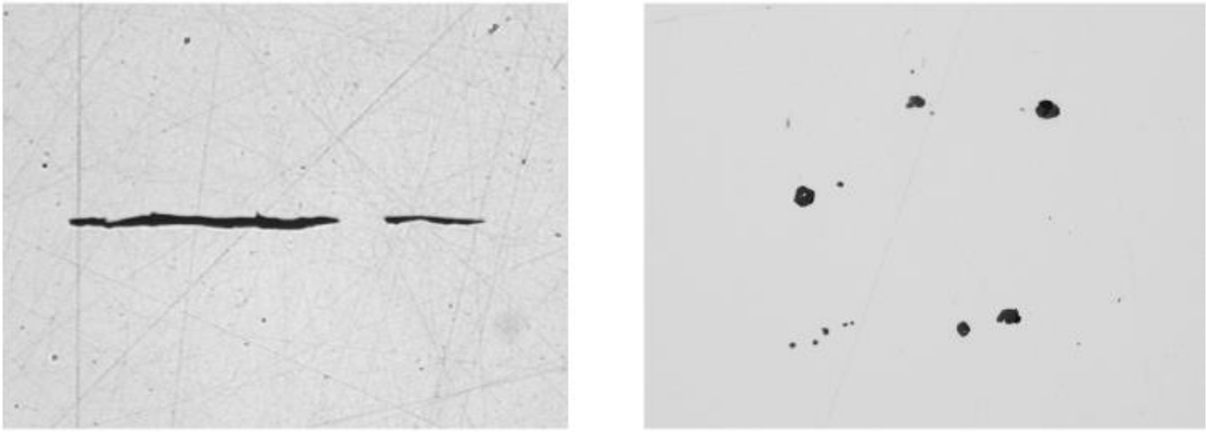

C) Silicate

D) Globular Oxide

Fig. 62 Morphological features of different types of oxides [31].

A disadvantage of the microscopic methods is that individual rating fields are very small (0.50 mm^2), see Fig. 64, thus, in case of large specimen characterization it would take a prohibitive number of fields to provide any statistical confidence [26, 28, 29].

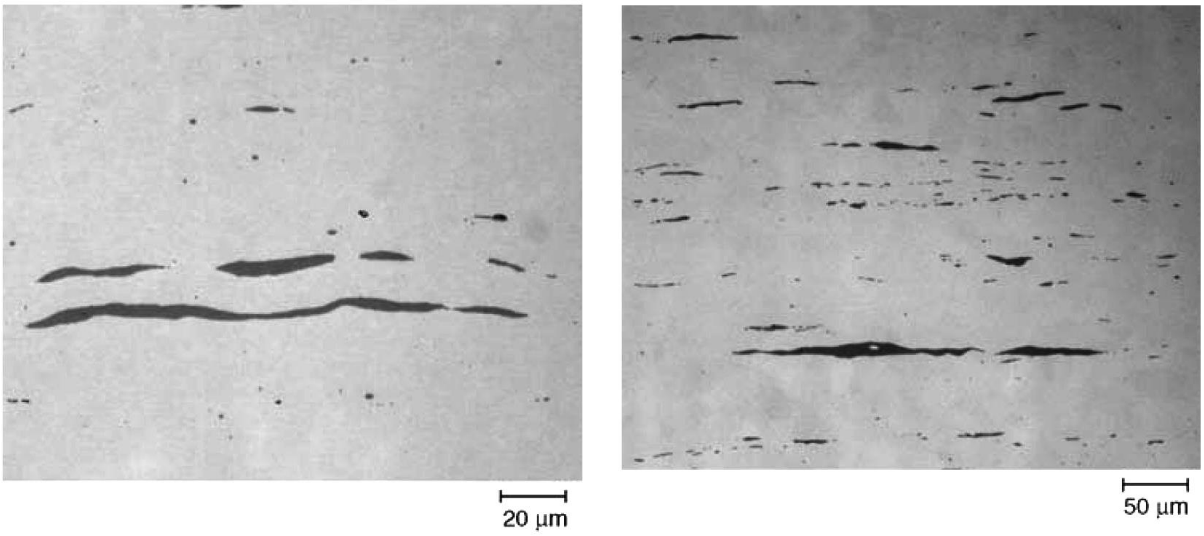

Fig. 63 Manganes sulfides in stainless steel [25].

The first systematic rating of inclusions in steel was developed in Sweden by the Swedish Ironmasters' Association called Jernkontoret (literally Iron Office). It has become known as the **JK inclusion rating system**, derived from the association's name [28].

TABLE 5 Minimum Values for Severity Level Numbers (Methods A, D, and E)^{A,B}

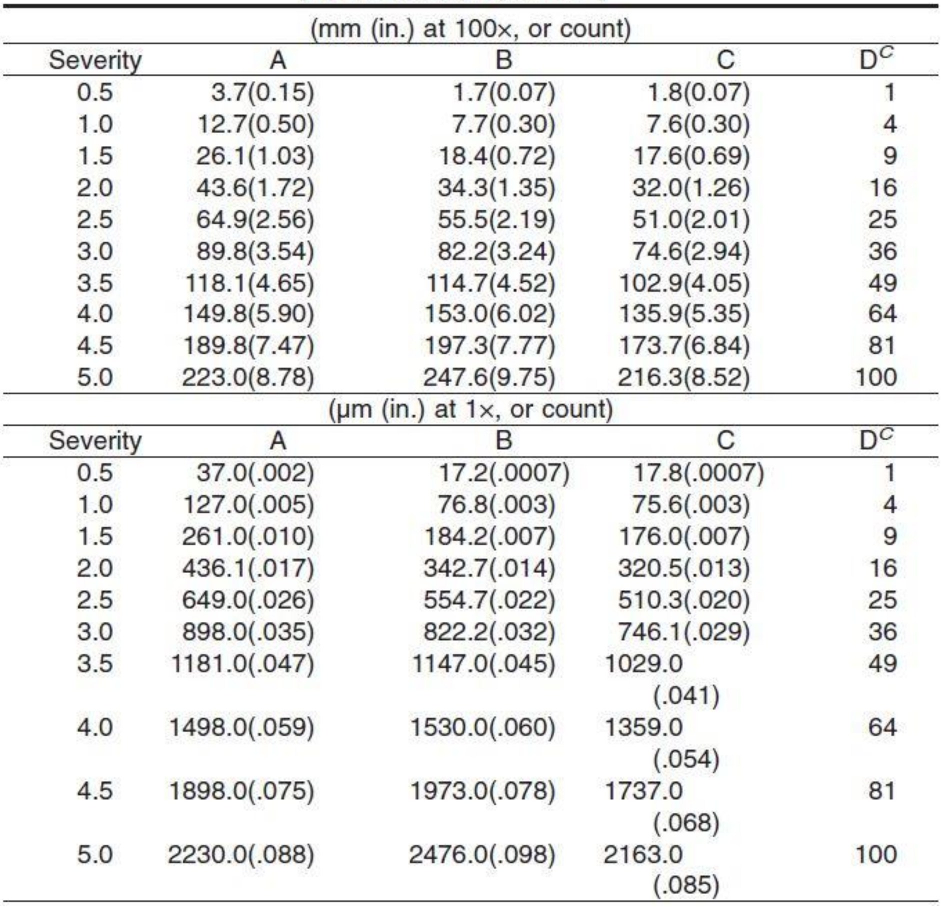

(mm (in.) at 100×, or count)				
Severity	A	B	C	D^{C}
0.5	3.7(0.15)	1.7(0.07)	1.8(0.07)	1
1.0	12.7(0.50)	7.7(0.30)	7.6(0.30)	4
1.5	26.1(1.03)	18.4(0.72)	17.6(0.69)	9
2.0	43.6(1.72)	34.3(1.35)	32.0(1.26)	16
2.5	64.9(2.56)	55.5(2.19)	51.0(2.01)	25
3.0	89.8(3.54)	82.2(3.24)	74.6(2.94)	36
3.5	118.1(4.65)	114.7(4.52)	102.9(4.05)	49
4.0	149.8(5.90)	153.0(6.02)	135.9(5.35)	64
4.5	189.8(7.47)	197.3(7.77)	173.7(6.84)	81
5.0	223.0(8.78)	247.6(9.75)	216.3(8.52)	100

(µm (in.) at 1×, or count)				
Severity	A	B	C	D^{C}
0.5	37.0(.002)	17.2(.0007)	17.8(.0007)	1
1.0	127.0(.005)	76.8(.003)	75.6(.003)	4
1.5	261.0(.010)	184.2(.007)	176.0(.007)	9
2.0	436.1(.017)	342.7(.014)	320.5(.013)	16
2.5	649.0(.026)	554.7(.022)	510.3(.020)	25
3.0	898.0(.035)	822.2(.032)	746.1(.029)	36
3.5	1181.0(.047)	1147.0(.045)	1029.0 (.041)	49
4.0	1498.0(.059)	1530.0(.060)	1359.0 (.054)	64
4.5	1898.0(.075)	1973.0(.078)	1737.0 (.068)	81
5.0	2230.0(.088)	2476.0(.098)	2163.0 (.085)	100

The microscopic methods in ASTM E45 [26] are using refined comparison charts: **Method A** (Worst Fields), **Method D** (Low Inclusion Content) and **Method E** (SAM Rating) use charts based on the JK chart, while **Method C** (Oxides and Silicates) uses the SAE chart. ISO Standard 4967 also uses the JK chart[9]. **Method B** (Length) is used to determine inclusion content based on their length. Only inclusions 0.127 mm or longer are recorded regardless of their type. From this method one may obtain data such as length of the longest inclusion and average inclusion length.

No chart can represent all the various types and forms of inclusions. The use of any chart is thus limited to determining the content of the most common types of inclusions, and it must be kept in mind that such a determination is not a complete metallographic study of inclusions [26].

The European Standard EN 10247:2017 defines a method of microscopic non-metallic endogenous inclusion assessment using picture charts. The method does not apply to particles of a length or diameter less than 3,0 µm or a width smaller than 2,0 µm. However, based on specific product standard or an agreement between the involved parties for certain special products, inclusions with a width below 2,0 µm can be evaluated by length alone [26].

---

[9] JK Chart - Jernkontoret's inclusion chart II for quantitative assessment of the content of non-metallic inclusions in metals and alloys [Swedish Institute for Standards].

5.2. Working procedure

The microscopic methods are not intended for assessing the content of exogenous inclusions (those from entrapped slag or refractories). For that types of inclusions could be applied methods like Ultrasonic Testing or one of the macroscopic methods previously described.

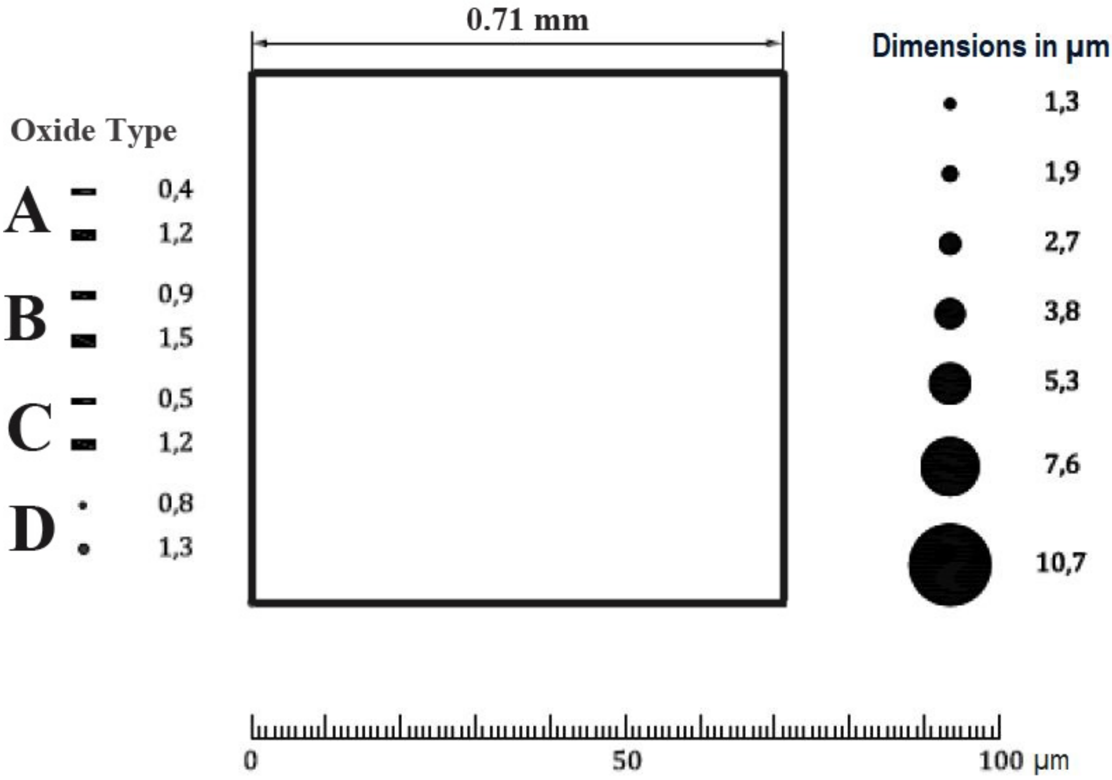

Fig. 64 Pattern reticle for microscope eyepieces with the test grid area is 0,50 mm^2 at the image plane [26].

The four categories or Types are partitioned into Severity Levels based on the number or length of the particles present in a 0.50 mm^2 field of view. A graphic representation of the maximum thickness of the Thin and Heavy series of Types A, B, C, and D is on the left. Several oversized Type D are depicted on the right, Fig. 64 and Table 5.

Depending on the method used for microstructure analysis, the examination with the microscope may use one of two practical methods below:

- by projection on to ground glass,
- by observation by means of an eyepiece, see Fig.64.

The image within the test square is compared to the standard pictures on the chart:

- Fig. 66 and Fig. 67 for Type A inclusions (sulfides)
- Fig. 68 and Fig. 69 for Type B inclusions (aluminates)
- Fig. 70 for Type C inclusions (silicates)
- Fig. 71 for Type D inclusions (globular types)

Each chart depicts the inclusions for Thin and Heavy series, for each type of oxides groups (A, B, C, or D). The students should measure the total length of oxides (µm) in the field, then based on the result obtained, they should rate the inclusion severity level accordingly (i=0.5 … 5.0).

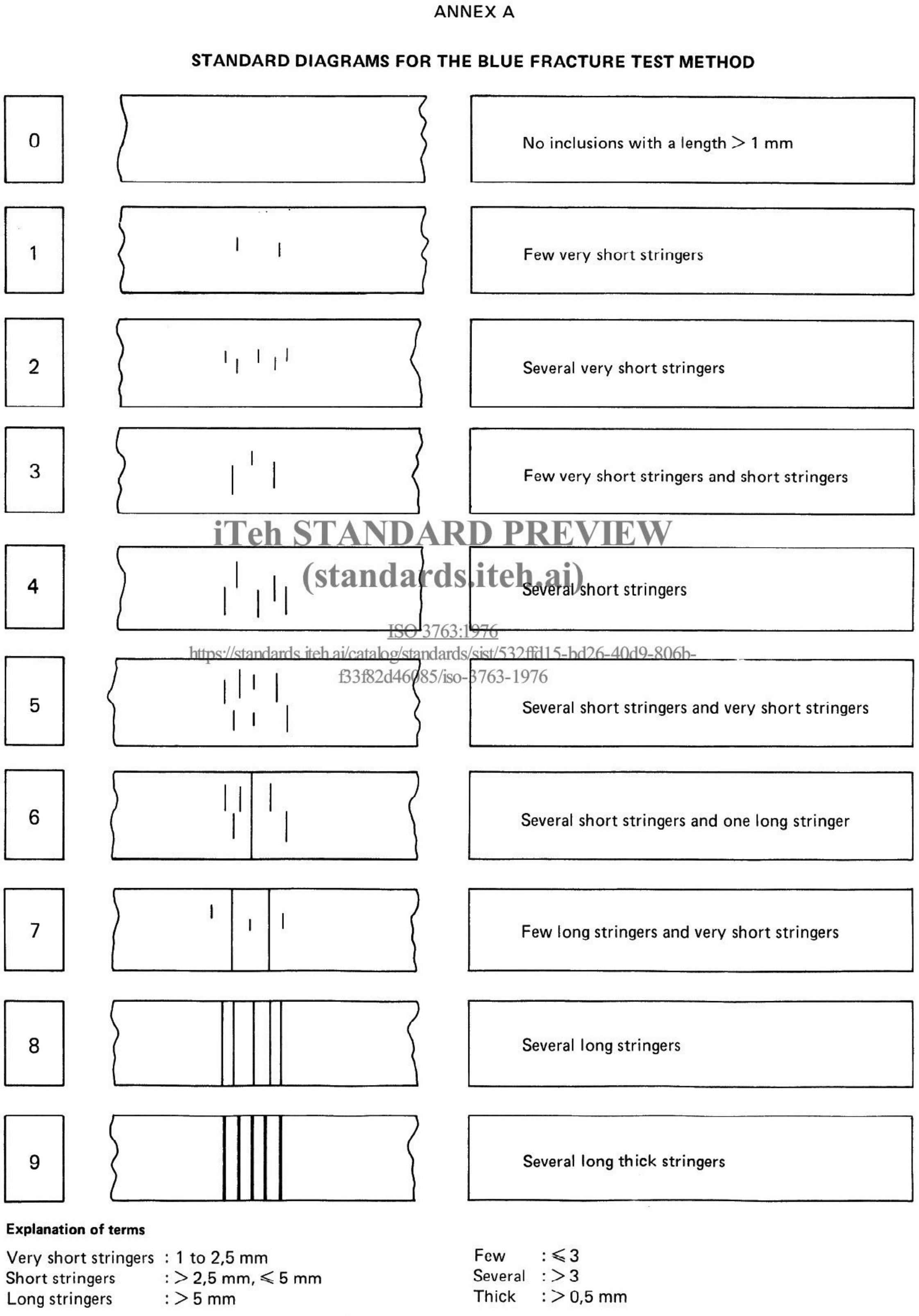

ANNEX A

STANDARD DIAGRAMS FOR THE BLUE FRACTURE TEST METHOD

0	No inclusions with a length > 1 mm
1	Few very short stringers
2	Several very short stringers
3	Few very short stringers and short stringers
4	Several short stringers
5	Several short stringers and very short stringers
6	Several short stringers and one long stringer
7	Few long stringers and very short stringers
8	Several long stringers
9	Several long thick stringers

Explanation of terms

Very short stringers : 1 to 2,5 mm
Short stringers : > 2,5 mm, ⩽ 5 mm
Long stringers : > 5 mm

Few : ⩽ 3
Several : > 3
Thick : > 0,5 mm

Fig. 65 Blue Fracture Test Method Chart, for rating macro inclusions larger than 0.5 mm [32].

Fig. 66 ISO Chart diagram for Sulfide Inclusions, Type A. Total sulfide lengths per field is measured [33].

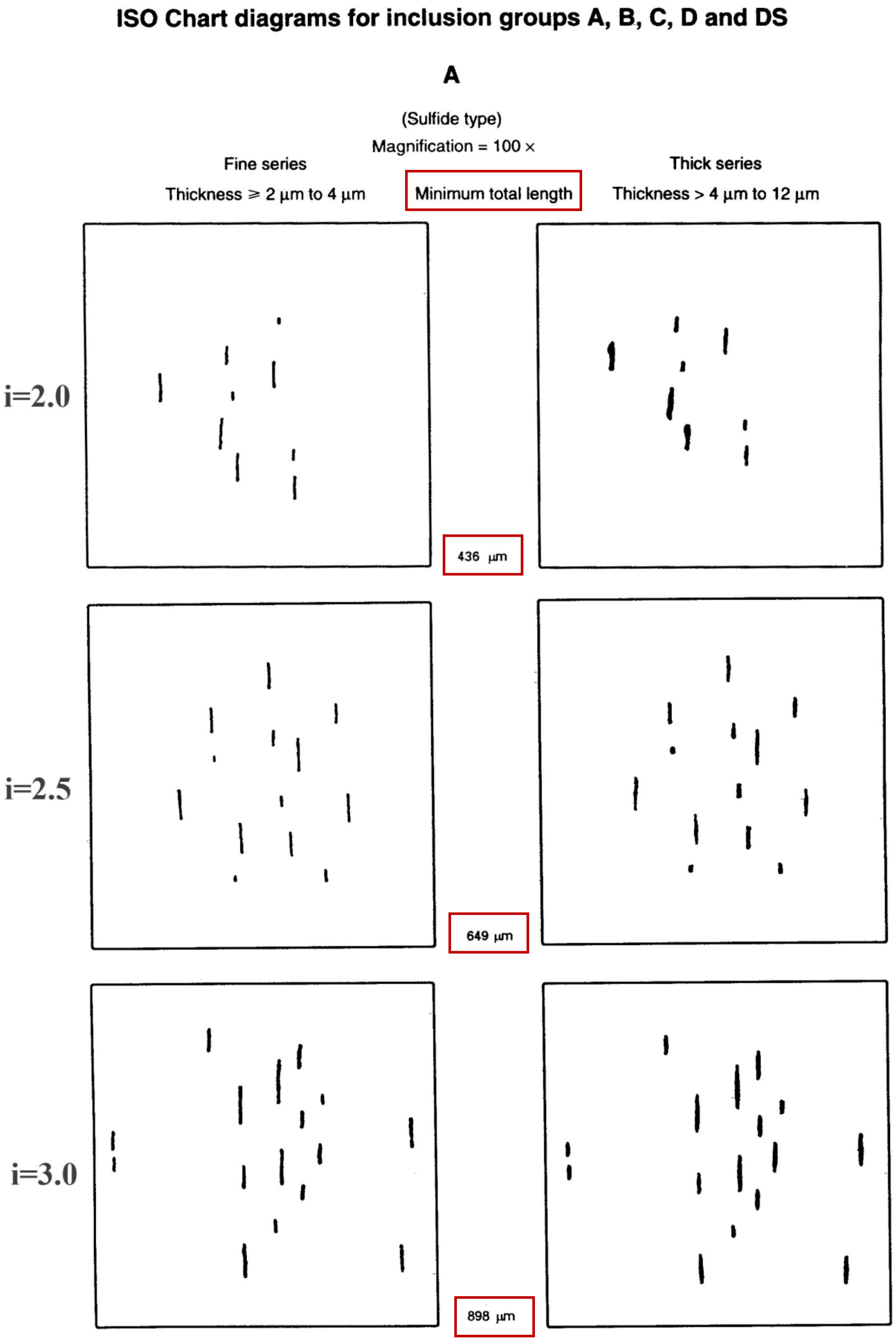

Fig. 67 ISO Chart diagram for Sulfide Inclusions, Type A. Total sulfide lengths per field is measured [33].

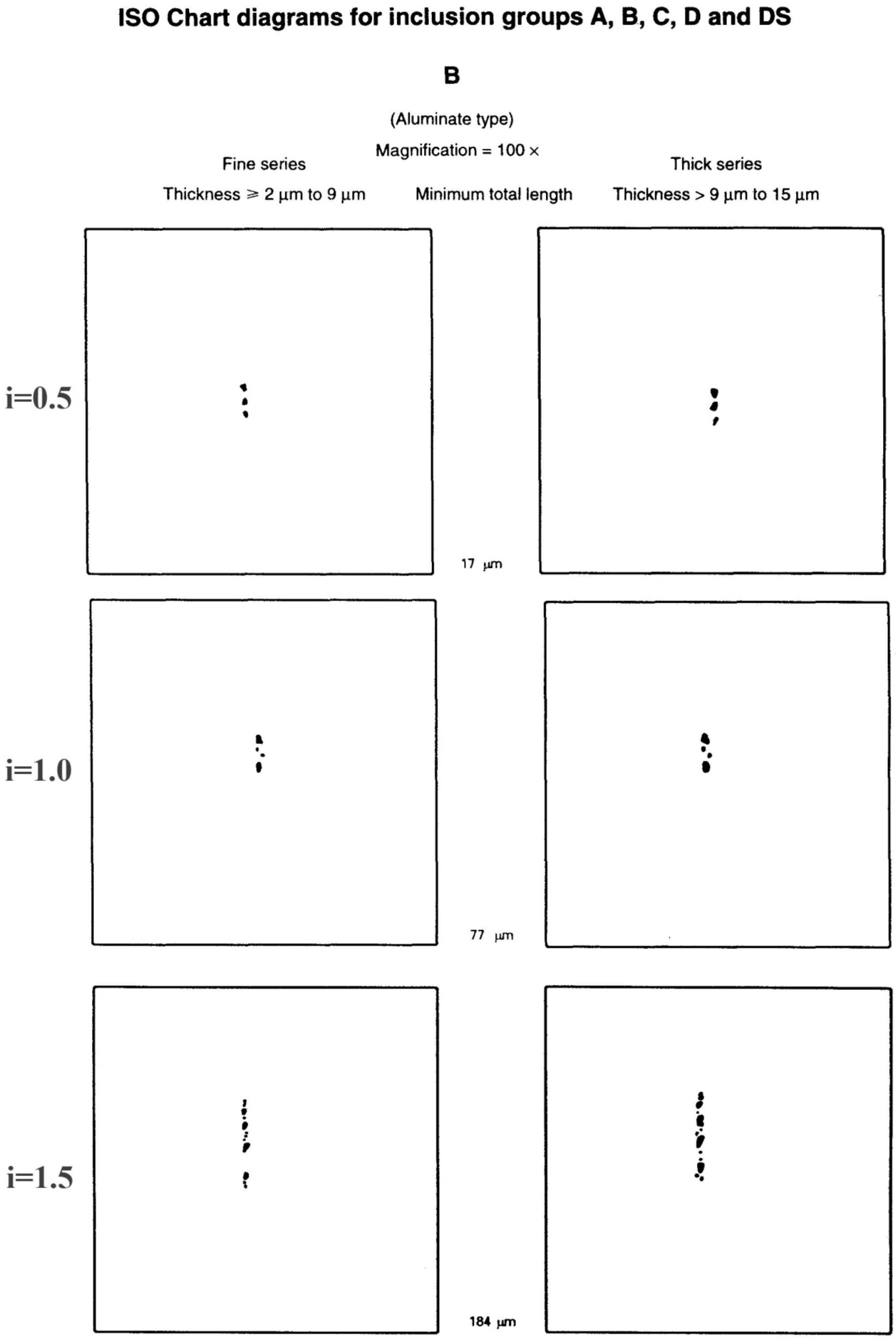

Fig. 68 ISO Chart diagram for Aluminate Inclusions, Type B. Total length of fragmented stringer inclusions per field is measured [33].

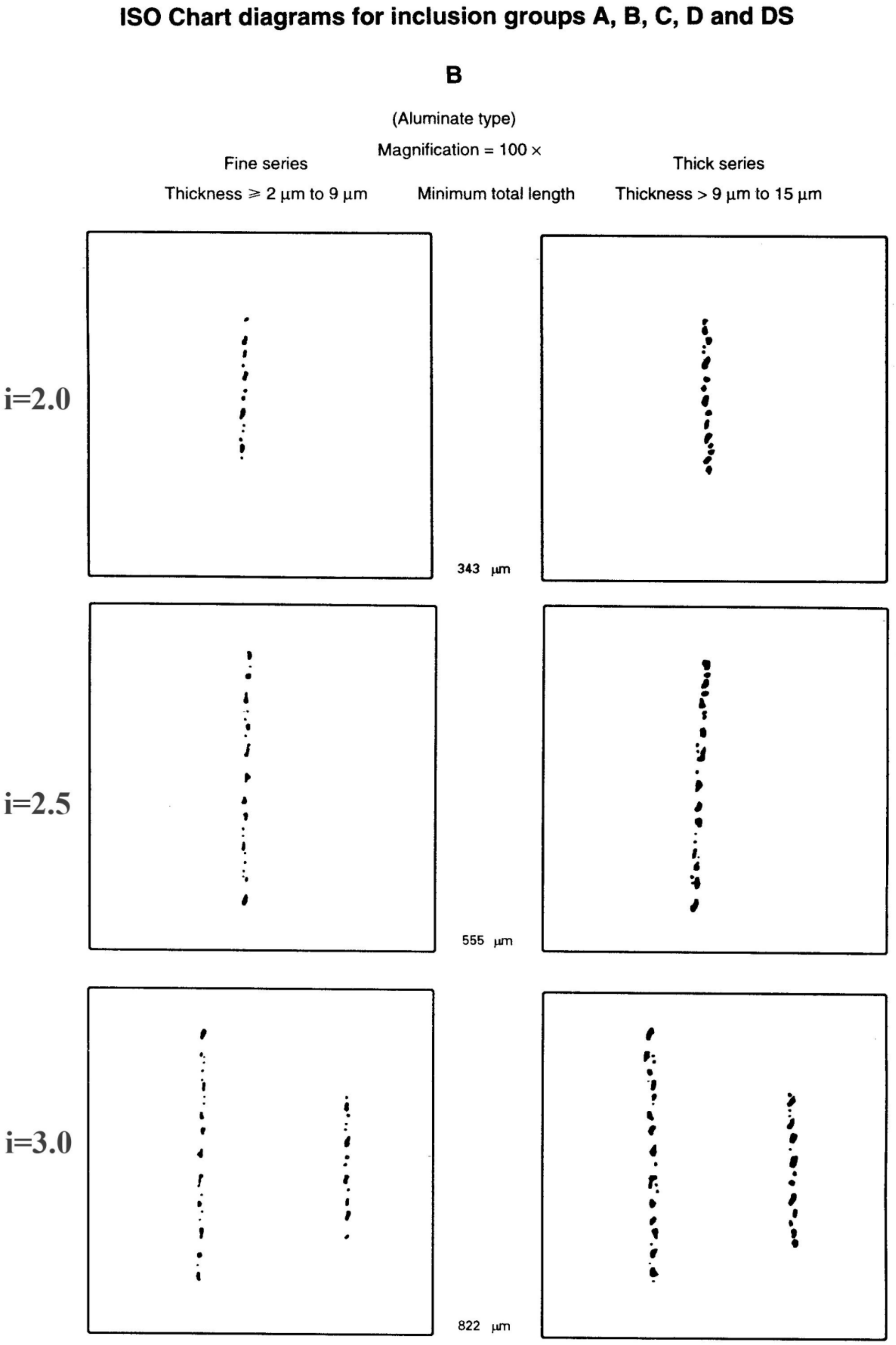

Fig. 69 ISO Chart diagram for Aluminate Inclusions, Type B. Total length of fragmented stringer inclusions per field is measured [33].

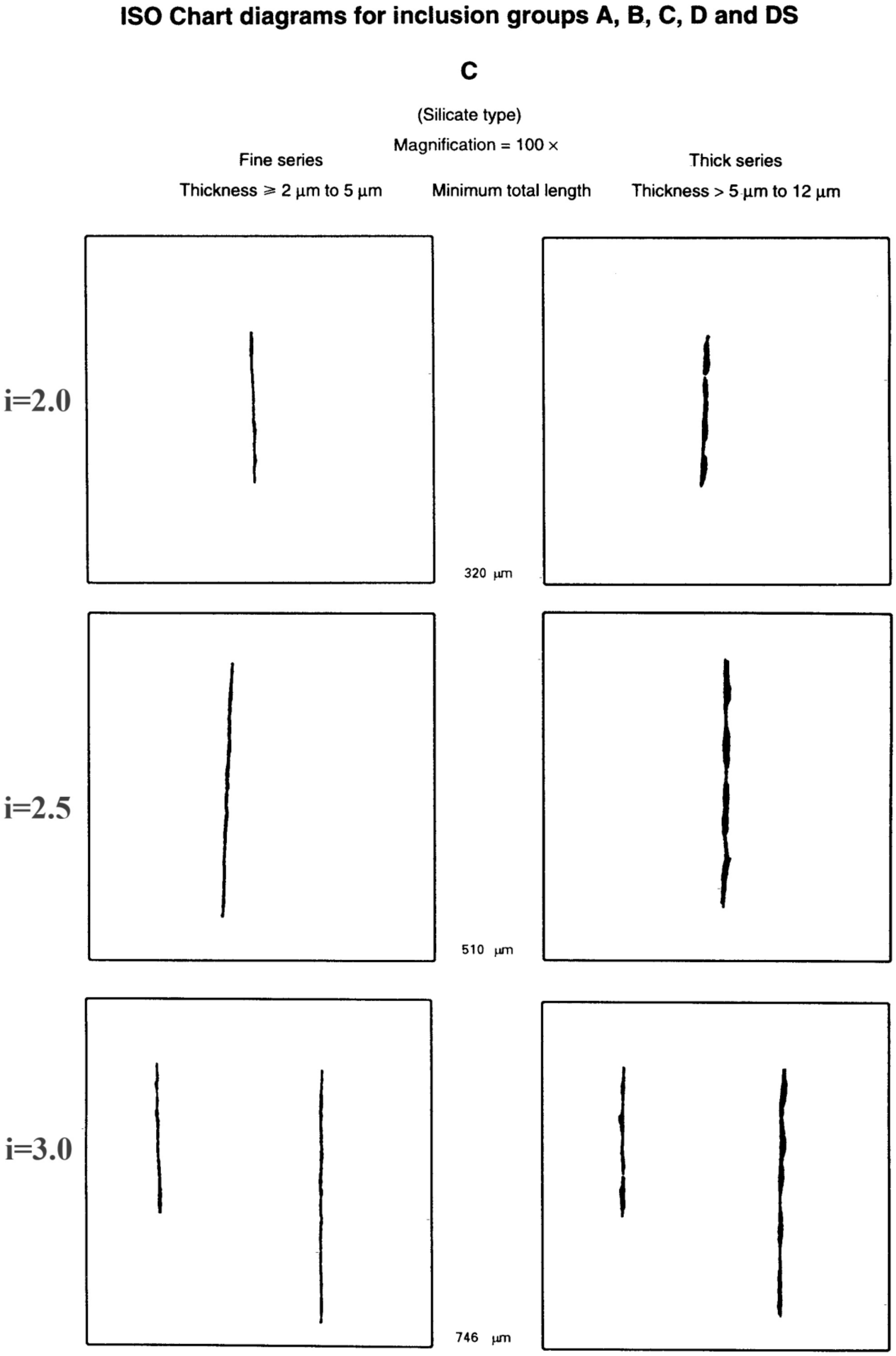

Fig. 70 ISO Chart diagram for Silicates Inclusions, Type C. Total length of fragmented stringer inclusions per field is measured [33].

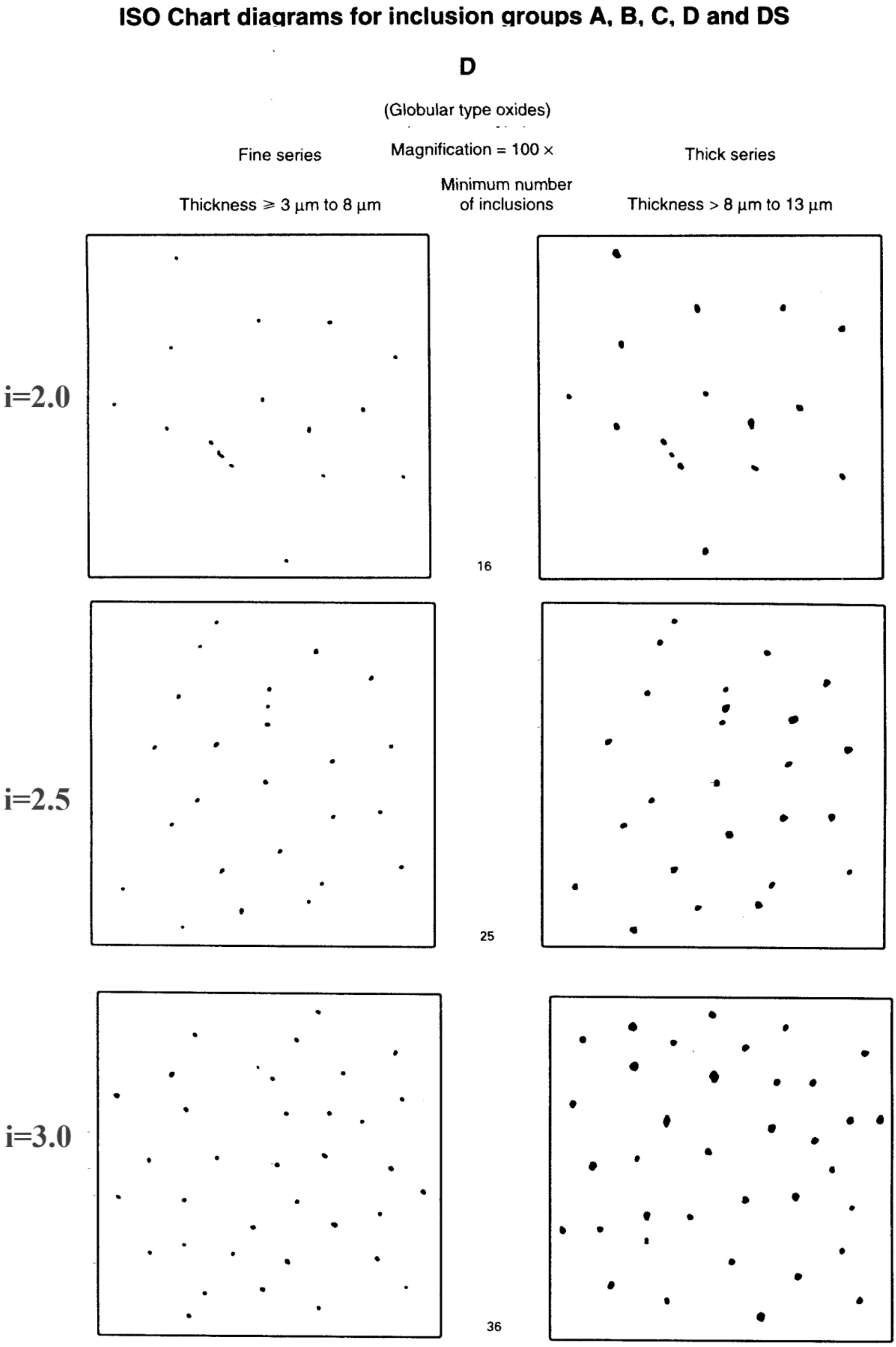

Fig. 71 ISO Chart diagram for Globular Inclusions, Type D [33].

5.3.Discussion and results interpretation

Materials Science Laboratory

Materials Science and Engineering Department

eReport

Type of the work	Determination of non-metallic inclusions in steels
Scop of inspection	Short description of the work:
Specimen Steel designation	Photo/Microstructure 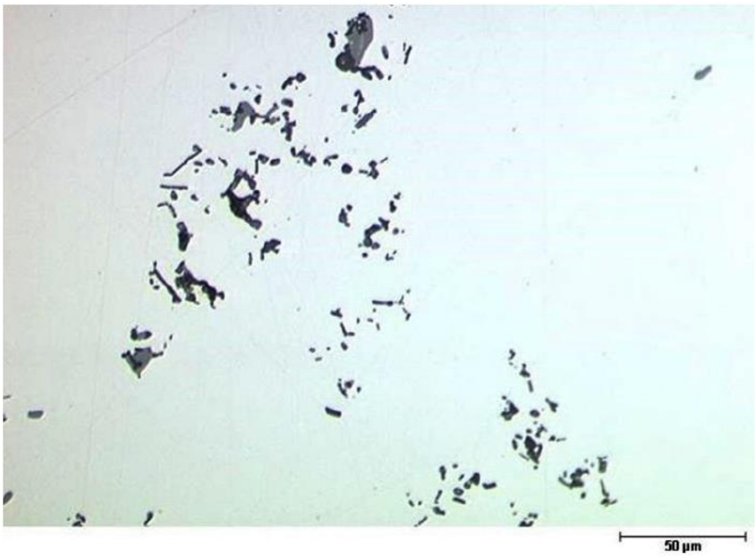
Preparation Polished, non-etched	
Manufacturing Technology Rolled Steel	
Magnification 100 X	
Equipment Metallographic microscope	
Observations Method of examination (A,B,C,D, E) Standard used: ASTM E45 - 18a ASTM E1245 ISO 3763:1976 ISO 4967:2013. SR EN 10247:2017 The number of observed fields or the total area examined____________	Specimen characterization. Results Analysis Non-inclusion type (A, B, C, D), Thin/Heavy During reduction from the cast shape by rolling or forging, the inclusions are elongated and broken up according to the degree of reduction of the steel cross section. In reporting results of inclusion determinations, therefore, the size, shape, and method of manufacture of the steel from which the specimens were cut must be stated.

Date:	Specialization:	Authorization Student Name

Selection of Analysis Method

Specimen preparation

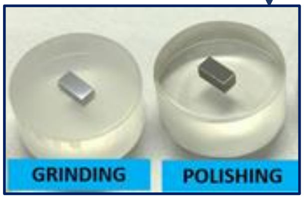

Method A (Worst Fields)

Method B (Length)

Method C (Oxides and Silicates)

Method D (Low Inclusion Content)

Method E (SAM Rating)

Selection of examination method.

All methods require a survey of a 160 mm^2 polished surface area of the specimen at 100X. The field size shall equal an area equivalent to 0.50 mm^2 on the specimen surface as defined by a square with 0.71 mm sides, Fig.64.

Method A (Worst Fields)

Each field is compared to the square fields depicted in Fig.66 to Fig.71 in a search for the worst field, that is, the highest severity rating of each inclusion Type A, B, C, and D for both the Thin and Heavy series.

Method B (Length)

This method utilizes a pattern of parallel lines, the distance between lines is equivalent to 0.127 mm on the specimen surface when viewed at 100×. This distance shall be referred to as one unit. Only inclusions in this field that are one unit long or longer are measured.

Method C (Oxides & Silicates)

The non-deformable alumina oxide and deformable silicate stringers and rated by comparison SAE Charts. The longest stringer of each inclusion type (“O” for alumina oxides and “S” for silicates) shall be reported.

Method D (Low Inclusion Content)

This test method is intended for application to steel with low inclusion contents. Every square 0.50 mm^2 field on the polished surface is examined for inclusion Types A, B, C, and D and compared with the square fields depicted on ISO Charts. Record the Severity Level Number for each inclusion type (A, B, C, and D) that most resembles the field under observation.

Method E (SAM Rating)

This test method is used to rate the inclusion content of steels in a manner that reflects the severity and frequency of occurrence of the larger B and D-Type inclusions based on JK Charts. It will result in a survey of a 160 mm^2 polished surface of the specimen at 100×.

Notes:

1. Method A (Worst Fields) is a rating in which the specimen is rated for each type of inclusion by assigning the value for the highest severity rating observed of that inclusion type, anywhere on the specimen surface.
2. Method B (Length) is used to determine inclusion content based on their length. Only inclusions 0.127 mm or longer are recorded regardless of their type.
3. Method C (Oxides and Silicates) uses the SAE[10] Charts (SAE Recommended Practice J422 of the SAE Handbook).

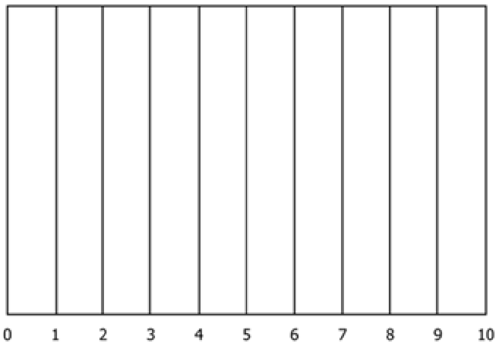

NOTE 1—One unit equals 0.127 mm (0.005 in.) on the specimen surface.

Suggested Reticle or Overlay Grid for Method B

---

[10] SAE International, formerly named the Society of Automotive Engineers, is a United States-based, globally active professional association and standards developing organization for engineering professionals in various industries.

5.4. Case study

5.4.1. The Metallurgy of the RMS Titanic

The Titanic ship was assembled using some 3,000,000 hydraulically driven rivets. These were drawn from wrought iron, a mass of iron and iron silicate that extruded into a layered structure. These rivets were made of wrought iron, which consists of a relatively pure iron matrix containing 2-3% (by volume) iron silicate slag.

Quantitative metallography was performed on a cross-section of a hull rivet that had been cut and polished. This showed that this rivet contained 9.3% ±0.3% slag on average, which is more than 3 times the amount normally expected in wrought iron [34].

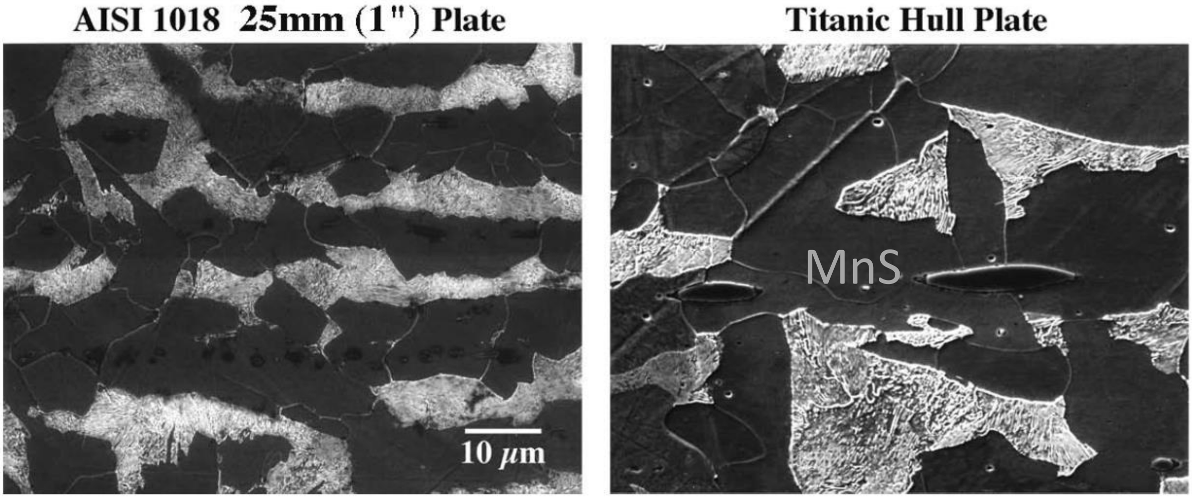

Scanning electron microscope image of the polished and etched longitudinal sections of steel from the hull of the *Titanic*, and for comparison a modern hot-rolled 25 mm (1") AISI 1018 plate. Note the differences in grain size, pearlite lamella spacing, and MnS particle sizes.

Fig. 72 Metallurgy of the RMS Titanic, NIST Interagency/Internal Report [34].

MnS and oxide particles are evident throughout the material, and were quite large, occasionally exceeding 100 μm in length. The MnS particles were deformed into lenticular shapes instead of being melted into stringers. Cleavage patches on the surface, made up of 4 to 15 cleaved grains, were seen to originate at fractured MnS particles.

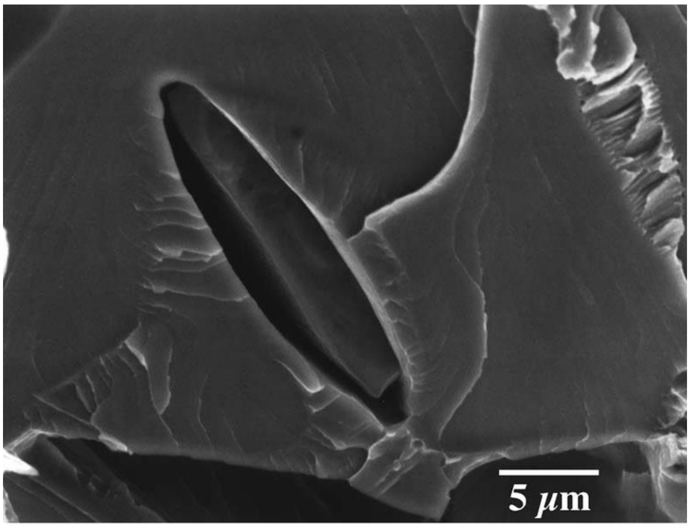

Fig. 73 SEM fractograph showing the MnS particle that fractured and nucleated a patch of 15 cleaved grains [34].

The steel from the Titanic hull presents a ferritic-pearlitic microstructure, with large ferrite grains (ASTM number 4 to 5, 100 µm to 130 µm equivalent diameter) and large, coarse pearlite colonies (roughly 0.2 µm lamella thickness). The microstructure shows a large amount of banding in the rolling direction. The slag had an almost bimodal type of distribution of sizes, ranging from a large amount in very long stringers (>200 µm long) to many small oblate spheroid particles (1 µm to 5 µm diameter). The mechanical behavior of wrought iron, and especially the fracture behavior, is known to be highly anisotropic, and in the transverse orientation of rivets, the slag stringers present a very large area that can nucleate a crack.

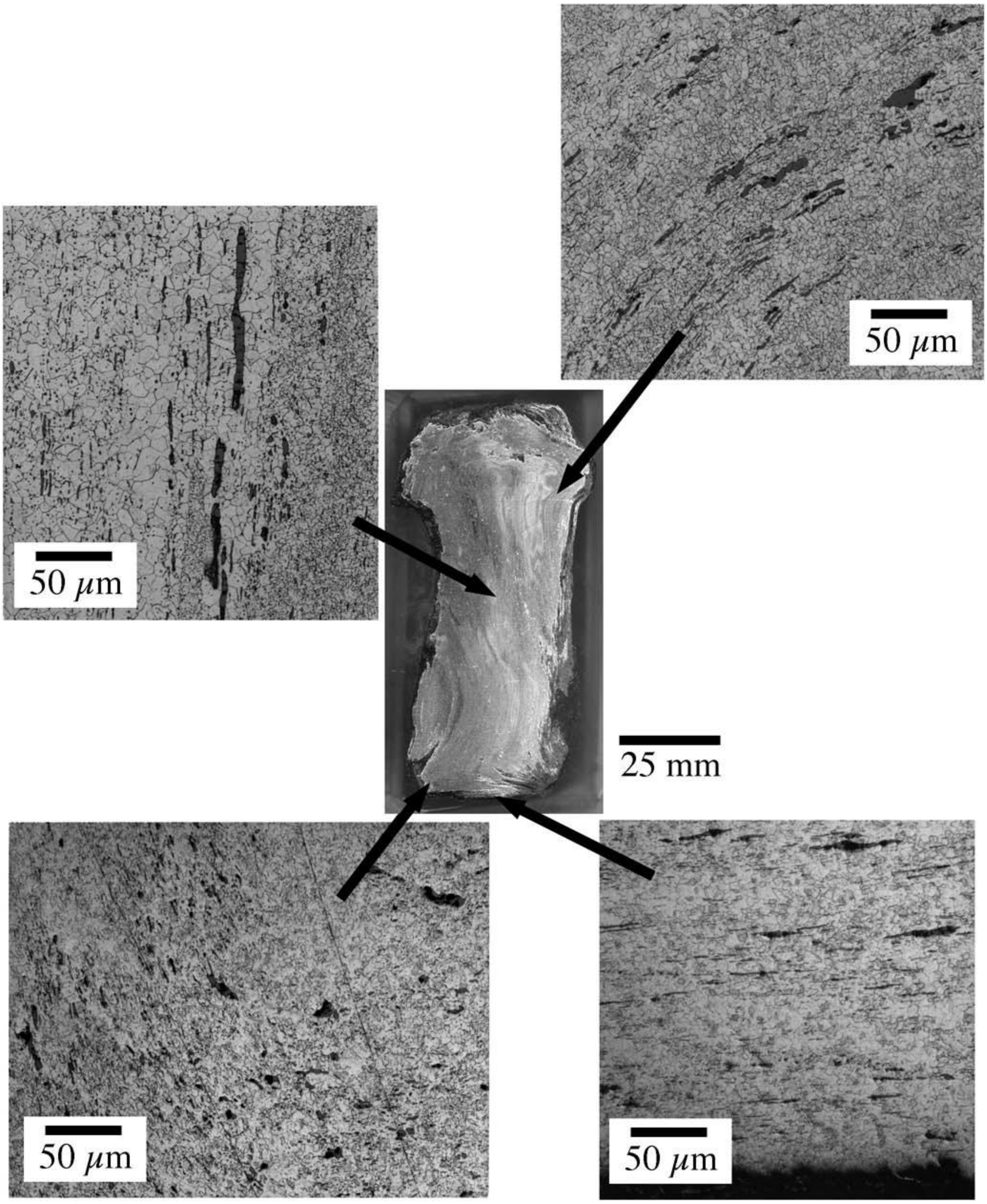

Fig. 74. Montage of micrographs showing the orientation of silicate slag at various locations within a cross-section of a *Titanic* hull rivet.

From Fig. 74 (bottom area) one can observe that the slag stringers are oriented perpendicular to the tensile axis, very near to the fracture surface, where the inner rivet head popped off. This nefavorable orientation and distribution of slag stringers within the rivet, with the high amount of the incorporated slag, would have degraded the mechanical performance of the rivets.

Metallurgical and mechanical analyses performed on the steel rivet samples recovered from the wreck of the RMS Titanic showed that the steel possessed a ductile-to-brittle transition temperature that was very high with respect to the service temperature, making the material brittle at ice-water temperatures. This has been attributed to both chemical and microstructural factors of the Titanic's steel, and due to elevated amount of incorporated slag and its orientation within the rivets.

5.4.2. Advanced method for statistical relevant determination on non-metallic inclusions in steel

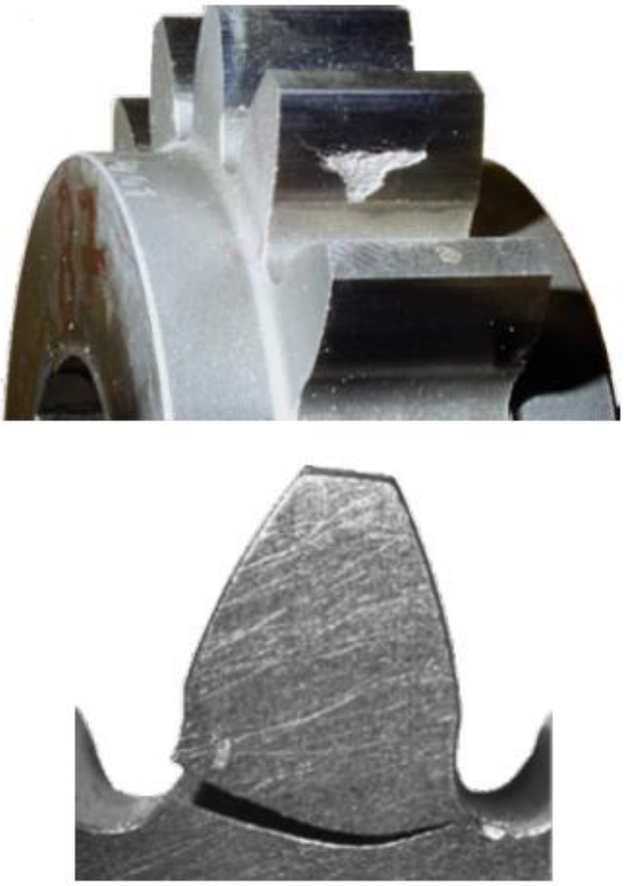
Fig. 75 Fatigue failure is a major challenge for gear design [29].

The drive for higher levels of fuel efficiency requires powertrain components to be lighter, stronger and capable of resisting ever greater and more complex loads. In many cases it is fatigue strength that is the most critical factor when selecting a powertrain steel components since fatigue accounts for the majority of all mechanical service failures [29].

The issue is that current international standards for steel inclusions do not reflect the recent major advances in steel quality, particularly when inclusions are small and/or widely dispersed [29].

It is no exaggeration to say that current steel standards are obsolete in that they offer no effective guidance for designers in considering clean steels. Therefore a new approach to quantification has been developed that brings together a range of methods providing a full and statistically valid picture of the inclusion population in a steel sample.

ISO 4967, ASTM E45 and DIN 50602 are the current standards that apply when assessing micro inclusions. However, modern clean steels have very few inclusions above 25 µm, and the size of the assessed area in standard ASTM and DIN tests using optical methods is too small to provide any statistical confidence, Fig. 76 [29].

Blue fracture is currently used to reveal macro inclusions larger than 0.5 mm. But invariably, using this method a clean steel producer will generate only zero ratings for macro inclusions. It is performed on a bar cross-section area that has been hardened, fractured and then tempered blue to increase the visibility of defects. This technique is used by Ovako only due to customer demand. It is of little relevance in clean steel though**, as it is over 30 years since an inclusion has been found using this method**.

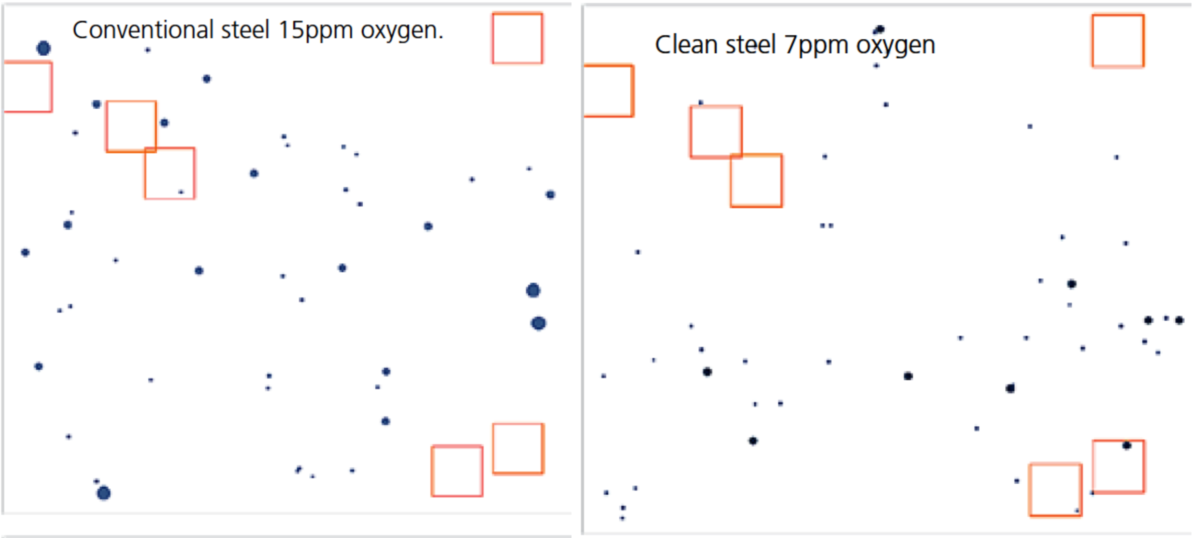

Fig. 76 Possible errors in rating the non-metallic inclusions using LOM (Light Optic Microscopy) [29].

A specific issue with LOM is the small sample size as shown in the schematic illustration presented in Fig.76 (not to scale). The normal procedure is to examine 6 samples. But their small size does not represent the true size and distribution of inclusions. In the case from Fig. 76, it is even possible to obtain the false impression that standard steel (left) has fewer and smaller inclusions than clean steel (right). The field size of analysis is equal to an area equivalent to 0.50 mm^2 on the specimen surface, being defined by a square with 0.71 mm sides, depicted in Fig.76 with orange color.

Ovako Co. has developed an internal standard that enables the powertrain designers to utilize the advanced fatigue properties of clean steels to optimize their components. This is based on a new approach, based primarily on 10 MHz ultrasonic testing of specimens to correctly identify the size and nature of inclusions, codified in Ovako's new standard. It is particularly in the use of 10 MHz immersed ultrasonics that Ovako has made advances in limiting the defects that have the most influence on the final performance of the finished component, Fig. 77. This is also a method that can be readily adopted by most steel producers. SEM of large areas as a method alone, will take more time to become established as a standard cross-industry procedure.

Fig.77 Immersed ultrasonic testing of steels specimen at Ovako [29].

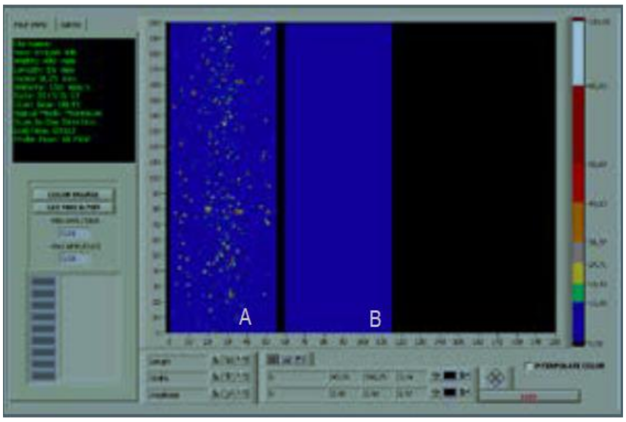

Fig. 78 Ultrasonic C-Scan (10MHz) of two steels A, B.

The ultrasonic and SEM-evaluation revealed a major difference in cleanliness between the two steels (A, B see Fig.78), whereas the traditional micro inclusion rating by ASTM-E45 method did not reveal any significant difference [29]. Immersion ultrasonic testing (by C-Scan 10MHz) compared to LOM, offers both a higher detectability and allows testing of a more significant volume of material.

Thus, a new approach that combines the traditional technique of light optical microscopy (LOM) with the modern techniques of scanning electron microscopy (SEM) and immersed ultrasonics has been developed at Ovako. This approach provides a comprehensive overview of the size and distribution of micro and macro inclusions, Fig. 79.

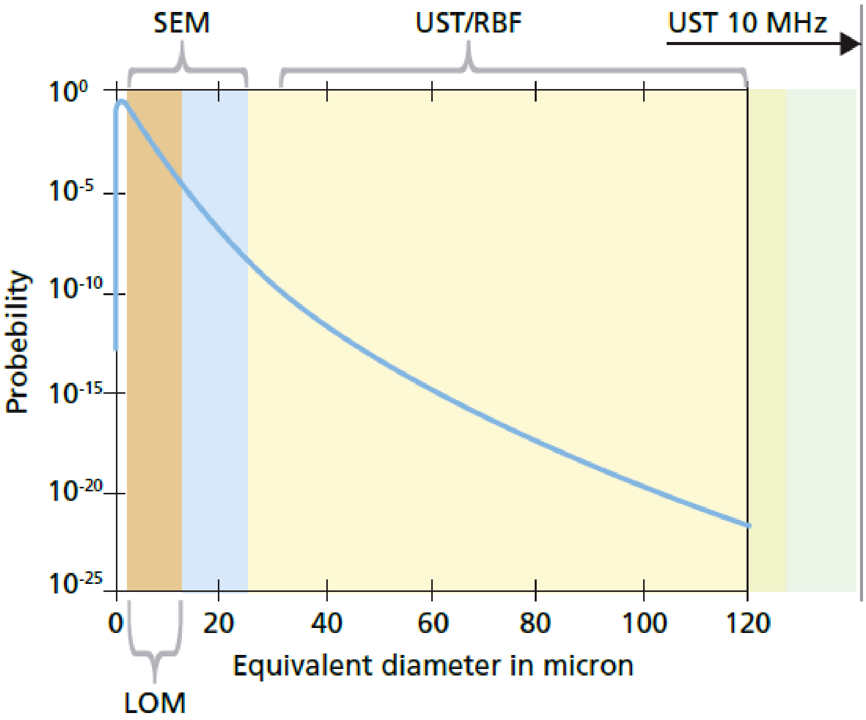

SEM- Scaning Electron Microscopy, UST-Ultrasonic Testing, RBF- Rotating Bending Fatigue testing
Fig.79 Summary of inclusion quantification methods at Ovako [29].

Key summary:

1. Using clean steels for powertrain components can offer a significantly enhanced fatigue life, up to 50% in some cases. The use of clean steel is known to offer a dramatic improvement in the fatigue life of critical automotive powertrain components. This is due mainly to the precise engineering of the inclusions that initiate fatigue failures. The inclusions act as local stress raisers that multiply the nominal load to above the component's safe fatigue limit.

2. As today's international standards do not provide reliable information about the true size and real distribution of inclusions, due to their small size and limited area size of analysis. Thus, the current standards that have been applied historically for conventional steels are not sufficient today to quantify the much smaller and more dispersed inclusions in modern steels.

3. In contrast to LOM, SEM can assess large areas – typically 5,000 mm^2 and provides rich data on inclusion chemistry, morphology and their size. The chemistry of inclusions is vital for process development, while morphology and size are vital for product development. This quantification method is used for inclusions between 2 μm and 25 μm.

4. The microscopic test methods are employed to characterize inclusions that form because of deoxidation or due to limited solubility in solid steel (indigenous inclusions). The microscopic test methods rate inclusion severities and types based on morphological type (by size, shape, concentration, and distribution), but not specifically by composition.

6. Carbon and low alloyed steels microstructures

6.1. Theoretical background

Carbon and low alloyed steels play a pivotal role in various industrial applications, serving as the backbone of structural components, machinery, and infrastructure. These steels, characterized by their predominantly carbon composition with controlled amounts of alloying elements, are favored in specialized industries due to their desirable mechanical properties, cost-effectiveness, and versatility.

In the realm of industrial engineering, carbon steels exhibit exceptional strength, toughness, and weldability (low carbon steels). Low alloyed steels, enriched with alloying elements such as manganese, chromium, nickel, and molybdenum, further enhance specific properties to meet the stringent requirements of diverse applications. The applications of carbon and low alloyed steels span a multitude of industries, including but not limited to:

1. **Automotive Manufacturing**: Carbon and low alloyed steels find extensive use in the automotive sector, where their high strength, formability, and durability contribute to the production of lightweight yet robust components. These steels are employed in chassis structures, body panels, and critical safety components, ensuring optimal performance and crashworthiness.
2. **Construction and Infrastructure**: The construction industry relies heavily on carbon and low alloyed steels for the fabrication of buildings, bridges, and other infrastructure. Their superior strength, toughness, and ease of fabrication make them essential in structural applications, providing the necessary support and longevity required in construction projects.
3. **Oil and Gas Exploration**: In the challenging environments of oil and gas exploration, carbon and low alloyed steels play a crucial role. These materials are utilized in pipelines, drilling equipment, and offshore platforms, where corrosion resistance, high tensile strength, and resistance to extreme temperatures are vital for reliable performance.
4. **Power Generation**: Power plants, both conventional and renewable, rely on carbon and low alloyed steels for components such as boilers, turbines, and pressure vessels. Their ability to withstand high temperatures and pressures makes them indispensable in the generation of electricity across various platforms.
5. **Heavy Machinery and Equipment**: The manufacturing of heavy machinery and equipment demands materials that can withstand significant mechanical stresses. Carbon and low alloyed steels provide the required strength and toughness, ensuring the reliability and longevity of components in industries ranging from mining to manufacturing.

As specialists in the field, understanding the relation between carbon and low alloyed steels properties and their microstructure, is essential for optimizing material selection, ensuring structural integrity, and meeting the stringent performance requirements demanded by modern industrial processes, supporting efficiency, sustainability, and innovation.

The carbon steels can be classified in respect to the carbon content as:

- **Ferritic** or α-Ferrite Steels (max. 0.05% C, typically < 0.022% carbon).
- **Hypo-eutectoid** (0.05 ‑ 0.77% C)
- **Eutectoid** (~0.77% C)
- **Hyper-eutectoid** (0.77 ‑ 2.11% C).

Ferritic Steels

The microstructure of ferritic steels is composed of ferrite, which is a body-centered cubic (BCC) iron structure. Ferritic steels have relatively low strength and hardness but exhibit good ductility. They are often used in applications where toughness is critical, such as pipelines.

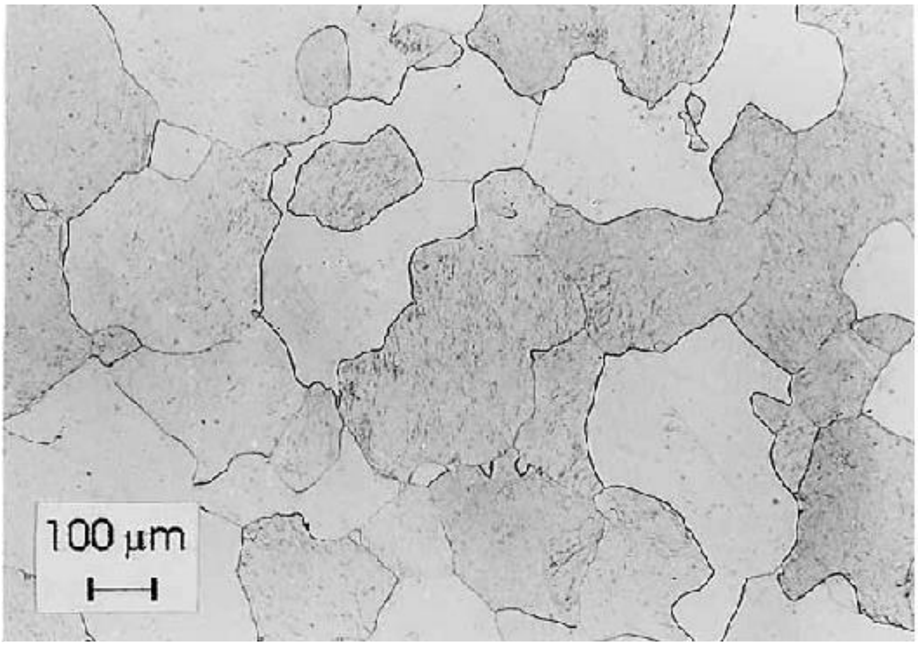

C	Mn	Si	N	Al	P	Cr	Ni
0.002	0.05	-	0.004	-	0.003	-	-

Fig. 80 Ferritic steels microstructure. Average ferrite grain diameter 158 µm ±28 µm [more info].

It's important to note that the term "ferritic steel" is often used broadly to describe steels with a predominant ferrite phase, and there are variations within this category. Ferritic stainless steels, for instance, are a specific type of ferritic steel alloyed with elements like chromium for enhanced corrosion resistance. Ferritic stainless steels will be studied in another chapter, respectively in High alloys microstructures.

Hypo-Eutectoid Steels

The microstructure of hypo-eutectoid steels is composed of ferrite (body-centered cubic BCC) and pearlite, that is a heterogeneous constituent formed by cementite and ferrite lamellae, see SEM detail from Fig.81).

Microstructural constituents can be calculated according to the lever rule, see Fe-Fe$_3$C diagram:

$$Ferrite = \frac{0.77-\%\,C\ in\ steel}{0.77-0.01}\ x\ 100\ (\%)\ \text{and}\ Pearlite = \frac{\%\,C\ in\ steel-0.01}{0.77-0.01}\ x\ 100\ (\%)$$

The phases can be calculated according to the lever rule:

$$Ferrite = \frac{6.67-\%\,C\ in\ steel}{6.67-0.01}\ x\ 100\ (\%)$$

$$Cementite = \frac{\%\,C\ in\ steel - 0.01}{6.67 - 0.01}\ x\ 100\ (\%)$$

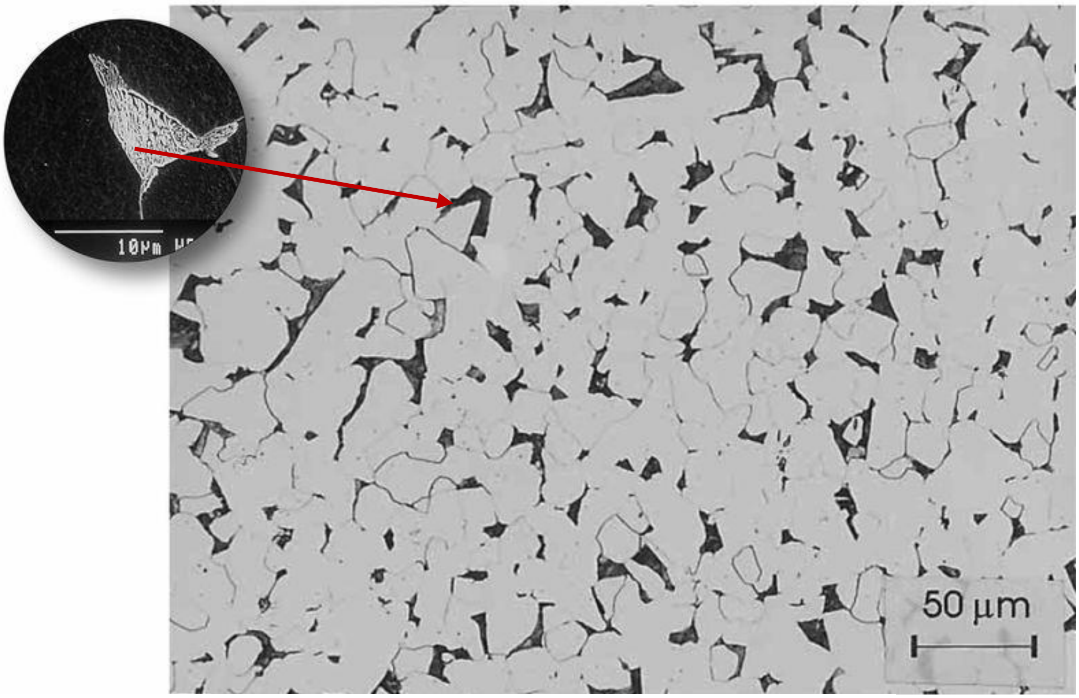

C	Mn	Si	N	Al	P	Cr	Ni
0.11	0.50	0.028	0.004	0.046	0.015	0.012	0.020

Fig. 81 Low carbon–manganese steel. Microstructure by 89 % ferrite and 11 % pearlite. [more info]. Notes that in LOM ferrite is light and pearlite is dark (Nital attack), while in SEM the ferrite grains are black, and pearlite appear light [video].

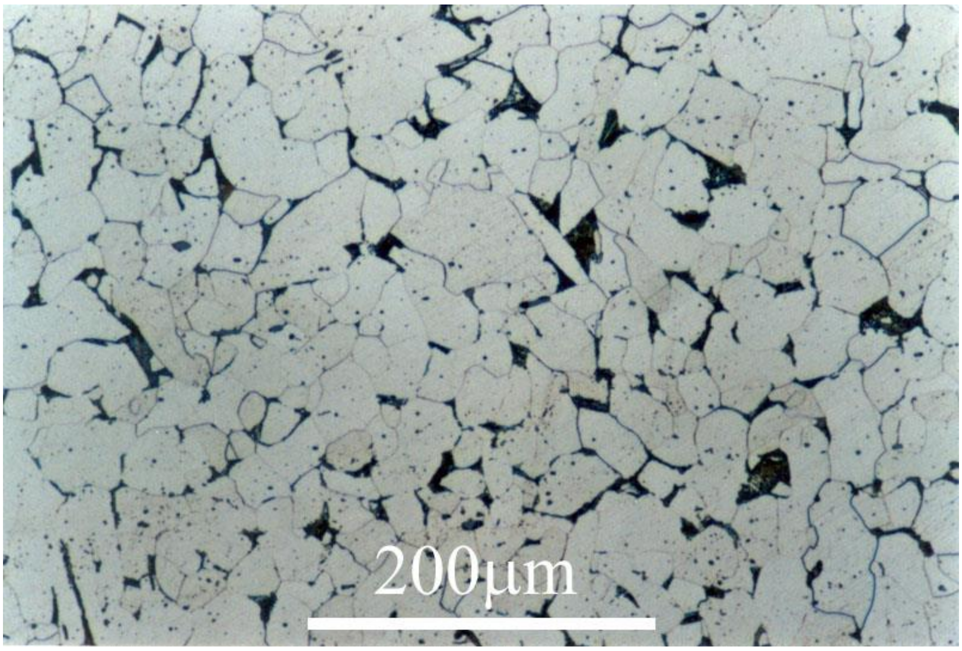

Fig.82 Normalized carbon steel Fe, C 0.08%wt. Low carbon steel with a microstructure consisting mostly of ferrite with the darker pearlite regions around the ferrite grains [more info © DoITPoMS, University of Cambridge].

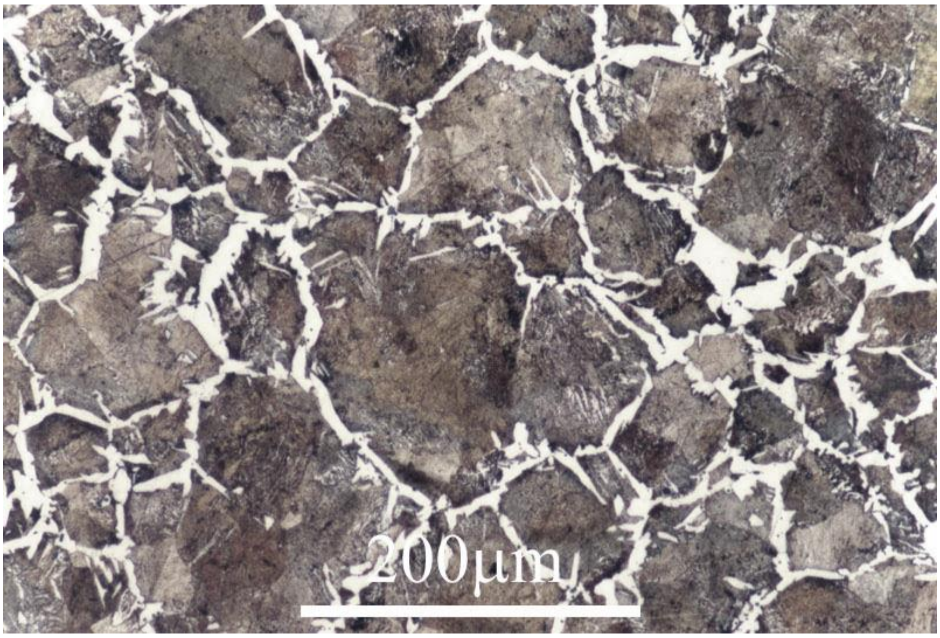

Fig.83 Hypo-eutectoid steel Fe, C 0.4 (wt%), normalized at 1100°C [more info © DoITPoMS, University of Cambridge].

The first phase formed upon cooling from the austenite phase field is proeutectoid ferrite. Due to the lower solubility of carbon in ferrite, carbon is partitioned into the remaining austenite. At the eutectoid point the remaining carbon enriched austenite transforms to pearlite (a heterogeneous mixture of ferrite and cementite) which is the darker region of the micrograph. The proportion of pearlite is dependent upon the overall composition [video].

The light areas network is formed by allotriomorphic ferrite [video]. The allotriomorphic ferrite or grain boundary ferrite nucleates on the austenite grain boundaries and hence follows the shape of the boundaries. The remaining austenite transforms to pearlite and is surrounded by the ferrite. The large size of the areas of pearlite arises due to the high normalization temperature which causes the austenite grains to grow large.

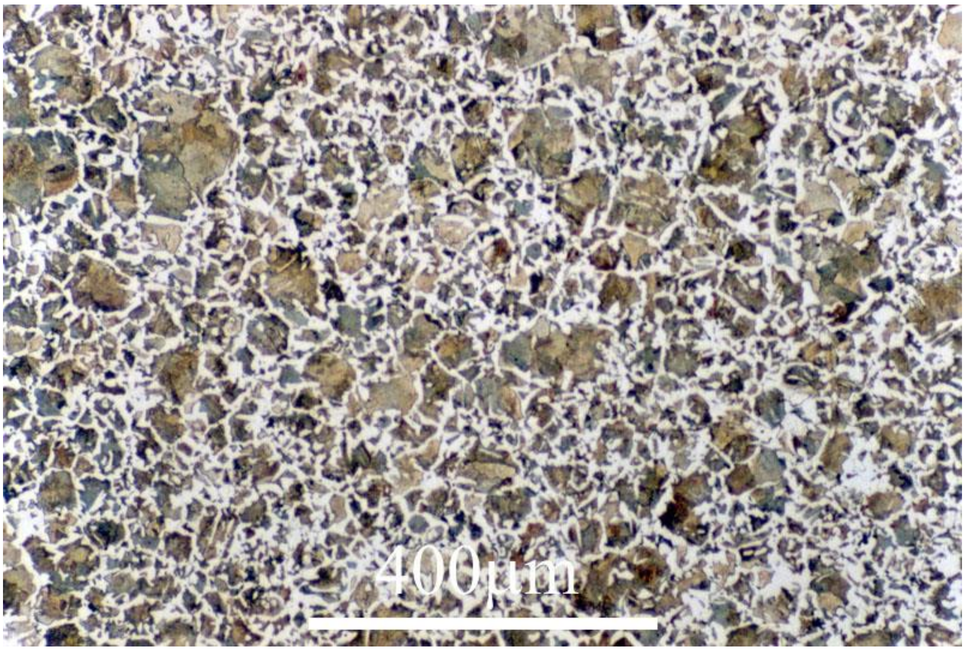

Fig.84 Hypo-eutectoid steel Fe, C 0.4 (wt%), normalized at 950°C [more info, © DoITPoMS, University of Cambridge].

Eutectoid Steels

Eutectoid steels represent a specific class of carbon steels that undergo a eutectoid reaction during cooling (at 727ºC or A_1 temperature), resulting in the formation of a microstructure known as pearlite [video]. This transformation involves the decomposition of austenite, into two distinct phases: ferrite and cementite. Eutectoid steels have a carbon content of approximately 0.77% wt C.

The microstructure resulting from the eutectoid reaction is known as pearlite, which consists of alternating layers of ferrite and cementite. The lamellar structure of pearlite provides a balance of strength and ductility.

The pearlitic microstructure imparts a balance of strength and ductility, making these steels valuable for a range of applications, particularly in situations where wear resistance and mechanical performance are critical. The fine lamellar structure contributes to these mechanical properties, making eutectoid steels suitable for a variety of applications.

Eutectoid steels, find applications in the production of some cutting tools due to their hardness and wear resistance (e.g. Katana sword), springs due the balance of strength and ductility which makes eutectoid steels suitable for the manufacturing of springs, where both elasticity and toughness are essential. Some eutectoid steels are used for railway tracks due to their ability to withstand wear and deformation.

The kinetics of the eutectoid reaction and the cooling rate significantly influence the resulting microstructure. Factors such as alloying elements and heat treatment parameters play a role in controlling the evolution of the microstructure.

$$\text{Austenite} \xrightarrow{\text{Eutectoid}} \text{Ferrite} + \text{Cementite}$$

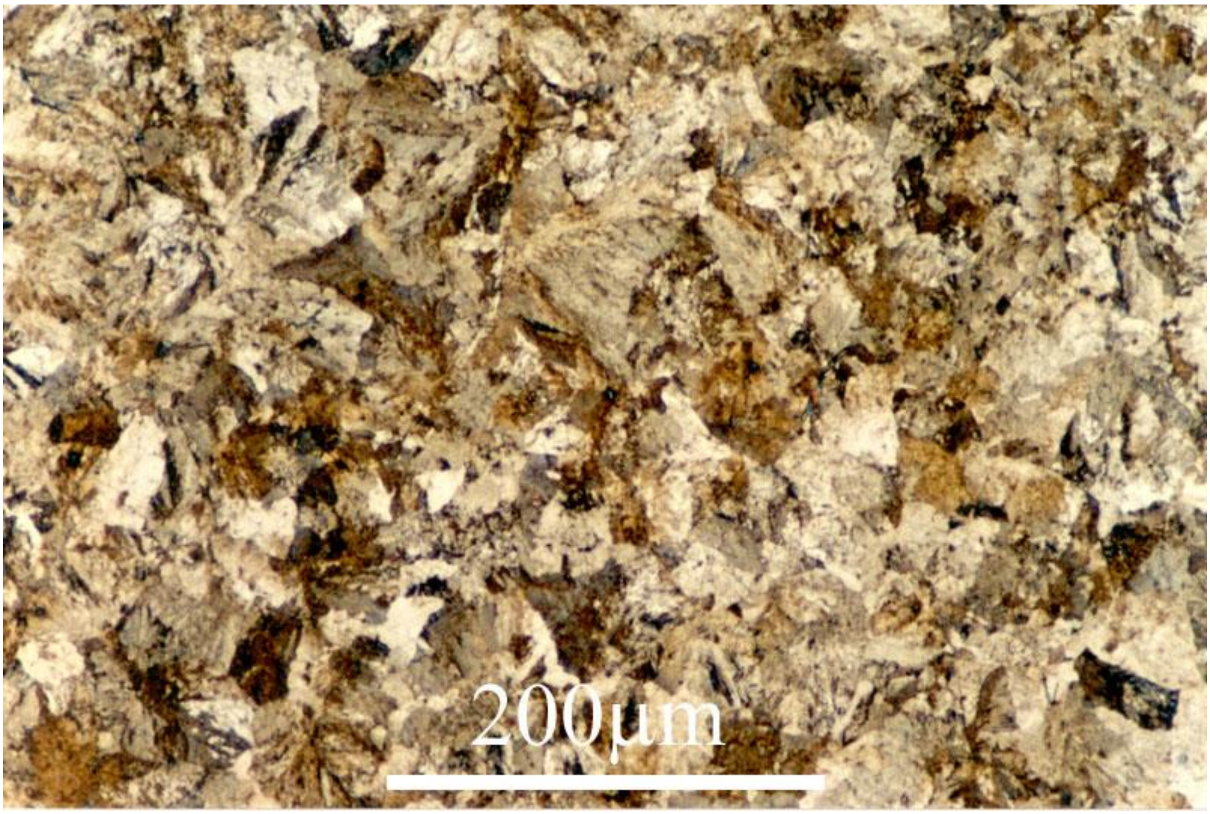

Fig.85 Eutectoid steel Fe, C 0.8 (wt%) [more info, © DoITPoMS, University of Cambridge].

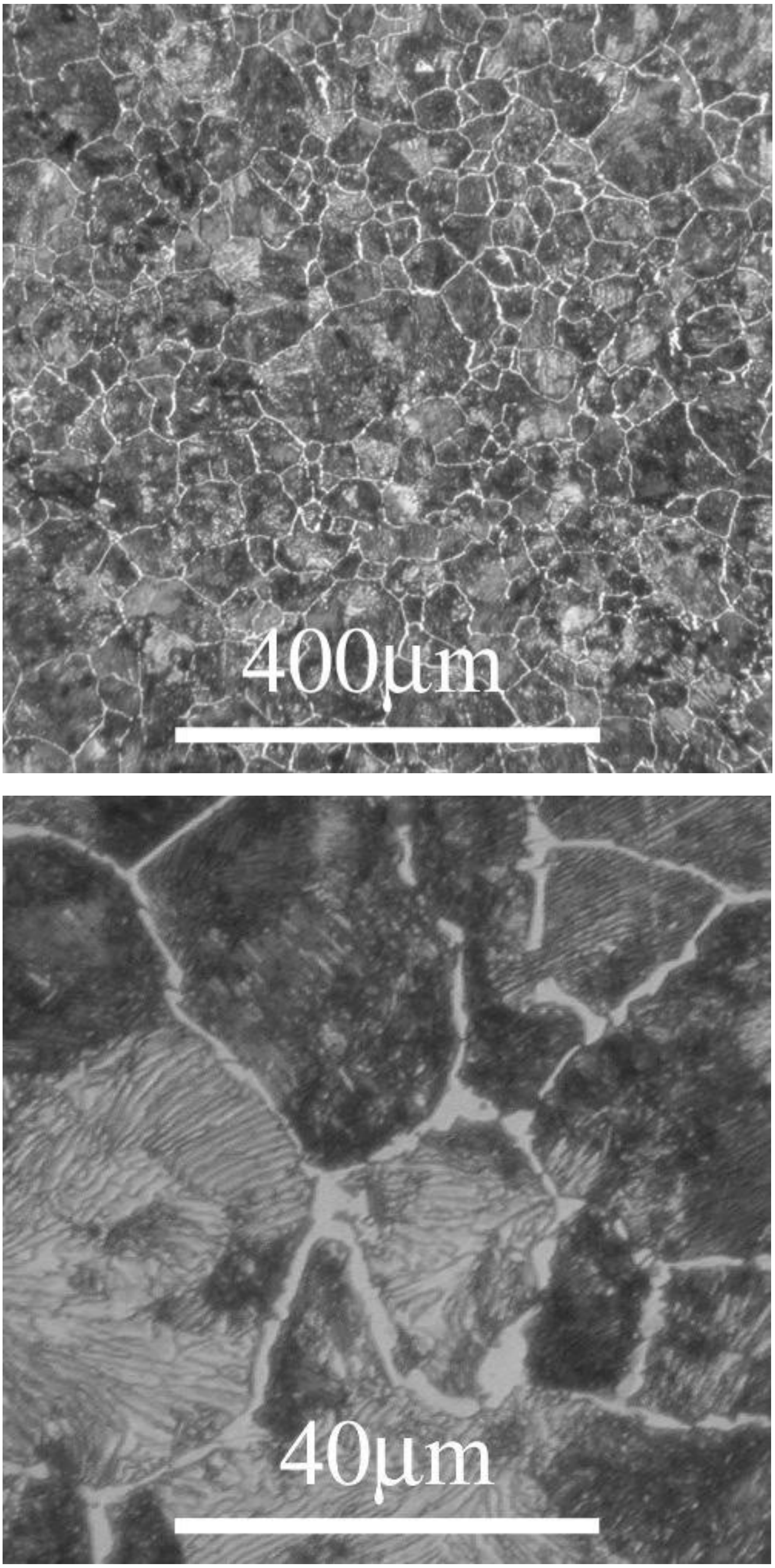

Fig.86 Hyper-Eutectoid steel Fe, C 1.0 (wt%) [more info, © DoITPoMS, University of Cambridge].

Figure 86 presents the microstructure of a hyper-eutectoid steel with 1.0 wt % carbon, normalized, and etched in 3% Nital. At higher magnification, the lamellae structure of the pearlite becomes clearly visible, while at lower magnification in LOM the pearlite appears darker, surrounded by a network of secondary cementite.

The first phase formed from the austenite is proeutectoid cementite. With faster cooling there is less time for carbon to diffuse and the microstructure is more refined and may form the initial cementite as Widmanstätten side plates, aspect illustrated in the SEM image presented in Figure 87, [video].

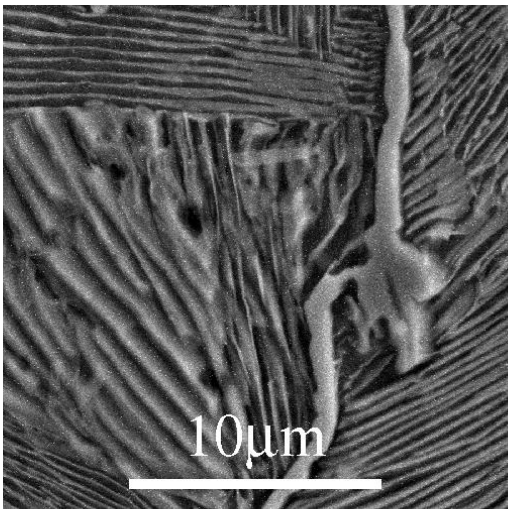

Fig. 87 SEM aspects of pearlite [more info, © DoITPoMS, University of Cambridge].

This scanning electron image SEM shows the cementite delineating prior austenite grain boundaries with a thin layer. The amount of proeutectoid phase is very low, with the majority of the area being taken by the pearlite eutectoid. Each pearlite cell has a different crystalline orientation with the ferrite phase being selectively etched [35].

6.2. Working procedure

The specimens available in laboratory are labeled and should be prepared according to instructions given in Laboratory no 2 for metallographic specimen preparation and etching. The microstructure image can be captured using the digital camera from microscope or can be photographed using a smartphone camera. All relevant information should be filled in the *e*-Report file, and for each microstructure should be calculated the microstructural constituents and phases ratio according to the lever rule. Also, using Heyn Lineal Intercept Procedure, can be calculated the ratio of phases within the microstructure. Both values, calculated and measured, should be compared.

6.3. Discussion and results interpretation

For each microstructure, relevant information is provided, e.g. Steel Designation and Delivery State, Chemical Composition, Manufacturing Technology, Heat Treatments applied, or other processing technologies (e.g. welding, additive manufacturing, hot/cold deformation, casting etc.).

Depending on the application where the steel is used, we expect that the material will provide a series of mechanical properties and a certain behavior in exploitation (e.g. fatigue strength, creep strength, corrosion resistance, good weldability etc.).

Based on that information, the students should comment the analyzed microstructure and the non-conformities that they have identified (grain size, microstructural constituents' morphology and distribution, secondary phases, inclusions, material imperfections etc.).

Materials Science Laboratory

Materials Science and Engineering Department

eReport

Type of the work	Carbon and low alloyed steels microstructures
Scop of inspection	Short description of the work:

Specimen

Steel designation

Preparation

Etched

Manufacturing Technology

Magnification

Equipment

Metallographic microscope

Photo/Microstructure

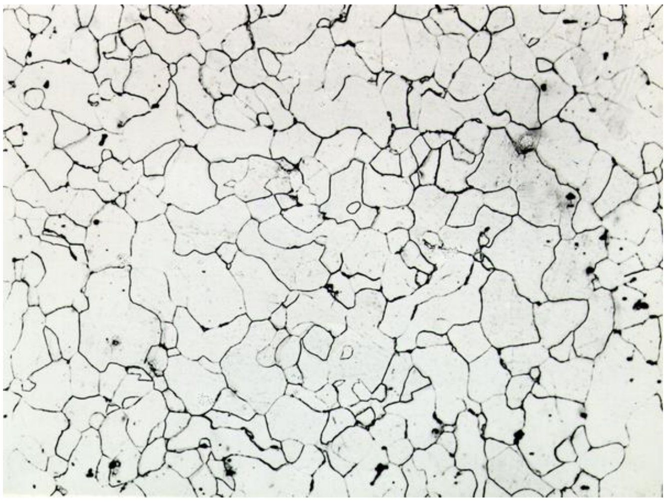

Observations

$$\alpha = \frac{0.77 - \%\,C\ in\ steel}{0.77 - 0.01}\ x\ 100\ (\%)$$

$$P = \frac{\%\,C\ in\ steel - 0.01}{0.77 - 0.01}\ x\ 100\ (\%)$$

$$Fe_3C = \frac{\%\,C\ in\ steel - 0.01}{6.67 - 0.01}\ x\ 100\ (\%)$$

Specimen characterization. Results Analysis

Method of measurement grain size:

Grains Mean Diameter ________ [μm]

Identified phases and microstructural constituents.

Name	Ferrite [%]	Pearlite [%]	Cementite [%] Phase
Calculated			
Measured LOM			

Date:	Specialization:	Authorization Student Name

6.4. Case study

6.4.1. The forensic analysis in structural failures

As mechanical engineers, understanding the nuanced applications of carbon and low alloyed steels is essential for optimizing material selection, ensuring structural integrity in a various field of applications, like Automotive Manufacturing, Construction and Infrastructure, Oil and Gas Exploration, Power Generation or Heavy Machinery and Equipment.

Forensic analysis of structural failures, especially those involving steel structures, is a crucial aspect of engineering investigations. Such analyses aim to understand the reasons behind structural failures, be it due to design flaws, material issues, manufacturing and construction errors, fatigue, external forces, or failure due to natural disasters. Some historical cases and reports are presented below:

Fig. 88 Opening Ceremonies for the Tacoma Narrows Bridge on July 1, 1940, and Fig. 89 Collapse of the Tacoma Narrows Bridge on November 7, 1940 [video].

- **Bridge Failures**. Bridge failures often lead to forensic investigations. One notable example is the collapse of the Tacoma Narrows Bridge in 1940. The forensic analysis revealed design flaws and the role of aerodynamic forces in the collapse [37].
- **Building Collapses.** Forensic analysis has been conducted on various building collapses to understand the failure mechanisms. This includes investigations into the collapse of the Ronan Point apartment tower in London in 1968 and the Hyatt Regency walkway collapse in Kansas City in 1981.
- **Failure Due to Fire.** Understanding how steel structures respond to fire is crucial. The Station nightclub fire in 2003 led to investigations into the impact of fire on structural elements.

Organizations such as the National Academy of Forensic Engineers (NAFE) play a role in advancing the field of forensic engineering. Forensic engineers often work on cases involving structural failures to determine the root causes and contribute to lessons learned for future designs. The specifics of forensic analysis depend on the context of each case, and the methodologies can vary based on the nature of the failure. In-depth analysis often involves collaboration between structural engineers, materials scientists, and forensic experts.

6.4.2. The forensic analysis of the World Trade Center Buildings 1, 2 and 7

The forensic analysis of the World Trade Center (WTC) towers primarily refers to investigations carried out after the terrorist attacks on September 11, 2001. The collapse of the towers led to extensive efforts to understand the events, causes, and consequences.

Various organizations and experts, including the National Institute of Standards and Technology (NIST), conducted investigations and forensic analyses to determine the structural failures and contributing factors. NIST released its final reports on the collapses, providing detailed explanations for the sequence of events and contributing factors. The findings covered aspects like the inadequacy of fireproofing, the thermal weakening of structural components, and the overall response of the buildings to the impact and ensuing fires.

The collapse of World Trade Center Building 7 (WTC 7) is of significant engineering interest because it appears that its collapse was due primarily to fire, rather than any impact damage from the collapsing WTC 1 tower [39]. The summary of investigations and analyses results is presented below:

Buildings WTC 1 and 2 [38, 39]

1. The deterioration of the ASTM A36 steel was a result of hot corrosion.
2. Heating in an environment containing oxygen and sulfur resulted in intergranular melting which transformed to a FeO (Wüstite) and FeS eutectic mixture on cooling.
3. The reaction that results in the formation of this eutectic lowers the temperature at which liquid can form in this steel to about 940 °C or lower depending on Silicon and Carbon effects at the reaction interfaces.
4. The most likely source of the sulfur was the fire-retardant spray applied in 1993. After this report, WPI personnel performed experiments and proved that the sulfur had come from the fire-retardant spray.

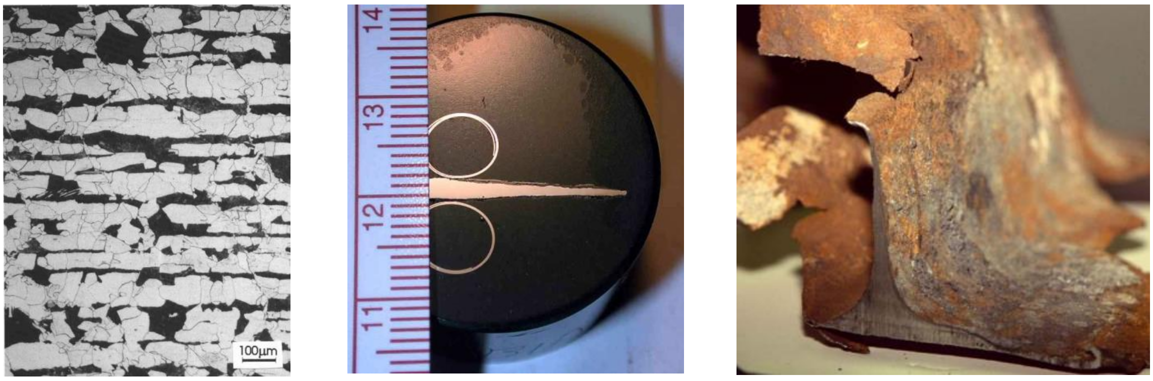

Ferrite-pearlite microstructure of an unaffected A36 beam area.

White: Ferrite,
Dark: Banded Pearlite

Pearlite forms in bands due to manganese segregation and prior hot working (hot rolling).

Severe loss of section thickness in the A36 beam and HSLA column sections.

In severely "eroded" areas in the A36 steel, where the thickness had been reduced by erosion substantially, heating in a hot-corrosive environment was evident in the steel's microstructure.

The interaction of heat in a corrosive fire environment resulted in making the steel susceptible to sulfidation and severe erosion.The severe erosion observed is a result of sulfidation caused by liquid penetration into the austenite grain boundaries, resulting in large grain pullout of material due to a liquid intergranular attack.

Severe thinning of the HSLA steel due to high temperature corrosion.

Fig.90 Metallography analysis of beams and HSLA columns from WTC 1 and 2 [39].

Severe thinning of the HSLA steel occurred by high temperature corrosion due to a combination of oxidation and sulfidation. Sulfidation of the grain boundaries in the HSLA steel accelerated the degradation of the steel. The high concentration of sulfides in the grain boundaries in the corroded regions of the steel involved copper diffusing from the alloy combining with iron, manganese, silicon and sulfur forming both discrete and continuous sulfides in the grain boundaries of the steel suggesting the presence of a liquid phase.

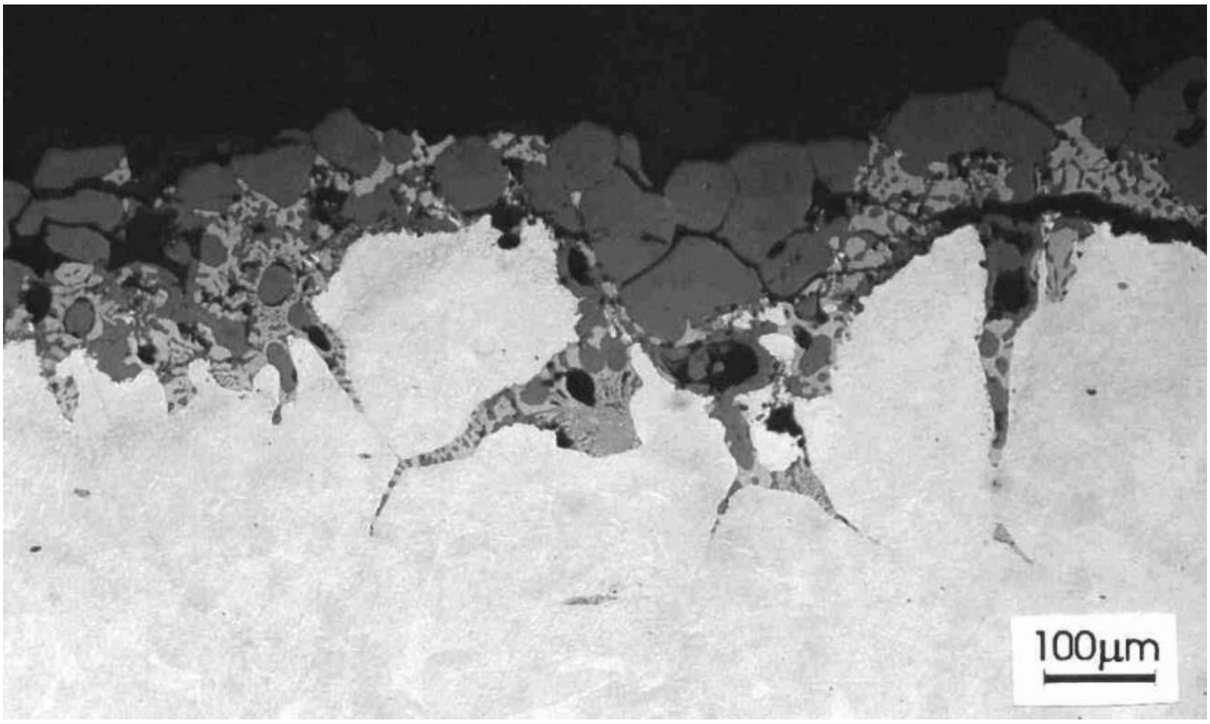

Fig. 91 Oxidation and Intergranular Attack of A36 Steel Beam, unetched [39].

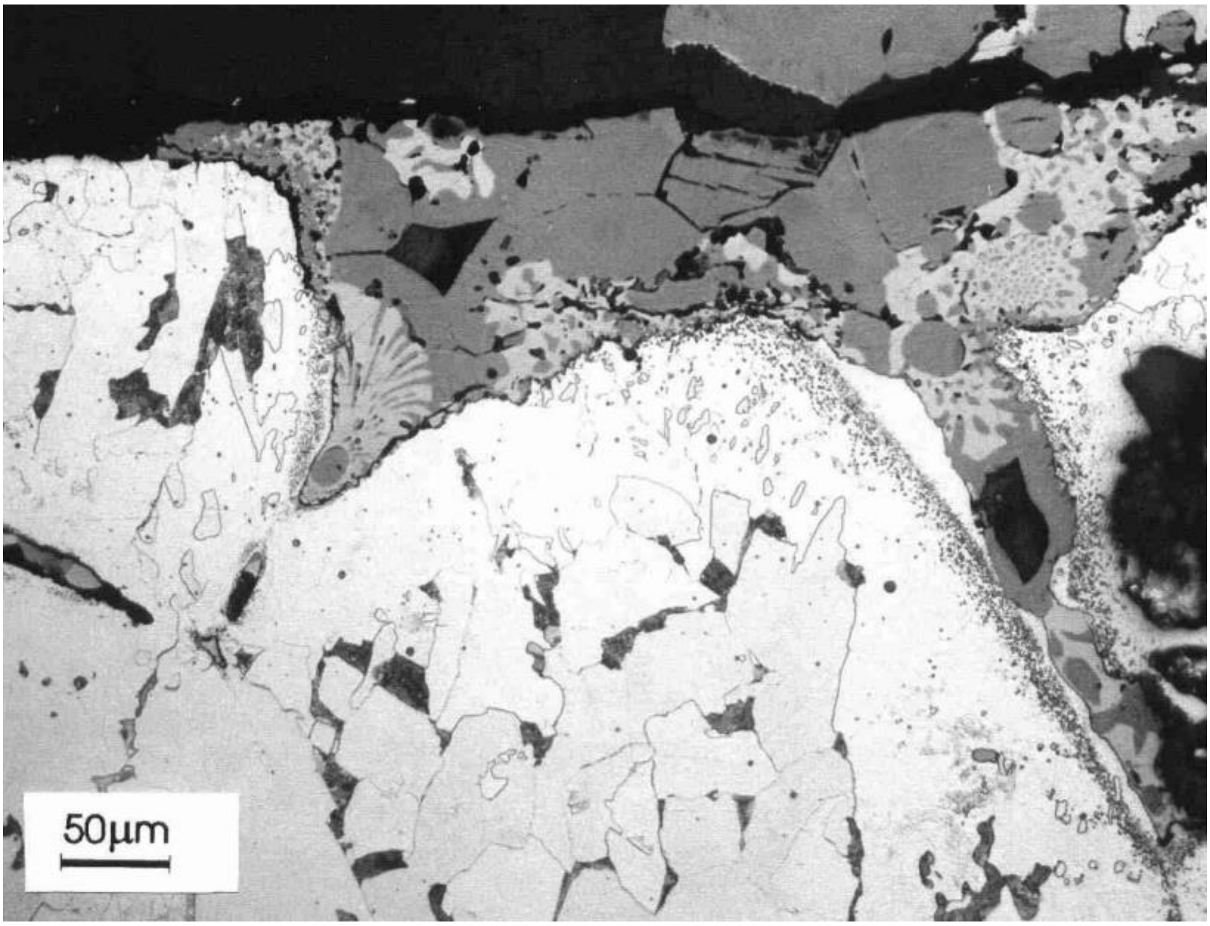

Fig. 92 Intergranular melting phenomena, FeO (Wüstite) and FeS eutectic, etched 4% Nital [39].

The severe thinning of the HSLA steel occurred by high temperature corrosion due to a combination of oxidation, sulfidation and liquid metal embrittlement. Sulfidation of the grain boundaries in the HSLA steel accelerated the corrosion and erosion of the steel, Fig. 91, Fig. 92 and Fig. 94.

The high concentration of sulfides in the grain boundaries in the corroded regions of the steel occurs due to copper diffusing from the HSLA steel combining with iron, manganese and sulfur making both discrete and continuous sulfides in the steel grain boundaries, facts supported by EDX analysis Fig. 93.

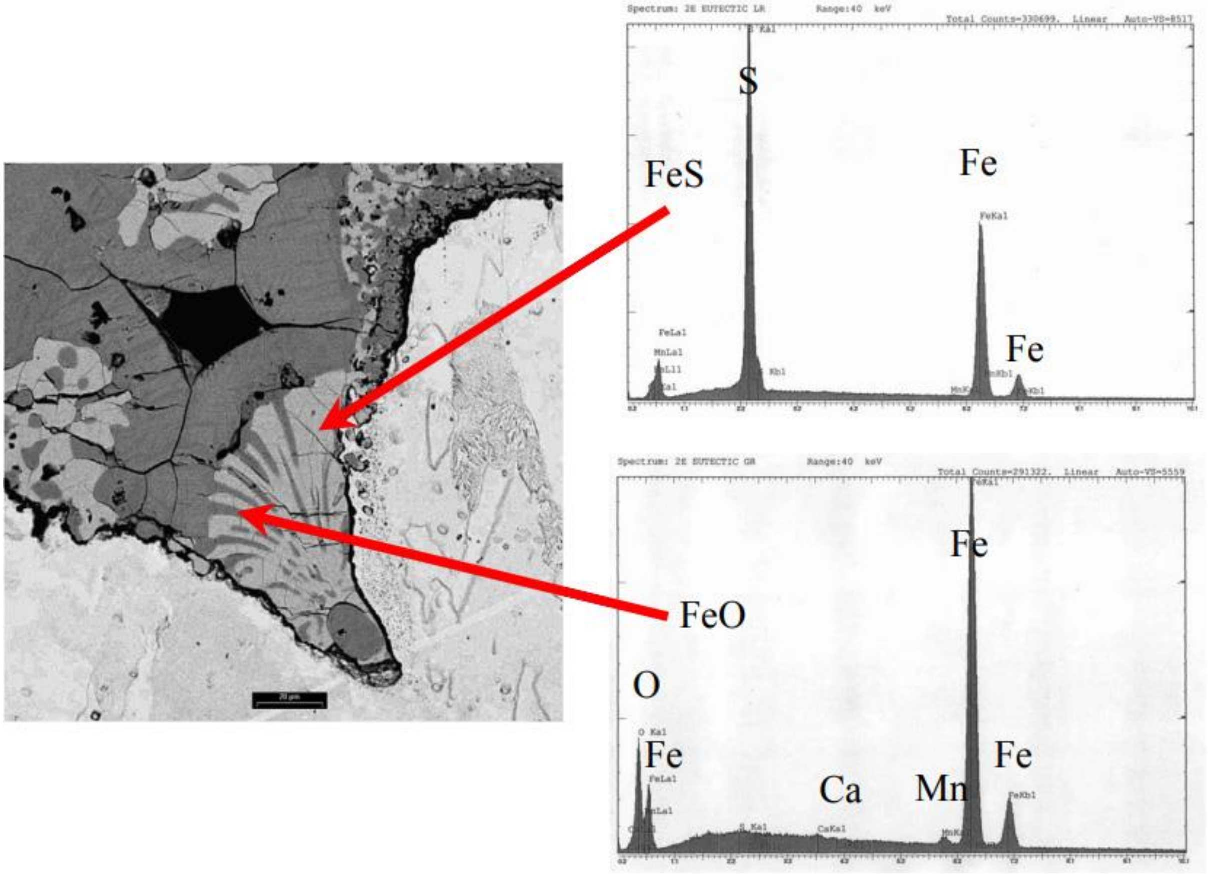

Fig. 93 EDX Analysis of Eutectic Region found in A36 Steel Beams [39].

The most likely source of the sulfur was the fire-retardant spray applied in 1993. After this report, WPI personnel performed experiments and proved that the sulfur had come from the fire-retardant spray. The maximum temperature reached by buildings 1, 2 and 7 was approximately 1100 °C [39].

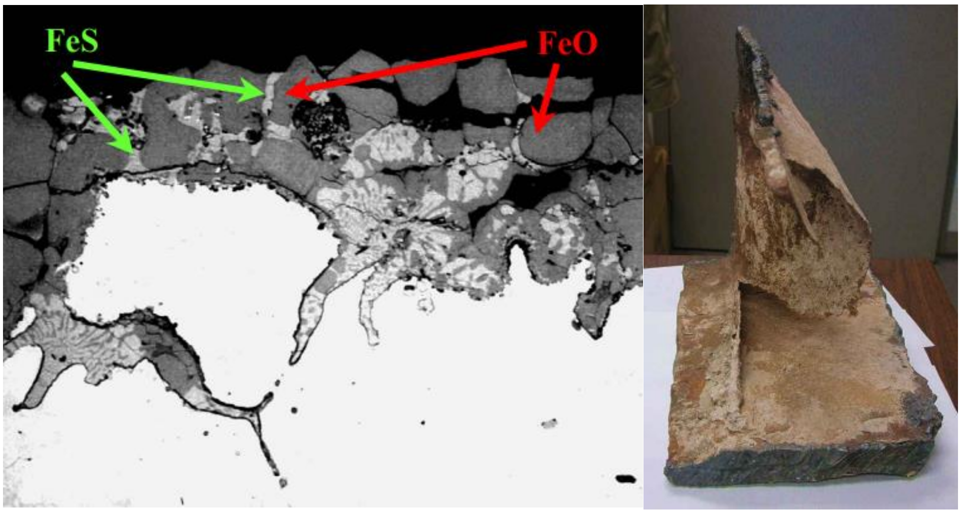

Fig. 94 Rapid deterioration of the A36 steel was a result of high temperature corrosion (combination of oxidation and sulfidation), intergranular melting and liquid metal embrittlement [39].

7. Heat-treated steels microstructures

7.1. Theoretical background

Heat treatment is a technological process used to control the microstructure of metals and alloys in order to achieve desired mechanical, physical, and chemical properties. This process is widely applied in various industries, including metallurgy, manufacturing, and aerospace.

The key factors of the heat treatments are summarized below:

- **Heating and Cooling Rates**. The rate at which a material is heated and cooled plays a crucial role in determining its final properties. Rapid cooling, or quenching, can result in a harder but more brittle material, while slow cooling leads to a softer but more ductile material.
- **Critical Temperature.** Materials have critical temperatures at which significant changes in their microstructure occur. For example, the critical temperature for steel is the austenite transformation to ferrite, pearlite and cementite.
- **Phase Transformation.** Different phases of a material (steel), such as austenite, ferrite, pearlite, and martensite, are formed during the heating and cooling process. The distribution of these phases determines the material's properties.
- **Controlled Grain Growth.** Heat treatments can be used to control the grain size of materials, influencing their mechanical and thermal properties (e.g. important for welded structures).

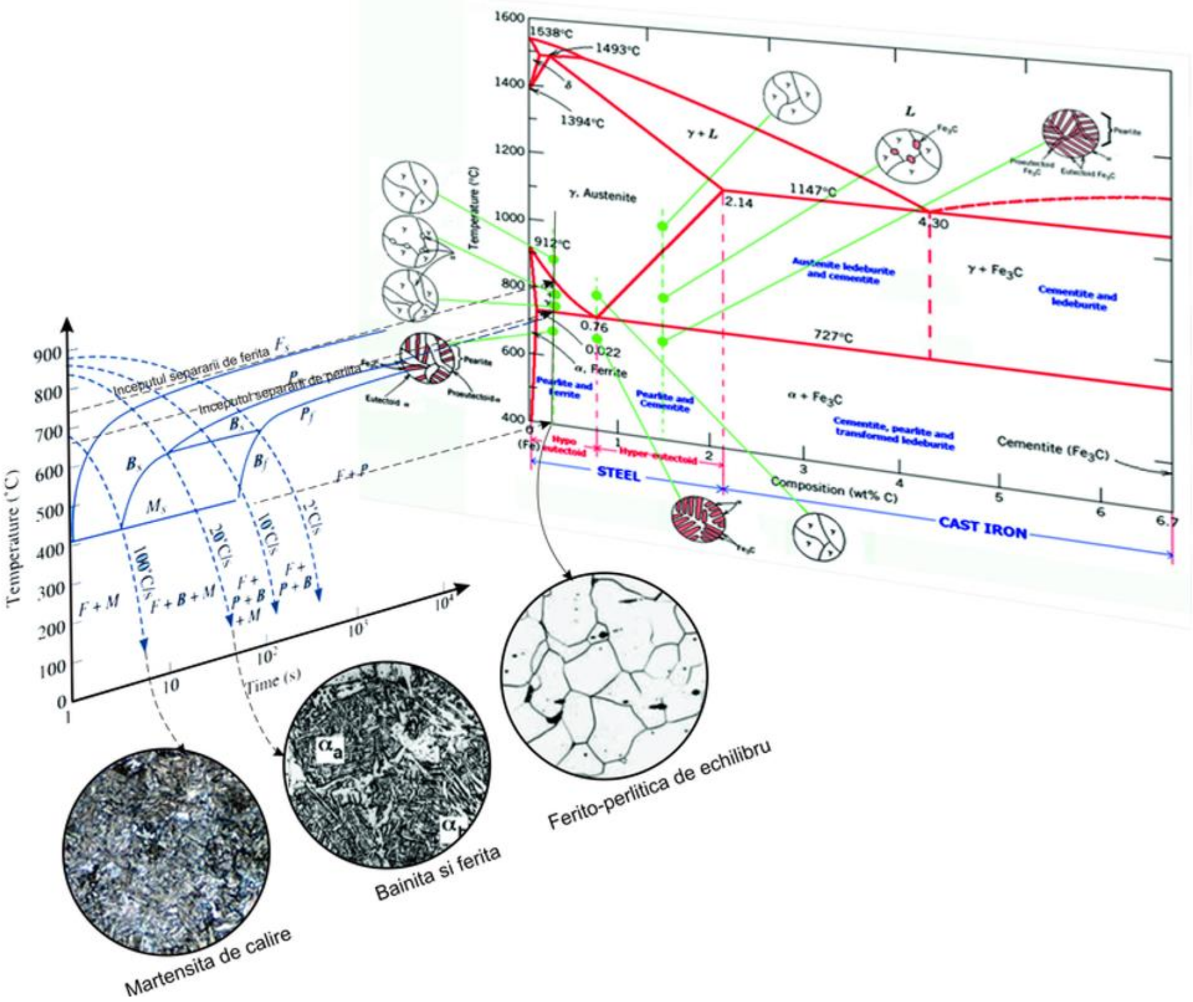

Fig. 95 Steel's microstructure control by using different cooling rates in metallurgical processes.

The delivery heat treatment conditions for steels can vary depending on the specific type of steel and the desired properties and performance requirements for the end product. The steel suppliers provide information on the heat treatment conditions for specific steel grades to guide manufacturers and end-users in achieving the desired material characteristics, see Annex II.

The common heat treatments are summarized below:

- **Annealing**. The steel is heated to a specific temperature and then slowly cooled to relieve internal stresses, improve machinability, and achieve desired mechanical properties. Annealing is often used for structural steels, carbon steels, and low-alloy steels to soften the material for further processing or to improve its formability and machinability. This is important in processes like cold working or deep drawing.
- **Normalizing.** The process is similar to annealing, but the steel is air-cooled in a still environment. Normalizing refines grain structure and enhances mechanical properties. It is commonly applied to carbon and low-alloy steels to improve uniformity in grain size and mechanical properties.
- **Quenching** is the rapid cooling of a material to achieve specific properties. It is often used to harden materials like steel by transforming austenite into martensite. The steel is heated to a high temperature, followed by rapid cooling (quenching) to harden the material. Subsequently, it is tempered by reheating to a lower temperature to reduce brittleness, while maintaining strength. The process is often used for medium to high carbon steels, alloy steels, and tool steels to achieve a balance between hardness and toughness.
- **Tempering** involves reheating a quenched material to a lower temperature to reduce brittleness and improve toughness. This process is crucial for achieving a balance between hardness and toughness in certain materials.
- **Stress Relief.** Heat treatment is applied to relieve internal stresses in materials, improving dimensional stability and reducing the risk of distortion.
- **Precipitation Hardening (Aging).** Involves a combination of solution treatment (heating) and aging to form fine precipitates within the steel, resulting in increased strength and hardness. Can be applied for certain stainless steels and non-ferrous alloys, providing improved mechanical properties.
- **Carburizing.** The steel is heated in a carbon-rich atmosphere to allow carbon diffusion into the surface layers, followed by quenching. This increases hardness at the material surface. Applied for low-carbon steels to enhance surface hardness, commonly employed in gear and bearing applications.
- **Nitriding.** Nitrogen is introduced into the surface of the steel at elevated temperatures, forming hard nitride compounds that improve surface hardness and wear resistance. Applied to alloy steels to improve surface properties, particularly in components subjected to sliding or abrasive wear. Processes like carburizing and nitriding are used to harden only the surface layer of a material, providing wear resistance while maintaining a tough core.

Because alloying elements play a key role in steel’s behavior during/after heat treatments, the alloys designed for heat treatments are elaborated very carefully with strict conditions on purity and composition. The heat treatment processes are then employed to optimize the microstructure and properties of the steel based on its alloy composition.

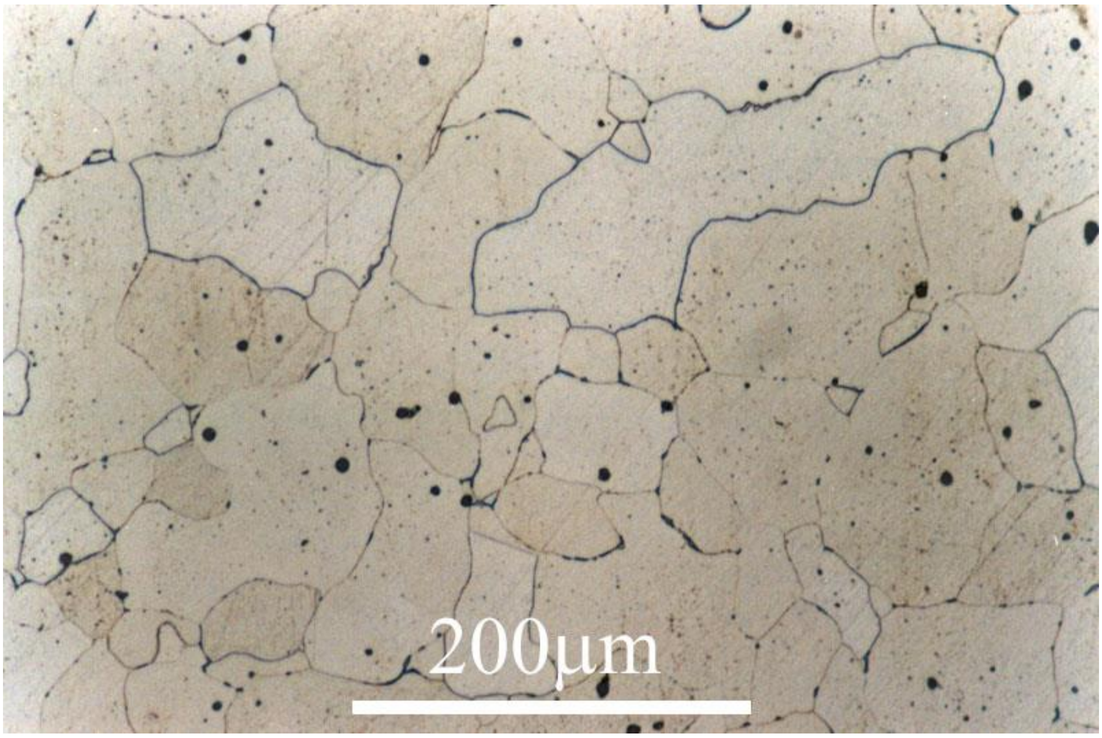

Fig. 96 Annealed low carbon steel at 1050ºC [more info, © DoITPoMS, University of Cambridge].

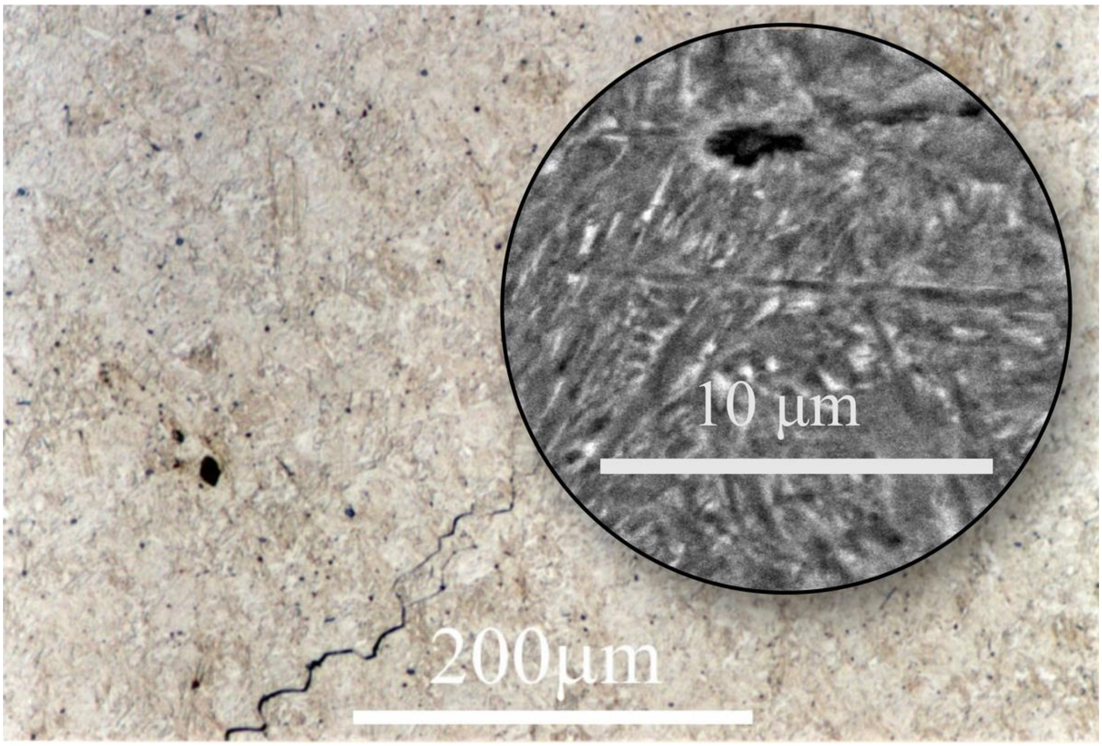

Fig. 97 Steel C=0.40 (wt%), quenched, martensitic microstructure [more info, © DoITPoMS, University of Cambridge].

The steel has been rapidly quenched. This leads to a rapid volume change due to thermal expansion. In this case the steel has been unable to plastically deform to accommodate this change. This leads to the nucleation of cracks in the metal. This is exacerbated by the fact that the quenching of steel promotes the formation of the brittle phase martensite. This steel was quenched from the austenite phase field too rapidly for carbon to diffuse out and form cementite. This resulted in the formation of the brittle martensite phase [35].

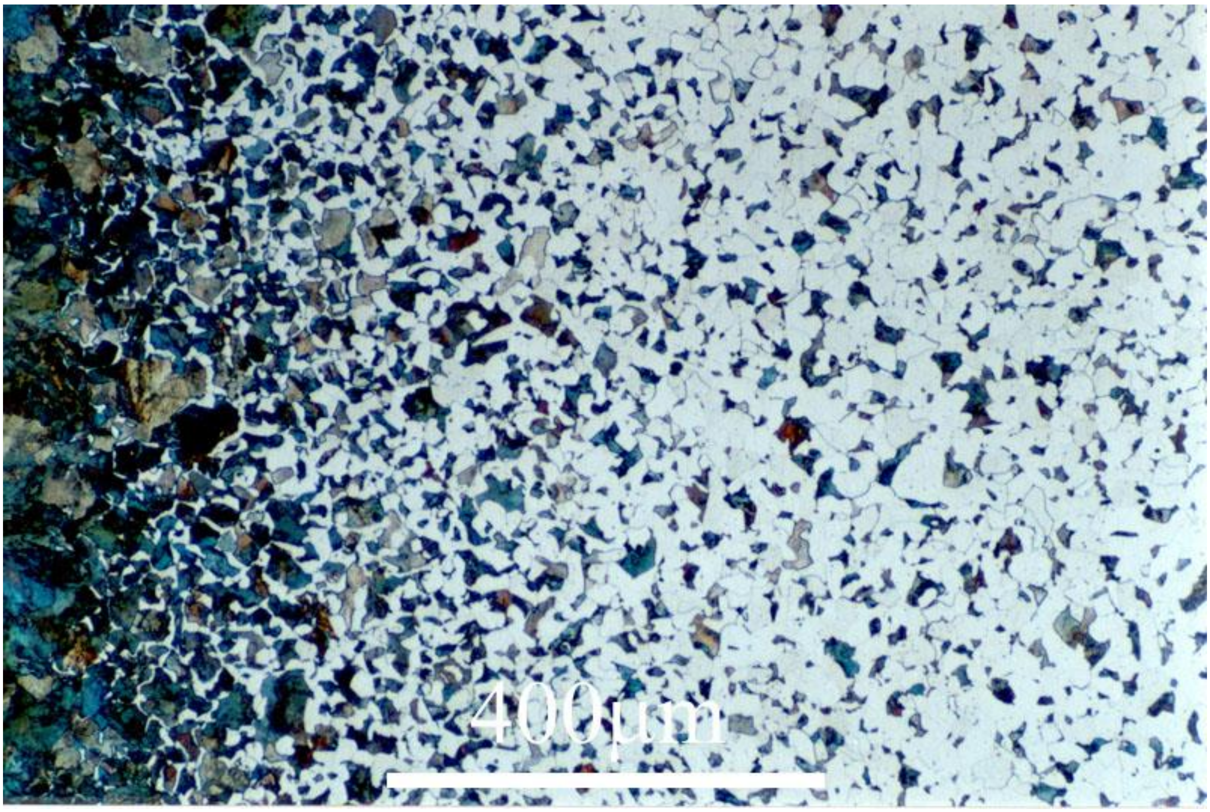

Fig. 98 Carburized and case hardened steel, C=0.2 (wt%) [more info, © DoITPoMS, University of Cambridge].

After initial casting of this steel it was subject to a process known as carburization. The metal is heated above the ferrite-austenite transition in a carbon rich atmosphere. This establishes a concentration gradient and hence carbon diffuses into the steel. Usually the steel is then hardened by quenching. This produces what is known as a case-hardened steel - with a hard surface (case) surrounding a tough core. The carbon gradient can be seen in the changing shade of the sample from left to right, with high carbon concentration at the left (surface) and hence a martensitic phase, changing to the lighter shade consisting of mostly ferrite [35].

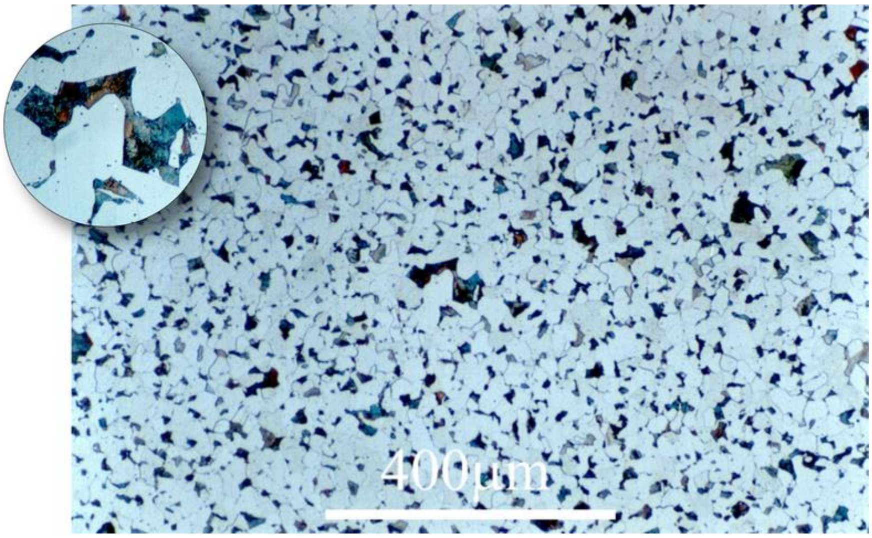

Fig. 99 Carburized and case-hardened steel, C=0.2 (wt%) in the bulk material. Non-affected by thermo-chemical process of carburization and quenching.

This micrograph has been taken from the bulk of the sample presented in the Figure 98, showing that carbon does not diffuse significantly into the interior of a case hardened steel [more info].

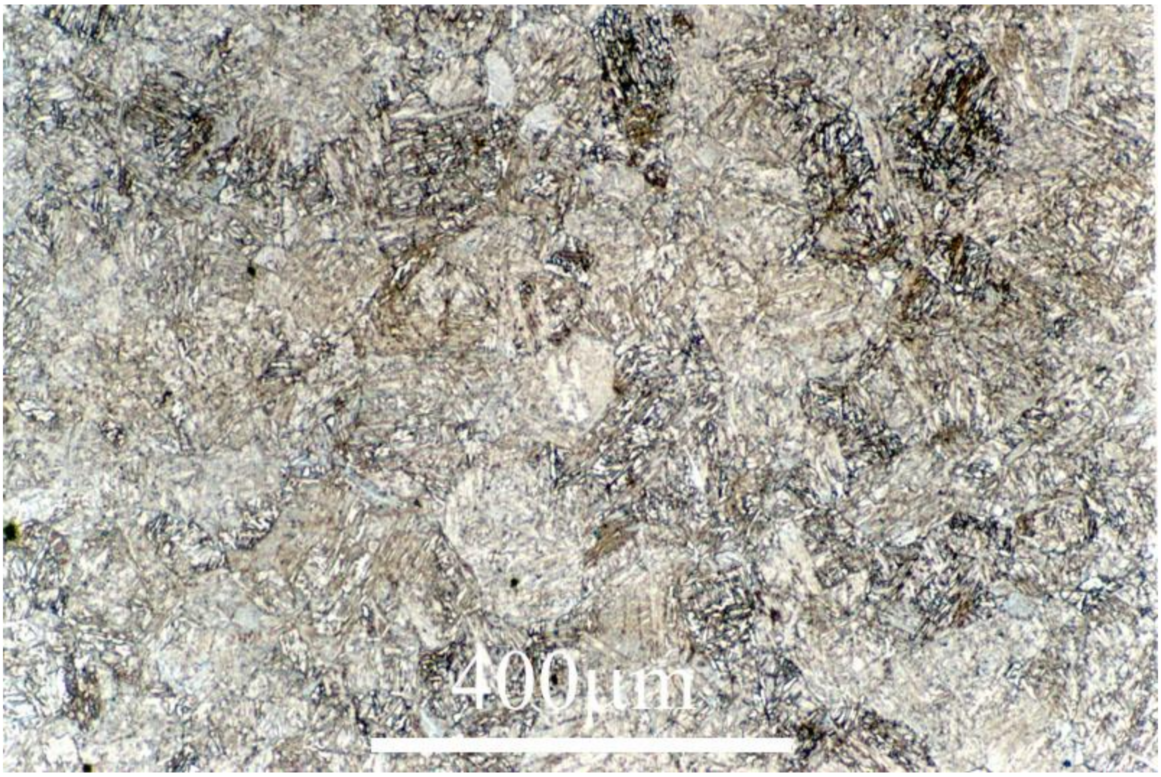

Fig. 100 Quenched & Tempered Steel (C=0.3 wt %), [more info, © DoITPoMS, University of Cambridge].

Medium carbon steel after quenching is producing martensite and should be subsequently tempered in order to achieve a balance between hardness and toughness for optimal performance in many applications, such as:

- **Tool Steels.** Tempering is commonly applied to tool steels to achieve a combination of hardness and toughness suitable for cutting, machining, and forming applications.
- **Structural Steels.** Tempering is used to enhance toughness, making the material more resistant to fracture and providing better performance in construction applications.
- **Automotive and Aerospace Components.** Tempering is crucial for components in the automotive and aerospace industries, where a balance of strength and toughness is essential for safety and reliability.
- **Machine Components.** Gears, shafts, and other machine components often undergo tempering to achieve the necessary combination of hardness and toughness for optimal performance.

During tempering, there are three stages that can be identified:

- Initial Stage - Formation of Carbides. As the steel is heated during tempering, the initial stage involves the decomposition of retained austenite and the formation of carbides. This contributes o an increase in hardness.
- Intermediate Stage - Transformation of Martensite. The hard phase formed during quenching, occurs during this stage. This transformation involves the precipitation of fine carbides, leading to a reduction in hardness.
- Final Stage - Microstructural Changes. Further heating allows for microstructural changes, such as the coarsening of carbides and the transformation of retained austenite into other phases. These changes result in a balance between hardness and toughness.

In many applications the dimensional stability is an important requirement of the manufactured parts. During the heat treatment processes metastable phases form, playing a crucial role in the final properties of metallic components.

It's important to note that the stability of these metastable phases is influenced by factors such as temperature, time, and the chemical composition of the material. Subsequent heat treatments, like tempering, can lead to the transformation of metastable phases into more stable ones, affecting the final mechanical properties of the material.

- **Martensite** is a metastable phase that forms during rapid quenching (cooling) of austenitic steel. It has a body-centered tetragonal (BCT) crystal structure. It is very hard and very brittle, especially at high carbon content in alloys.
- **Lath Martensite** is a specific microstructure of martensite that forms as laths or thin plates during the martensitic transformation. Lath martensite is metastable, and its stability can be influenced by subsequent tempering or aging processes.
- **Bainite** forms during the austempering process, which involves quenching the steel to a temperature above the martensitic start temperature and holding it at that temperature until the transformation is complete. It forms also during continuous cooling in certain conditions [video][11].
- **Acicular Ferrite or** Needle-like Martensite is a product with characteristics between martensite and bainite. The nucleation of acicular ferrite takes place on specific inclusions, the needle-shaped structure can form in certain alloy steels during the cooling process (e.g. in welding).
- **Retained Austenite** has a face-centered cubic (FCC) structure and can remain in the steel matrix after quenching. It often forms during the quenching process, especially when there are alloying elements that stabilize austenite. Retained austenite is metastable, and its stability depends on factors such as temperature, stress, and the presence of other phases. It can transform into martensite or other phases during subsequent mechanical or thermal treatments.

In automotive sector are used a series of modern and advanced steels with complex microstructure providing specific combinations of strength, ductility, and formability:

- **Dual-Phase (DP) steel** - DP steels typically consist of a combination of ferrite and martensite phases [video]. Ferrite provides ductility, while martensite contributes to strength. DP steels are produced by subjecting the material to a two-step heat treatment. The first step involves partial austenitization followed by quenching to form martensite, and the second step involves further annealing to produce ferrite. DP steels exhibit a balance of strength and ductility. The combination of these phases results in improved formability and resistance to fracture, making DP steels suitable for applications like automotive body parts.
- **Transformation-Induced Plasticity (TRIP) Steel -** TRIP steels are characterized by the presence of retained austenite and other phases like ferrite and bainite. Alloying elements such as manganese and silicon are often added to stabilize retained austenite.

---

[11] The 3D-structure is an artistic interpretation of an electron-microscopic image (2D) with a magnification of 4000x. The displayed type of bainite is composed of bainitic ferrite and martensitic-austenitic constituents (M/A). The SEM-image was produced at the Steel Department (IEHK) and the Central Facility for Electron Microscopy (GFE) at RWTH Aachen University.

TRIP steels are produced by controlled cooling or isothermal transformation. The goal is to retain a certain amount of austenite during the quenching process. TRIP steels offer a combination of high strength and high ductility due to the strain-induced transformation of retained austenite during deformation. This enhances energy absorption and makes TRIP steel suitable for crash-resistant automotive components.

- **Twinning-Induced Plasticity (TWIP) Steel -** TWIP steels are characterized by a high manganese content (often more than 20%) to promote twinning. TWIP steels rely on the deformation-induced twinning of grains during mechanical loading. Twinning is a crystallographic process that increases the material's ductility. TWIP steels exhibit exceptional ductility and formability due to the twinning mechanism. They also show high work hardening capacity, making them suitable for applications that require excellent energy absorption and resistance to deformation.

DP, TRIP, and TWIP steels are widely used in the automotive industry for structural and safety-related components. Their combination of strength, ductility, and formability makes them suitable for applications like car body panels, chassis parts, and crash-resistant structures.

In structural engineering, these steels can be utilized for components that require a balance between strength and deformation capacity. Dual-phase DP, TRIP, and TWIP steels are examples of advanced high-strength steels designed for specific applications where a balance of strength and ductility is crucial. Their unique microstructures and properties are achieved through careful alloying and heat treatment processes, making them valuable materials in industries requiring high-performance materials.

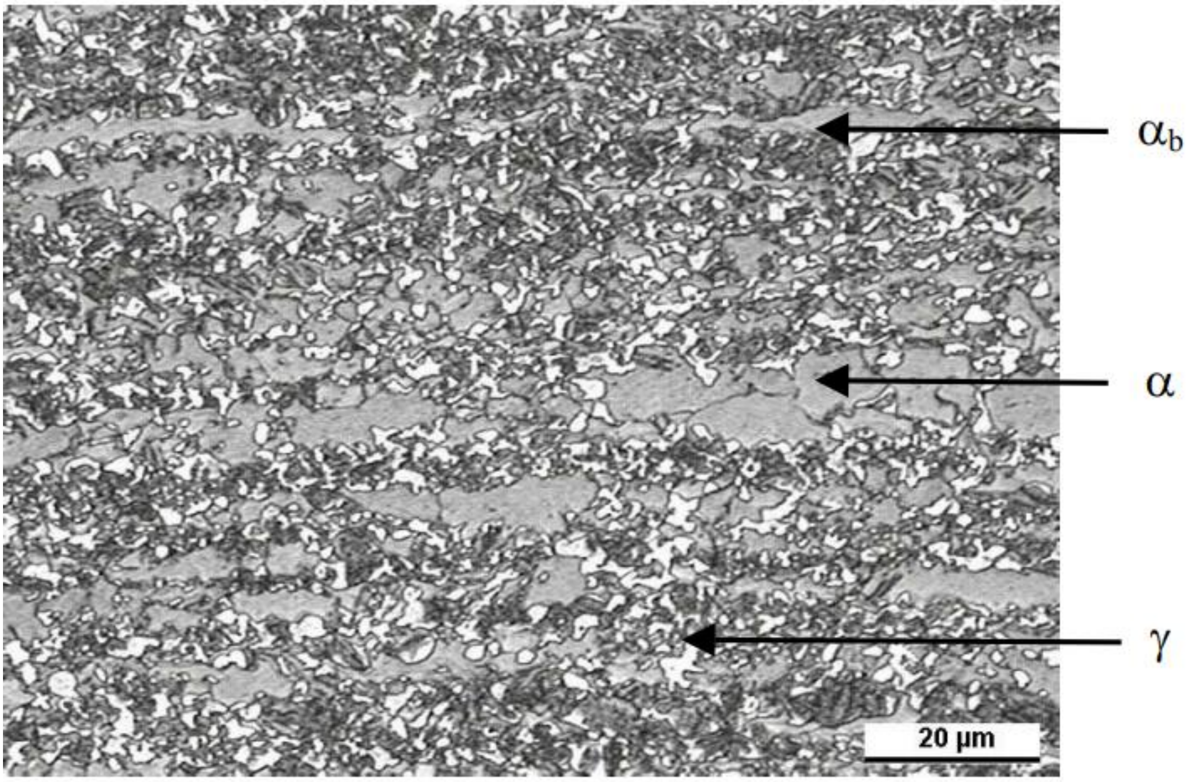

Fig. 101 Typical microstructure for TRIP steels. Etchant: LePera [41].

The TRIP steel microstructure shown in Figure 101 consists of a ferrite matrix, α (grey) containing a dispersion of retained austenite, γ (bright) and bainite, α_b (dark) [41].

During the deformation of TRIP steels, the retained austenite also transforms to martensite with increasing strain, which results in an increase of the work hardening rate at higher strain. At low carbon levels, the retained austenite transforms almost immediately upon deformation, increasing work hardening rate and formability during the stamping process. At high carbon contents, the retained austenite is more stable and begins to transform only at strain levels beyond those produced during stamping and forming, and the retained austenite is still present in the final part. It can then transform to martensite during a crash, and thereby provide greater crash energy absorption [41].

7.2. Working procedure

The specimens available in laboratory are labeled and should be prepared according to instructions given in Laboratory no 2 for metallographic specimen preparation and etching. The microstructure image can be captured using the digital camera from microscope or can be photographed using a smartphone camera. All relevant information should be filled in the *e*-Report file, and for each microstructure should be calculated the microstructural constituents and phases ratio according to the lever rule. Also, using Heyn Lineal Intercept Procedure, can be calculated the ratio of phases within the microstructure. Both values, calculated and measured, should be compared.

It is recommended to measure the hardness for each specimen and record the values in a specimen catalog. Thus, the students have more information that can be correlated with the observed microstructures.

7.3. Discussion and results interpretation

For each microstructure, relevant information is provided, e.g. Steel Designation and Delivery State, Chemical Composition, Manufacturing Technology, Heat Treatments applied, or other processing technologies (e.g. welding, additive manufacturing, hot/cold deformation, casting etc.).

Depending on the application where the steel is used, we expect that the material will provide a series of mechanical properties and a certain behavior in exploitation (e.g. hardness, wear resistance, toughness, fatigue strength, creep strength, corrosion resistance, good weldability etc.).

Based on that information, the students should comment the analyzed microstructure and the non-conformities that they have identified (cracks and microcracks, grain size, microstructural constituents' morphology and distribution, secondary phases, non-metallic inclusions, material imperfections etc.).

All information related to the specimens analyzed shall be filled in the *e*Report Form together with the investigation results: what phases and microstructural constituents, or secondary phases have been identified (they should be labeled on the microstructure image), if has been observed problems related to the heat treatments (e.g. decarburization, oxidation, presence/absence of cracks, macro-deformations) or any aspect that could impact the material performance in exploitation.

It is highly recommended to note all known parameters used during the heat treatment, such as austenitization temperature, cooling rate or cooling environment. Also, if the specimen was subjected or not to tempering process and what were the tempering conditions.

As an optional work, the students can search over the internet for mechanical parts that have been subjected to similar heat treatments, and they can add to the *e*-Report Form additional photos of these parts and relevant information about the applications where those parts are used.

The individual study on this topic can continue by reading numerous technical reports and expertise's available on the internet, for important failure cases.

Materials Science Laboratory

Materials Science and Engineering Department

eReport

<table>
<tr><td>Type of the work</td><td colspan="4">Heat-treated steels microstructures</td></tr>
<tr><td>Scop of inspection</td><td colspan="4">Short description of the work:</td></tr>
<tr><td>Specimen
Steel designation</td><td colspan="4" rowspan="5">Photo/Microstructure
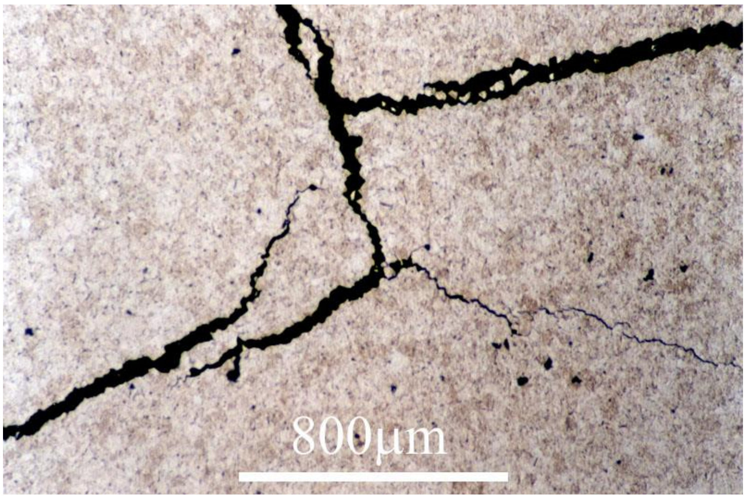

Heat Treatment parameters</td></tr>
<tr><td>Preparation
Etched</td></tr>
<tr><td>Manufacturing Technology</td></tr>
<tr><td>Magnification</td></tr>
<tr><td>Equipment
Metallographic microscope</td></tr>
<tr><td rowspan="4">Observations:
Hardness ______________</td><td colspan="4">Specimen characterization. Results Analysis
Identified phases and microstructural constituents.</td></tr>
<tr><td></td><td></td><td></td><td></td></tr>
<tr><td></td><td></td><td></td><td></td></tr>
<tr><td></td><td></td><td></td><td></td></tr>
<tr><td>Date:</td><td colspan="2">Specialization:</td><td colspan="2">Authorization
Student Name</td></tr>
</table>

7.4. Case study

The study is based on the work presented in [36][12], that presents a metallographic study on a traditional Japanese sword, produced by the *2nd* generation of Muramasa[13] swordsmiths. The *1st* generation of *katana* was made during the 11th-16th century, the *2nd* generation was made during 16th-18th century and the *3rd* generation sword was made during the 18th-19th century.

Japanese sword and Damascus sword are famous in the world historically and technically. Japanese sword has a long history, more than one thousand years. The *katana* is a traditional Japanese sword that has become a symbol of Japan's rich cultural heritage and martial prowess [video].

Symbolism. The *katana* has deep cultural and historical significance in Japan. It is often associated with the samurai, the warrior class of feudal Japan, and embodies the samurai's values of honor, loyalty, and discipline. The sword is considered a sacred object, and its forging is seen as a spiritual process. It is sometimes believed to contain the spirit of the swordsmith. The *katana* is often paired with a smaller companion sword called a *wakizashi*, and together they form the *daisho*, a symbol of the samurai's social status.

Katana represents a combination of exceptional craftsmanship, functional design, and cultural significance. Its association with the samurai and the values they upheld has elevated it to a symbol of pride for the Japanese people, both historically and in contemporary times.

Katanas are often made using a specific Japanese sword smithing technique called *tamahagane*, which involves the smelting of iron sand. The process requires a high level of skill and precision. Traditional *katanas* are made by folding the steel multiple times during the forging process. This folding helps to remove impurities and create a blade with a unique grain pattern. The *katana* typically has a gentle curve, enhancing its cutting efficiency. This design is known as the *sori*.

The metallurgical characterization of the *2nd* generation of Muramasa traditional Japanese sword has revealed the following:

- The microstructure of the sharp edge is lath martensite whereas that of the side and central parts is the fine or coarse pearlite structure.
- The micro-hardness was found maximum in the sharp edge, which is consistent with the structure and carbon content of that zone.
- The non-metallic inclusions in the sword are more than those in ordinary steel. The amount of non-metallic inclusion in the sword is 50-100 times as much as ordinary steel. None of deoxidizers had been used in *Tatara* iron making process which is different from modern iron process.
- The inclusions in the sharp edge are finer and the amount of inclusions is fewer than those in the side and central part. The dominant inclusions are SiO_2, TiO_2, FeO and Al_2O_3. The presence of these oxides justifies that the sword studied has been made by smelting iron sand using *Tatara* process.

---

[12] Open Access article distributed under the terms of the Creative Commons Attribution-Noncommercial License (http://creativecommons.org/licenses/by-nc/3.0/), which permits unrestricted use, distribution, and reproduction in any noncommercial medium, provided the original work is properly cited.

[13] Swordsmith. After Masamune the name of Muramasa is probably the best known of all swordsmiths. He was a native of Kuwana in Ise Province who worked in the early sixteenth century. His earliest recorded dated blade is marked 1501, and there are signed blades dating to the 1530s and 1570s believed to be by the second and third generations, whose works are very similar [The British Museum].

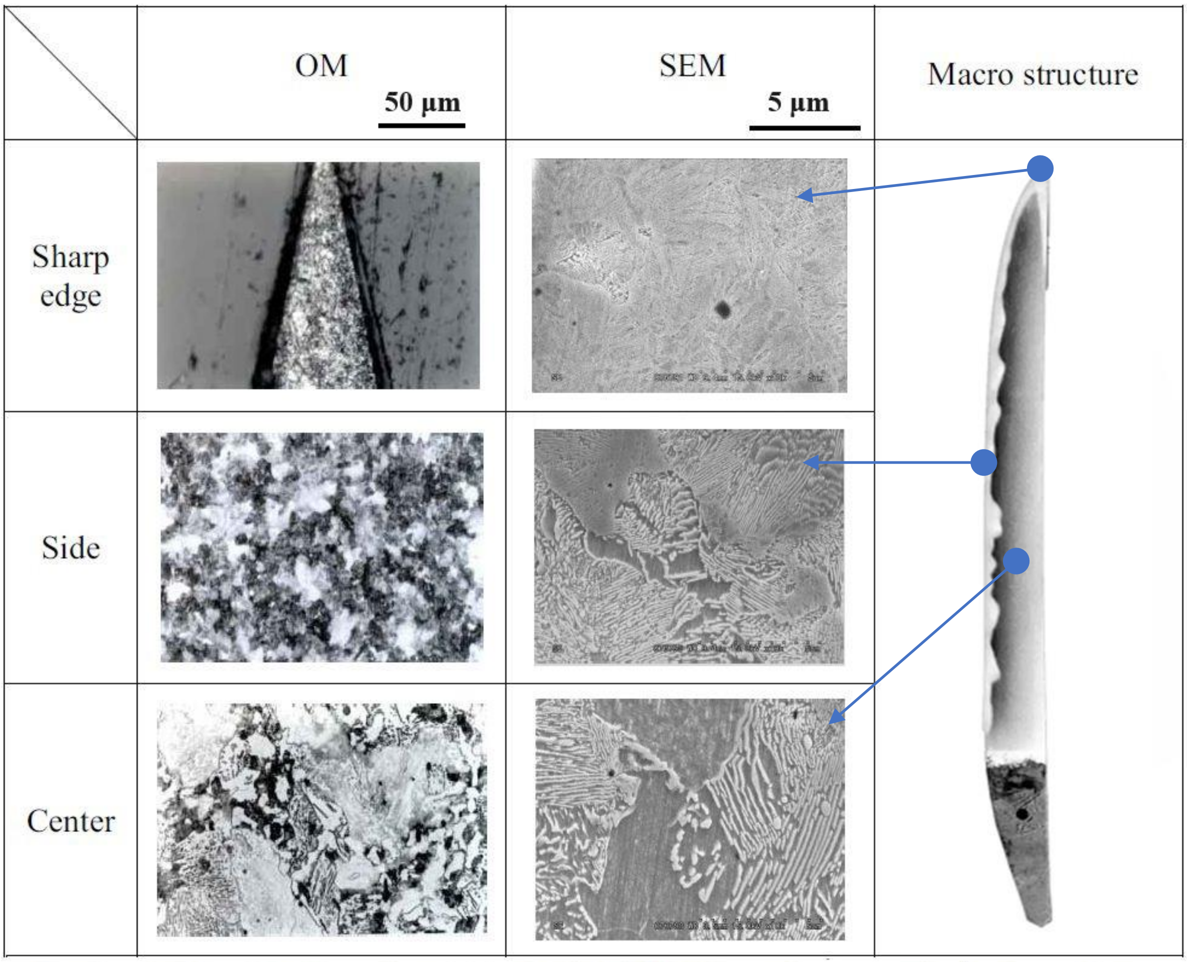

Fig. 102 The microstructures in cross section of a Muramasa, 2nd generation of katana swords by optical microscopy (OM) and scanning electron microscopy (SEM) [36].

The grain size of sharp edge part is observed to be very fine, about 10-15µm due to the effect of ten several times-forgings in sword making process. The distribution of martensite structure is limited only to the sharp edge of the sword and in other areas fine pearlite or coarse pearlite structures are observed dominantly. The morphology of the martensite in the sharp edge is lath type.

The maximum hardness[14] of the sharp edge is 720-730 HV. This hardness level almost corresponds to the hardness of martensite which contains 0.78 mass% carbon. It has been found that the hardened area was limited to the sharp edge.

At a short distance from the sharp edge, the hardness decreases drastically. In the center part of the blade, the slow quench allows to grow soft pearlite, improving the toughness, Fig. 102.

Fig. 103 Clay coating of the blade before quenching.

By coating the blade in clay before heating and quenching it, which results in a distinctive pattern on the edge of the blade known as the *hamon*.

---

[14] Other similar studies reported a maximum hardness level in the sharp edge about 700-820 HV [36].

8. Welded steels microstructures

8.1. Theoretical background

The industries in which welding is a critical enabling technology account for 59% of the total value of production by all Manufacturing, Construction, and Mining industries. Durable goods manufacturing industries in which welding is a critical enabling technology[15] account for 90% of total U.S. durable goods value of product [more info].

Materials joining and forming are essential cross-cutting technologies, contributing around $200 billion in value to US-manufactured products annually. The industries that use welding to manufacture their products are the driving force of a modern economy. They are largely responsible for the infrastructure, capital goods, and commercial products that sustain a relatively high standard of living for billions of people across the world. Welding-related industries construct power plants, factories, bridges, vehicles, and pipelines.

These welding related industries employ a large portion of U.S. workers and generate a significant part of the nation's wealth. Manufacturing alone employs more than 12 million people and accounts for 12% of GDP. In 2014, the automotive industry spent about $120 billion on research and development. That's about 16% of the total amount spent on R&D across all industries worldwide.

The impact of welding technologies on the Gross Domestic Product (GDP) can be analyzed through various lenses, considering both direct and indirect effects. Welding technologies play a crucial role in various industries, and their influence on GDP can be substantial.

- **Manufacturing Sector Contribution**. Welding is integral to the manufacturing sector, especially in industries such as automotive, aerospace, construction, and shipbuilding. As these industries grow, driven by technological advancements in welding, they contribute significantly to global GDP.
- **Infrastructure Development.** Welding is essential in construction and infrastructure development. The construction of buildings, bridges, pipelines, and other infrastructure projects relies heavily on welding technologies.
- **Productivity and Efficiency.** Advanced welding technologies enhance productivity and efficiency in manufacturing processes. This, in turn, can lead to cost savings and increased output, positively impacting the overall economic productivity and contributing to GDP growth.
- **Innovation and Research**. Investments in research and development of welding technologies can foster innovation. The development and adoption of new welding techniques and materials can lead to the creation of high-tech products and industries, driving economic growth.
- **Job Creation**. Growth in welding-related industries creates job opportunities. The employment generated directly and indirectly by the welding sector contributes to income levels and, consequently, consumer spending, which is a significant driver of economic activity.
- **Global Competitiveness**. Countries with advanced welding technologies and skilled workforce can enhance their global competitiveness. This can lead to increased exports and a favorable trade balance, positively affecting the GDP.

---

[15] Welding-Related Expenditures and Productivity Measurement in U.S. Manufacturing, Construction, and Mining Industries Report, WEP Report AR (aws.org)

- **Energy and Resource Efficiency**. Welding technologies that promote energy efficiency and sustainable practices can have positive economic implications. Cost-effective and environmentally friendly welding processes contribute to long-term economic sustainability.
- **Supply Chain Effects**. The welding sector is often part of complex supply chains. Efficiency improvements in welding processes can positively impact the entire supply chain, leading to overall economic benefits.

It's important to note that the impact on GDP can vary by region and depend on the level of industrialization, technological adoption, and government policies. Additionally, economic impacts may not be immediate, as the full effects of technological advancements in welding may take time to materialize. Overall, advancements in welding technologies can contribute significantly to economic growth and development.

Welding technologies, when not applied correctly or when there are deficiencies in the welding process, can contribute to failure cases in various industries. Failure in welded components can have serious consequences, ranging from structural failures to safety hazards.

Metallography analysis plays a crucial role in assessing the quality of welded structures. It involves the microscopic examination of the microstructure of welded joints and evaluation of the weld's integrity, identifying potential defects, and ensuring that the material meets specified quality standards.

The metallographic analysis of the welded samples includes the following aspects:

- **Identification of Microstructural Features** within the weld zone. This includes the analysis of weld metal, heat-affected zone (HAZ), and base metal. By understanding the microstructure, one can assess the impact of welding processes on the welded metallic structure behavior.
- **Grain Structure Evaluation**. Metallography helps in evaluating the grain structure of the weld and adjacent regions. The size, shape, and distribution of grains can provide insights into the thermal history of the weld and its mechanical properties. Abnormalities in grain structure can indicate potential issues like overheating or rapid cooling.
- **Detection of Weld Defects**. Metallography is effective in detecting and characterizing weld defects such as porosity, cracks, inclusions, and lack of fusion. The analysis helps determine the size, shape, and distribution of these defects, providing information about their potential impact on the structural integrity of the weld.
- **Phase Analysis**. Different welding processes and parameters can result in changes in the phases present in the microstructure. Metallography allows for the identification and analysis of these phases, helping to ensure that the material has the desired mechanical and metallurgical properties.
- **Assessment of Heat-Affected Zone (HAZ).** Welding induces thermal changes in the HAZ, which can affect the material properties. Metallography helps assess the microstructural changes in the HAZ, allowing for an understanding of potential issues such as softening, hardening, or the formation of undesirable phases.
- **Evaluation of Weld Penetration**. Metallography is used to assess the depth of weld penetration into the base metal. Incomplete penetration or excessive penetration can be identified through microscopic examination, providing insights into the quality of the welding process.

- **Quality Control and Assurance**. Manufacturers can ensure that the welding processes meet specified standards and that the resulting structures have the required mechanical properties.
- **Failure Analysis**. In the event of a welding-related failure, metallography can be instrumental in conducting failure analysis. Examining the microstructure of failed welds helps in determining the root cause of the failure and developing corrective measures to prevent similar issues in the future.

Thus, metallography analysis is a powerful tool for assessing the quality of welded structures by providing detailed insights into the microstructure and identifying potential defects and issues. This information is invaluable for ensuring the reliability, safety, and performance of welded components in various industries.

The morphology and characteristics of the microstructural constituents in the welded materials are strongly dependent on the chemical composition of the base metal and the thermal cycle of the welding process. In technical literature can be found many articles that refer to these aspects. In the next part, are described and presented a series of microstructures depicting specific phases and constituents that can be found in welded specimens.

Widmanstätten Ferrite Granular Bainitic Ferrite Bainitic Ferrite

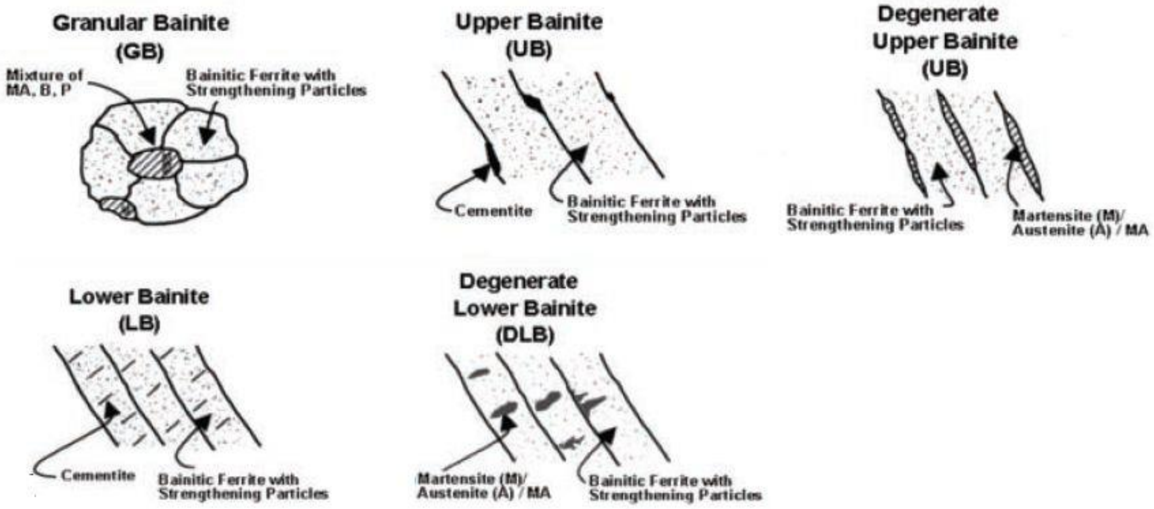

Fig. 104 Microstructural aspects of ferritic microstructures in low carbon steels [more info].

Due to large experimental data and different terminology used for characterizing such microstructures, one could be confused by the different names used in the specific literature.

In this respect, we recommend the terminology adopted by the ISIJ Bainite Committee[16], an internationally recognized organization, Table 6.

Table 6. Symbols and nomenclature for ferritic microstructures according to ISIJ Bainite Committee.

Nr.	**Symbol**	**Nomenclature**
Major matrix-phase		
1.	α_p	Polygonal ferrite
2.	α_q	Quasi-polygonal ferrite
3.	α_w	Widmanstätten ferrite
4.	α_B	Granular bainitic ferrite
5.	α^0_B	Bainitic ferrite
6.	α'_m	Dislocated cubic martensite
Minor secondary phases		
7.	γ_r	Retained austenite
8.	MA	Martensite-austenite constituent
9.	α_M	Martensite
10.	aTM	Auto-tempered martensite
11.	B	BII, B2: upper bainite Bu: upper bainite
12.		B_L: lower bainite
13.	P’	Degenerated pearlite
14.	P	Pearlite
15.	θ	Cementite particle

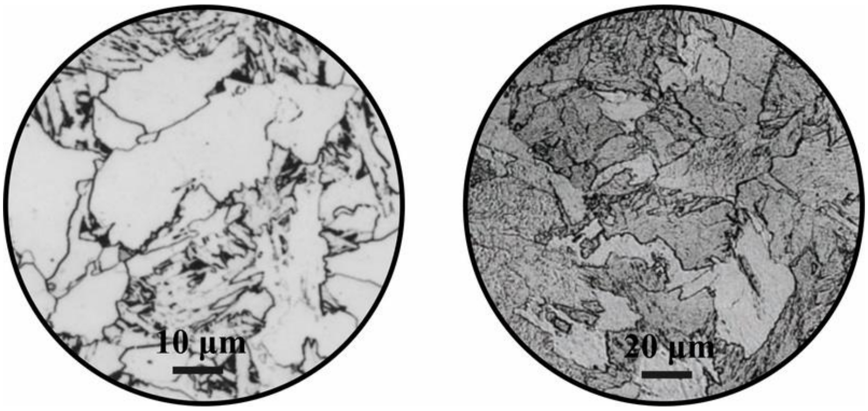

Fig. 105 Microstructural aspects of quasi-polygonal ferrite in HAZ of welded steels.

Polygonal or Equiaxed Ferrite (α_p) forms at high temperatures and for slow cooling rates and is nucleated at the grain-boundary allotriomorph ferrite and grows into equiaxed grains. Accordingly to International Institute of Welding (IIW), this phase is called primary ferrite. In some scientific articles is referred as Massive Ferrite. Depending on the nucleation site, the IIW makes distinction between primary ferrite nucleated on grain boundaries PF(G) and primary ferrite nucleated inside grains, PF(I).

The coarse, elongated crystals of ferrite are referred to as Widmanstatten ferrite (α_W), Fig. 104. The Widmanstatten ferrite nucleates at austenite grain boundaries or from polygonal ferrite allotriomorphs.

---

[16] The ISIJ Bainite Committee classification identifies and names all the microstructures usually obtained in low carbon microalloyed steels, including two bainitic microstructures: granular ferrite and bainitic ferrite, commonly called granular bainite and lath-like bainite, respectively.

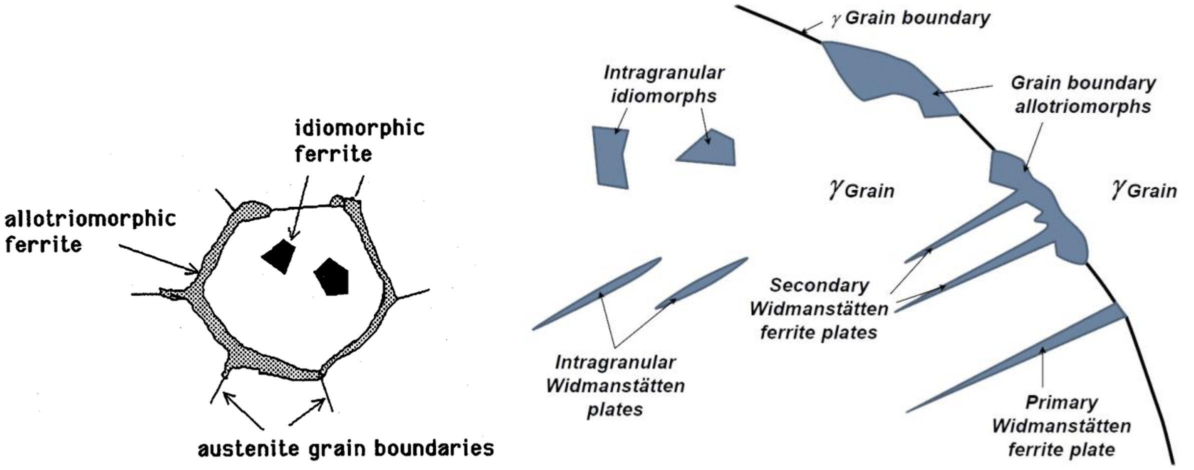

Fig. 106 Schematic representation of the ferritic microstructures.

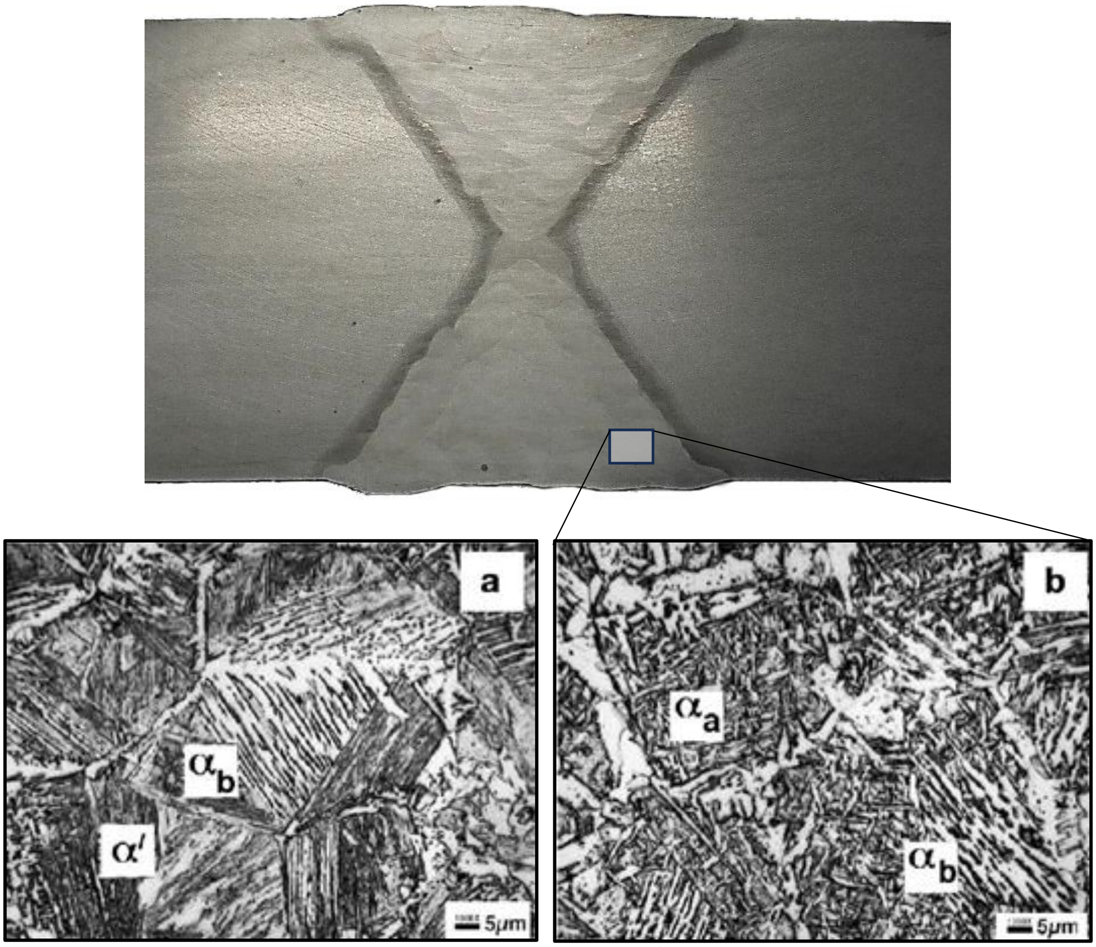

Fig. 107 Typical aspects of bainitic ferrite (α_B), martensitic (α'_m) and acicular ferrite in weld metal (α_a).

As can be observed in Figure 108, the microstructural ferrite/pearlite bands of the parent metal are clearly illustrated, that is specific to hot rolled products used in various structural metallic constructions.

In Figure 109 is depicted the microstructure of the weld metal, which is preponderantly bainitic with ferritic grains (light color), having quasi-polygonal shapes, which suggest slow and moderate cooling conditions of the weld. Near the fusion line, some grown granular bainitic grains (α_b) can be observed in the parent metal (in the coarse-grain area). Also, in the HAZ a network of allotriomorphic ferrite grains (light color) can be distinguished, indicating the prior size of the austenite grains.

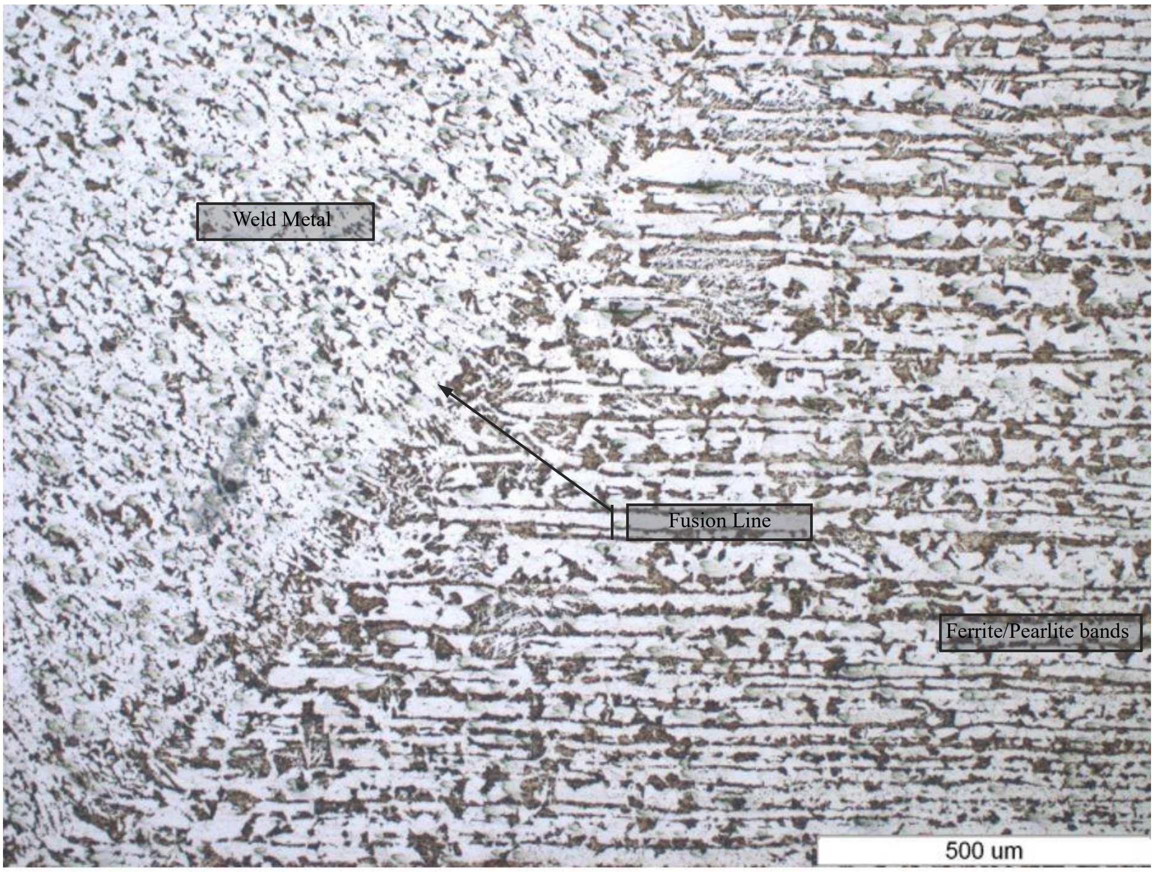

Fig. 108 Parent metal microstructure, S355 J2, Nital 2%, x100.

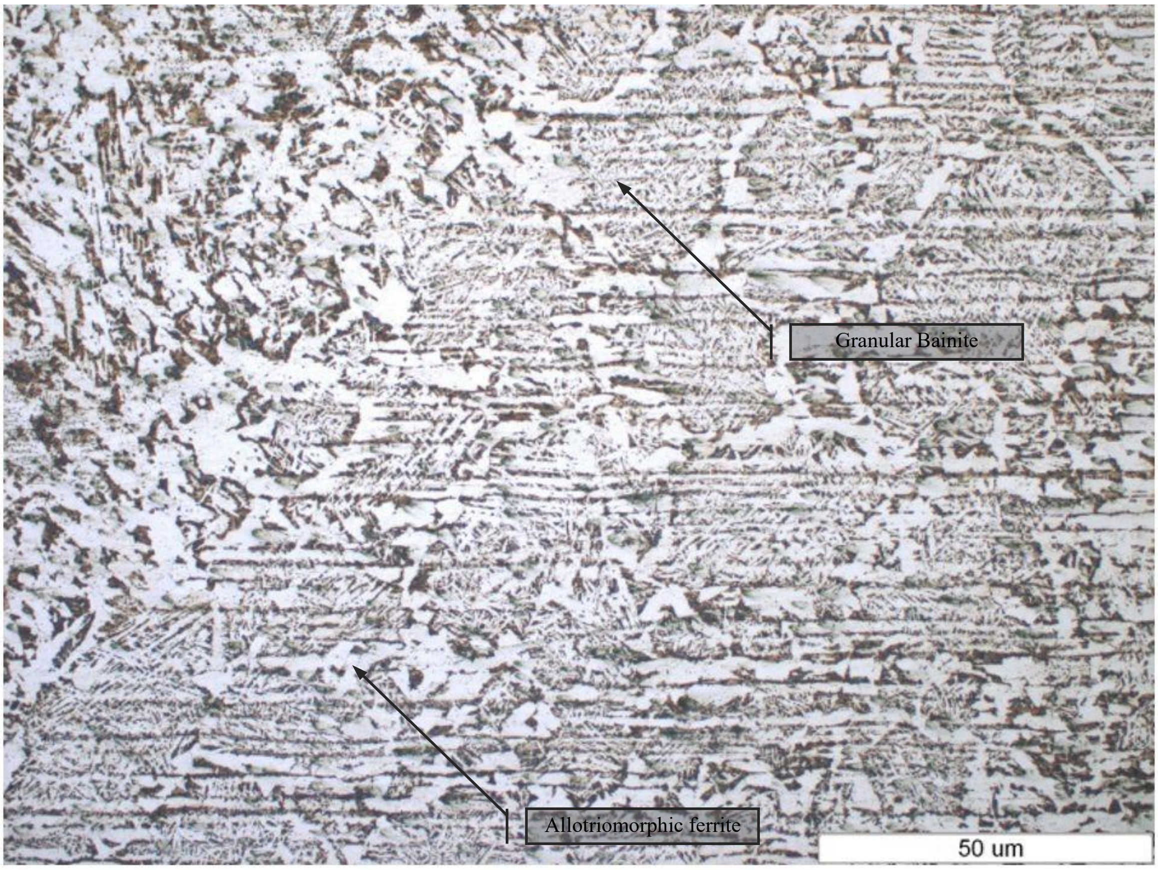

Fig. 109 Microstructural aspects of S355 J2 steel in weld deposit and in HAZ (Nital 2%), x1000.

Some degenerate pearlite grains with discontinuous lamellae or rods (called microphases – because occur in very small fractions), can be observed also in Figure 108. By the time the weld deposit cools to about 500 ºC, most of the austenite has been transformed already. The small quantity of remaining austenite (about 5%) is enriched in carbon and either transforms to martensite, or into pearlite which is degenerate because it does not have the opportunity to establish a lamellar structure [more info].

The degenerate pearlite consists of 'block' (a region in which ferrite orientations are nearly the same) and 'colony' (a region containing cementite particles of nearly the same orientation), both of which are similar to those in lamellar pearlite of the parent metal. The microstructural transformation of austenite from low to intermediate, to high cooling rate can be summarized as:

ferrite-pearlite → ferrite-degenerate pearlite → bainitic ferrite

Although degenerate pearlite is also formed by a diffusion process, a discontinuous lamellae morphology developed, the difference being attributed to insufficient carbon diffusion in order to develop continuous lamellae structure.

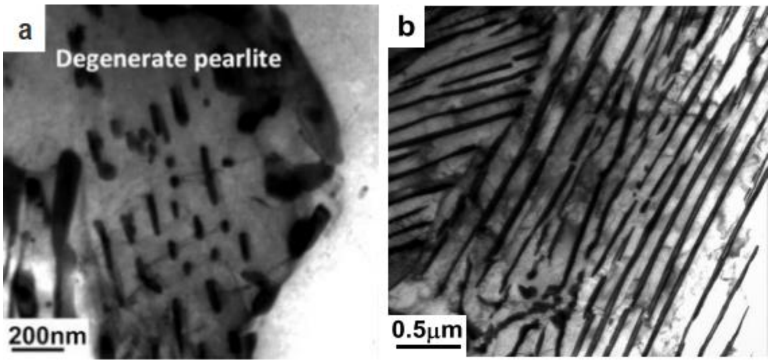

Fig. 110 Details of degenerate pearlite morphology, bright field TEM micrographs [more info].

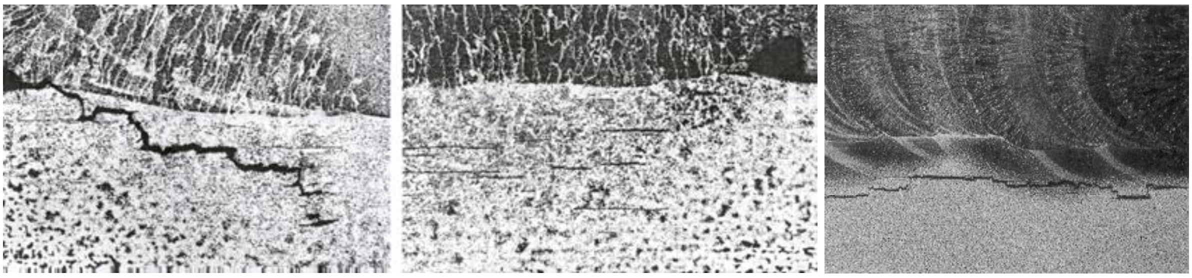

Fig. 111 Aspects of lamellar tearing that occur in welded structures [more info].

A specific defect that appears in welded structures is lamellar tearing. It occurs normally in T-butt and fillet welds, parallel to the fusion weld boundary and the plate surface, Figure 111. The lamellar tearing is associated with a high concentration of elongated inclusions oriented parallel to the surface of the plate, tearing being trans-granular with a stepped appearance [TWI].

Thus, lamellar tearing is a form of cracking that occurs in the base metal of a weldment due to the combination of high localized stress and low ductility of the plate in the through-thickness direction.

8.2.Working procedure

The specimens available in laboratory are labeled and should be prepared according to instructions given in Laboratory no 2 for metallographic specimen preparation and etching. The microstructure images can be captured using the digital camera from microscope or can be photographed using a smartphone camera. All relevant information should be filled in the *e*-Report file.

8.3.Discussion and results interpretation

For each welded specimen, relevant information should be provided, e.g. Material Designation and Delivery State, Chemical Composition, Heat Treatments applied.

After the proper specimen preparation, a macro examination should be conducted. The students should inspect the welded specimens, looking after:

- Undercuts
- Craters
- Cracks
- Slag inclusions
- Underfilled zones
- Lack of fusion
- Geometric non-conformities of the weld
- Porosity in weld.

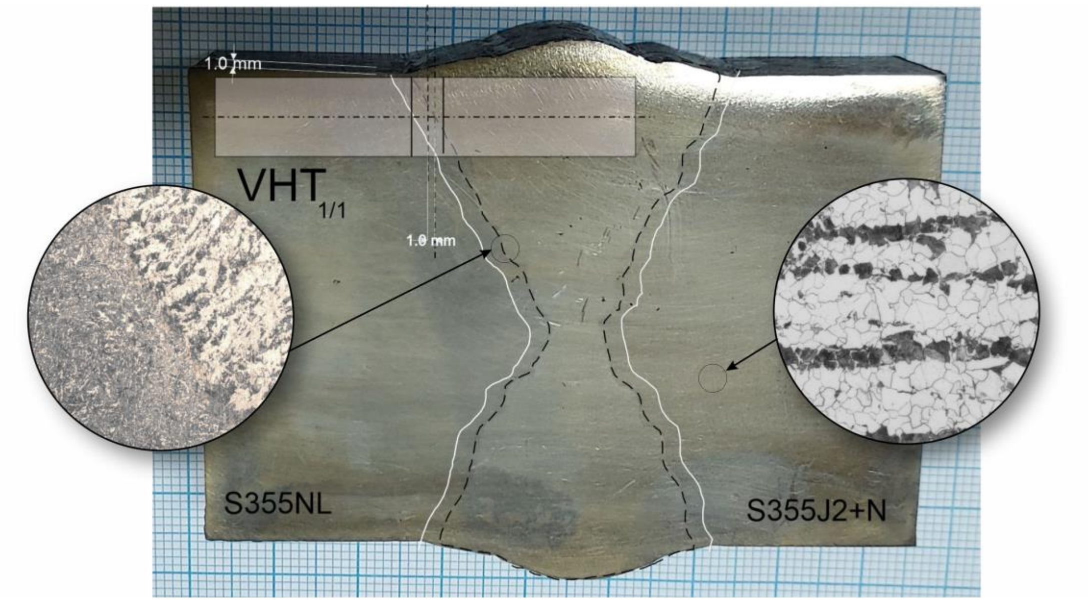

Fig. 112 Macro aspects of a butt-welded specimen.

The microstructural analysis should be performed in parent metals, weld metal and in HAZ (see delimitations of those areas in Figure 112). The students should check the specimens to detect possible cracks and microcracks, to measure the grains size of different phases, to characterize the morphology and distribution of secondary phases, non-metallic inclusions, etc.

Some simple geometric measurements can be performed, like the width of HAZ, the depth of weld penetration, weld reinforcement, and weld size. It would be very useful to have data about the hardness measured in parent metals, HAZ and weld metal.

For welds, measuring the hardness is important to ensure that hydrogen cracking or sulphide stress corrosion cracking does not occur. Depending on the welded materials, some limits are imposed (check CR ISO 15608). A hardness of up to 350HV (for structural steels) is often the maximum allowed for welding procedure qualification, in order to ensure that hydrogen cracks are avoided.

All information related to the welded specimens analyzed shall be filled in on the *e*-Report Form together with the investigation results. The individual study on this topic can be continued by reading numerous technical reports and expertise’s available on the internet.

Materials Science Laboratory

Materials Science and Engineering Department

eReport

Type of the work	Welded Steels Microstructures
Scop of inspection	Short description of the work:
Specimen Steel designation	Photo/Microstructure 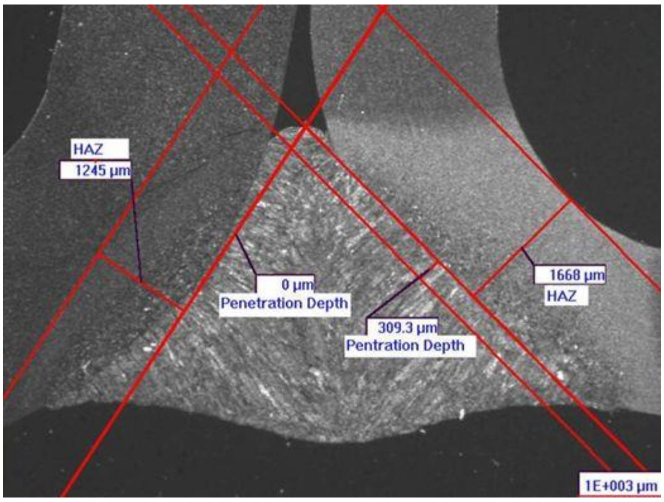 Welding parameters
Preparation Etched	
Manufacturing Technology	
Magnification	
Equipment Metallographic microscope	
Observations: Hardness ______________	Specimen characterization. Results Analysis Identified phases and microstructural constituents.

Date:	Specialization:	Authorization Student Name

8.4. Case study

Modern economy relies on industries in which welding is a critical enabling technology (e.g. over 90% of total U.S. manufactured durable goods depends critically on welding technologies).

"Tak ada gading yang tak retak" is an ancient Indonesian proverb that in Romanian could be translated as "*Nu există fildeş care să nu fie crăpat*." In the world of welded metallic structures, the Indonesian proverb could be translated as "*there will be no design without flaw and there will be no construction without defect*".

On the internet are available a series of failure databases associated with material failures due to fatigue, corrosion, creep, design flaw and welding defects that had lead to material failure in oil and gas production, hydrocarbon industry, oil and gas distribution network, energy power plants, naval and railway transports, petrochemical industry etc.

In Figure 111 has been shown the aspects of lamellar tearing that can occur in large, welded structures. As an example, lamellar tears were produced when attempting the repair of lack of root penetration in a brace weld from BP Forties platform, Fig. 113 (lamellar tearing is associated with high concentration of extended inclusions, parallel to the surface of the plate, and tearing is trans-granular with stepped appearance. Fig. 111).

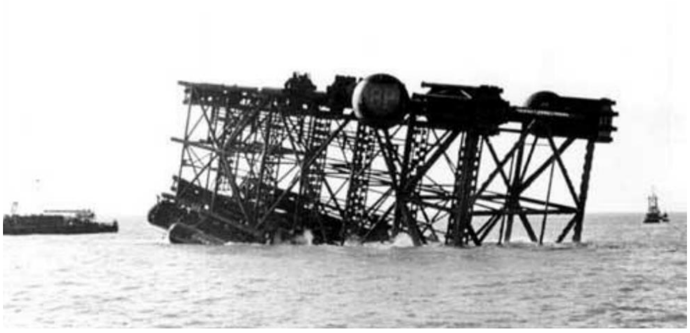

Fig. 113 BP Forties platform, the second largest oil field in the North Sea [more info].

Read more about at: The 50 Major Engineering Failures (1977-2007) | Integrity Engineering

Instead of viewing one of the severe failure cases due to welding associated problems and defects, the case study in this chapter will present a very unusual phenomena related to welding processes, namely the cold-welding phenomena.

NASA launched "Galileo" spacecraft into space on October 9, 1989, with the main aim of gathering data about Jupiter. When Galileo spacecraft reached Jupiter on April 10, 1991, NASA tried to open its high gain antenna, but three ribs of antenna got cold welded to the body and they wouldn't open which caused antenna failure.

The incident of cold welding in space nearly destroyed NASA's space operation, the mission costs being several billion dollars. Considering the considerable distance between the earth and Jupiter, the scientists at NASA had designed a special antenna to complete the mission (the antenna after becoming functional, should have transmitted roughly 80Kb data per second, to the earth station).

What has happened?

Cold welding or contact welding is a solid-state welding process in which joining takes place without fusion or heating at the interface of the two parts to be welded. Unlike in fusion welding, no liquid or molten phase is present in the joint.

Spacecraft subsystems contain a variety of engineering mechanisms that exhibit ball-to-flat surface contacts. These may be periodically closed up to several thousand times during ground testing and the operational life of the spacecraft. These contacts are usually designed to be static, but in reality, they are often subjected to impact forces.

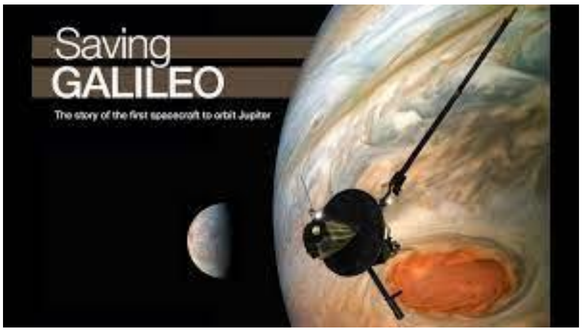

[video]

On the ground it is unusual to witness adhesion between metallic interfaces independently of whether they are subjected to impact or fretting. This is because the surfaces are re-oxidized after each opening, so that the next closing is made on new oxide layers. In space, the oxide layers are broken irreversibly. Therefore, the following closing is metal–metal contact, thereby enabling cold welding effects.

In 2009 the European Space Agency (ESA) published a peer reviewed paper detailing why cold welding is a significant issue that spacecraft designers need to carefully consider [read more at ESA STM-279 Cold Welding due to Impact and Fretting under Vacuum].

Impacts during closing can eventually degrade the metal's surface layers, whether they are natural oxides, chemical conversion films or even metallic coatings. This can dramatically increase the tendency of these contacting surfaces to 'cold weld' to each other.

Another, even more dangerous effect is fretting. Vibrations occurring during launch or during the movement of antennas in space, for example, can lead to small oscillating movements in the contact, which are referred to as 'fretting'. This lateral motion can cause even more severe surface layers destruction than impact and may lead to cold welding effects similar to bonding techniques.

In summary, under impact and fretting conditions, contaminant layers (oxides) are removed much more quickly than under static contact, and cold welding occurs much sooner than expected. This may not only reduce the lifetime of a satellite, but can also endanger space missions, since any opening or ejection mechanism may fail due to cold-welded contacts.

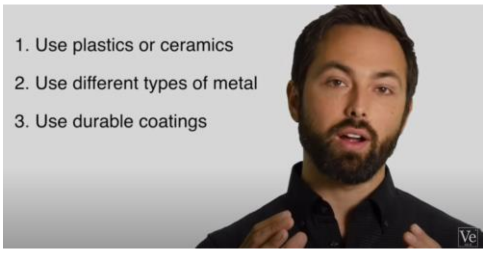

An interesting video material about cold-welding can be watched, by using the following link:

Why Metals Spontaneously Fuse Together in Space - YouTube

While cold-welding can pose serious problems for spatial missions, the same phenomena can be used successfully in the nanofabrication processes. Scientists have discovered that very thin nanowires of gold having a diameter of 10 nm can be cold-welded within seconds, just by bringing them in contact by applying minimal pressure. Studies have shown that the welds are nearly perfect, with the same crystal orientation, strength and electrical conductivity as the rest of the nanowire. Another possible application for cold welding is spacecraft repairing in case of collisions with micrometeoroids from space [more info].

9. Cast iron microstructures

9.1.Theoretical background

Cast iron is a ferrous casting alloy characterized by its high carbon content (2.1% up to 6.67% C that correspond to cementite – Fe_3C), and the presence of silicon.

The cast iron microstructure contains graphite in various forms, influencing their mechanical and physical properties. The graphite shapes, size and distribution from the cast iron, imparts unique characteristics such as brittleness, hardness, and excellent castability. The cast iron can be further classified into distinct types, including:

- Gray iron with its characteristic graphite flakes,
- White iron distinguished by cementite structures,
- Ductile iron featuring spheroidal graphite nodules for improved thoughness,
- Malleable iron produced through heat treatment of white iron, enhancing its malleability.

Advanced formulations of cast iron may incorporate alloying elements, refining the material's properties to meet specific engineering requirements. These alloys find applications across diverse industries, including automotive, construction, and manufacturing, owing to their exceptional strength, heat resistance, and versatility in intricate casting shapes. The nuanced microstructural variations and alloy compositions within cast iron alloys allow for tailored solutions catering to a spectrum of technological demands and applications. Below are presented the main characteristics of each cast iron type:

Gray Iron (Graphite Flake Iron)

- Microstructure: Contains graphite flakes in a matrix of ferrite and pearlite, Fig. 115.
- Properties: Good casting properties, high wear resistance, and excellent machinability. It has good damping capacity and is suitable for applications like engine blocks, pipes, and cookware.

White Iron (Chilled Iron)

- Microstructure: Contains cementite (iron carbide) in a pearlitic matrix, Fig. 116.
- Properties: Extremely hard and brittle, with excellent wear resistance. Commonly used for applications where abrasion resistance is crucial, such as in crushing machinery, grinding balls, and excavator teeth.

Ductile Iron (Nodular Iron or Spheroidal Graphite Iron)

- Microstructure: Contains graphite in the form of nodules, which provides flexibility and ductility, Fig. 117.
- Properties: Improved tensile strength, toughness, and ductility compared to gray iron. Used in components requiring higher strength and toughness, such as pipes, automotive parts, and hydraulic components.

Malleable Iron

- Microstructure: White iron castings are heat-treated to decompose the cementite compound into irregularly shaped nodules of graphite in a matrix of ferrite or pearlite, depending on the cooling conditions, Fig. 118.
- Properties: Combines the strength of white iron with the ductility of nodular iron. Used for components that require a combination of strength and ductility, such as pipe fittings and certain automotive parts.

Compacted Graphite Iron (CGI)

- Microstructure: Similar to gray iron but with a different graphite structure, Fig. 119.
- Properties: Offers a balance between the strength of ductile iron and the thermal conductivity of gray iron. Used in high-performance engine components, such as cylinder heads and exhaust manifolds.

Alloyed Cast Iron

- Microstructure: Contains additional alloying elements such as vanadium, nickel, chromium, or molybdenum, Fig. 120.
- Properties: Enhanced mechanical properties and improved resistance to corrosion and wear. Used in specialized applications where specific properties are required, such as in chemical and corrosive environments.

The choice of cast iron type depends on the specific requirements of the application, considering factors like strength, hardness, ductility, machinability, and resistance to wear or corrosion. Engineers and specialists carefully select the appropriate type of cast iron based on the demands of the end-use application. Some key applications of cast iron, are illustrated below:

Engineering Components

Automotive Industry: Cast iron is commonly used for engine blocks, cylinder heads, and brake components due to its high strength and good heat dissipation properties.

Machinery and Equipment: Cast iron is utilized for manufacturing various components in heavy machinery, such as gears, pulleys, and flywheels.

Pipes and Pipe Fittings

Water and Sewer Systems: Ductile iron, a type of cast iron, is often used for pipes and fittings in water and sewer systems due to its durability and corrosion resistance.

Railway Industry:

Railway Components: Cast iron is used for manufacturing components like brake shoes, brake discs, and railcar couplings due to its high wear resistance and strength.

Pumps and Valves:

Fluid Handling Equipment: Cast iron is commonly employed in the production of pumps, valves, and other fluid-handling equipment due to its corrosion resistance and strength.

Fig. 114 Exemples of applications for cast iron alloys.

Fe, C 3.52, Si 3.26, Mn 0.47 (wt%) (Grey cast iron)
Fig. 115 Grey cast iron microstructure [more info, © DoITPoMS, University of Cambridge].

The addition of a substantial amount of silicon to a relatively low carbon cast iron serves to induce the cementite to transform to ferrite and graphite flakes. This is improving machining and wear resistance. The graphite flakes are very soft and have low density so compensate for freezing contraction upon solidification, however they also act effectively as cracks making the cast iron is brittle, Figure 115.

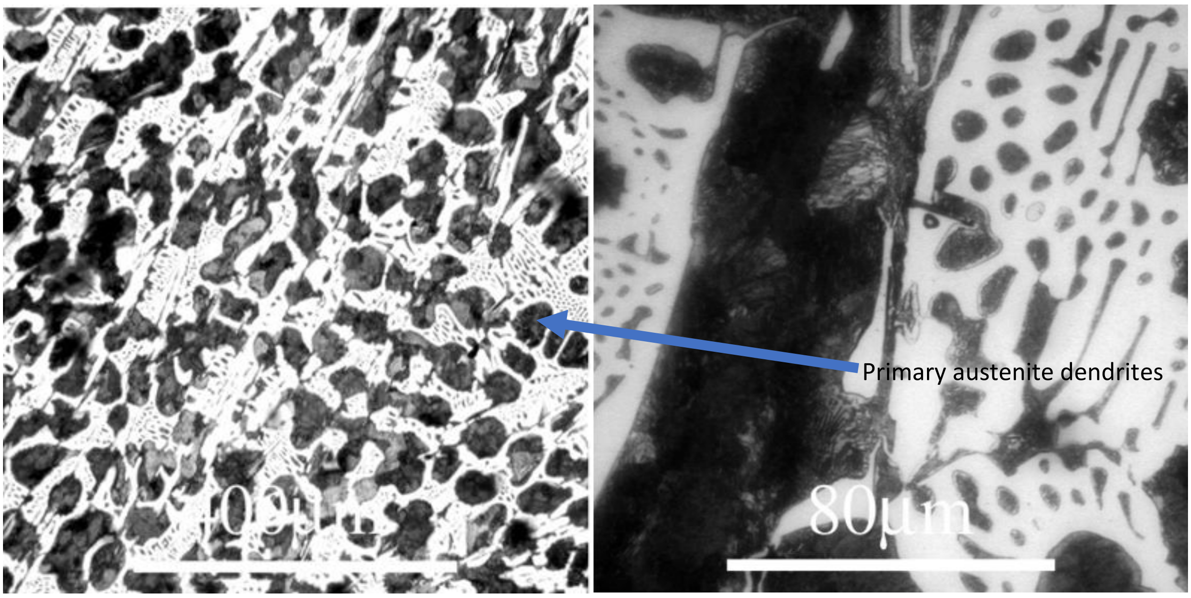

Fig. 116 White cast iron microstructure (2.4 wt % C), [more info, © DoITPoMS, University of Cambridge].

With a carbon equivalent less than the eutectic composition a hypoeutectic white cast iron is formed. Primary austenite dendrites (dark) are first to form from the liquid. At the eutectic the remaining liquid transforms to a mixture of austenite and cementite (light) with further transformation of the austenite to ferrite and pearlite at low temperatures (A_1), Figure 116.

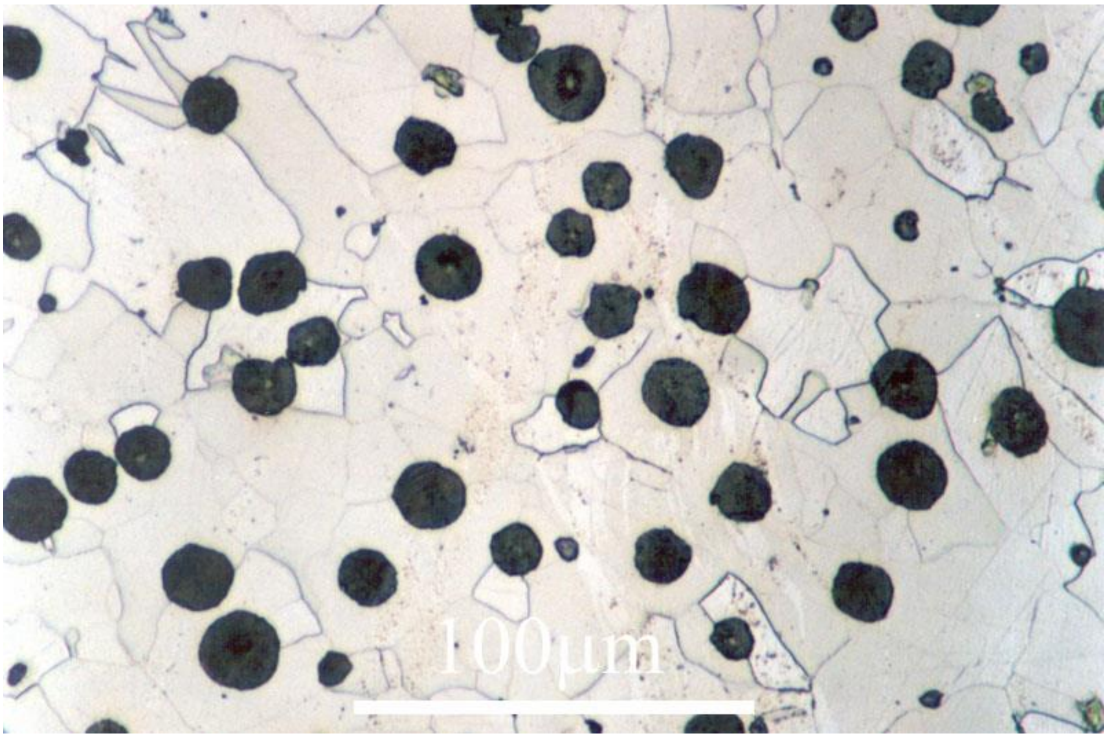

Fe, C 2.40, (wt%) (Ductile cast iron with magnesium induced spheroidised graphite)
Fig. 117 Ductile cast iron microstructure [more info, © DoITPoMS, University of Cambridge].

Cast iron is a brittle material and it is advantageous to process it in such a way to improve its ductility. The brittleness is partially due to the graphite flakes which act as nucleation sites for cracks. Therefore it is an advantage to have graphite present as nodules. This can be achieved by a heat treatment regime or by the addition of a small amount of Mg at elaboration, which poisons the graphite growth directions.

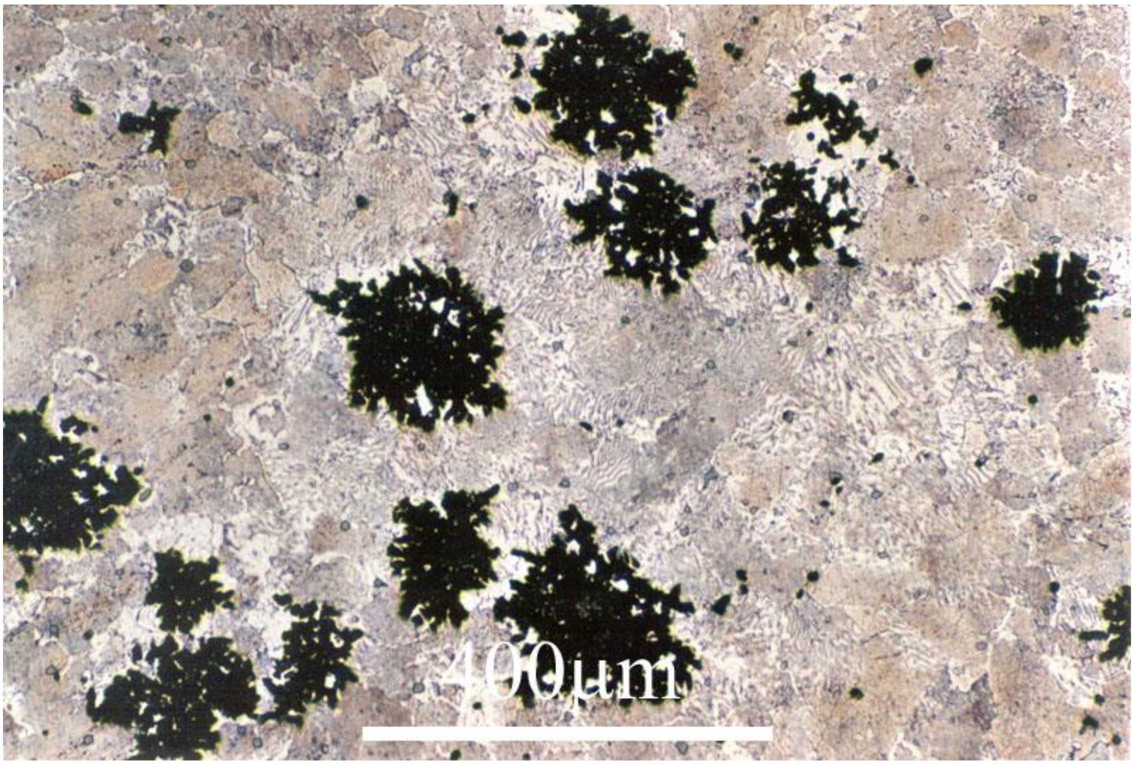

Fe, C 2.4, Si 1.1, Mn 1.1 (wt%). Upon cooling the austenite transforms to pearlite at the eutectoid temperature, leaving a microstructure of pearlite and graphite.
Fig. 118 Pearlitic malleable cast iron [more info, © DoITPoMS, University of Cambridge].

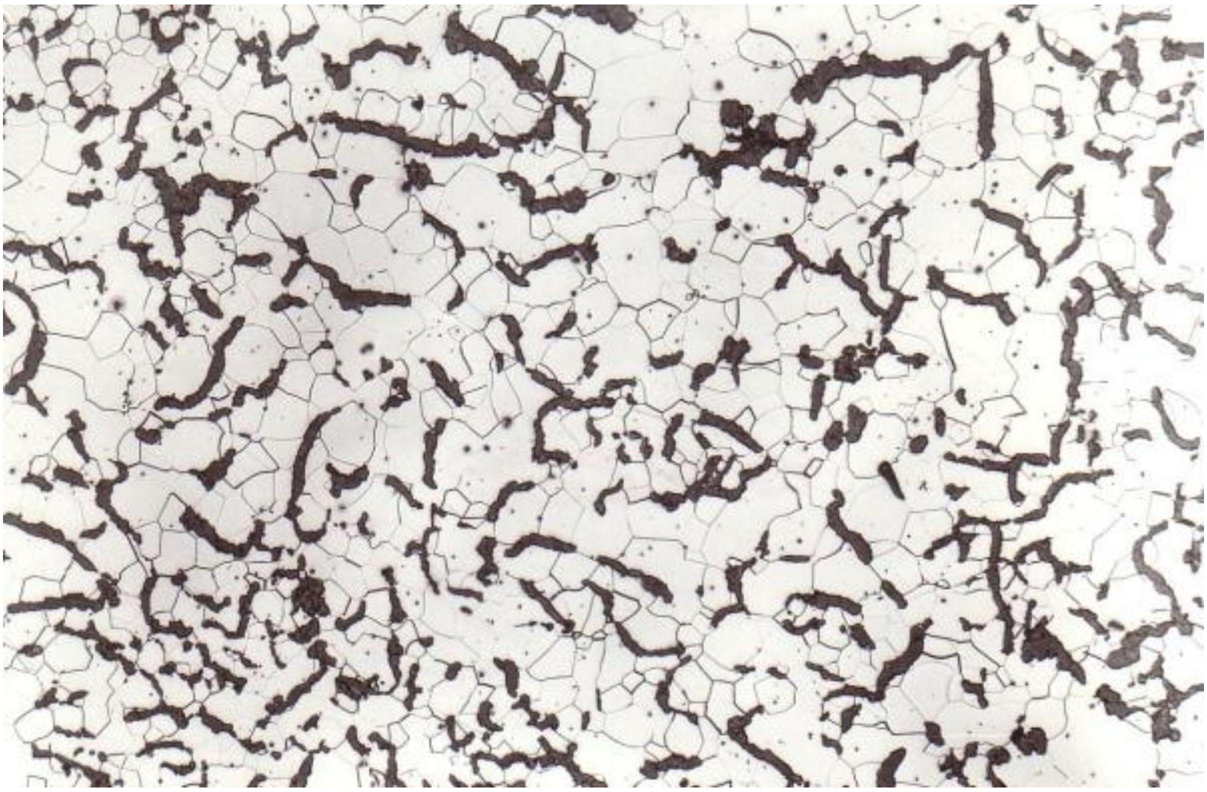

Fig. 119 Compacted graphite cast iron [more info].

Accordingly with the cooling conditions, the matrix of compacted graphite (vermicular) cast iron may be formed as ferritic, pearlitic/ferritic, or mainly pearlitic structure. Cast iron, including the vermicular graphite or compacted graphite iron is standardized by EN 1560.

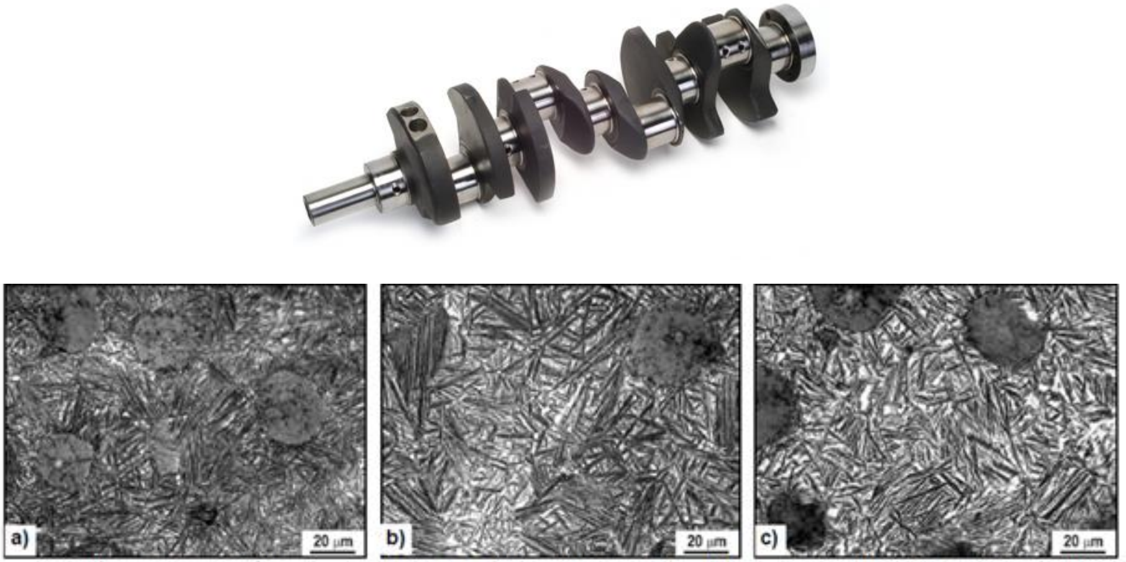

Microstructure of unalloyed ADI material austempered for 1 hour at: a) 300°C; b) 350°C; c) 400°C

Fig. 120 Austempered Ductile Iron (ADI) microstructures [more info, video].

ADI is the abbreviation of “Austempered Ductile Iron”, Figure 120. According to German standardization it is referred to as “Bainitic nodular graphite cast iron”, although it does not contain any bainite, which can be defined as “non-lamellar ferrite-carbide aggregate”. In Europe, the material is standardized according to EN 1564 and in the USA to ASTM A897.

The ausferritic microstructure is achieved by heat treatment (austempering) and is characterised by needle-shaped ferrite that is present in a carbon-supersaturated matrix named Ausferrite.

Below the temperature of 400 to 500°C, the pearlite transformation is no longer possible. Instead, short-term diffusion takes place and the carbon displaced from the ferrite accumulates in the austenite, whose carbon content may increase up to 2 wt% due to this process. This stabilizes the austenite down to low temperatures and the resulting structure comprises a mixture of finely acicular ferrite and austenite, called Ausferrite, see Figure 120 [see more ADI microstructures].

ADI crankshafts were fitted into engines where noise and vibration measurements were undertaken followed by engine durability testing.

Due to ADI castings excelent characteristics, some steel forged parts have been replaced by ADI in key applications, like the crankshafts manufacturing for high performance engines, Figure 120.

9.2. Working procedure

The cast iron specimens available in laboratory are labeled and should be prepared according to instructions given in Laboratory no 2 for metallographic specimen preparation and etching. The microstructure images can be captured using the digital camera from microscope or can be photographed using a smartphone camera. All relevant information should be filled in the *e*-Report file. For quantitative analysis, the students should refer to the procedure described in Laboratory no 3.

9.3. Discussion and results interpretation

Based on the microstructures analysed and on chart for graphite classification presented in Figure 121, the students should identify the graphite type and the size class, also the graphite distribution (on polished specimens), see Figure 122:

- Type I graphite is nodular in shape and is the normal and desirable graphite form in ductile iron.
- Type II graphite consists of slightly irregular nodules.
- Type III is the graphite form most often seen in malleable iron[17] castings after annealing. Some malleable irons may also contain Type I or II graphite particles.
- Type IV is the predominant graphite form in compacted (vermicular) graphite iron.
- Type V is the spiky graphite form occasionally seen in ductile iron in conjunction with Types I and II.
- Type VI is the exploded nodule graphite form occasionally seen in ductile iron in conjunction with Types I and II.
- Type VII is the flake graphite form usually seen in gray iron.

The designation of cast iron specimens should be specified according to EN 1560: 2011. The standard ASTM A 247 A-19 categorizes graphite particles by size, into eight classes, see Table 7.

Table 7. Graphite particles size, ASTM A245 A-19.

Size class	Dimension range [µm]
1	≥ 640
2	320 to < 640
3	160 to < 320
4	80 to < 160
5	40 to < 80
6	20 to < 40
7	10 to < 20
8	≤ 10

---

[17] Grafit în cuiburi (RO)

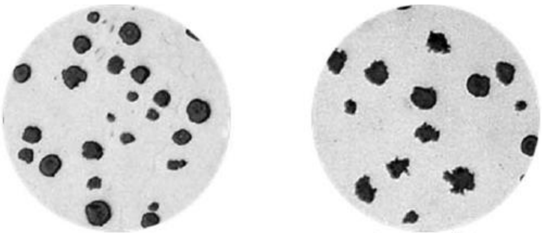

Type I Graphite Type II Graphite

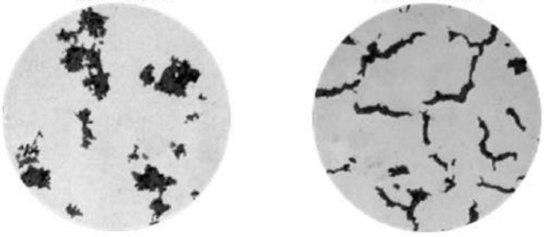

Type III Graphite Type IV Graphite

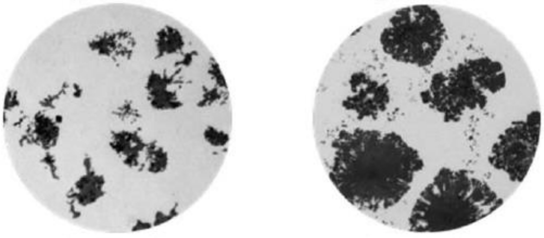

Type V Graphite Type VI Graphite

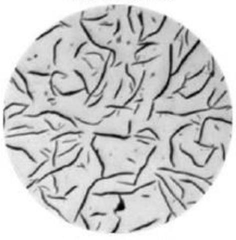

Type VII Graphite

Fig. 121 Graphite Types Chart[18] according to ASTM A 247 A-19.

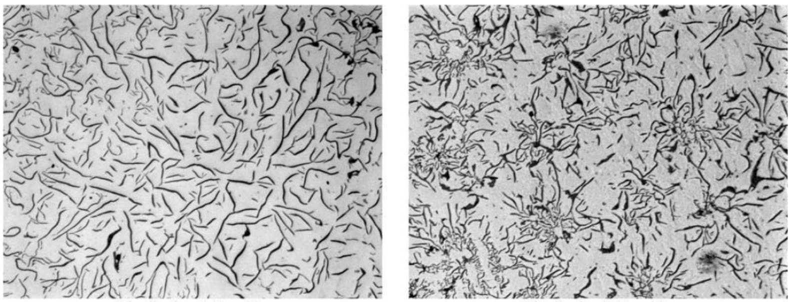

Distribution A Graphite Distribution B Graphite

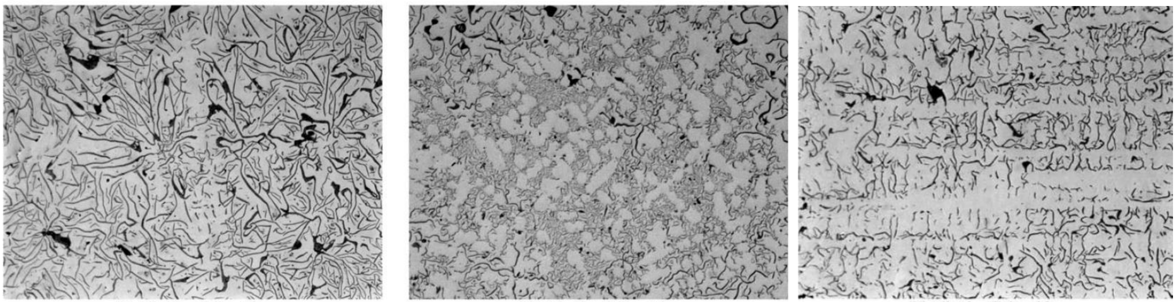

Distribution C Graphite Distribution D Graphite Distribution E Graphite

Fig. 122 Graphite Distribution used to rate Type VII Flake Graphite in Gray Iron (100×) [44].

---

[18] ASTM Standard Test Method for Evaluating the Microstructure of Graphite in Iron Castings.

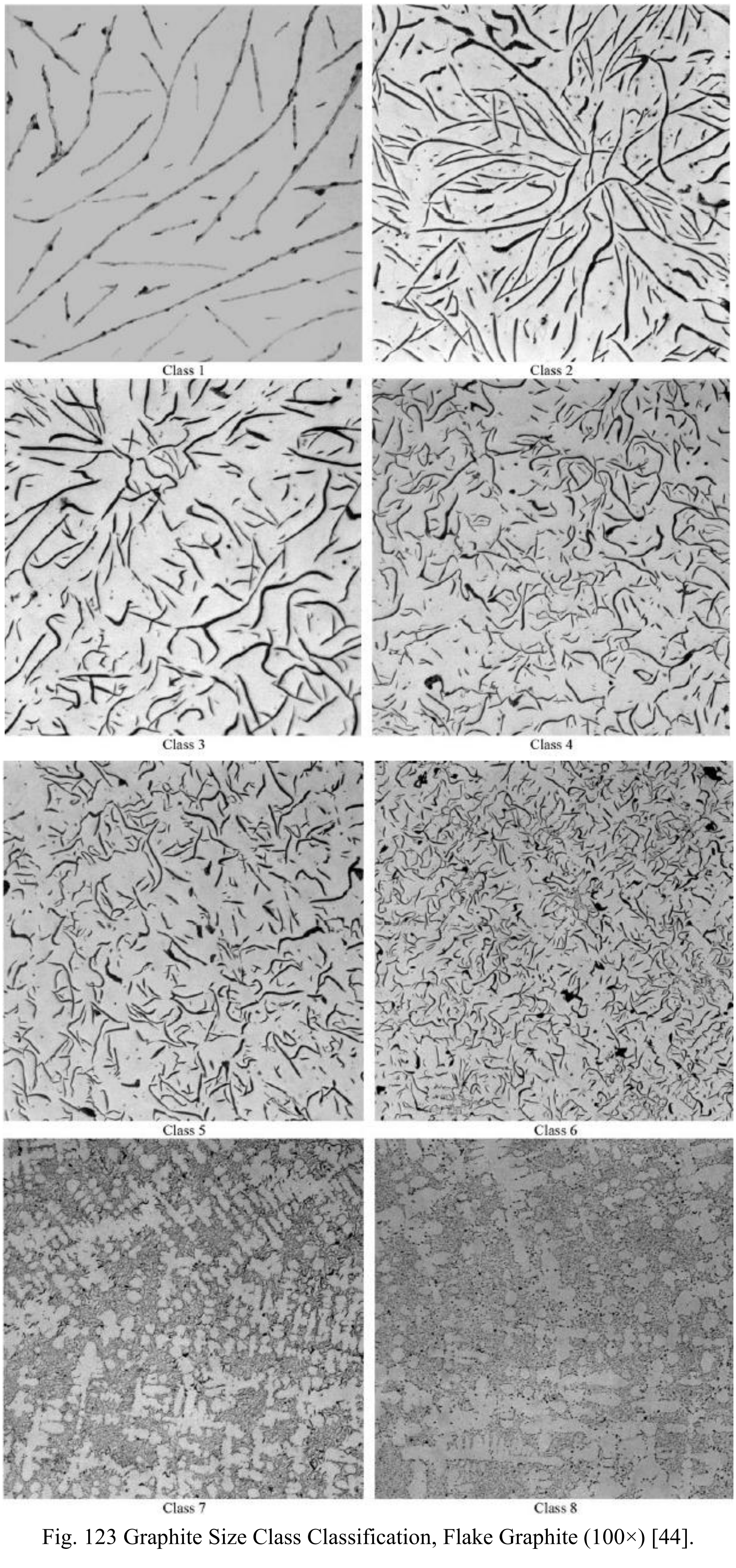

Class 1
Class 2
Class 3
Class 4
Class 5
Class 6
Class 7
Class 8

Fig. 123 Graphite Size Class Classification, Flake Graphite (100×) [44].

For microstructure direct comparison with the size classes presented in Figure 123, and Figure 124 the specimen to be evaluated shall be captured at the magnification of 100×. Where a mixture of one or more sizes occurs in the same sample, the sizes may be reported as percentages of the total graphite area represented by the sizes involved. It is a common practice in malleable irons to use nodule count per unit area instead of a comparison chart as given here. The nodule count is a measure of calculated average nodule area [44].

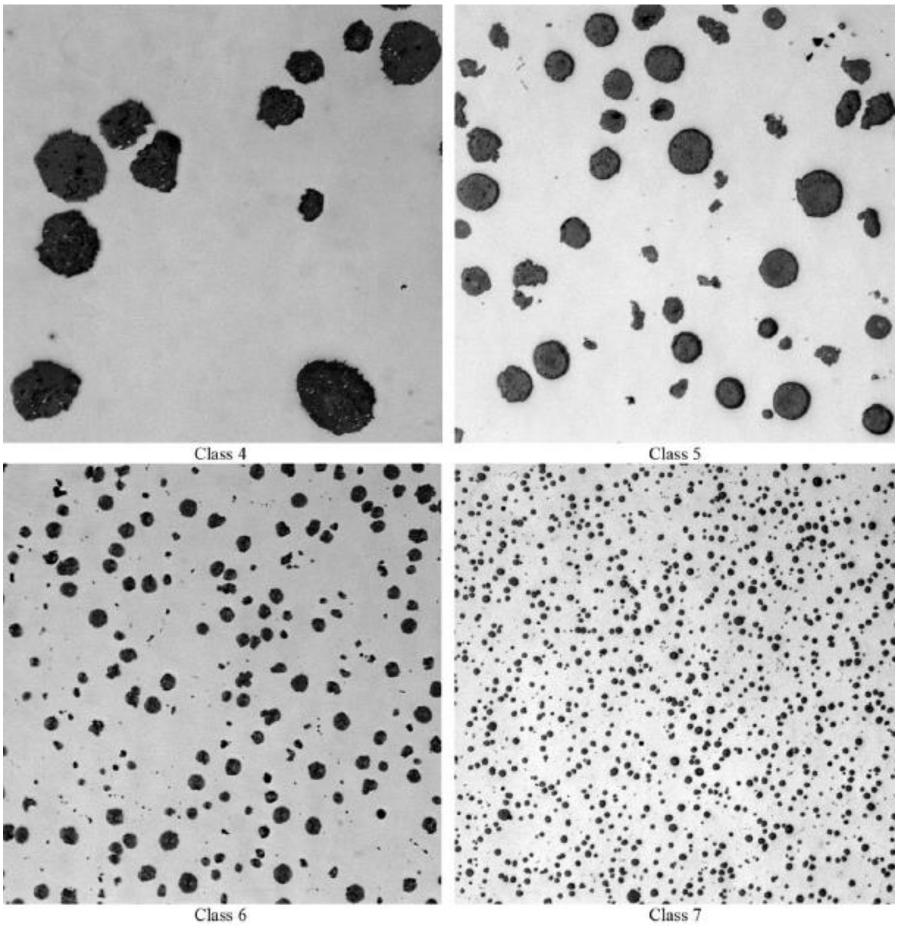

Fig. 124 Graphite Size Class Classification Chart, Nodular Graphite (100×) [44].

Different graphite shape factors are used to express the deviation of the graphite particle morphology from a sphere as the maximum possible compactness degree. Usually, the Roundness Shape Factor (RSF) is used as a ratio between the graphite particle area and the area of a circle corresponding to the maximum size of the graphite particle [45].

In commercial ductile cast iron [more info], depending on the deviation from a sphere, as expressed by RSF values, there are different graphite morphologies defined, according to ISO 945-4-2019:

- Spheroidal (RSF > 0.8, Type VI),
- Slightly irregular spheroidal (RSF = 0.6–0.8, Type V),
- Irregular spheroidal (RSF = 0.45–0.6, Type IV),
- Vermicular/compacted (RSF = 0.1–0.45, Type III),
- Lamellar (RSF < 0.1, Type I) morphology.

$$RSF = \frac{4 \times Graphite\ Particle\ Area}{\pi \times D_{Feret}^2}$$

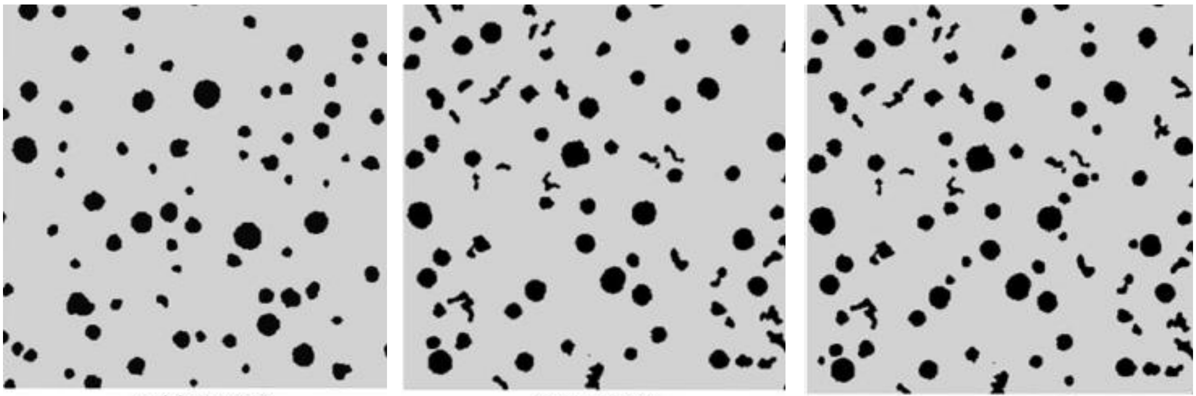

Nodularity 100%

Nodularity 90%

Nodularity 80%

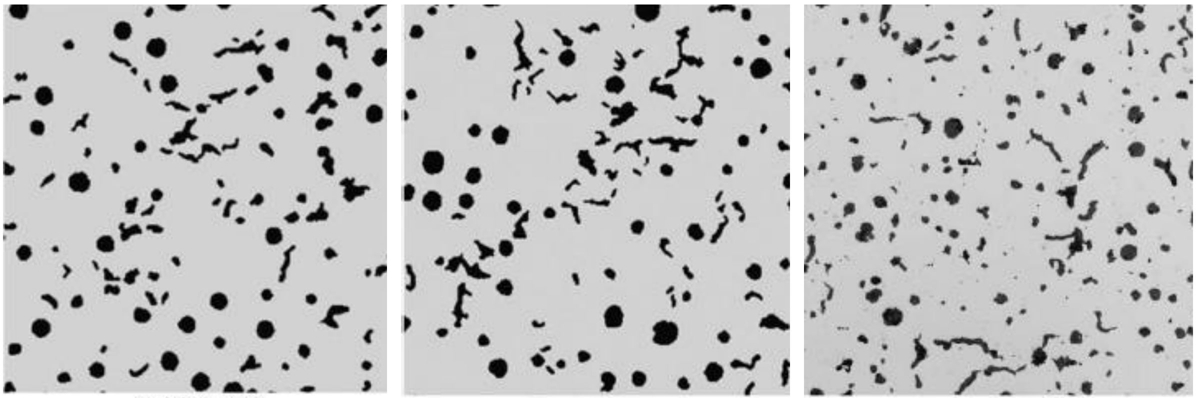

Nodularity 70%

Nodularity 60%

Nodularity 50%

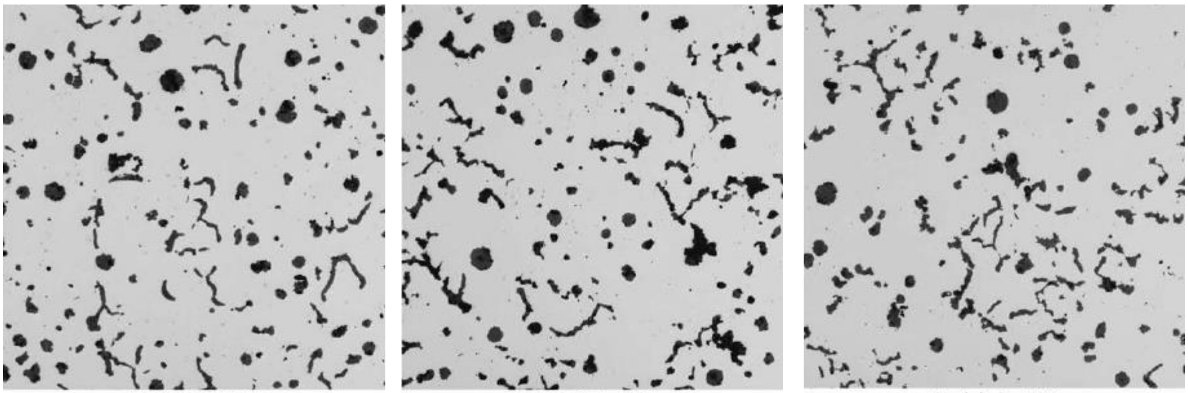

Nodularity 40%

Nodularity 30%

Nodularity 20%

Fig. 125 Compacted Graphite Iron Nodularity Rating Chart (Wall Chart).
Available from SinterCast, www.sintercast.com

Nodularity is expressed by counting the nodular particles and reporting the results as a percentage of the total amount of graphite present in the microstructure. Ductile irons typically exhibit a nodularity between 80 to 100 %, gray irons a nodularity of 0 %, and compacted graphite irons a nodularity of 0 to 20 %. Nodularity should be assessed by evaluating more than one field of view. The *e*Report should state the number of fields of view or area of the sample evaluated, Figure 125.

Graphite distribution is always designated for flake graphite irons but may be omitted for malleable and ductile iron. Nodule count is expressed as the number of graphite nodules/mm^2 and is performed at a magnification of 100×. Generally, a high nodule count indicates good metallurgical quality [44].

Nodularity can be measured using Image Analysis Software (see ASTM E2567-16A) or it can be measured using ultrasonic testing. There is a consistent difference in sound velocity between pure iron, nodular cast iron, and gray cast iron. Typically, *Fe* has a velocity of approximately 5.9 mm/µS, nodular iron has a velocity of 5.6 mm/µS, and gray iron has a velocity of approximately 4.8 mm/µS.

Materials Science Laboratory

Materials Science and Engineering Department

eReport

Type of the work	Cast Iron Microstructures
Scop of inspection	Short description of the work:
Specimen Cast iron designation. EN 1560: 2011	Photo/Microstructure 
Preparation Polished/Etched	
Manufacturing Technology Casting	
Magnification	
Equipment Metallographic microscope	

Observations:

Hardness:

Chemical composition:

Specimen characterization. Results Analysis

Graphite Types

Graphite Distribution

Graphite Size Class

Nodularity

RSF Factor

Identified phases and microstructural constituents.

Date:	Specialization:	Authorization Student Name

9.4.Case study

TVR Tuscan Speed Six

Fig. 126 Tuscan Speed Six sport car [video The TVR Tuscan Review With Richard Hammond].

Tuscan will go down as one of the brand's most iconic models of British company TVR[19]. some of the most beautiful and exciting cars on the roads. The TVR Tuscan Speed Six (Figure 126) made its debut in 1999 for sale to the UK and Japan as a right-hand drive only vehicle.

The TVR Tuscan Speed Six is a high-performance automobile, by any measure. This low volume sports car weighs 1,100 kg and is powered by a 4-litre in-line six-cylinder engine that develops over 350 bhp[20]. TVR Engineering selected an Austempered Ductile Iron (ADI) crankshaft for its combination of low cost, low weight and high torsional strength. ADI presents a useful set of properties for the design engineers. With ever increasing specific power requirements for new engine designs, new material and process combinations for engine components are being explored.

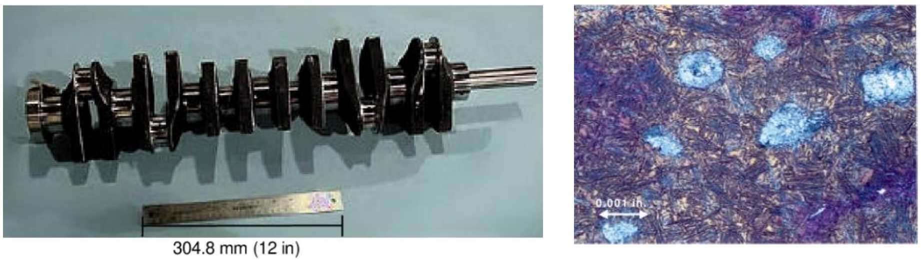

Fig.127 Austempered Ductile Iron (ADI) crankshaft for TVR Tuscan Speed Six car [read more].

Striking in appearance and power, the Tuscan Six accelerates from 0-100 km/h in 4.2 seconds and reaches a top speed of 289.6km/h. To achieve a such performance, the designers had combined aerodynamic styling with a high power to weight ratio, where the engine car plays the key role.

Below, are summarized the key aspects for the Austempered Ductile Iron material:

- Strength comparable to steel: Because of its equivalent strength, nearly 80% of all cast and forged steels can be replaced with some grade of ductile iron or ADI.
- Lower density than steel: The relative weight per unit of strength of ADI allows economy in design without loss of performance. For a given shape, an ADI component will be 10% lighter than steel.

---

[19] TVR Engineering in Blackpool

[20] BHP vs HP. A simple yet crucial difference between BHP and HP is how they're measured in the car. While horsepower measures the power generated by the engine, brake horsepower measures how much of the power produced by the engine is sent to the wheels which makes the car accelerate.

- ADI is three times stronger than the best cast or forged aluminium parts and weighs only 2.5 times as much. Because it is twice as stiff, a properly designed ADI part can replace aluminium at a weight saving.
- Excellent fatigue strength: ADI's dynamic properties exceed those of forged, cast and microalloyed steels. Unlike aluminium, ADI's endurance limit remains nearly constant after tens of millions of cycles.
- Improved noise damping: The presence of graphite in the ADI matrix improves noise damping, for quieter, smoother running components. ADI's internal damping characteristics also gave the engine superior noise properties compared to engines with steel or ductile iron crankshafts.
- Superior wear and abrasion resistance: ADI's abrasion resistance exceeds that of conventionally processed steels and irons at a lower 'bulk' hardness level. Unlike carburised steel, which loses wear resistance as the carburised layer is removed, ADI improves in service. Wear resistance is superior to steel at any given hardness level, making it ideal for earth moving and other high abrasion applications [46].

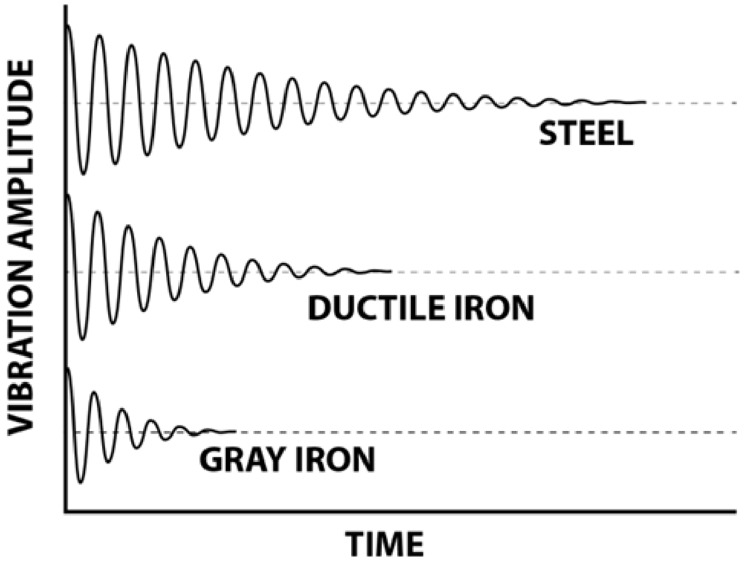

Fig. 128 Comparison of steel and cast-iron damping capabilities [more info]. Individual study: Read more about Measuring of Vibration-Damping Properties of Cast Iron and Numerical modal analysis for vibration-damping properties of ductile cast.

Cast iron has a high damping capacity, meaning it can absorb and dissipate vibrational energy. This property makes it useful in applications where minimizing vibrations is important, such as:

- Machinery Bases: Cast iron is commonly used as a material for machine bases and frames. Its damping properties help reduce the transmission of vibrations from machinery to the surrounding environment.
- Automotive Applications: In the automotive industry, cast iron is used in components such as engine blocks, crankshats and brake components due to its ability to absorb and reduce vibrations, contributing to smoother operation and improved performance.

Machine vibration impacts on machines lifetime, reliability, and could cause machine damage or accidents. To mitigate the negative impact of vibrations on machines, engineers employ various strategies, including designing for vibration resistance, using vibration isolators, implementing damping materials, and conducting regular maintenance and monitoring programs.

10. High alloys microstructures

10.1. Theoretical background

High-alloy steels refer to steels that contain a significant amount of alloying elements beyond carbon steels. These alloying elements may include chromium, nickel, molybdenum, titanium, and others.

High alloys are known for their superior corrosion resistance, strength, and other specialized properties. Here are some common applications of high alloys:

- Stainless Steel
    - Chemical, Pharmaceutical and Food Processing: Stainless steels, which often contain chromium and nickel, are widely used in the chemical and food processing industries due to their corrosion resistance and hygiene properties.
    - Oil and Gas Industry: High-alloy steels are employed in the oil and gas industry for corrosion-resistant pipelines and equipment that come in contact with corrosive substances. This helps prevent corrosion and ensures the integrity of the infrastructure.
    - Reaction Vessels and Piping: High-alloy steels are used in chemical processing plants for the construction of reaction vessels, piping, and other equipment where resistance to corrosive chemicals is essential.
    - Automotive Industry: High-alloy steels, including stainless steel, are used in the manufacturing of automotive exhaust systems due to their resistance to corrosion and high temperatures.
    - Power Generation: High-alloy steels are used in the power generation industry for components exposed to high temperatures and corrosive environments, such as steam generators and boiler tubes.
    - Medical Equipment: High-alloy steels are used in the manufacture of medical instruments and equipment because of their corrosion resistance and biocompatibility.
- Superalloys
    - Superalloys, also known as high-performance alloys, are a class of metallic materials designed to exhibit exceptional mechanical strength, high-temperature stability, corrosion resistance, and other specialized properties. These alloys are primarily used in extreme environments, such as high-temperature and high-stress conditions, where conventional materials would fail. Superalloys find extensive applications in aerospace, gas turbine engines, power generation, chemical processing, and other industries.
    - Aerospace and Aircraft Components. High-alloy steels, particularly those containing nickel and cobalt, are used in the construction of jet engines and turbines due to their ability to withstand high temperatures and resist corrosion/oxidation.
    - Key characteristics of superalloys include high temperature strength, oxidation and corrosion resistance, creep resistance, thermal fatigue resistance and wear resistance.
- Tool Steels
    - Contain tungsten, molybdenum, cobalt, and other alloying elements. These steels are designed for high wear resistance, hardness, and toughness. Common types include high-speed steels and cold-work steels, which are used in the production of cutting tools, dies, and molds for manufacturing processes such as metal forming and machining.

According to the EN10020:2003 definition, stainless steel is an alloy of Fe, which contains minimum 10.5 wt.% Cr and maximum 1.2% wt. Carbon. Chromium leads the formation of an adherent film of Cr_2O_3 oxide on the metal surface, which ensures the steel's resistance to corrosion (through passivation).

Stainless steels are further subdivided in accordance with their main properties into corrosion resisting steels, heat resisting steels and creep resisting steels.

The microstructure of high-alloy steels is crucial to their mechanical properties, including strength, hardness, toughness, heat and corrosion resistance. The microstructure is determined by the alloying elements present in the steel and the heat treatment processes it undergoes, Figure 129.

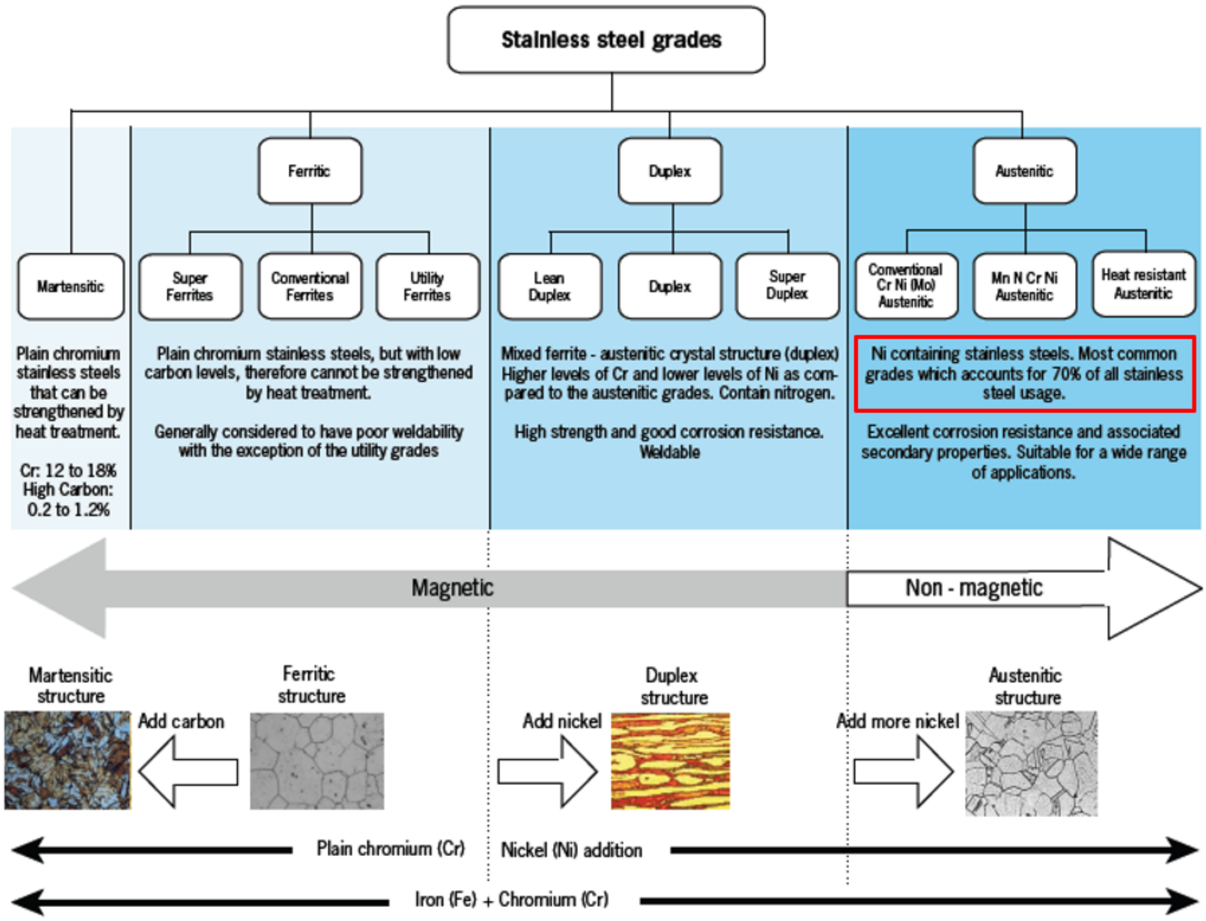

Plain chromium stainless steels that can be strengthened by heat treatment.

Cr: 12 to 18%
High Carbon: 0.2 to 1.2%

Plain chromium stainless steels, but with low carbon levels, therefore cannot be strengthened by heat treatment.

Generally considered to have poor weldability with the exception of the utility grades

Mixed ferrite - austenitic crystal structure (duplex) Higher levels of Cr and lower levels of Ni as compared to the austenitic grades. Contain nitrogen.

High strength and good corrosion resistance. Weldable

Ni containing stainless steels. Most common grades which accounts for 70% of all stainless steel usage.

Excellent corrosion resistance and associated secondary properties. Suitable for a wide range of applications.

Fig. 129 Stainless steel classification and properties [Euro Inox Publications].

The global cost of corrosion is estimated to be US$2.5 trillion, which is equivalent to 3.4% of the global GDP. According to data from the Financial Times, corrosion in its many forms is estimated to cost the global economy $3 trillion a year due to damage to steel buildings and infrastructure [read more].

According to a study by NACE International, implementing corrosion prevention best practices could result in global savings of 15-35% of that cost, or $375-$875 billion. Stainless steels provide excellent corrosion resistance properties, being used in many applications.

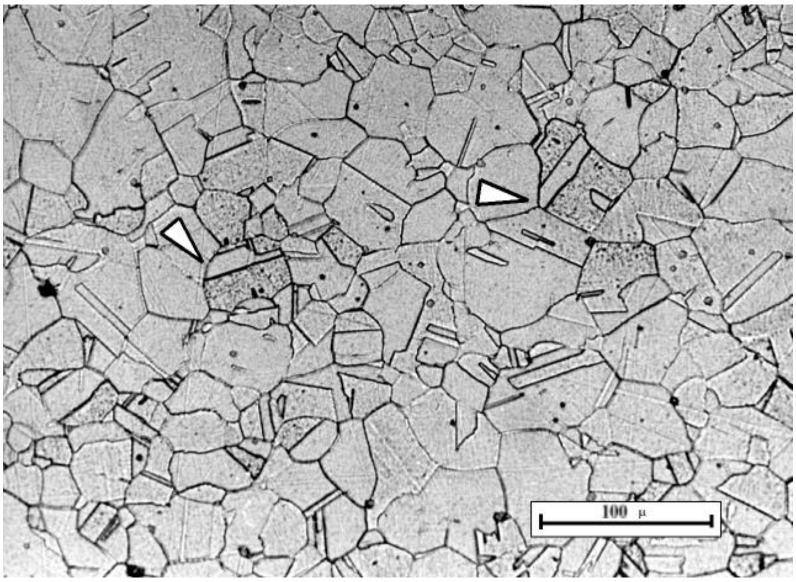

Fig. 129 Austenitic stainless steel [more info, © DoITPoMS, University of Cambridge].

Austenite has a face-centered cubic (FCC) crystal structure that provides good formability and corrosion resistance. Figure 129 presents the grain structure of an austenitic stainless steel NF709, observed using light microscopy on a specimen polished and etched electrolytically using 10% oxalic acid solution in water. Many of the grains contain annealing twins. NF709 is a creep-resistant austenitic stainless steel used in the construction of highly sophisticated power generation units.

On the Schaeffler diagram, the austenitic region is typically found in the upper right corner see Figure 130. The Schaeffler diagram is a graphical method used to predict and assess the microstructure of stainless steels and other alloys based on their chromium (Cr) and nickel (Ni) equivalent content. It was developed by German metallurgist Schaeffler in the 1930s and is particularly useful in predicting the phase balance, and thus the corrosion resistance and mechanical properties, of stainless steels.

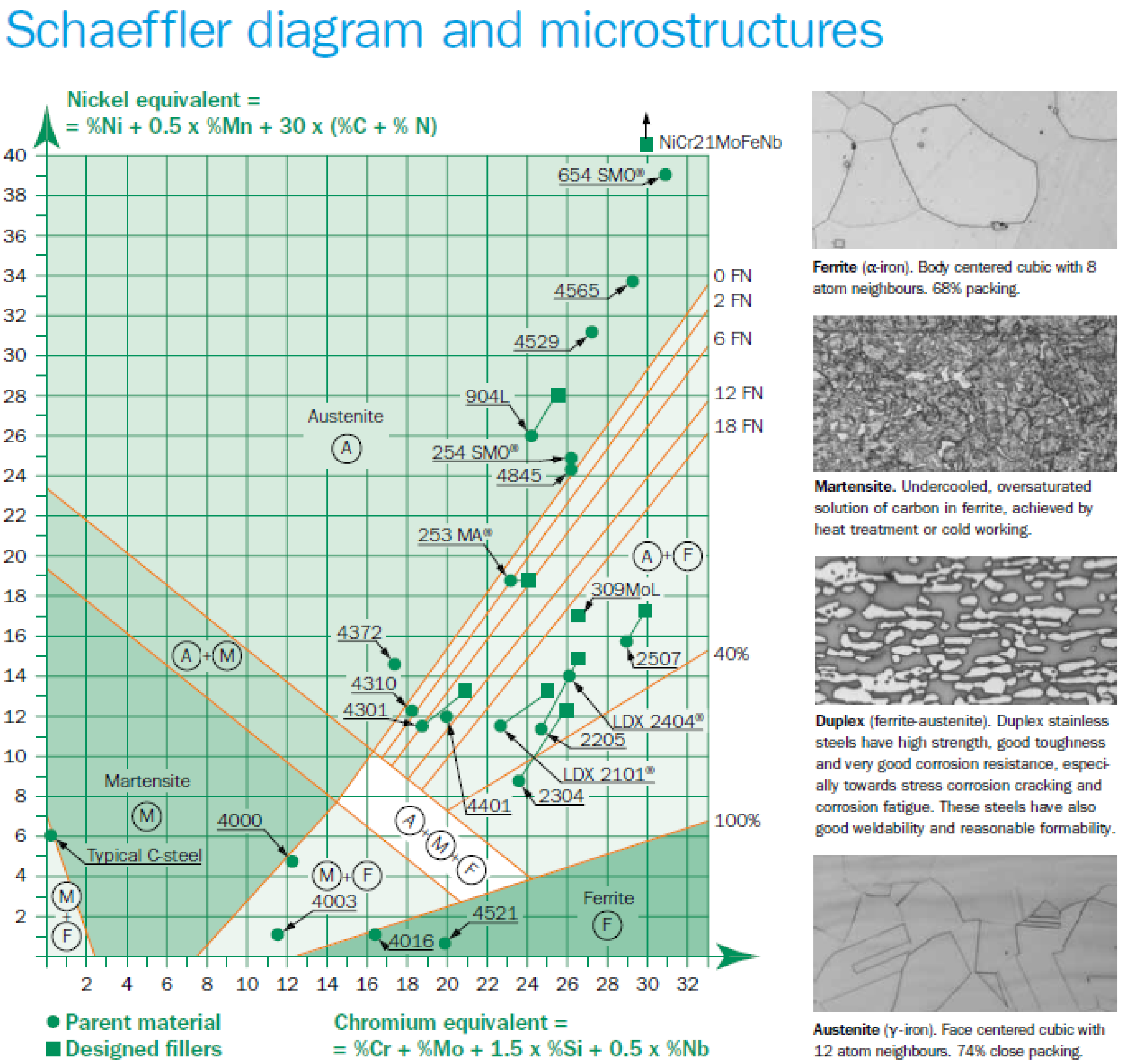

Ferrite (α-iron). Body centered cubic with 8 atom neighbours. 68% packing.

Martensite. Undercooled, oversaturated solution of carbon in ferrite, achieved by heat treatment or cold working.

Duplex (ferrite-austenite). Duplex stainless steels have high strength, good toughness and very good corrosion resistance, especially towards stress corrosion cracking and corrosion fatigue. These steels have also good weldability and reasonable formability.

Austenite (γ-iron). Face centered cubic with 12 atom neighbours. 74% close packing.

Fig. 130 Schaeffler diagram of stainless steels [Euro Inox Publications].

The Schaeffler diagram is essentially a composition chart, Figure 130, that helps determine the likely phases that will form in a stainless-steel alloy based on its chemical composition. The primary phases considered in the Schaeffler diagram are austenite, ferrite, and martensite.

The position of a stainless-steel alloy on the Schaeffler diagram is determined by its chromium equivalent (Cr_{eq}) and nickel equivalent (Ni_{eq}) values. These equivalents are calculated based on the alloy's composition and are used to locate the alloy within the diagram, Figure 130.

At lower temperatures or with specific alloy compositions, high-alloy steels may have a ferritic microstructure. Ferritic stainless steels, for example, contain high chromium but limited nickel, resulting in a ferritic structure, Figure 131.

Ferrite is a body-centered cubic (BCC) crystal structure and is stable at lower temperatures. Ferrite provides strength and hardness but may have reduced corrosion resistance compared to austenite. The ferritic region is usually in the lower right corner of the Schaeffler diagram.

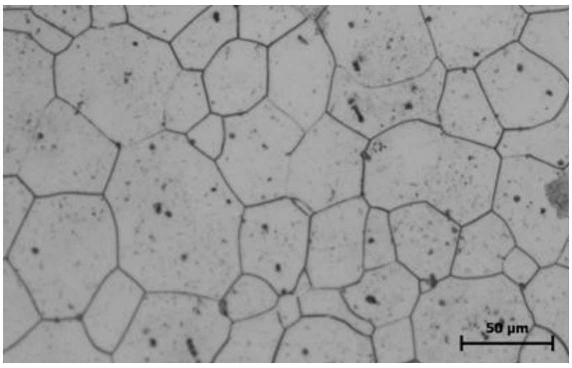

Fig. 131 Ferritic stainless steel X3CrTi17, EN 10088-2:2014 or AISI[21] 439
Ti-stabilized 17% chromium ferritic stainless steel with improved weldability, [read more].

The Schaeffler diagram is particularly useful in predicting the balance between austenitic and ferritic phases in duplex stainless steels, which are alloys designed to have a combination of both phases to achieve a balance of strength and corrosion resistance.

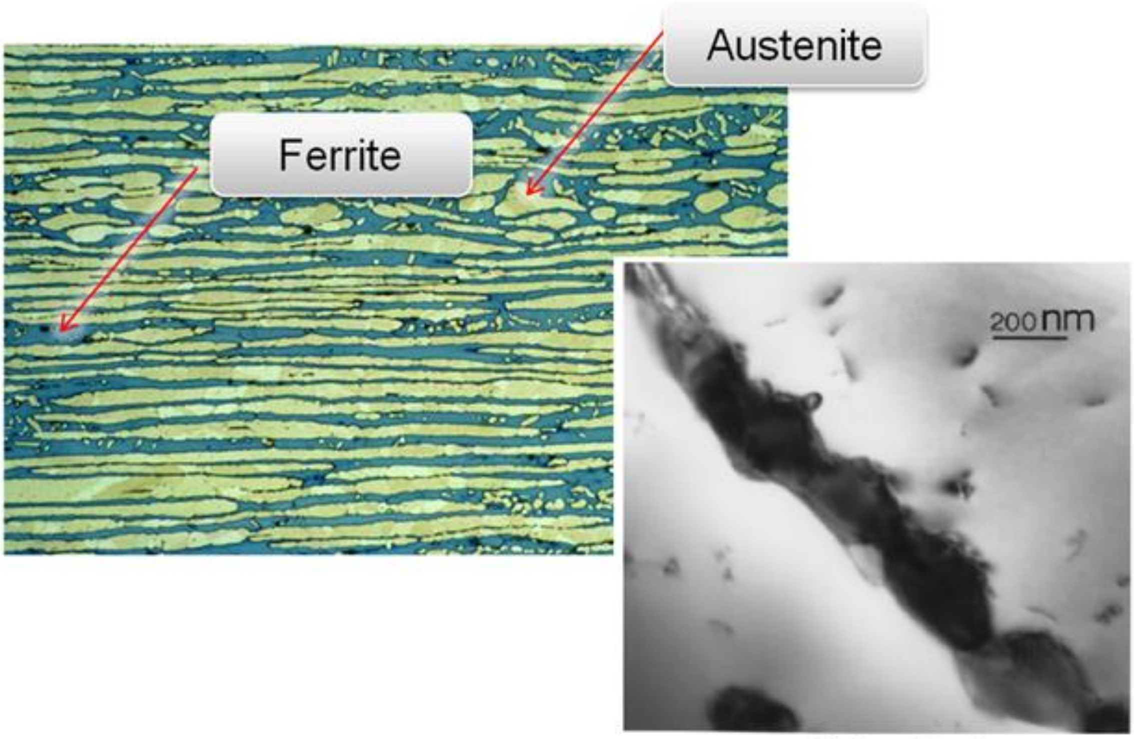

$M_{23}C_6$ on grain boundary.

Fig. 132 Duplex stainless-steel microstructure [Euro Inox Publications].

Duplex stainless steels have a dual-phase microstructure, consisting of both austenitic and ferritic phases, Figure 132. This combination provides a balance of strength and corrosion resistance. The duplex microstructure is achieved through careful alloying, typically with a mix of chromium, nickel, and sometimes nitrogen.

---

[21] AISI – American Iron and Steel Institute

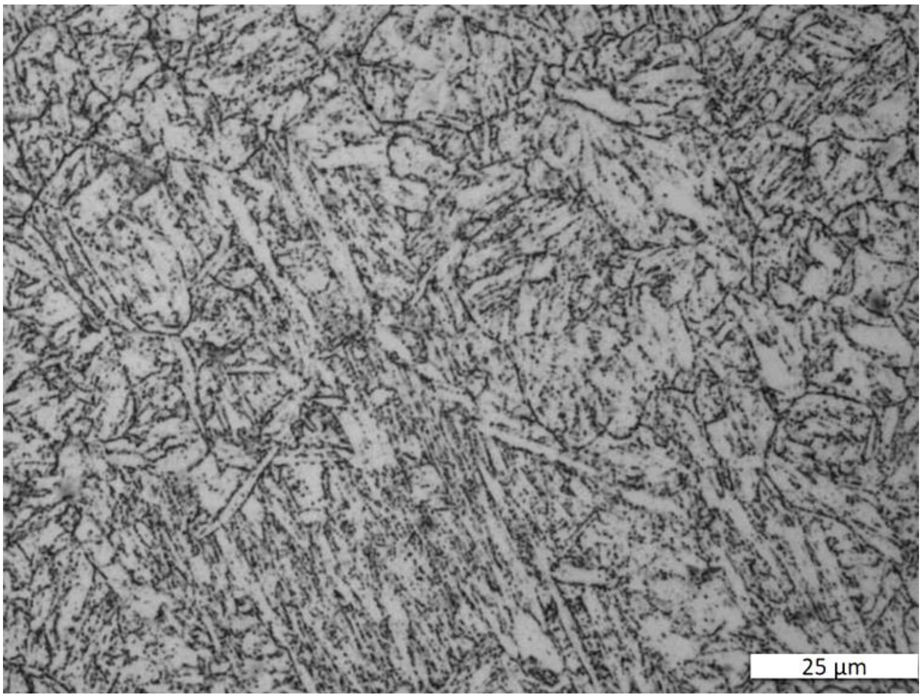

Fig. 133 Martensitic stainless-steel microstructure, electrolytically polished and etched with A2. Bright field.

Martensite is very hard, brittle, and body-centered tetragonal crystal structure. High carbon content, along with alloying elements like chromium and molybdenum, contributes to the formation of martensite during quenching.

Martensitic stainless steels respond to heat treatment. Martensite is formed through rapid cooling and properties can then be optimised by subsequent tempering treatment. The alloys are magnetic. Depending on the thermal treatment the microstructure can range from pure martensitic structure to fine tempered martensite [47].

Delta ferrite is usually an unwanted phase because long annealing times of steels[22] with high chromium content, at temperatures between 700 and 950°C, can change the delta ferrite into the hard and brittle iron-chromium intermetallic sigma phase. Sigma phase (σ) has a negative impact on corrosion resistance and mechanical properties. Heating up to 1050°C and subsequent quenching removes the sigma phase and with it the steel embrittlement.

Table 8. Intermetallic phases and temperature range for formation.

Intermetallic phases	Chemical formula	Temperature range (°C)
Sigma	Fe-Cr-Mo	600–1000
Chi	$Fe_{36}Cr_{12}Mo_{10}$	700–900
Nitrides	CrN/Cr_2N	700–900
Carbides	$M_7C_3/M_{23}C_6$	550–650
R	Fe-Cr-Mo	550–800
Π	$Fe_7Mo_{13}N_4$	550–600
Prime alpha (α') phase	Fe-Cr	475

During welding stainless steels, a series of intermetallic phases can form, such as sigma (σ) phase, which can negatively impact corrosion resistance and mechanical properties. Others intermetallic phases that can form are presented in Table 8.

---

[22] Sigma phase can form also in welded stainless steels.

10.2. Working procedure

The stainless-steel specimens available in Material Science Laboratory are labeled and should be prepared according to instructions given in Laboratory no 2 for metallographic specimen preparation and etching. A more detailed procedure for metallographic preparation of stainless steels is given here.

The microstructure images can be captured using the digital camera from microscope or can be photographed using a smartphone camera. All relevant information should be filled in the *e*-Report file. For quantitative analysis, the students should refer to the procedure described in Laboratory no 3.

10.3. Discussion and results interpretation

Metallography of stainless steels is an important part of the overall quality control of the production process. The scope of the metallographic tests of stainless steels specimens are:

- Grain size measurement,
- Identification of delta ferrite and sigma phase,
- Evaluation and distribution of carbides.

Based on this information the students can perform further failure analysis, investigating corrosion or oxidation mechanisms in different stainless-steel specimens.

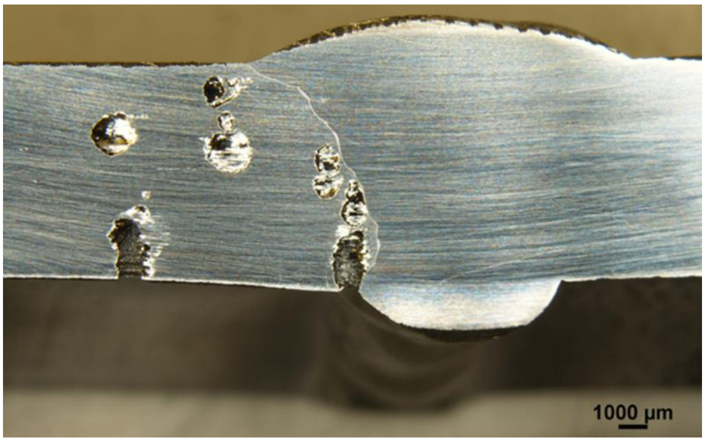

Macro analysis of the specimens can reveal some material damage due to different forms of corrosion: pitting, crevice, galvanic, intergranular, stress corrosion cracking, selective, through cavitation and microbiological, see Figure 134 and Figure 135.

Fig. 134 Stainless steel welded specimen which presents pitting corrosion.

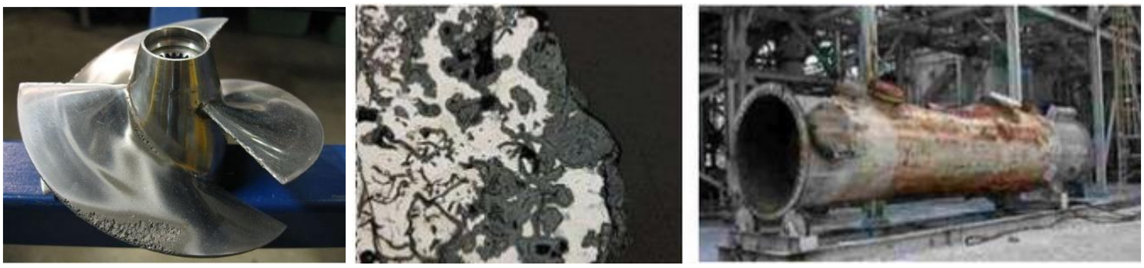

Fig. 135 Cavitation and selective corrosion in stainless steels.

Based on the chemical composition of the stainless-steel specimen, the students should calculate the chrome and nickel equivalent and identify the type of steel using the Schaeffler diagram, Fig.130.

All the observations made should be noted in the *e*Report Form together with other details related to the specimen: macro analysis results, technique of preparation, etchant used etc.

For grain size measurements should be used comparison or intercept method in compliance with EN ISO 643 or ASTM E 112 described in Laboratory no 3. Detailed procedure for austenitic stainless steel is presented here.

Materials Science Laboratory

Materials Science and Engineering Department

*e*Report

Type of the work	Stainless Steels Microstructures
Scop of inspection	Short description of the work:
Specimen Steel designation.	Photo/Microstructure 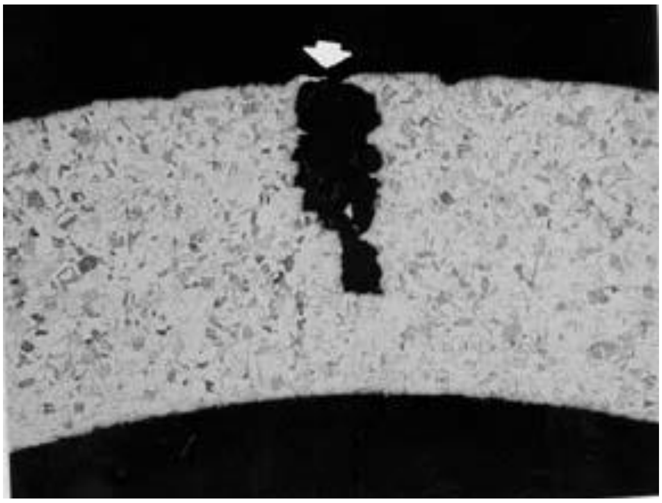 Pitting Corrosion
Preparation Polished/Etched	
Manufacturing Technology	
Magnification	
Equipment Metallographic microscope	
Observations: Hardness: ☐ Chemical composition:	Specimen characterization. Results Analysis Stainless Steel Type ☐ Chrome equivalent ☐ Nickel equivalent ☐ Corrosion Resistance PRE= %Cr + 3,3·(%Mo) + 16·(%N) Identified phases and microstructural constituents.

Date:	Specialization:	Authorization Student Name

10.4. Case Study

Philadelphia Energy Solutions refinery in Philadelphia

In the early morning of June 21, 2019, a fire and multiple explosions occurred at the Philadelphia Energy Solutions refinery in Philadelphia, Pennsylvania (PES). A release of hydrocarbons and hydrofluoric acid in the refinery's alkylation unit caused a ground-hugging vapor cloud which rapidly ignited, leading to three separate explosions minutes apart. The largest explosion sent a bus-size 17 tons vessel fragment flying 610 m across the Schuylkill River, Figure 136. The refinery announced it would shut down operations the same month and filed for bankruptcy a month later.

Fig. 136 Explosion occurred at Philadelphia Energy Solutions refinery in Philadelphia (PES) [video].

According to the EPA, between 2007 and 2017, there were 1,517 reportable accidents at facilities using hazardous chemicals — nearly 150 incidents a year over 10 years. Nearly 500 of those accidents affected residents in surrounding communities (almost 500,000 people evacuated or sheltered-in-place), being responsible for 59 deaths, 17,099 people were injured or sought medical treatment, and over $2 billion in property damages have been recorded.

The root cause for the Philadelphia refinery incident has been identified in a severe coroded elbow pipe that has ruptured and released flammable hydrocarbons gas (primarily butylene, isobutane, and butane) and hydrofluoric acid in the air.

Fig. 137 Image showing the 17 tons vessel that flew across the Schuylkill River when the third explosion occurred at 4:22 a.m. June 21, 2019 (Credit: Global News).

At 4:01am, one of the operators reported seeing a ground-hugging vapor cloud, estimated by another to be 3.0 m high due to a released gas from a ruptured pump pipe elbow.
At 4:22 a.m., a vessel containing flammable hydrocarbons (primarily butylene, isobutane, and butane) detonated, causing the largest explosion.

The final investigation report (published at October 11, 2022) by CBS[23] says that an estimated 5,239 pounds of hydrofluoric acid (HF) released from piping and equipment during the incident. It estimated that 1,968 pounds of the released HF was contained by water spray within the unit and was processed in the refinery wastewater treatment plant, and that 3,271 pounds of HF has been released to the atmosphere and was not contained by water spray. PES also estimated that about 676,000 pounds of hydrocarbons were released during the event, of which an estimated 608,000 pounds were combusted[24].

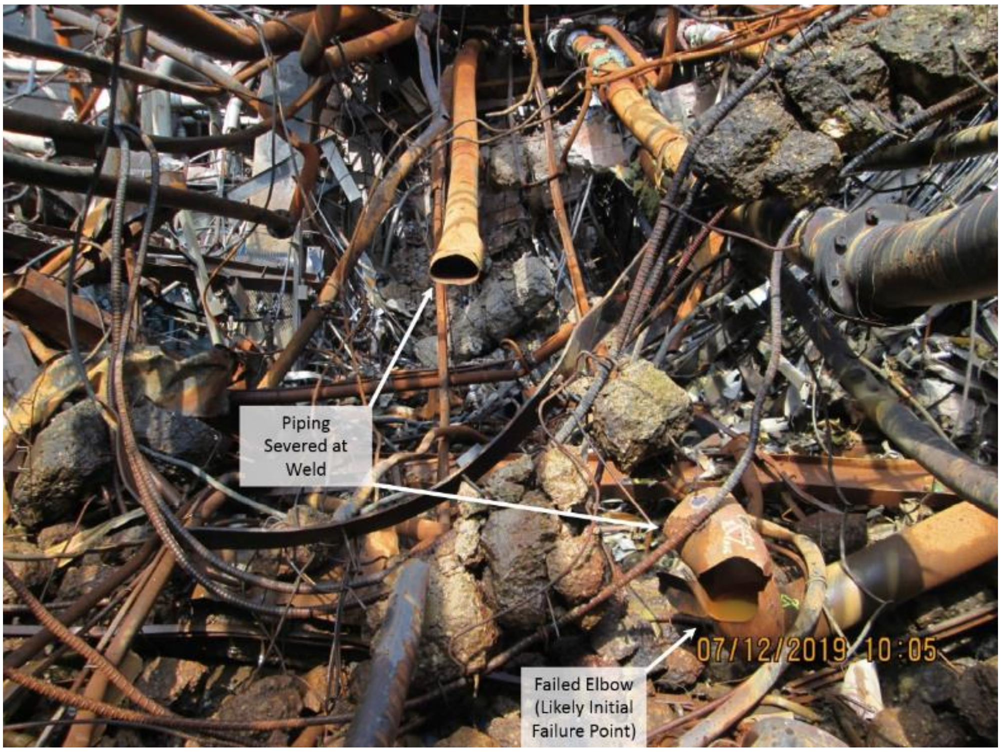

Fig. 138 A post-incident photo of the elbow pipe that ruptured and allowed flammable process fluid containing hydrofluoric acid to leak, (Credit: PES).

Hydrofluoric acid is one of the deadliest industrial chemicals in use. Integral to the creation of high-octane gasoline, it is used as a catalyst and has been combined with highly flammable hydrocarbons at about 48 alkylation units in the United States — including the now-closed South Philadelphia refinery.

Swallowing just a small amount of HF or getting small splashes on the skin can be fatal, according to the Centers for Disease Control and Prevention. In a gaseous state, the CDC says, low levels of HF can irritate the eyes, nose and respiratory tract. Breathing it at high levels "can cause death from an irregular heartbeat or fluid buildup in the lungs."

---

[23] CSB is an independent federal agency charged with investigating, determining, and reporting to the public in writing the facts, conditions, and circumstances and the cause or probable cause of any accidental chemical release resulting in a fatality, serious injury, or substantial property damages.

[24] Koopman (senior scientist at the Lawrence Livermore National Laboratory, where he worked for 36 years) conducted the definitive experiment on the release of hydrogen fluoride back in 1986. He said the HF that was released at PES was likely dispersed by the intense explosion. "*The explosion is nasty, it could kill people, but it's not the principal hazard*," he said. "*It's the toxic gas [HF] that could continue to be toxic downwind. Sometimes, the explosion and the fire are your friend*". Koopman's experiment in 1986 released 1,000 gallons of HF at a Nevada test site. The results shocked him. A video of the experiment shows white billowing clouds of poisonous gas expanding and traveling rapidly across the desert. Highly toxic levels of HF were detected miles away.

The elbow pipe was only 0.3 mm (0.012 inches) thick, less than 10% the lowest recommended thickness. PES had a policy that **any pipe thinner than 4.5 mm (0.18 inch) would be replaced**. CBS's investigation found that the ruptured pipe was only 0.3 mm thick — less than a tenth of the thickness that would have triggered a replacement!

John Jechura, professor of practice at the Colorado School of Mines, said deciding where to test is always a probability issue. "*You can't check every square inch of pipe*," he said.

As a rule of thumb, he said, the areas most vulnerable to corrosion and thus potential cracks and leaks, are places in the pipe where there is a change in the flow direction: T's, Y's, and elbows.

Key summary of PES incident

1. The explosions and fire that destroyed a critical part of the PES refinery has led to PES bankruptcy and the layoffs of more than 1,000 workers.
2. The exploasion took place due to spilled hydrocarbons and HF gas, released by an elbow pipe ruptured due to advanced corrosion (the elbow thickness was just 10% from the lowest value recommended).
3. The quick action[25] of one employee helped avoid further catastrophe for workers and nearby residents by transferring the majority of the deadly hydrofluoric acid from the alkylation unit to a tank far away from the fire.
4. HF corrosion has been found to be strongly affected by steel composition and localized corrosion rates can be subtly affected by local chemistry differences.
5. Another issue was the pipe material. The pipes in the PES alkylation unit were installed in 1973, when industry standards did not specify how much nickel or copper they should contain. In 1995, however, those standards were updated, specifying that pipes should be no more than 0.4% each nickel and copper. The ruptured pipe contained 1.74% nickel and 0.84% copper.
6. The corrosion monitoring in such facilities can prevent further catastrophes, but it remains a problem of statistics and costs.

Daniel Horowitz, a former managing director at the Chemical Safety Board (CSB), said explosions due to faulty, old equipment also occurred at the Tesoro refinery in Anacortes, Washington, in 2010 and at Chevron's Richmond, California, refinery in 2012.

Tubes in Sanicro 28 proved to be a safe choice to fight hydrogen induced cracking in the heat exchangers of a large Indian oil refinery. Five years after the installation, thorough inspection showed no signs of corrosion.

Fig.139 Duplex steels in refineries.

---

[25] The control room operator, Barbara McHugh, acted quickly and within 30 seconds activated the Rapid Acid Deinventory, or "RAD," system, which transferred the majority of the deadly hydrofluoric acid from the alkylation unit to a tank far away from the fire. About 340,000 pounds of HF at the facility has since been neutralized. Refineries typically have water spray mechanisms to contain HF, which were also activated at PES. Koopman said fast action is critical because once the HF is airborne, it can kill people at high concentrations.

11. Non-ferrous alloys microstructures

11.1. Theoretical background

Non-ferrous alloys are alloys that do not contain iron as a primary component. They are typically composed of elements such as aluminum, copper, zinc, tin, nickel, and others. Non-ferrous alloys are widely used in various industries such as aerospace, automotive, electronics, construction, and more due to their desirable properties, including corrosion resistance, conductivity, and lightweight characteristics. Some non-ferrous alloys in industry:

- Aluminum Alloys
  - Aerospace: Used in aircraft components and structures due to its lightweight properties.
  - Automotive: Used in vehicle bodies, engine components, and wheels.
  - Packaging: Aluminum cans and foils for food and beverage packaging.
  - Construction: Widely used in structural components and building materials.
- Copper Alloys
  - Electrical Wiring: Copper is an excellent conductor of electricity, making it ideal for electrical wiring and cables.
  - Plumbing: Copper pipes and fittings due to corrosion resistance.
  - Electronics: Connectors, switches, and various electronic components.
- Zinc Alloys:
  - Die Casting: Used in various die-cast components for the automotive and electronics industries.
  - Galvanization: Zinc-coating for steel to prevent corrosion.
  - Battery Components: Zinc is used in some types of batteries.
- Lead Alloys
  - Batteries: Lead-acid batteries for vehicles and backup power systems.
  - Radiation Shielding: Due to its high density, lead is used for shielding against radiation.
  - Soldering: Lead-based solders for electronic assembly.
- Nickel Alloys:
  - Aerospace: Used in aircraft engines and components due to high-temperature resistance.
  - Chemical Processing: Corrosion-resistant equipment for chemical plants.
  - Power Generation: Turbine blades and components in power plants.
- Titanium Alloys:
  - Aerospace: Titanium's high strength-to-weight ratio is valuable in aircraft and spacecraft.
  - Medical Implants: Biocompatible titanium alloys are used in medical implants.
  - Military Applications: Titanium is used in military aircraft and armor.
- Magnesium Alloys:
  - Aerospace: Lightweight magnesium alloys are used in aircraft components.
  - Automotive: Magnesium is used in certain automotive parts to reduce weight.
  - Portable Devices: Magnesium alloys in the casing of laptops and cameras.
- Tin Alloys:
  - Soldering: Tin-based solders for electronic and electrical applications.
  - Food Packaging: Tin-plated steel for food cans.
- Precious Metal Alloys:
  - Jewelry: Gold and silver alloys are widely used in jewelry making.
  - Electronics: Platinum and palladium in electronic components.
- Bismuth Alloys:
  - Medical Imaging: Bismuth alloys are used in some types of X-ray shielding.

The selection of a non-ferrous alloy for a given application depends on factors such as strength, corrosion resistance, thermal and electric conductivity, service temperature, and weight characteristics.

It should be mentioned also that technological properties like formability, machinability, weldability, and others are equally important in the material selection process.

COPPER ALLOYS

The sample from Figure 140 (bronze) was subject to an annealing treatment (after casting operation), which served to recrystallise the sample. Evidence of this can be found in the annealing twins visible in several of the grains. These are a consequence of growth accidents during recrystallisation. Their shape is determined by the need to minimise interfacial energy. There is no strain energy associated with such twins and hence they do not have pointed ends.

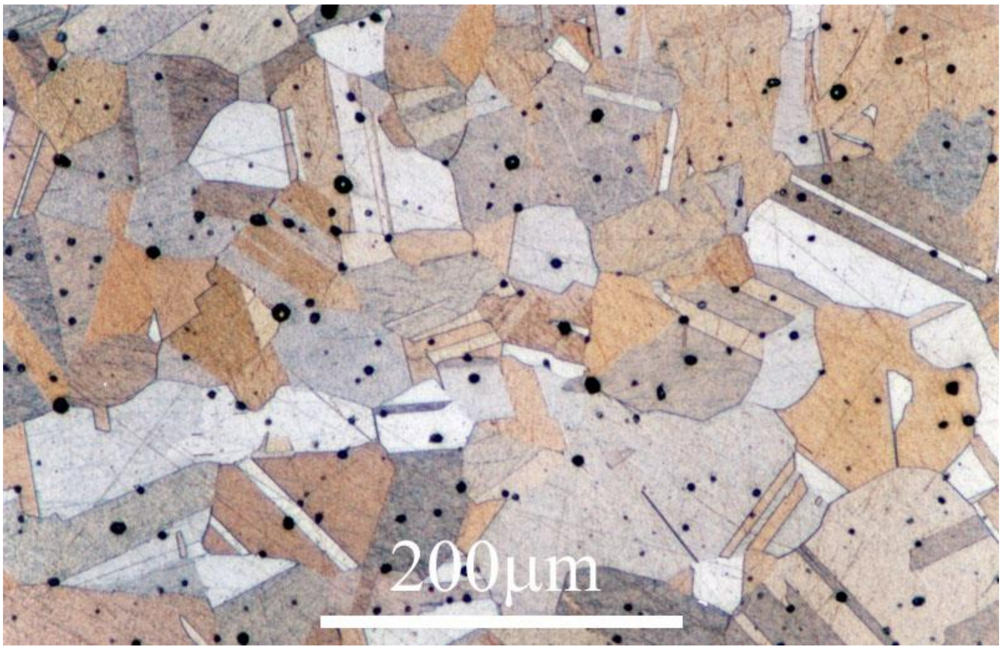

Fig. 140 Annealed bronze Cu 85, Sn 15 (wt%) [more info, © DoITPoMS, University of Cambridge].

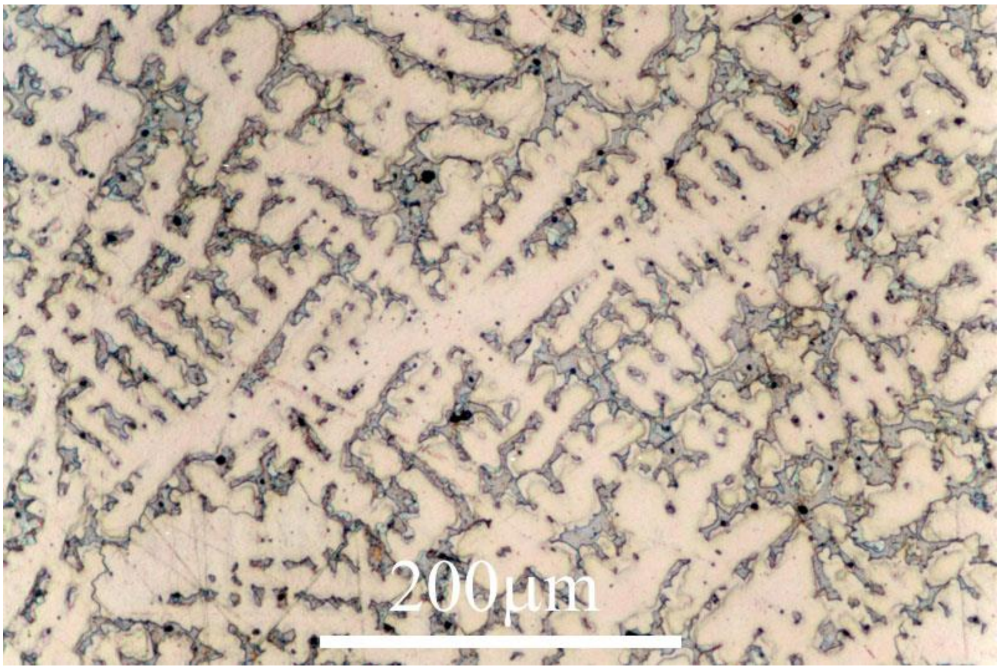

Fig. 141 Cu 80, Sn 20 (wt%) bronze, exhibiting dendritic solidification [more info, © DoITPoMS, University of Cambridge].

ALUMINUM ALLOY

Duralumin. The 2024 aluminium alloy is an aluminium alloy, with copper as the primary alloying element. It is used in applications requiring high strength to weight ratio, as well as good fatigue resistance. It is weldable only through friction welding and has average machinability. Due to poor corrosion resistance, it is often clad with aluminium or Al-1Zn for protection, although this may reduce the fatigue strength. In older systems of terminology, 2XXX series alloys were known as duralumin, and 2024 aluminium alloy was named 24ST.

2024 aluminum alloy is a kind of high-strength duralumin, which belongs to the Al-Cu-Mg series aluminum alloys. It is mainly used to make various high-load parts and components and can be strengthened by heat treatment. It has moderate plasticity in quenched and just quenched conditions. It has good spot welding and has a tendency to form intergranular cracks when using gas welding. The alloy has good machinability after quenching and cold work hardening. This alloy is mainly used to make various high-load parts and components (but not stamping forgings) such as aircraft skeleton parts, skins, bulkheads, ribs, spars, rivets and other working parts below 150°C, Figure 142 [more info].

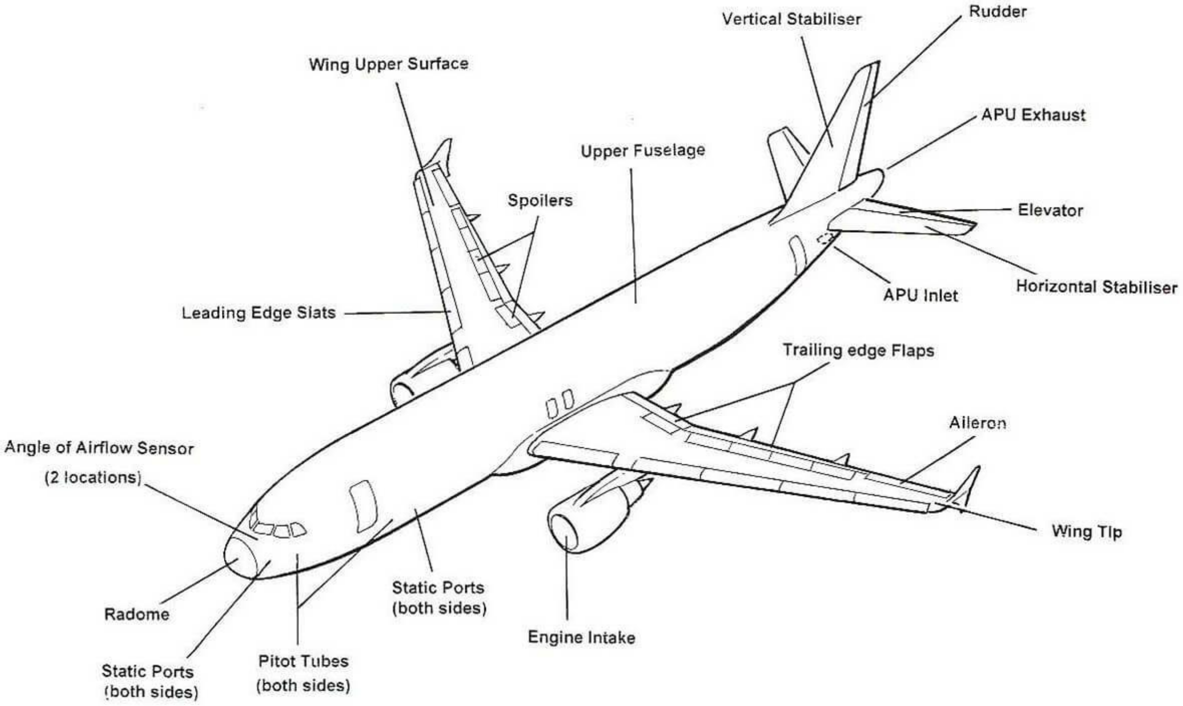

Fig. 142 Application for 2024 aluminum in aviation industry.

In the aviation industry, due to the low density, high strength and corrosion resistance, 2024 aluminum is the main material for aircraft structure. In recent years, as aircraft put forward higher requirements for maneuverability and speed, the aircraft itself will bear more complex load spectrum effects. Compared with ordinary aluminum alloys, aircraft aluminum alloys have higher requirements for strength, hardness, toughness, fatigue resistance, and plasticity. It is an ideal aviation structural material.

Metallography of aluminum is used in quality control for grain size determination and to determine microstructure defects on polished and etched specimens. In addition, specimens are often checked for impurities, such as oxides or zirconium aluminides. Cast alloy aluminum is evaluated for shape, distribution of phases and possible porosity. In wrought material, defects from the rolling and extrusion process are investigated and plating thicknesses measured [49].

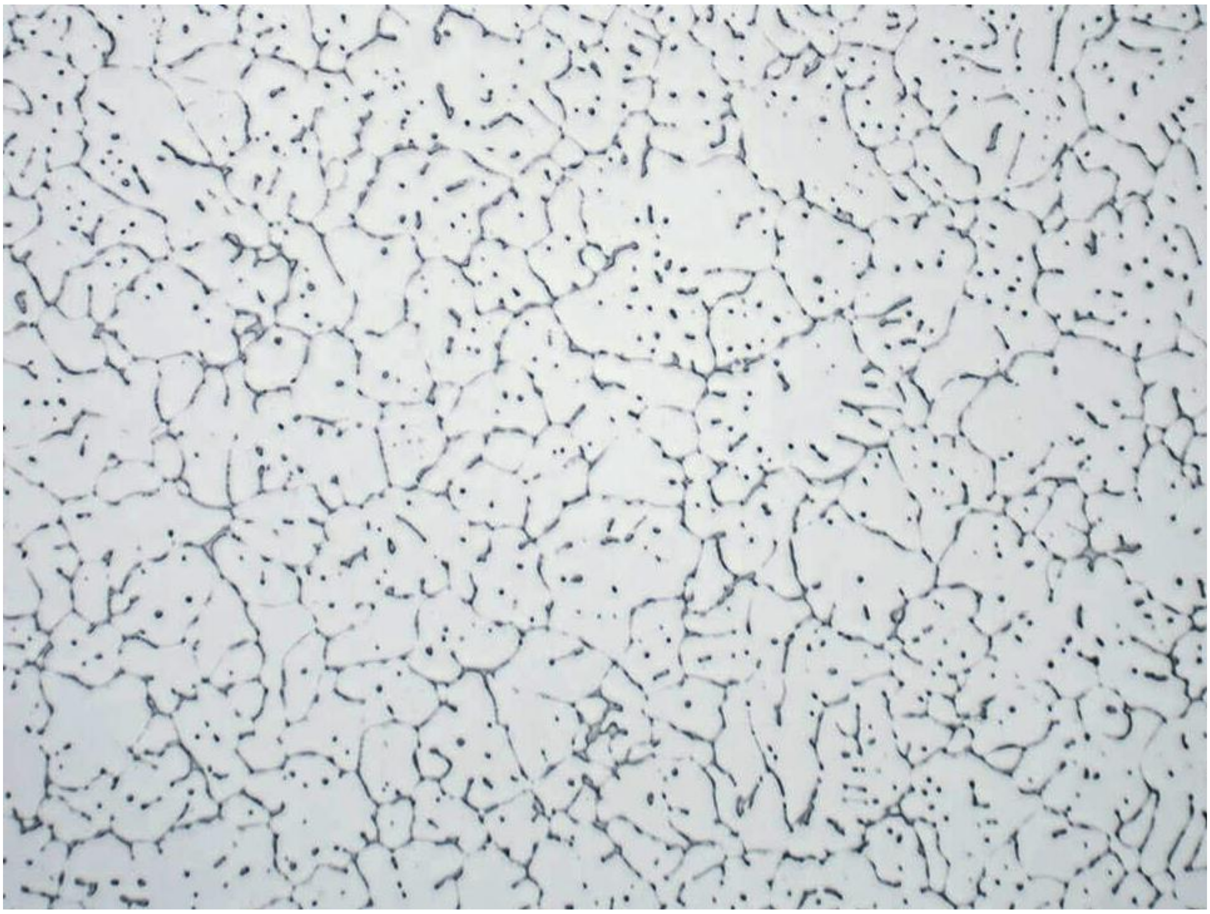

Fig.143 Aluminum alloy 2024, cast, showing eutectic precipitation on grain boundaries, unetched, 200x [more info].

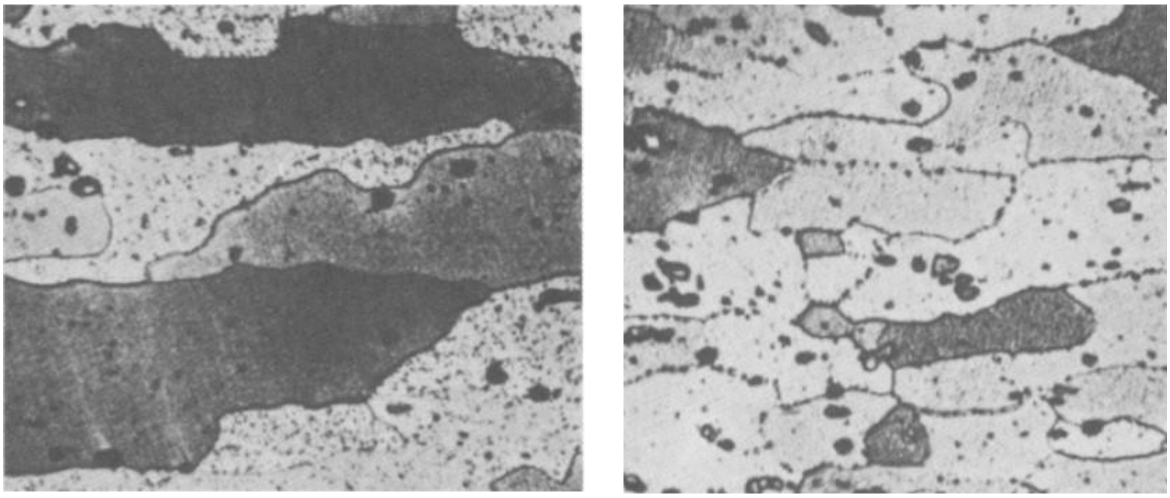

Alloy 2024-T3 sheet, solution heat treated at 495 ºC and quenched in cold water. Longitudinal section. Dark particles are $CuMgAl_2$, Cu_2MnAl_{20}, and Cu_2FeAl_7. Keller’s reagent. Magnification: 500x

Alloy 2024-T3 sheet, solution heat treated at 495 ºC but cooled in an air blast. The lower cooling rate resulted in increased precipitation of $CuMgAl_2$ at grain boundaries. Keller’s reagent. Magnification 500x

Fig. 144 The full microstructure of AA2024 alloys can only be seen through an electron microscope. They have a very complex structure, in order to increase strength, corrosion resistance and to control grain size. When the content of copper is 3,5-5 % they can be seen in the light microscope by etching reagent Keller [more info].

Materials Science Laboratory

Materials Science and Engineering Department

eReport

Type of the work	Non-Ferrous Alloys
Scop of inspection	Short description of the work:
Specimen Alloy designation.	Photo/Microstructure 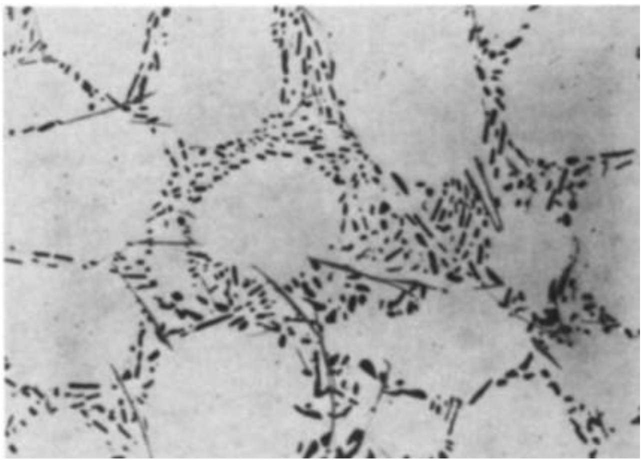
Preparation Polished/Etched	
Manufacturing Technology	
Magnification	
Equipment Metallographic microscope	
Observations: Hardness: ☐ Chemical composition: Applications: 	Specimen characterization. Results Analysis Identified phases and microstructural constituents.

Date:	Specialization:	Authorization Student Name

11.2. Case study

Bronze alloys for propellers in naval industry

Bronze alloys have been historically used for manufacturing propellers in ships due to their excellent combination of mechanical properties, corrosion resistance, and resistance to biofouling (the accumulation of marine organisms on submerged surfaces). The specific bronze alloy used for propellers can vary, but some common ones include:

- Manganese Bronze (C86300): This alloy is known for its high strength and excellent corrosion resistance in seawater. Manganese bronze is often used in marine applications, including propellers, because of its durability and resistance to wear.
- Aluminum Bronze (C95400, C95500): Aluminum bronze alloys are known for their high strength, corrosion resistance, and good anti-friction properties. They also offer excellent resistance to cavitation erosion, a common issue in propellers. The alloys C95400 and C95500 are frequently used in marine applications.
- Nickel Aluminum Bronze (C95800): This alloy is a variation of aluminum bronze that includes nickel for enhanced corrosion resistance. Nickel aluminum bronze is particularly well-suited for marine environments and is used in propellers, shipbuilding, and other marine applications.
- Tin Bronze (C90300, C90500): Tin bronze alloys offer good corrosion resistance, high strength, and excellent resistance to dezincification. These properties make them suitable for marine applications, including propellers.
- Phosphor Bronze (C51000, C54400): Phosphor bronze is known for its good wear resistance and corrosion resistance, particularly in marine environments. While it may not be as common as other bronze alloys for propellers, it is still used in some applications.

When selecting a bronze alloy for a propeller, factors such as the specific marine environment, the **size** and **type of the vessel**, and the **desired combination of properties** (strength, corrosion resistance, etc.) are considered. It's essential to balance these factors to ensure the propeller performs well over its intended lifespan in a maritime setting. Additionally, manufacturers may employ specific heat treatment processes to further enhance the properties of the chosen bronze alloy for propeller applications.

Since the first manufacture of aluminium bronze in the 1850s, there has been a progressive development in elemental additions to improve the mechanical properties and corrosion resistance. The early alloys were binary systems of copper and aluminium with aluminium in the range 6-11%.

Nowadays, there is a large market for nickel aluminium bronze in naval applications, particularly for the submarine fleets of the world [50]. The main applications are in seawater piping and valve systems, weapons handling, flexible couplings, sonar equipment, seawater external hatches, hydraulic valves and bearings, fasteners and sealing flanges, low noise propellers, propulsion equipment and periscope assemblies, Figure 145.

Nickel aluminium bronze is one of the main alloys used for ship propellers on commercial vessels and cruise liners. Its high resistance to cavitation, coupled with reasonable cost and the ease of repair when damaged, makes it a leading contender for this application. The alloys also exhibit good anti-damping properties, twice that of steel, which is important in submarines in suppressing sound for silent operations. Non-sparking and wear resistance become particularly important in weapons' handling systems [50].

Here is a short video that presents the bigest ship propellers in the world (2019) and the manufacturing proces.

Submarine propeller Ocular box submarine periscope Queen Elizabeth's propeller[26]

Fig. 145 Some applications for nickel aluminium bronze [50].

Fig. 146 Propeller's surface erosion due to cavitation.

Cavitation is the formation and implosion of cavities in liquids. It occurs when the hydrostatic pressure falls below the evaporation pressure of the liquid due to high flow velocities. Vapor bubbles are formed, which are entrained by the flowing liquid into areas of higher pressure, where the vapor in the cavities suddenly condenses and the vapor bubbles collapse, Figure 146.

The propeller ship is the greater source of cavitation due to induced high local velocities (or low pressures) around the blades. The consequnces of the cavitation of propellers are multiple, such as:

- raising onboard noise and vibration,
- material erosion and surface degradation of the propeller blades, accelerating wear and reducing the service life of the propellers,

---

[26] Adjustable bolted propeller - one of two 33 tonne propellers from the Queen Elizabeth class aircraft carrier capable of producing 40 MW of thrust (Courtesy Rolls Royce Marine), [50].

- reduction of propeller efficiency and thrust, decreasing ship speed and increasing the fuel consumption,
- increasing the structural fatigue strees,
- increasing operational costs for ship owners,
- increasing the cost maintenance, propellers may require more frequent inspections and repairs.

The greatest challenge for designers of ship propellers is to use the available engine power as efficiently as possible in order to minimize fuel consumption and therefore operating costs: a mid-size container ship will consume bunker fuel at a rate of more than 100 tons per day. At a cost more than $300 per ton, even marginal improvements in fuel economy will lead to significant savings [more info].

To mitigate the adverse effects of cavitation, engineers employ various design strategies, including optimizing blade shapes, adjusting operating conditions, and using specialized coatings. Additionally, selecting appropriate materials, such as bronze alloys with good cavitation resistance, can help minimize the impact of cavitation on propeller performance and longevity [more info].

The largest ship propellers in the world weight over 100 tons and have over 10 m in diameter. The cost for a ship propeller about 6 m in diameter is around £1 -1.5 million [movie]. Thus, we can understand the importance of maintenance and repairing of such expensive components. Studies[27] have shown that non-conformities detected in material chemical composition, as well as the presence of internal and surface flaws could be considered as the main contributors of the premature failure of propellers.

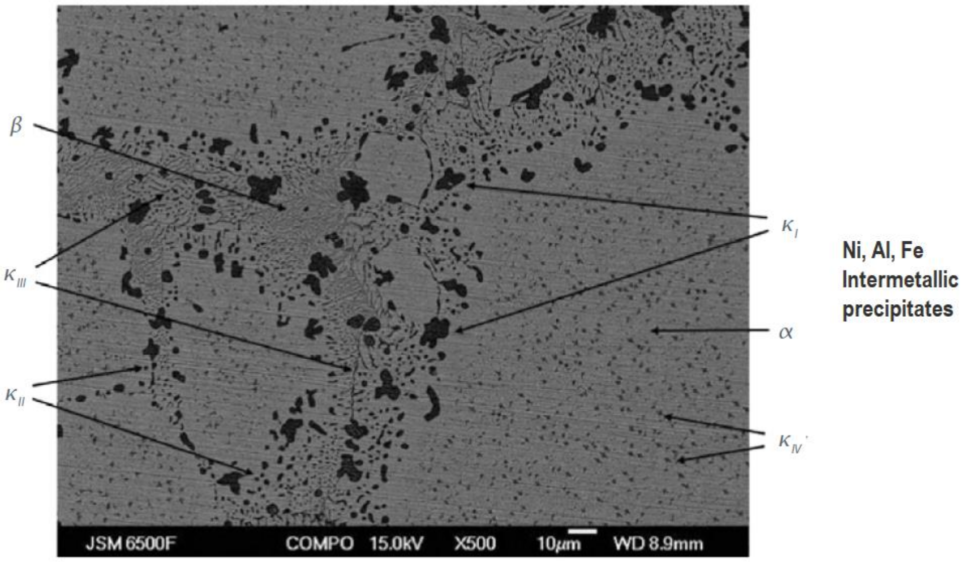

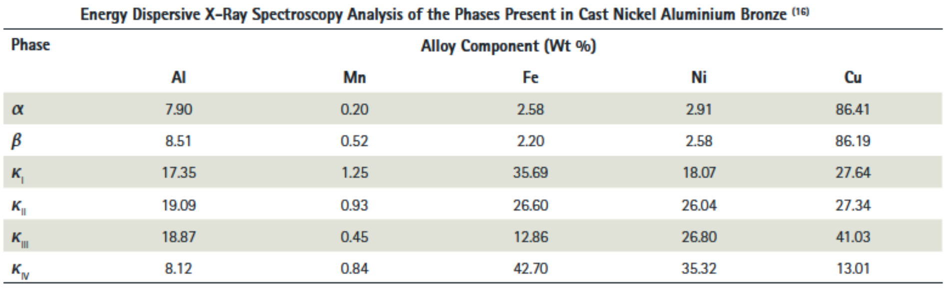
Energy Dispersive X-Ray Spectroscopy Analysis of the Phases Present in Cast Nickel Aluminium Bronze (16)

Phase	Alloy Component (Wt %)				
	Al	Mn	Fe	Ni	Cu
α	7.90	0.20	2.58	2.91	86.41
β	8.51	0.52	2.20	2.58	86.19
K_I	17.35	1.25	35.69	18.07	27.64
K_{II}	19.09	0.93	26.60	26.04	27.34
K_{III}	18.87	0.45	12.86	26.80	41.03
K_{IV}	8.12	0.84	42.70	35.32	13.01

Fig. 147 Nickel Aluminium Bronze microstructure [50].

---

[27] Chemical analysis, visual inspection, optical microscopy, fractographic evaluation, SEM/EDS analysis, and hardness testing were used as the principal analytical tools for the propeller failure investigation.

Table of Contents

List of Case Studies

1. Advanced image software for quantitative analysis
2. Sayano-Shushenskaya dam
3. The Metallurgy of the RMS Titanic
4. Advanced method for statistical determination of non-metallic inclusions in steel
5. The forensic analysis in structural failures
6. The forensic analysis of the World Trade Center Buildings 1, 2 and 7
7. Metallographic study on a Muramasa Japanese sword
8. Cold Welding. Galileo NASA mission
9. TVR Tuscan Speed Six. Austempered Ductile Iron (ADI) crankshaft
10. Philadelphia Energy Solutions refinery in Philadelphia
11. Bronze alloys for propellers in naval industry

Annex I – Fe-Fe_3C diagram

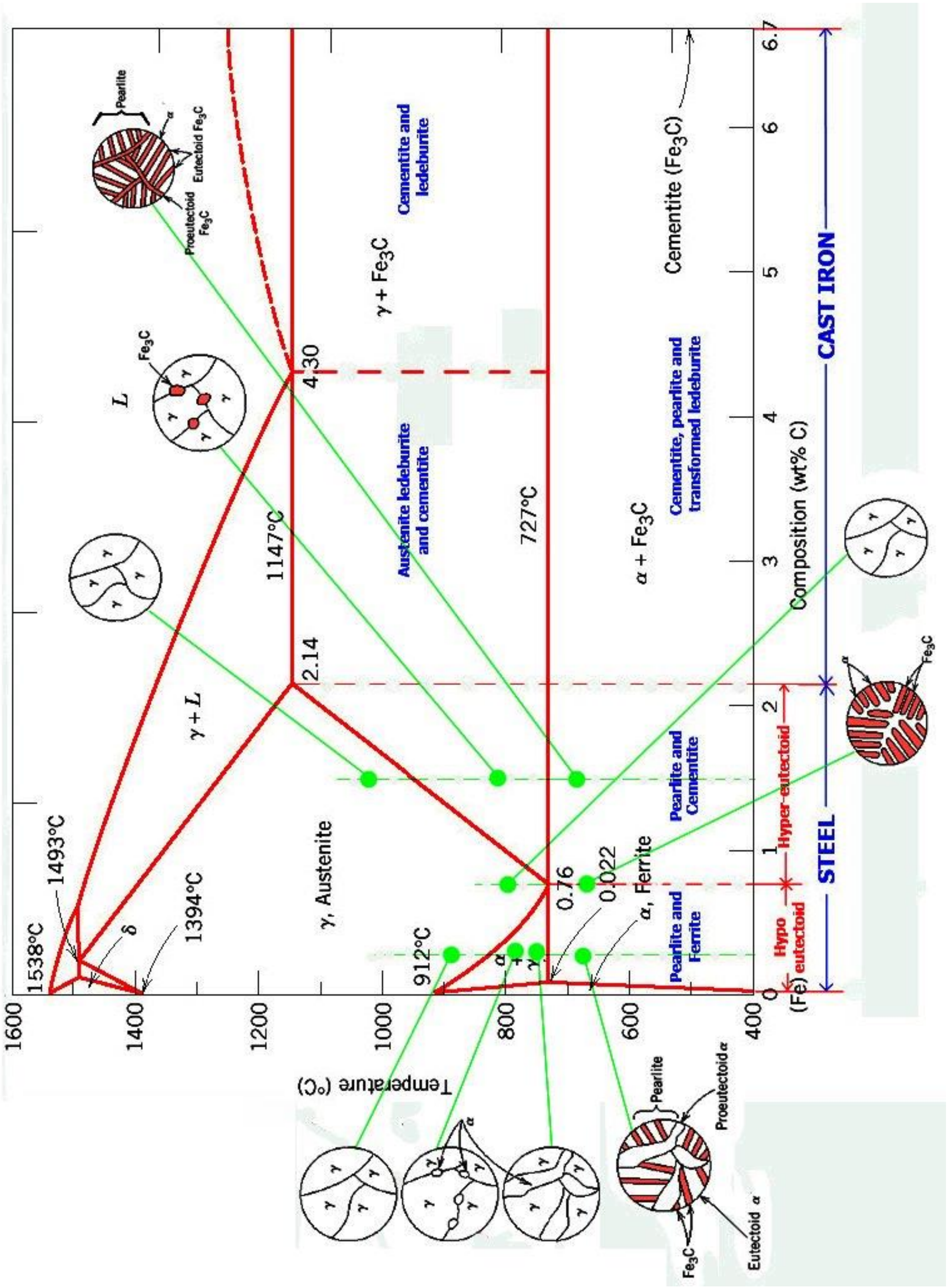

Annex II – Symbols for steel products indicating heat treatment condition.

Accordingly to EN 10027:1-2016

Symbol	Treatment Condition
+A	Soft annealed
+AC	Annealed to achieve spheriodised carbides
+AR	As rolled (without any special rolling and/or heat treatment conditions)
+AT	Solution annealed
+C	Cold work hardened
+Cnnn	Cold work hardened with a minimum tensile strength of nnn MPa
+CPnnn	Cold work hardened with a minimum 0,2 % proof strength of nnn MPa
+CR	Cold rolled
+DC	Delivery condition at manufacturer's discretion
+FP	Treated to ferritic-pearlite structure and hardness range
+HC	Hot rolled followed by cold hardening
+I	Isothermically treated
+LC	Skin passed (temper rolled or cold drawn)
+M	Thermomechanically formed
+N	Normalized or normalized formed
+NT	Normalized and tempered
+P	Precipitation hardened
+Q	Quenched
+QA	Air quenched
+QO	Oil quenched
+QT	Quenched and tempered
+QW	Water quenched
+RA	Recrystallization annealed
+S	Treated for cold shearing
+SR	Stress relieved
+T	Tempered
+TH	Treatment to hardness range
+U	Untreated
+WW	Warm worked

Annex III – Schmitz Microstructure Database

The database contains more than 620 case studies and failure cases. The microstructures are sorted by material type, being available at different magnification scales.

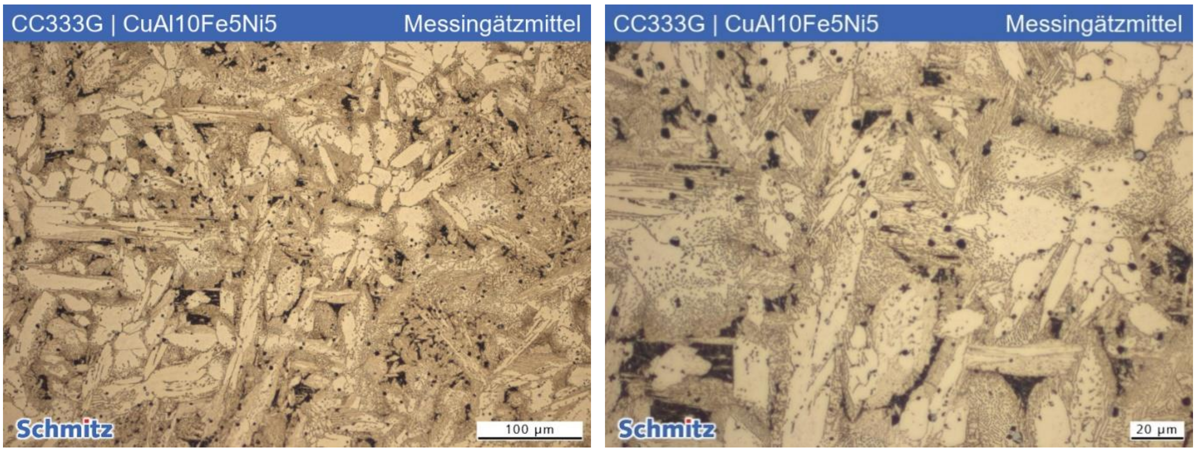

CuAl10Fe5Ni5 - The bronze has high strength values and very good corrosion resistance and is easily weldable, which is why it is used as a construction material in many sectors. The hardness here is 200 HB2.5/62.5. The microstructure consists of α-solid solution and inter metallic precipitations based on Fe3Al and NiAl (κ phase, gray).

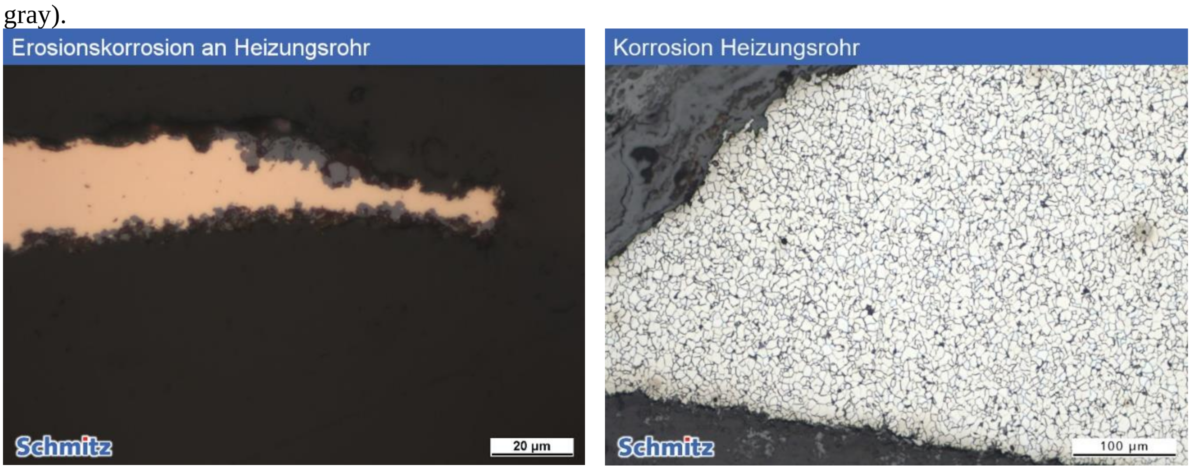

The damage mechanism leading to leakage is erosion-corrosion caused by solid particles in the (hot) water. Preferably in the area of bends or cross-section variations, these particles "grind" along the pipe wall on a microscopic level and finally lead to a hole-shaped wall perforation (pitting corrosion type II).

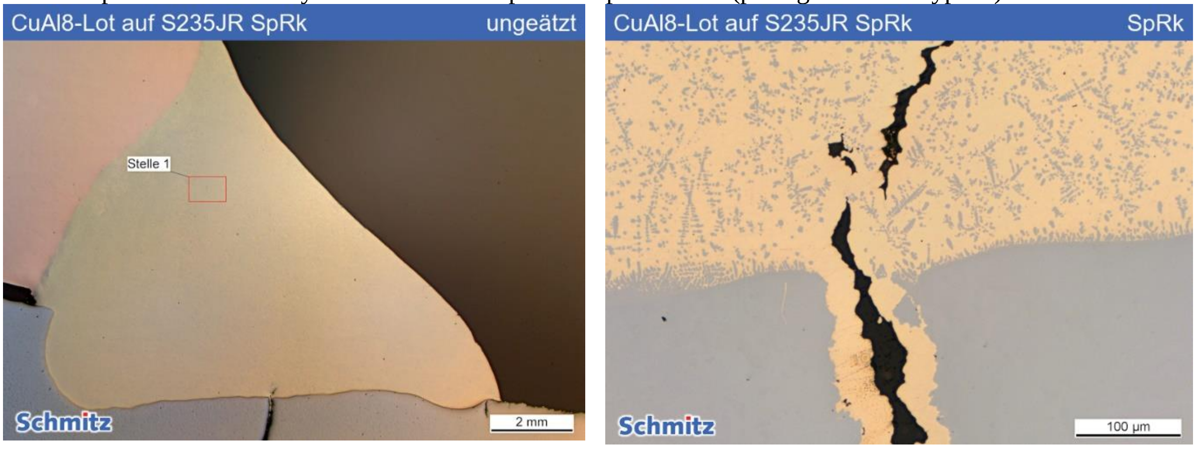

CuAl8 solder on S235JR - The microstructural pictures impressively show the diffusion of Cu into Fe. Iron has a decreasing solubility of maximum 2.2 wt.% Cu at 850 °C. The Cu diffuses along the grain boundaries of the iron and embrittles them. In the crack, the Cu concentrates to approx. 90 %.

References

1. BBC News, Alexander Kielland relatives seek answers 43 years on - BBC News
2. Solutions for Materials Preparation, Testing & Analysis, Sectioning - Buehler - Metallography Equipment & Supplies for Sample Preparation
3. Guide for abrasive blade selection, Blades for Abrasive Cutters - Buehler - Metallography Equipment & Supplies for Sample Preparation
4. Schmitz Metallographie GmbH, Abrasive Cut-Off Wheels, Abrasive Cut-Off Wheels (metallographie.shop)
5. YouTube - Metallography Part II - Microscopic Techniques - YouTube
6. Cold mounting, Metallographic cold mounting insight | Struers.com
7. Struers, Silicon Carbide Foils and Papers grinding consumables | Struers.com
8. George F. Vander Voort, Buehler Ltd. Metallography and Failure Analysis
9. Perrin Walker, William H. Tarn, Handbook of Metal Etchants, ISBN 0-8493-3623-6.
10. Elmet LLC, Microstructure and the Origins of Metallography — Elmet (elmetlabs.com)
11. World's Best Microscope Can Produce Images Less Than Diameter of Single Hydrogen Atom | ScienceDaily
12. Eyepieces (Oculars), Anatomy of a Microscope Eyepiece (Oculars) | Microscopy Primer | Olympus LS (olympus-lifescience.com)
13. Microscope Objectives Introduction, Microscope Objectives - Introduction | Olympus LS (olympus-lifescience.com)
14. Microscope Objectives , ZEISS Microscopy Online Campus | Microscopy Basics | Objectives (fsu.edu)
15. The Reflected Light Microscope, ZEISS Microscopy Online Campus | Microscopy Basics | Reflected Light Microscopy (fsu.edu)
16. Köhler illumination system, Köhler Illumination - Köhler Illumination in Reflected Light | Olympus LS (olympus-lifescience.com)
17. George F. Vander Voort Consultant – Struers Inc., Wadsworth, Illinois USA, Grain Size Measurements Using Circular or Rectangular Test Grids, https://doi.org/10.3139/147.110208, Practical Metallography 50(1):17-31, 2013.
18. LEICA, How to Adapt Grain Size Analysis of Metallic Alloys to Your Needs, 2019.
19. Graticules Optics Ltd., Microscope Eyepieces Reticles. Catalog 2023.
20. ASTM E112 − 13-R21, Standard Test Methods for Determining Average Grain Size, Reapproved 2021.
21. An Investment Casting Institute Publication, Atlas of Casting Defects, 2017.
22. Schmitz Metallographie, S355J2 Fatigue fracture of a hitch – Schmitz Metallographie GmbH (schmitz-metallographie.de)
23. Schmitz Metallographie, Etching – Schmitz Metallographie GmbH (schmitz-metallographie.de)
24. Bryan Leyland MSc, Leyland Consultants Ltd., Lessons from the accident at the Sayano-Shuskenaya hydropower station, EEA Conference & Exhibition 2010, 17-18 June 2010.
25. V. Ramachandran, A.C. Raghuram, R.V. Krishnan, and S.K. Bhaumik, Failure Analysis of Engineering Structures. Methodology and Case Histories, National Aerospace Laboratories, Bangalore, ASM International 2005.
26. ASTM E45-18 (R 2018). Standard Test Methods for Determining the Inclusion Content of Steel.
27. Kip O. Findley*, E.B. Damm, The Effects of Non-Metallic Inclusions on Mechanical Properties and Performance of Steel, Colorado School of Mines.
28. Dionis Diez, Ph.D.James DeRose, Thomas Locherer, Leica Microsystems, Overview of standard analysis methods and practical solutions for evaluating steel inclusions, Free Webinar and Report, April 28, 2020.
29. How clean is your steel? Erik Claesson, Joakim Fagerlund, Lily Kamjou and Patrik Ölund, OVAKO.
30. Wolfram Stets, Foseco Nederland BV, Non-Metallic Inclusions in Ductile Cast Iron, Steel, and Aluminium Castings, Foundry Practics 271.
31. Olympus Industrial Resources, Nonmetallic Inclusion Analysis in Steel, accessed dec. 2023.
32. ISO 3763 -1976. Wrought steels - Macroscopic methods for assessing the content of non-metallic inclusions.
33. ISO 4967:2013. Steel. Determination of content of non-metallic inclusions. Micrographic method using standard diagrams.

34. Foecke, T. (1998), Metallurgy of the RMS Titanic, NIST Interagency/Internal Report (NISTIR), National Institute of Standards and Technology, Gaithersburg, MD, Accessed December 28, 2023.
35. DoITPoMS Teaching and Learning Packages, About DoITPoMS[28]
36. M. Yaso, T. Takaiwa, Y. Minagi, K. Kubota, S. Morito, , T. Ohba, A. K. Das, Study of Microstructures on Cross Section of JAPANESE SWORD, ESOMAT 2009, DOI:10.1051/esomat/200907018.
37. J. Paul Guyer, P.E., R.A., Fellow ASCE, Fellow AEI, Ethical Issues from the Tacoma Narrows Bridge Collapse, Continuing Education and Development, 2010.
38. Tech Talks, Famous Failures: 9/11 Microstructural Steel Analysis of the World Trade Center, Higgins Armory/WPI MCSI Symposium Ronald R. Biederman, WPI June 8, 2005.
39. R. R. Biederman, Erin Sullivan1, George F. Vander Voort, and R. D. Sisson, Jr., Microstructural Microstructural Analysis of Steel from the World Trade Center Buildings 7, & 1 or 2, MCSI Symposium, 2005.
40. Erasteel, Heat Treatment of High Speed Steel, Accessed December 28, 2023.
41. Christophe Mesplont, Phase transformations and microstructure - mechanical properties relations in Complex Phase high strength steels, Laboratorium voor Algemene Metallurgie, Siderurgie en Fysische Metaalkunde, Accessed December 28, 2023.
42. Krawiec, H.; Lelito, J.; Mróz, M.; Radoń, M. Influence of Heat Treatment Parameters of Austempered Ductile Iron on the Microstructure, Corrosion and Tribological Properties. *Materials* **2023**, *16*, 4107. https://doi.org/10.3390/ma16114107
43. Chatterley, T. C., and P. Murrell. "ADI Crankshafts - An Appraisal of Their Production Potential." *SAE Transactions*, vol. 107, 1998, pp. 436–53. *JSTOR*, http://www.jstor.org/stable/44724158, Accessed 2 Jan. 2024.
44. ASTM A 247-19, Standard Test Method for Evaluating the Microstructure of Graphite in Iron Castings.
45. Riposan I, Anca D, Stan I, Chisamera M, Stan S. Graphite Nodularity Evaluation in High-Si Ductile Cast Irons. Materials (Basel). 2022 Nov 1;15(21):7685. doi: 10.3390/ma15217685. PMID: 36363275; PMCID: PMC9656566.
46. ADI Treatments Ltd, Doranda Way, ADI solutions aid vehicle design, https://www.foundry-planet.com/fileadmin/redakteur/pdf-dateien/technical-reports/ADsolutionsvehicleesign.pdf, Accessed 2 Jan. 2024.
47. STRUERS, Stainless Steel. Metallographic preparation of stainless steel, Application Note, Accessed 2 Jan. 2024.
48. CSB, Investigation Report - Fire and Explosions at Philadelphia Energy Solutions Refinery Hydrofluoric Acid Alkylation Unit, Published: October 11, 2022.
49. STRUERS, Metallographic Preparation of Aluminum and Aluminum Alloys, Application Note, Accessed 6 Jan. 2024.
50. Ivan Richardson, Guide to Nickel Aluminium Bronze for Engineers, Guide to Nickel Aluminium Bronze for Engineers (copper.org), Copper Development Association Publication No 222, Jan.2016.

---

[28] The copyright in the DoITPoMS Library of Teaching and Learning Packages resides with the University of Cambridge. DoITPoMS and the University of Cambridge must be acknowledged in any text, images or other material. Such acknowledgement must be visible within any teaching material produced and accompanying literature if applicable e.g. © *DoITPoMS, University of Cambridge* and include the webpage URL where appropriate. Copies of the images cannot be sold or made available under loan. Commercial reproduction is prohibited, and multiple distribution of any kind is prohibited except for educational use.